UNIVERSIDADE FEDERAL DO RIO GRANDE DO SUL
ESCOLA DE ENGENHARIA
DEPARTAMENTO DE ENGENHARIA QUÍMICA
PROGRAMA DE PÓS-GRADUAÇÃO EM ENGENHARIA QUÍMICA

Desenvolvimento de Biomateriais Eletrofiados, Biorreatores e Modelos Fenomenológicos para a Engenharia de Tecidos

TESE DE DOUTORADO

Ágata Paim

Porto Alegre
2017

UNIVERSIDADE FEDERAL DO RIO GRANDE DO SUL
ESCOLA DE ENGENHARIA
DEPARTAMENTO DE ENGENHARIA QUÍMICA
PROGRAMA DE PÓS-GRADUAÇÃO EM ENGENHARIA QUÍMICA

Desenvolvimento de Biomateriais Eletrofiados, Biorreatores e Modelos Fenomenológicos para a Engenharia de Tecidos

Ágata Paim

Tese de doutorado apresentada como requisito para obtenção do título de Doutor em Engenharia Química.

Área de concentração: Projeto, Simulação, Controle e Otimização

Orientadores:
Prof[a]. Dr[a]. Isabel Cristina Tessaro

Prof. Dr. Nilo Sérgio Medeiros Cardozo

Co-orientadora:

Prof[a]. Dr[a]. Patricia Lucas Helena Pranke

Porto Alegre

2017

UNIVERSIDADE FEDERAL DO RIO GRANDE DO SUL

ESCOLA DE ENGENHARIA

DEPARTAMENTO DE ENGENHARIA QUÍMICA

PROGRAMA DE PÓS-GRADUAÇÃO EM ENGENHARIA QUÍMICA

A Comissão Examinadora, abaixo assinada, aprova a Tese de Doutorado *Desenvolvimento de Biomateriais Eletrofiados, Biorreatores e Modelos Fenomenológicos para a Engenharia de Tecidos*, elaborada por Ágata Paim, como requisito para obtenção do título em Engenharia Química.

Comissão Examinadora:

Profª Drª Alessandra Nejar Bruno

Profª Drª Márcia Rosângela Wink

Profª Dra Rosane Rech

Agradecimentos

Ao Laboratório de Hematologia e Células-tronco, ao Instituto de Pesquisas com Células-tronco, ao Programa de Pós-Graduação em Engenharia e à CAPES por terem viabilizado a execução desta tese.

À colega Daikelly I. Braghirolli, sem a qual a parte experimental com cultivo de células deste trabalho não teria sido possível.

Aos meus orientadores Isabel C. Tessaro e Nilo S. M. Cardozo, e coorientadora Patricia H. L. Pranke, pela orientação, incentivo, apoio e compreensão.

Aos colegas do laboratório, pelos ensinamentos e por participar de momentos decisivos na construção da metodologia utilizada neste trabalho.

À Martina Soares, pela amizade e por ter plantado em mim a vontade de trabalhar com células-tronco e engenharia de tecidos.

À minha família, pelo amor e incentivo, especialmente ao meu irmão, pelo suporte técnico, e ao meu pai, pelo apoio moral e financeiro.

Às amizades que construí no laboratório, pelo carinho e apoio.

À Fiji, minha fiel companheira.

Resumo

Uma potencial alternativa para o transplante de tecidos é a engenharia de tecidos. Células-tronco mesenquimais e *scaffolds* eletrofiados são comumente utilizados nesta área devido à capacidade multipotente de diferenciação destas células e à rede de poros interconectados destas estruturas fibrosas. Além disso, bioreatores de perfusão podem ser utilizados para melhorar o transporte de nutrientes e reduzir o acúmulo de metabolitos tóxicos. Neste contexto, uma maneira de estudar e otimizar o sistema de cultivo é utilizar técnicas de modelagem para descrever interações ou processos individuais envolvidos no crescimento celular. Deste modo, o objetivo geral deste estudo é realizar o cultivo de células-tronco mesenquimais da polpa de dente decíduo (DPSCs) utilizando *scaffolds* tridimensionais eletrofiados de policaprolactona (PCL), biorreatores e técnicas de modelagem. Inicialmente foram testadas diferentes misturas de solventes (clorofórmio e metanol), a fim de produzir *scaffolds* com poros adequados ao cultivo tridimensional. Os diâmetros de fibra e de poro foram determinados por microscopia eletrônica de varredura (MEV). O crescimento e o metabolismo das células foram avaliados através da determinação da atividade metabólica e das concentrações de glicose e lactato do meio de cultivo, e a infiltração celular foi observada com a marcação do núcleo celular. Depois de estabelecidos os parâmetros de eletrofiação, o efeito da perfusão direta no desprendimento de DPSCs de *scaffolds* eletrofiados de PCL foi estudado. A atividade metabólica das células foi determinada para diferentes tempos de adesão, vazões e densidades de semeadura, e a tensão de cisalhamento na parede do poro foi calculada para cada vazão. A morfologia das células foi avaliada através de imagens de microscopia confocal e MEV. Paralelamente, foram realizadas simulações utilizando o software OpenFOAM para estudar como os parâmetros e variáveis de entrada (concentração inicial de glicose, porosidade e espessura do *scaffold*) afetam as saídas (fração volumétrica de células e concentração de substrato) de um modelo de proliferação celular que considera a difusão e o consumo de glicose. As contribuições do teor de oxigêno na cinética de crescimento de *Contois* e da variação da porosidade com o tempo devido à degradação do polímero também foram avaliadas. Inicialmente, foi observado que apenas um tamanho de poro maior que o diâmetro da célula permitiu a infiltração das células no *scaffold*. Então, observou-se que o aumento do tempo de adesão acarretou em maior espalhamento das células e, assim como a diminuição da densidade de semeadura e da tensão de cisalhamento, resultou em uma redução do desprendimento das células sob perfusão. Quanto ao modelo fenomenológico, observou-se maior sensibilidade à concentração inicial de glicose e à porosidade do *scaffold*, e aos parâmetros adimensionais relacionados à proliferação e morte celular e ao consumo de nutrientes. Além disso, o número inicial de células apresentou maior impacto no transporte de massa do que no crescimento celular. Neste estudo, foi possível obter *scaffolds* eletrofiados e conduções de cultivo dinâmico adequadas ao cultivo tridimensional de DPSCs, e elucidar os efeitos da limitação do transporte de massa e do oxigênio no crescimento celular, e da degradação do polímero no transporte de massa.

Palavras-chave: células-tronco da polpa de dente, *electrospinning*, policaprolactona, biorreator de perfusão, modelagem computacional.

Abstract

A potential alternative to tissue transplant is tissue engineering. Mesenchymal stem cells and electrospun scaffolds are commonly used in this field due to the multipotent differentiation capacity of these cells and the interconnected pore network of these fibrous structures. In addition, perfusion bioreactors can be used to enhance nutrient transport and reduce the accumulation of toxic metabolites. In this context, one way to study and optimize the culture system is to use modeling techniques to describe interactions or individual processes involved in cell growth. Thus, the objective of this study is to perform the three-dimensional culture of mesenchymal stem cells of dental pulp (DPSCs) using electrospun polycaprolactone (PCL) scaffolds, bioreactors and modeling techniques. Initially, different solvent mixtures (chloroform and methanol) were tested to produce scaffolds with pores suitable to three-dimensional culture. Fiber and pore diameter was determined using a scanning electron microscope. Cell growth and metabolism were evaluated through the metabolic activity and the culture medium concentration of glucose and lactate, and the cell infiltration was observed with cell nuclei staining. After the establishment of the elesctrospinning parameters, the effect of direct perfusion on DPSCs detachment from PCL electrospun scaffolds was investigated. The metabolic activity of the cells was determined for different adhesion times, flow rates and seeding densities and the pore wall shear stress was calculated for each flow rate. The cell morphology was evaluated through scanning electron and confocal microscopy imaging. In parallel, simulations with the software OpenFOAM were performed to study how parameters and inputs (initial glucose concentration, porosity and thickness of the scaffold) affect the outputs (cell volume fraction and substrate concentration) of a model of cell proliferation and glucose diffusion and consumption. The contribution of the oxygen in the *Contois* growth kinetics and the porosity variation with time due to polymer degradation was also evaluated. Initially, it was observed that only a pore size higher than the cell diameter allowed the infiltration of the cells through the scaffold. Then, it was observed that a higher adhesion time leaded to higher cell spreading in static conditions and, similar to smaller seeding densities and shear stresses, reduced cell detachment under perfusion. Regarding the phenomenological model, it was observed that the model is more responsive to the initial glucose concentration and scaffold porosity, and to the dimensionless parameters related to cell proliferation, death and nutrient uptake. Furthermore, the initial cell number had a more significant impact on mass transport than on cell growth. In this study, it was possible to obtain an electrospun scaffold and dynamic culture conditions suitable for the three-dimensional culture of DPSCs, and to elucidate the effects of transport limitations and of oxygen on cell growth, and of polymer degradation on mass transport were elucidated.

Keywords: dental pulp stem cells, electrospinning, polycaprolactone, perfusion bioreactor, computational modeling.

Sumário

Lista de figuras

Lista de tabelas

Capítulo 1

Introdução

A engenharia de tecidos, ciência multidisciplinar que aplica princípios básicos de engenharia para restauração, manutenção e/ou aperfeiçoamento funcional de tecidos representa uma alternativa potencial aos transplantes. Um desafio desta ciência é o desenvolvimento de um suporte (*scaffold*) para proliferação, diferenciação e migração celular que seja capaz de mimetizar as propriedades da matriz extracelular do tecido a ser regenerado. Uma das técnicas utilizadas para a produção de *scaffolds* com poros interconectados é a eletrofiação. Esta técnica permite a utilização de uma ampla faixa de polímeros naturais e sintéticos, sendo um deles a policaprolactona (PCL), a qual tem sido bastante utilizada na engenharia de tecidos devido às suas propriedades mecânicas (força e elasticidade). Entre as diferentes células utilizadas na engenharia de tecidos, destacam-se as células-tronco mesenquimais, devido a sua capacidade de se auto-renovar e de se diferenciar em diferentes tipos celulares. A utilização de células-tronco em estudos experimentais deve atender a muitos requisitos quanto à contaminação e reprodutibilidade, de modo que sistemas dinâmicos podem ser utilizados para reduzir o esforço experimental e superar limitações de transporte de massa. Modelos preditivos também podem ser utilizados para simular diferentes experimentos ou estratégias de tratamento que possuem custo elevado ou que são eticamente impraticáveis. Além disso, modelos matemáticos podem elucidar as ciências básicas do crescimento celular e do transporte de massa dentro de *scaffolds* porosos, o que favorece a identificação de componentes-chave na regeneração de tecidos e o desenvolvimento de melhores estratégias de tratamento. Assim, torna-se interessante o desenvolvimento de *scaffolds* eletrofiados de PCL e

de biorreatores para o cultivo de células-tronco mesenquimais de dente, assim como a modelagem fenomenológica da proliferação celular e do transporte de massa para o estudo do desenvolvimento de tecidos.

1.1 Relevância e objetivos

O transplante de órgãos e de tecidos é uma terapia amplamente aceita para o tratamento de pacientes com órgãos e tecidos danificados em casos de acidentes, traumas ou câncer. No entanto, o transplante autólogo é limitado pela morbidade no sítio doador, pelo risco de infecção e pela exposição do paciente ao ser submetido a uma segunda cirurgia. Fontes alternativas de tecidos com origem de outro indivíduo ou animal também apresentam restrições, principalmente devido à resposta imunológica do paciente quanto ao implante e à escassez de doadores compatíveis. Essas questões têm motivado muitos estudos envolvendo o cultivo de células-tronco mesenquimais em *scaffolds* tridimensionais para a engenharia de tecidos.

No cultivo de células em *scaffolds* tridimensionais tem-se a formação de gradientes de concentração dos diferentes compostos presentes no processo, de modo que a disponibilidade e a distribuição dos nutrientes influenciam no metabolismo celular. Muitos estudos buscam a minimização destas limitações de transporte através do uso de biorreatores e de técnicas de modelagem. No entanto, a maioria dos estudos utiliza estruturas com poros de tamanho médio superior a 100 μm para o cultivo de células-tronco mesenquimais em *scaffolds* tridimensionais. Além disso, não foram encontrados estudos do transporte de massa e da proliferação de células-tronco em *scaffolds* tridimensionais eletrofiados que considerassem o gradiente de concentração de nutrientes na determinação da taxa de consumo de nutrientes.

Neste contexto, o presente estudo foi desenvolvido considerando as hipóteses listadas a seguir.

→ O crescimento celular é modulado pela disponibilidade de nutrientes.

→ A célula é capaz de migrar através de uma estrutura 3D com poros de diâmetro maior que o diâmetro da célula em suspensão.

→ A célula é capaz de se proliferar com a perfusão direta do meio de cultivo, contanto que a tensão de cisalhamento não ultrapasse um limite crítico.

→ A perfusão do meio de cultivo proporciona maior disponibilidade de nutrientes ao longo do *scaffold*.

→ A técnica de *electrospinning* é capaz de produzir *scaffolds* de PCL com fibras micrométricas e poros grandes o suficiente para permitir a infiltração das células para dentro da matriz.

Desta forma, o objetivo geral deste trabalho é realizar o cultivo de células-tronco mesenquimais da polpa de dente decíduo utilizando *scaffolds* tridimensionais eletrofiados de PCL, biorreatores e técnicas de modelagem. De acordo com esta meta geral, os objetivos específicos deste estudo são:

a. estabelecer o protocolo de eletrofiação de *scaffolds* com poros de diâmetro adequados para o cultivo tridimensional de DPSCs;
b. comparar o tempo de dobramento e as taxas de consumo de glicose e de produção de lactato das células em cultivos bidimensionais e tridimensionais;
c. estabelecer protocolo de cultivo dinâmico de células-tronco mesenquimais da polpa de dente em *scaffolds* de PCL;
d. modelar a proliferação celular e o transporte de massa em *scaffolds* porosos;
e. realizar análise de sensibilidade (simulação com diferentes valores de parâmetros e entradas) para determinar os parâmetros significativos do modelo;
f. avaliar a contribuição da adição de complexidade ao modelo e estabelecer os fenômenos que devem ser descritos;

1.2 Estrutura da Tese

Este trabalho apresenta-se dividido em oito capítulos, conforme descrito a seguir.

O Capítulo 1 trata da introdução ao tema a ser abordado na tese, dos objetivos e da relevância do estudo. Neste capítulo também são esclarecidas as hipóteses iniciais da tese e é apresentada a estrutura do trabalho.

No Capítulo 2 é feita uma revisão bibliográfica acerca dos principais fenômenos envolvidos no desenvolvimento de um tecido e da utilização de técnicas de modelagem para a análise destes fenômenos. Com foco em células-tronco mesenquimais e *scaffolds* tridimensionais, são revisados o transporte de massa e outros processos, como a síntese da matriz extracelular, a vascularização, a proliferação, a adesão, a migração, a morte e a diferenciação celular.

No Capítulo 3, são revisadas as propriedades dos *scaffolds* e as condições de semeadura e de cultivo que afetam a atividade de células-tronco mesenquimais em *scaffolds*

eletrofiados. Além disso, foi discutida utilização de técnicas de modelagem computacional para a otimização destes fatores.

O Capítulo 4 apresenta um estudo acerca do efeito da adição de metanol como não-solvente na morfologia e tamanho das fibras produzidas através da eletrofiação de uma solução de PCL e clorofórmio. Também foi discutido o tamanho dos poros e a influência da concentração de PCL no diâmetro das fibras. Por fim, é avaliada a influência do substrato no metabolismo e no crescimento celular.

O Capítulo 5 apresenta o estudo do efeito da vazão de perfusão no arraste de células-tronco mesenquimais de polpa de dente decíduo, pré-aderidas em *scaffolds* eletrofiados de PCL. O efeito do tempo de adesão, em condições estáticas, na força de adesão também é abordado, assim como a influência da densidade de células da semeadura estática no posterior arraste de células sob perfusão.

O Capítulo 6 apresenta a análise de sensibilidade de um modelo de transporte de massa, consumo de glicose e crescimento celular em meio poroso em cultivo estático. Também foi avaliada a influência da densidade inicial de células, da concentração inicial de glicose, da espessura e da porosidade do *scaffold* na fração volumétrica de células e na concentração de glicose do meio ao longo do tempo.

O Capítulo 7 apresenta um estudo comparativo entre três modelos matemáticos do crescimento celular e do transporte de massa em *scaffolds* tridimensionais, para engenharia de tecidos. Uma análise do efeito das variáveis de entrada na concentração de nutrientes e na fração volumétrica de células foi realizada a fim de averiguar a contribuição da adição da concentração de oxigênio na cinética de proliferação de Monod e da variação da porosidade com o tempo devido à degradação do *scaffold*.

No capítulo de considerações finais, (Capítulo 8) é feita uma retomada do tópico, objetivos, questões de pesquisa e hipóteses, e apresentado um resumo dos principais resultados obtidos e as conclusões gerais sobre o tema de pesquisa.

Por fim, no Capítulo 9 são discutidas as limitações do estudo e apresentadas as perspectivas para trabalhos futuros.

Os experimentos foram realizados no Laboratório de Hematologia e Células-Tronco da Faculdade de Farmácia da UFRGS. As simulações foram realizadas com o apoio do Centro Nacional de Supercomputação (CESUP), da UFRGS. A Figura 1 apresenta um fluxograma das etapas deste estudo que elucida a relação dos capítulos do trabalho descritos a seguir com os objetivos específicos apresentados anteriormente.

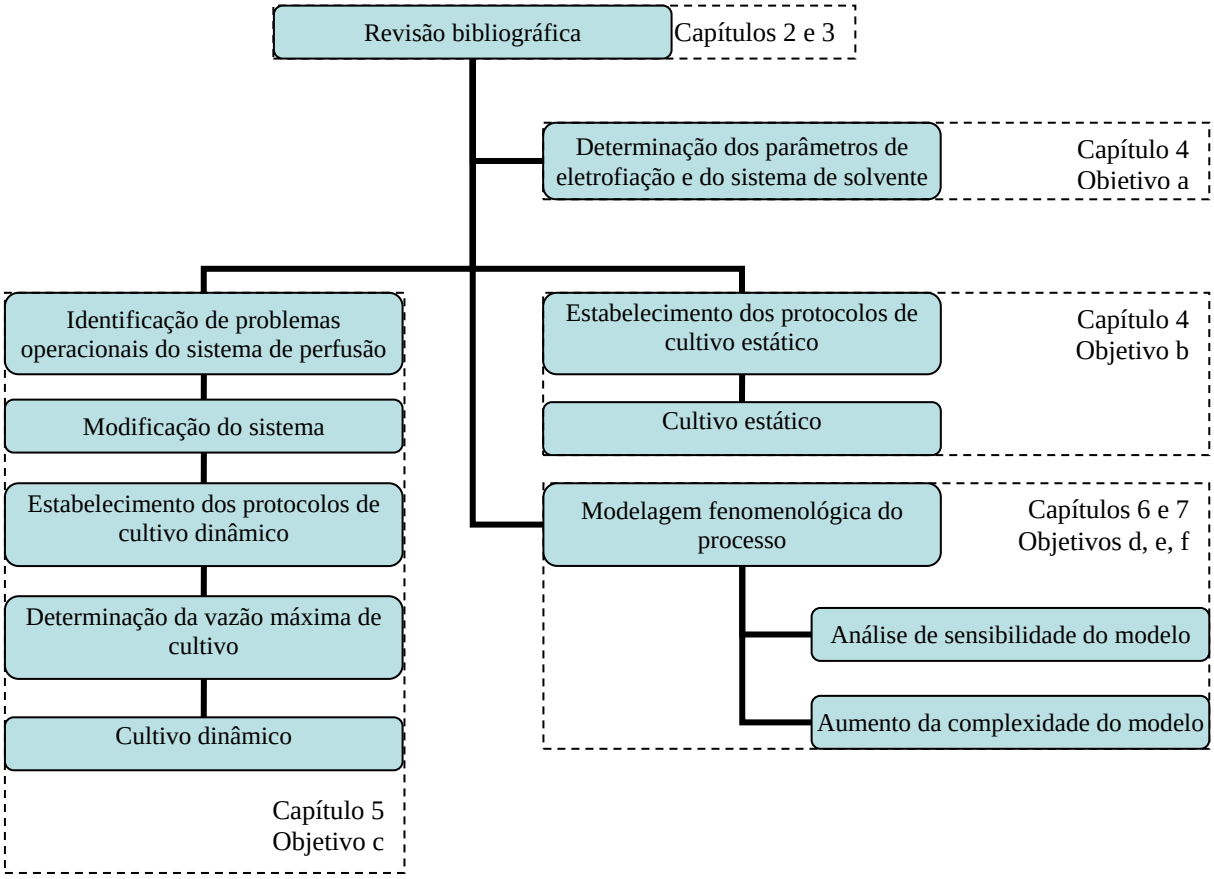

Figura 1.1: Fluxograma das etapas do projeto destacando os objetivos a serem atingidos em cada etapa

Capítulo 2

Fenômenos biológicos relevantes para o desenvolvimento de tecidos e modelagem fenomenológica

Um dos principais objetivos da engenharia de tecidos é reproduzir a complexidade natural de um tecido. Este capítulo tem como objetivo esclarecer a importância de alguns fenômenos envolvidos no desenvolvimento de tecidos *in vitro*. Inicialmente, é feita uma breve discussão acerca da utilização de células-tronco mesenquimais na engenharia de tecidos. Na sequência, são revisados os processos biológicos que governam a atividade celular e sua relação com o transporte de massa dentro de *scaffolds* tridimensionais. Por fim, é discutida a importância da modelagem dos diferentes fenômenos envolvidos no desenvolvimento de tecidos. Este capítulo está na forma de artigo de revisão, na língua inglesa, o qual foi submetido para a revista *Mathematical Biosciences* e está sendo analisado pelos revisores.

Artigo 1

RELEVANT BIOLOGICAL PROCESSES FOR TISSUE DEVELOPMENT WITH STEM CELLS AND THEIR MECHANISTIC MODELING

Ágata Paim[*1,2], Nilo S. M. Cardozo[2], Isabel C. Tessaro[1], Patricia Pranke[3]

[1,2]Department of Chemical Engineering, Universidade Federal do Rio Grande do Sul (UFRGS), R. Eng. Luis Englert, s/n. Porto Alegre, Rio Grande do Sul 90040-040, Brazil.

[3]Faculty of Pharmacy, Universidade Federal do Rio Grande do Sul (UFRGS), Av. Ipiranga, 2752. Porto Alegre, Rio Grande do Sul 90610-000, Brazil.

Corresponding author (Ágata Paim)

Present address: Department of Chemical Engineering, Universidade Federal do Rio Grande do Sul (UFRGS), R. Eng. Luis Englert, s/n. Porto Alegre, Rio Grande do Sul 90040-040, Brazil

Phone/Fax: +55 51 33085257

E-mail address: agata@enq.ufrgs.br

Abstract

A potential alternative for tissue transplants is tissue engineering, in which the interaction of cells and biomaterials can be optimized. Tissue development *in vitro* depends on the complex interaction of several biological processes such as extracellular matrix synthesis, vascularization and cell proliferation, adhesion, migration, death, and differentiation. The complexity of an individual phenomenon or of the combination of these processes can be studied with phenomenological modeling techniques. This work reviews the main biological phenomena in tissue development and their mathematical modeling, focusing on mesenchymal stem cell growth in three-dimensional scaffolds.

Keywords: stem cells, biological processes, tissue development, three-dimensional scaffolds, phenomenological modeling.

2.1 Introduction

Tissue and organs are composed of cells and well-organized networks called extracellular matrix (ECM) [1]. The general approach to engineer tissue is to cultivate cells in a scaffold, a device that provides an environment for tissue regeneration [2]. Scaffold properties can be determined by the material and by the method of fabrication. Several techniques can be used to manufacture scaffolds, such as gas foaming, fiber extrusion and bonding, electrospinning, solid free-form fabrication, three-dimensional printing, phase separation, solvent casting/particulate leaching, freeze-drying and emulsion freeze-drying [3].

In tissue engineering, transplanted cells can be removed from the same individual that is going to receive the engineered tissue transplant (autologous cells). However, in addition to the invasive nature of autologous cell sampling, the tissue biopsy does not always provide enough cells for further expansion or transplantation [4,5]. For instance, in cases of end-stage organ failure, stem cells can be applied due to their capacity of differentiation in several cell types [6]. Furthermore, mesenchymal stem cells have been used in clinical studies for tissue regeneration due to its high proliferative capacity and immunosuppressive properties [5,7,8].

To engineer a tissue, the stem cells must first proliferate to increase the pool of cells and the tissue mass, while they modify the micro-environment by the secretion of factors that induce tissue repair to further differentiate in the required cell type that will generate new tissue [9]. In the case of biodegradable materials, extracellular matrix synthesis and deposition occurs in a concurrent manner with scaffold degradation [10], affecting the nutrient transport and cell viability [11]. One way to describe the interactions or individual processes involved in tissue development or to optimize the culture system is to use mathematical and computational modeling techniques [12]. In this review, the main phenomena involved in tissue development *in vitro* are discussed with an emphasis on the culture of mesenchymal stem cells in three-dimensional (3D) porous scaffolds. Moreover, mechanistic modeling applications in tissue engineering are reviewed.

2.2 Stem cells

Stem cells can be multi-or pluripotent (Figure 2.1), meaning that they are able to differentiate to cells from their original dermal layer or in cells from the three embryonic germ layers (endo-, meso- and ectoderm), respectively [13].

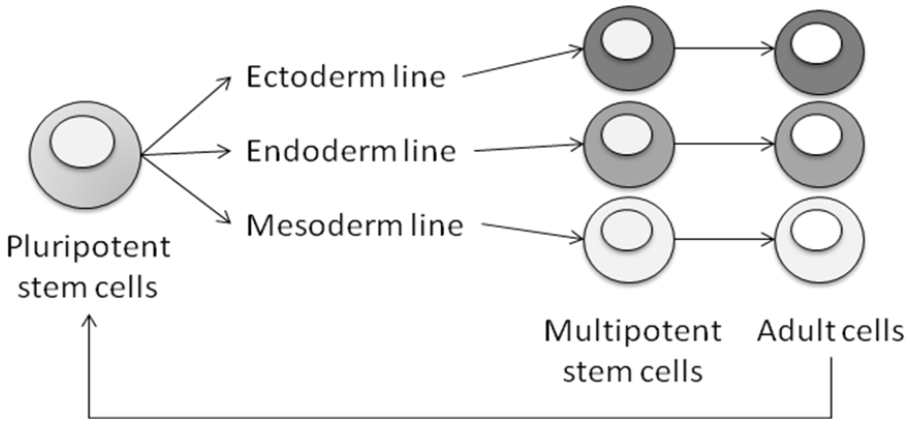

Figure 2.1: Diagram of stem cell hierarchy

Human embryonic stem cells (hESCs) are capable of self-renewing indefinitely while maintaining their capacity of differentiation in all adult human tissue, being classified as pluripotent cells [14]. However, hESCs are usually derived from blastocyst-stage embryos from *in vitro* fertilization treatment [15]. Despite the fact that the majority of countries which develop scientific research around the world allow the use of human embryonic stem cells [16,17], there are ethical and legislation constraints for the derivation of hESC's lines from excess *in vitro* fertilization embryos in many countries, such as Austria, Bulgaria, Costa Rica, Germany, Italy, Lithuania, Portland and Tunisia [18]. Furthermore, due to the allogenic nature of embryonic stem cells and differentiated derived cells, they can lead to rejection by the immune system of the transplanted tissue [19].

Induced pluripotent stem cells (iPSs) can be acquired by reprogramming adult cells with embryonic transcription factors (Oct3/4, Sox2, c-Myc, and Klf4) [20]. These cells can be autologous and have morphology, proliferation, gene expression, differentiation potential *in vitro*, and telomerase activity similar to the ones of hESCs [21]. Nevertheless, these cells can lead to tumor like teratoma formation, and acquire genetic and epigenetic modifications [22]. In addition, both autologous and allogenic IPS's and derivatives can lead to immune rejection [23,24]. Gao et al. [25] reported that both embryonic stem cells and IPS's can form tumors in mouse brains and lead to immune cell infiltration, while adult stem cells (mesenchymal and neural stem cells) presented no evidence of tumor formation and immune rejection.

Adult stem cells (ASCs) can be hematopoietic (HSCs), neural (NSCs) or mesenchymal (MSCs), and are multipotent due to their capacity to differentiate into blood and immune system cell types (HSCs), astrocytes, neurons and oligodendrocytes (NSCs), osteoblasts, chondrocytes, myocytes and adipocytes (MSCs), respectively [18,26]. HSCs can be found in

bone marrow, mobilized peripheral blood, and umbilical cord blood (in limited cell number), but their transplantation requires human leukocyte antigen (HLA) matching between the donor and the patient with the lack of compatible donors there is a current limitation for their clinical application [27]. NSCs can be obtained from developing and adult central nervous system tissue (e.g. brain and spinal cord), but insufficient cell quantities and heterogeneity of *in vitro* culture of NSCs are the main drawbacks for their use in tissue regeneration [28].

On the other hand, MSCs do not present tumor formation after transplantation [29] and can be obtained from several human organs and tissue – brain [30], pancreas [31], liver [32], lung [33], skin [34], placenta [35], bone marrow [36], umbilical cord blood [37], adipose tissue [38], gingival connective tissue [39], periodontal ligament [40], dental pulp and follicle [41]. Due to the non-invasive nature of dental MSCs sources and the capacity of differentiation into osteogenic, adipogenic and neurogenic cell lineages, dental MSC's can be a potential and promising alternative cell source for tissue engineering research [42].

Human MSCs are characterized by adherence to plastic, *in vitro* differentiation in to osteoblasts, adipocytes, chondroblasts, and specific surface antigen expression – positive phenotype expression (presented by $\geq$ 95 % of the cell population) of the markers CD105, CD90, CD 271, CD73; negative (not presented by $\leq$ 98 % of the cell population) expression of CD34, CD45, CD14 or CD11b, CD79a or CD19, MHC-II molecules, mainly HLA-DR [43,44]. Human MSCs (hMSCs) present high levels of HLA class I and major histocompatibility complex (MHC) class I, and can suppress the proliferation of T lymphocytes, natural killer (NK), T and B cells by cell contact and secretion of soluble immunomodulatory factors. hMSCs can also induce a more anti-inflammatory or tolerant phenotype by affecting the secretion of T cells and NK cells [45]. Despite these immunomodulatory properties, allogeneic MSCs (so termed when the cells come from another person) can provoke the immune system rejection and present limited persistence *in vivo* [46,47]. Furthermore, the success of the application of MSCs in tissue regeneration might be due to secretion of cytokines, chemokines and growth factors that promote paracrine actions. These paracrine mechanisms are related to the protection of the host tissue cells (by secreting anti-apoptotic and anti-oxidative factors), alteration of the extracellular matrix (e.g. inhibiting collagen synthesis), induction of neovascularization (through secretion of angiogenic factors) and stimulation of tissue regeneration through differentiation and cell fusion with native cells [48]. In addition to the suppression of inflammation, MSCs also play an important role in detection and elimination of pathogens during the initial phase of

inflammatory response [49,50]. For these reasons, the use of MSCs is one of the main alternatives in tissue engineering and regenerative medicine.

2.3 Main biologic processes involved in tissue development

In the process of tissue development, there are several phenomena that interrelate and govern cell behavior and response in three-dimensional matrixes. Thus, the main phenomena involved in tissue development and how they relate to the different variables affecting cellular response are discussed bellow.

2.3.1. Cell proliferation

Adherent cells in culture stop or reduce their proliferation when they reach confluence, which occurs at a characteristic population density and as the cells completely cover the surface on which they are being cultivated [51]. The mechanisms involved are the result of a combination of cell-cell contact, local or global deficiency of nutrients (e.g. glucose, oxygen) or growth factors, and production/accumulation of growth inhibitors (e.g. lactate, ammonia) [52]. According to Gray et al. [53], cell–cell contact stimulates RhoA signaling, which increases the formation of actin stress fibers and, as a result, enhances cell proliferation until it reaches a cell density in which the degree of cell contact with the surface is reduced, down-regulating proliferation.

The basal medium composition and the serum amount and type used in cell cultures affects the cell density, it being required that the medium provides the appropriate amount of nutrients and growth factors and is free of toxins and growth inhibitors. Mammalian cell growth is usually enhanced using a culture medium containing fetal bovine serum (FBS). FBS is added to the basal medium because it contains amino acids, fatty acids, lipids, hormones, vitamins, transport and adhesion proteins, and growth factors that stimulate cell adhesion and proliferation [54]. Despite the fact that its composition is not totally defined and presents lot-to-lot variability, FBS is the most used supplement in cell culture since it is easily obtained and is more economic than defined commercial culture media.

While cell proliferation can be inhibit by irradiation or mitomycin [55], growth factors and mitogens, such as hepatocyte growth factor (HGF) [56], epidermal growth factor (EGF) [57] and erythropoietin (EPO) [58], can be used to enhance MSCs proliferation. However, many growth factors concurrently affect other processes (e.g. cell migration, differentiation,

and survival): insulin-like growth factor-1 (IGF-1) and platelet-derived growth factor (PDGF) can stimulate cell migration [59,60]; fibroblast growth factor (FGF) can promote vasculogenesis [61], reduce cell death [62] and increase chondrogenic differentiation potential [63]; and nerve growth factor (NGF) can promote angiogenesis [64]. In addition, mammalian cell growth is also affected by physiological parameters such as pH (ideal range from 7.2 to 7.4), temperature (optimal at 37 °C) and osmolality (ideal range from 260 to 320 mOsm /kg) [52].

2.3.2. Extracellular matrix synthesis

Every tissue is composed of a cellular and an extracellular component, the latter being termed extracellular matrix (ECM). The ECM of a tissue is usually formed by different types of collagen, laminin, fibronectin, hyaluronic acid, proteoglycans and growth factors [65]. In scaffolds, adherent cells can secrete proteins that bind the material surface and form a layer of ECM [66]. While ECM molecules are mainly secreted by fibroblasts in several connective tissues, they can be produced by chondroblasts and osteoblasts in specialized connective tissues such as bone and cartilage [67]. However, endothelial [68–70], epithelial [68] and muscle [71,72] cells are also known to synthesize ECM, mostly through collagen, adhesion proteins (such as fibronectin) and/or glycosaminoglycans secretion and incorporation into an organized matrix. Furthermore, MSCs have shown their ability to synthesize EMC as well [73].

Growth factors, such as transforming growth factor β (TGF-β) [74–76], connective tissue growth factor (CTGF) [77,78] and hepatocyte growth factor (HGF) [79], can act as regulators of ECM synthesis for several cell types (e.g. chondrocytes, fibroblasts, endothelial and epithelial cells). While HGF can reduce collagen production and increase hyaluronic acid secretion of fibroblasts [79], TGF-β can increase collagen synthesis of fibroblasts [76] and epithelial cells [74], and stimulate proteoglycan synthesis by endothelial cells [69]. In addition, TGF-β have also been shown to increase fibroblasts collagen and fibronectin production under hypoxic conditions [75]. Moreover, CTGF can mediate the stimulation of ECM synthesis by TGF-β [78] and have been shown to enhance fibroblasts collagen secretion by itself [77].

ECM synthesis can also be stimulated by mechanical forces [80] and in dynamic culture systems (through shear stress) [81,82]. Besides this, other factors such as nutrient concentration and scaffold pore size can affect ECM deposition in a synthetic matrix. For

instance, cultures with high glucose concentrations [70,83] and low oxygen tensions [84,85] can increase ECM production from several cell types. On the other hand, the combination of hypoxic conditions with low glucose concentrations enhanced glycosaminoglycans and collagen production by bone marrow MSCs [86]. In addition, scaffolds with large pore sizes reduce cell growth and collagen synthesis, probably due to cell-cell interaction stimulation and growth inhibition by contact [87].

2.3.3. Cell adhesion

In the case of adherent cells, cell adhesion to a surface is critical for cell viability and growth because it precedes cell spreading and migration [88]. In addition, this process has an important role in cell organization in three-dimensional cell complexes and in the physiologic function of tissues and organs. Cells can adhere to one another and to the scaffold through surface receptors and extracellular matrix (ECM) proteins adhered on the biomaterial surface (Figure 2.2), respectively [89].

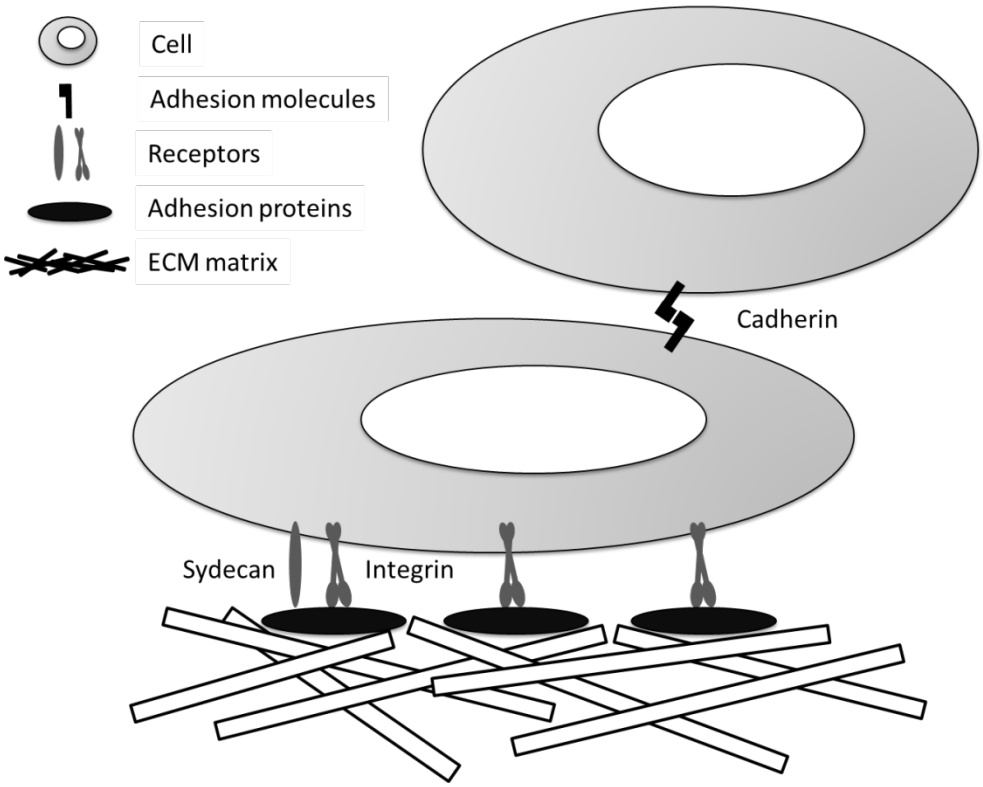

Figure 2.2: Cell-cell and cell-matrix adhesion

Cells can interact with each other using adhesion molecules (e.g. cadherins) to create a selective permeability wall and control substances transport to enhance the mechanical

resistance of the tissue or to communicate chemically [89]. These junctions can be dismantled in cell growth to allow cell movement, and in cell apoptosis to avoid damage to neighbor cells. In addition, the loss of adhesion can lead some adherent cells to a specific type of programmed death [90].

The adhesion of a cell to a biomaterial can be affected by several factors, such as roughness, hydrophobicity/hydrophilicity, electrical charges, stiffness and chemical composition of the biomaterial [91–93]. Synthetic scaffolds usually lack biological cues, but they are coated by a protein layer (which includes adhesion proteins) *in vivo* and *in vitro* when purified proteins or serum are added to the culture medium [94]. The shape and movement of the cells and the organization of the cytoskeleton are influenced by the interaction of ligands present on adhesion proteins (fibronectin, collagen, laminin, vitronectin) with adhesion receptors (integrins, syndecans) present in the cell membrane [91,95].

Integrins are the major cell adhesion receptor, whereas syndecans collaborate with integrins to regulate the formation of focal adhesions [96,97]. While integrins can present high specificity concerning their ligands, a single protein can have several ligand binding sites and bind with various integrins. Human MSC's can bind to collagens, laminins, fibronectin and vitronectin through the corresponding integrins $\alpha_1\beta_1/\alpha_2\beta_1$, $\alpha_3\beta_1/\alpha_7\beta_1$, $\alpha_4\beta_1/\alpha_5\beta_1$, and $\alpha_V\beta_3/\alpha_V\beta_5$, respectively [94].

2.3.4. Cell migration

The cell migration process is initiated with the polymerization of actin filaments and consequent polarization and extension of cell membrane protrusions towards a cue (Figure 2.3a). These protrusions are stabilized by adhesion through the interaction of the actin cytoskeleton with the ECM proteins (Figure 2.3b). Actomyosin contraction (Figure 2.3c) provokes traction forces on the ECM surface and the disassembly of adhesions at the rear of the cells (Figure 2.3d), inducing actin cytoskeletal reorganization and cell movement [95].

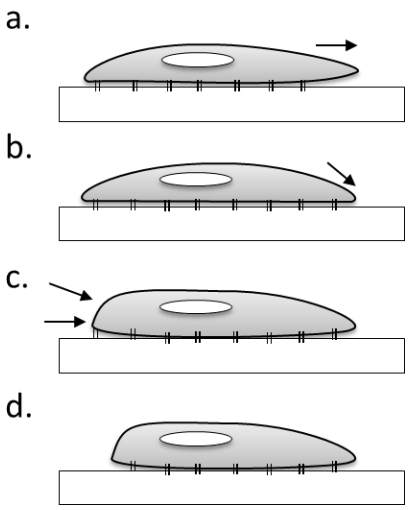

Figure 2.3: Cell migration steps: cell protrusion (a), formation of new adhesion (b), cell contraction (c) and loss of adhesion at the rear (d)

MSC migration can be induced by physical cues – ECM topography, stiffness, roughness and hydrophobicity – and chemical cues – ECM ligands, adherent molecules and chemoattractant gradients, which interact with cell membrane receptors to modulate cell mobility [95,98]. Shear stress produced by fluid flow in a parallel flow chamber system can also induce cell migration through the upregulation of stromal-derived factor-1 (SDF-1) secretion, which stimulate the CXC chemokine receptor 4 (CXCR4) expression in hMSCs [99].

Proteins Rac (ras-related C3 botulinum toxin substrate), Rho (ras homolog family), CDC42 (cell division control protein 42), and tyrosine phosphorylation are involved in signal transduction events that modulate actin polymerization and myosin generated tension [95]. On the other hand, bone morphogenetic proteins (BMPs) are able to increase cell migration and promote the rearrangement of the actin filaments through the activation of the CDC42 and α-isoform of the phosphoinositide 3-kinase (PI3Kα) [100]. Furthermore, other growth factors can induce MSC migration, such as hepatocyte growth factor (HGF) [101] and insulin-like growth factor-1 (IGF-1) [59].

Other molecules such as chemokines and glycoproteins have been used to promote cell migration. Stromal-derived factor-1 (SDF-1), a chemokine protein that binds CXCR4, can induce MSC migration [102] and have been shown to promote bone formation in PCL/gelatin electrospun scaffolds implanted in rat cranial defects [103]. By the regulation of the CXCR4/SDF-1 axis, the interleukin-3 (IL-3) has shown to enhance human bone marrow-

derived mesenchymal stem cells migration [104]. The cytokine tumor necrosis factor alpha (TNF-α) stimulates dental pulp stem cell migration by upregulating the integrin alpha-6 [105].

Fibronectin is a glycoprotein of the ECM that binds to cell membrane receptors (integrins) and has been shown to enhance MSC migration in fibronectin-coated surfaces. MSC adhesion to fibronectin depends on α5β1-integrin binding, which activates platelet derived growth factor receptor (PDGFR-β), and as a result, promotes phosphorylation of phosphoinositide 3-kinase (PI3K) and Akt, actin reorganization and cell migration [106].

Oxygen concentration gradients can induce cell migration towards more oxygenated sites, presenting higher cell growth rate and viability in these regions [107]. Similarly, due to enhanced actin–integrin adhesion complex formation in acidic regions, pH gradients can induce cell migration toward acid [108]. Furthermore, matrix pore diameter, adhesivity and elasticity can also have an influence in cell migration in three-dimensional scaffolds [109]. However, in environments with no gradients of mechanical, physical and/or chemical cues to promote the cell movement in one specific direction, cell migration is usually random [110].

2.3.5. Cell differentiation

In order to differentiate, stem cells undergo an asymmetric cell division, which results in one identical cell to the mother cell and another cell that differentiates into a specialized cell [111]. Cell differentiation is genetically regulated and stimulated by specific transcription factors, such as Runx2 (Runt-related transcription factor 2) [112], Sox9 (Sex-determining region of Y chromosome-related high-mobility-group box 9) [113] and PPARγ (Peroxisome proliferator-activated receptor gamma) [114] for osteoblastic, chondrogenic and adipogenic differentiation, respectively.

Conditioned medium can be used to induce cell differentiation *in vitro* due to the presence of secreted factors that can affect cell fate. Conditioned medium obtained from a culture of chondrocytes has been shown to promote chondrogenic differentiation of human bone marrow-derived mesenchymal stem cells [115]. Notochordal cell conditioned medium can also induce human mesenchymal stem cell from bone marrow toward a chondrogenic phenotype, but the presence of specific soluble factors result in cells with similar characteristics to nucleus pulposus cells [116]. Other conditioned medium such as the one obtained with retinal pigment epithelium cells, can stimulate the differentiation of mesenchymal stem cells toward cells with the phenotype of the cells used to produce the conditioned medium [117]. Recently, a conditioned medium from Sertoli cells has shown to

differentiate Wharton's jelly mesenchymal stem cells to germ-like cells when combined with a appropriated dosage of retinoic acid [118].

Cytoskeletal organization determines cell shape and has been shown to play an important role in cell differentiation [119,120]. Inhibition of cytoskeletal tension can reduce MSCs spreading, maintaining the cells in a round shape (Figure 2.4a) and thus favoring adipogenic and chondrogenic differentiation [119,121]. On the other hand, differentiation toward osteogenic lineages is favored when the cells present a spread and elongated shape (Figure 2.4b), being dependent on cytoskeletal tension and actomyosin contraction to form thick stress fibers [119,120].

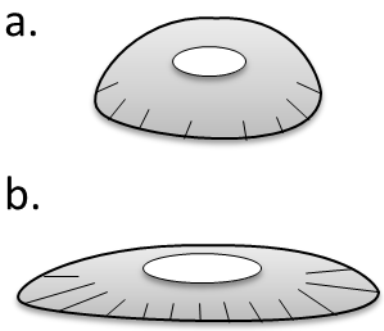

Figure 2.4: Cell shape types: round (a) and elongated (b)

Because interactions between ECM and the cell surface can affect cell shape and organization, scaffolds can be designed to transmit biophysical signals – topography [122], stiffness [123] and roughness [124] – and induce cell differentiation into a specific cell type. Furthermore, cell-cell contact [125] and the application of mechanical forces as shear, strain, compression and culture medium flow can also regulate and enhance cell differentiation [126,127].

For *in vitro* cultures, MSC differentiation can be induced by the addition of appropriate growth factors in the culture medium, such as bone morphogenetic proteins (BMP), transforming growth factor beta (TGFβ) and fibroblast growth factor (FGF) [63,125,128]. Moreover, the addition of serum to the culture medium can affect the differentiation potential of stem cells due to the presence of growth factors and hormones in their composition [129–131]. In addition, while hypoxic conditions are known to maintain the undifferentiated state of stem cells, the combination of low oxygen concentrations with other factors can induce cell differentiation towards specific lineages [131,132].

2.3.6. Cell death

Cell death can play an important role in developing and adult tissues, whether in cell number regulation, tissue remodeling or in maintaining tissue size and shape [133]. Cells can undergo different death types such as apoptosis, autophagy and necrosis, each with a particularity such as cellular shrinkage (Figure 2.5b), extensive presence of vesicles (Figure 2.5c), or generalized swelling of membranous organelles (Figure 2.5d), respectively [134].

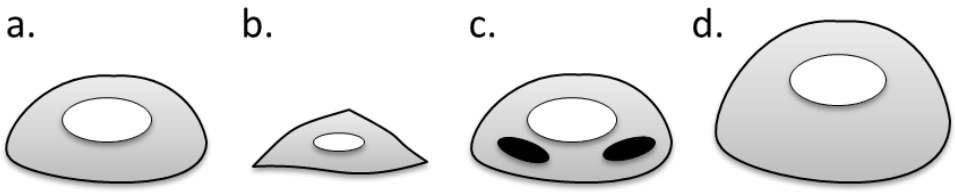

Figure 2.5: Cell morphology characteristics for different cell death types: normal cell (a), apoptotic cell (b), autophagic cell (black ellipses as vesicles) (c), necrotic cell (d)

Apoptosis is the main form of programmed cell death and is responsible for the removal of cells that are no longer necessary or that can be harmful to tissue development [135]. This death type is important because it does not induce inflammatory response and damage to neighbor cells, like other proinflammatory processes such as necrosis, and because it allows for the recycling of organic components of the dead cells through phagocytosis by neighboring cells or macrophages. Apoptosis depends on caspase activation through either an intrinsic or an extrinsic pathway. In intrinsic activation, the mitochondria is damaged and releases proteins such as cytochrome c into the cytosol, whereas in extrinsic activation an extracellular stimuli (involving death ligands such as tumor necrosis factor – TNF – superfamily and TNF-related apoptosis-induced ligands – TRAIL) activates death receptors on the cell surface [133,134,136]. Cytochrome c release is regulated by the inhibition of antiapoptotic proteins – by e.g. B-cell lymphoma 2 (BCL-2) and BCL-xL – and by the induction of proapoptotic proteins – BCL-2 associated protein x (Bax), BCL-2 homologues antagonist/killer (Bak), and BCL-2 homology 3 (BH3) interacting-domain death agonist (Bid) [136].

Several factors such as DNA damage and low concentration of growth factors can activate the intrinsic apoptotic pathway [134]. MSCs can undergo apoptosis when treated with homocysteine [137] or hydrogen peroxide [138] via activation of Jun N-terminal kinase (JNK) signal induced by reactive oxygen species (ROS). Apoptosis can also be promoted by

serum deprivation in MSC culture [139]. Combined serum deprivation and hypoxia (SD/H) has shown to induce MSC apoptosis, mostly due to the lack of growth factors essentials to cell activity and survival [140]. It is also important to observe that MSCs, as adherent cells, can undergo cell death when detached from their substrate or from other cells through an apoptotic response called anoikis [141].

Autophagy is another type of noninflammatory programmed cell death, but with cellular components degradation within the dying cell in autophagic vacuoles [142]. The process of autophagy is regulated by Atg (AuTophaGy-related) genes, and involves the lipidation of light chain 3 protein (LC3) and attachment of the lipidated LC3 (LC3-II) to the autophagosome membrane [134]. This process can enhance MSC survival under SD/H combined conditions by decreasing apoptosis [143]. Hypoxia itself has shown to induce MSC's autophagy and survival via activation of extracellular signal-regulated kinase ½ (ERK½) [144]. In addition, high glucose concentrations can stimulate ROS production, which leads to oxidative stress and activates autophagy, thus inducing MSC senescence [145]. Senescence is a process in which cell growth is irreversibly arrested with no cell death and in the case of MSC, this process can also be activated by heat shock and chemotherapeutic agents [146].

High levels of ROS can damage intracellular molecules and organelles and lead to DNA damage, activating p53, which may result in apoptosis, and poly (ADP-ribose) polymerase (PARP), which may cause necrosis by inhibiting glucose catabolism [147]. Necrosis is an important process in tissues with sustained damage or invasion because it allows for a defensive or reparative cellular response and it is characterized by swelling of the organelle, rupture and leakage of the plasma membrane and loss of adenosine triphosphate (ATP) production [147,148]. This proinflammatory process occurs through the caspase-independent loss of mitochondrial function promoted by the opening of the mitochondrial permeability transition pore (MPTP), which can be mediated by cyclophilin D (CypD), Bax and Bak [148].

Necrosis can be triggered by increased ROS generation, intracellular calcium increase, activation of calpains and cathepsins, and/or lack of co-factors required for ATP production [147]. In addition, extreme physical, chemical and/or mechanical stress factors by, for example irradiation, heat, osmotic shock, freezing, thawing, high levels of hydrogen peroxide, hypoxia, restricted nutrients supply, cytokines, pathogens and toxin exposure have been shown to promote cell necrosis [134].

2.3.7. Vascularization

The main challenges of tissue engineering are related to mass transport limitations, for both *in vitro* development and *in vivo* graft integration. In natural tissue formation, transport limitations are surpassed by new blood vessel formation (vasculogenesis), which occurs mainly in embryonic development, and by the expansion of the existing vascular network (angiogenesis). While the mass transport from the vessels to the capillary network occurs by perfusion, the transfer from the capillaries to the tissue occurs by diffusion [149].

Vascularization has an important role in nutrient and gases exchange, metabolic processes and removal of the residues of cell activity [150]. *In vitro* developed tissues need to allow nutrients to be transported *in vivo*, vascularization being a process of extreme importance for the graft integration and function. To enhance mass transfer inside the tissue, vascularity can be introduced by scaffold functionalization with angiogenic growth factors [151,152], or by the co-culture of endothelial and mesenchymal stem cells to stimulate the secretion of angiogenic factors [153,154].

In vitro capillary formation in MSC culture can be induced by several angiogenic factors, such as the vascular endothelial growth factor (VEGF) [153], nerve growth factor (NGF) [64], angiopoietin proteins (Ang) [155], erytropoietin (EPO) [156], basic fibroblast growth factor (bFGF) [61] and hepatocyte growth factor (HGF) [157]. These factors bind usually to cell receptors with tyrosine kinase activity, stimulating signaling pathways that regulate the activity of endothelial cells present in the existing vessels [64,158–161]. In addition, hypoxic or low oxygen concentration conditions enhance the cells production of angiogenic growth factors as VEGF [132,162], what can be related to the increased expression of hypoxia inducible factor (HIF)-1α under these conditions [163].

2.4 Modeling for tissue engineering

The biomechanical and biochemical environmental control of cell growth in scaffolds requires the knowledge of the complex interactions between the phenomena that rule tissue development process *in vitro*. However, these phenomena, described in the previous section, are extremely complex and so are the interactions between them. Additionally, some related parameters are difficult to obtain experimentally due to limitations of the available techniques, which constitute a serious drawback for model selection and validation of computational results. Consequently, at the current state of the art, the development of a complete model for

tissue growth in scaffolds is not yet possible. On the other hand, simplified models can be applied to capture specific features of the system behavior, despite the fact that it cannot represent all the events that occur experimentally [164]. For this reason, different modeling options and computational simulation techniques have been employed in tissue engineering to predict tissue development, reducing experimental costs and suggesting new investigation pathways [165,166].

2.4.1. Biological processes analysis

One the aspects to be considered in the modeling of tissue growth in scaffolds is the development of models for the analysis of the several biological processes involved, such as cell growth [167,168], ECM synthesis [169–172], cell adhesion and migration [173–176], cell differentiation [177,178], cell death [179–181], and angiogenesis [182,183].

2.4.1.1. Cell proliferation

Cell growth has been widely described through simplified models based on cell contact inhibition and nutrient availability. Mancuso et al. [168] studied the proliferation of MSC in monolayer cultures and compared a phenomenological logistic approach and a one-dimensional (1D) population balance model, based on contact inhibition at confluence. It was found that the population balance model could predict the experimental data better than the phenomenological logistic model. Galban and Locke [167] compared the Moser and the modified Contois models and an nth-order heterogeneous model of growth kinetics in the prediction of cell growth in porous structures. However, experimental data indicated that cell growth could not be described appropriately by any of the studied models, mainly due to the assumption of the non-variation of parameters in time and space. In 3D environments, nutrient transport can affect its distribution inside the matrices, being cell growth regulated by nutrient availability [184].

2.4.1.2. Extracellular matrix synthesis

ECM secretion is an important process in tissue development and its interaction with cell growth and mass transport has been investigated using mathematical models. The study of Saha and Mazumdar [169] proposed a mathematical model of cell growth and ECM synthesis which includes the ECM stimulation of cell growth and a negative feedback control mechanism for ECM formation (decay of the deposition of ECM components with increased

ECM synthesis). The model could predict that the ECM deposition presents an initial increasing concentration until reaching a maximum (overshoot) and subsequent with further slight decay to a final constant concentration of ECM. Recently, Lewis et al. [172] developed a mathematical model for the proteoglycans production as a function of the nutrient concentration, considering the mass transport of nutrients and proteoglycans inside a pellet of cells. The production of proteoglycans and the consumption of nutrients were described by the Michaelis-Menten kinectics, but cell proliferation and death were not considered. The results indicated that the heterogeneity of the ECM production could be associated to the nutrient gradient inside the pellet. Causin et al. [170] modeled the glycosaminoglycans (GAG) synthesis as a function of cell density and nutrient concentration and considered an inhibition term based on the saturation level of GAG. The amount of biomass inside the pore of a scaffold was considered to be dependent on the GAG content. The calculated biomass thickness was used to predict parameters such as porosity, effective permeability and diffusivity for a model of mass transfer to evaluate the oxygen delivery inside a direct perfusion bioreactor. These different models involving ECM synthesis could be used to predict ECM synthesis in different systems regarding cell type, matrix properties and culture type (static or dymanic).

2.4.1.3. Cell adhesion and migration

Because cell adhesion is important for the process of cell migration, cell-cell and cell-matrix adhesion models are usually included in migration models. Rey and García-Aznar [175] proposed a model of bi-dimensional (2D) cell migration considering the force that one cell exerts on another cell (cell-cell interaction), the force that the substrate exerts on the cell in opposition to its movement (drag), and the reaction of the propulsion force that one cell actively exerts on the substrate. Cell-cell interaction was modeled as a function of the distance between two cells because cell behavior can be regulated by mechanic-chemical signals. Cell propulsion was described as a combination of force magnitude, dependent on ECM stiffness, with the direction given by the polarization vector, defined in the beginning of the simulation as random or in a specific pattern of interest. This model could be used to understand 2D collective cell migration in monolayer cell cultures or in wound healing studies.

According to Zaman et al. [176], other mechanisms can affect cell migration other than matrix stiffness, such as the asymmetry of the cell, adhesive capacity of the matrix, and numbers of available ECM ligands and cell surface receptors. The authors described 3D cell

migration as the result of traction, drag and protrusion forces. The first was modeled as a two component force (traction in the forward and backward direction) dependent on the ligand-receptor complex. The force of this complex was described as a function of the matrix elastic modulus (stiffness), whereas the number of available receptors, the concentration of ligands, and binding strength between receptors and ligands was accounted for by an adhesion parameter. The drag force was proportional to the cell speed and the protrusion force was considered to have constant magnitude and random direction. The model could predict that the maximum migration speed is achieved at intermediate values of adhesiveness, and at high values of ECM stiffness and cell asymmetry.

Frascoli et al. [173] also considered the influence of the drag and traction forces on cell migration. Similarly to Zaman et al. [176], they described the traction force as a function of the force per ligand-receptor complex and of the number of interacting cell-matrix sites, and the drag force, of the cell speed. A distance dependent cell-cell interaction was accounted for in a similar way as in the work of Rey and García-Aznar [175], but the attraction and the repulsion forces were considered separately, and an overlapping term was included in the attraction model. The model was applied to study the behavior of two cells under several conditions, emphasizing the role of the force magnitude and number of sites of cell-cell and cell-matrix binding in determining cell aggregation and break-up events.

Another important type of migration is chemotaxis, which is regulated by chemical gradients and has been modeled by Painter [174]. The author used a continuous macroscopic partial differential equation model to describe cell migration of a two-population system. The continuous model was derived based on the populations' chemotatic efficiency and random motility in crowded and uncrowded regions. The model was capable of predicting cell migration into the ECM free space and into the occupied regions through displacement of other cells as a response to signal gradients.

Figure 2.6 presents all the main factors considered in the migration and adhesion models discussed above.

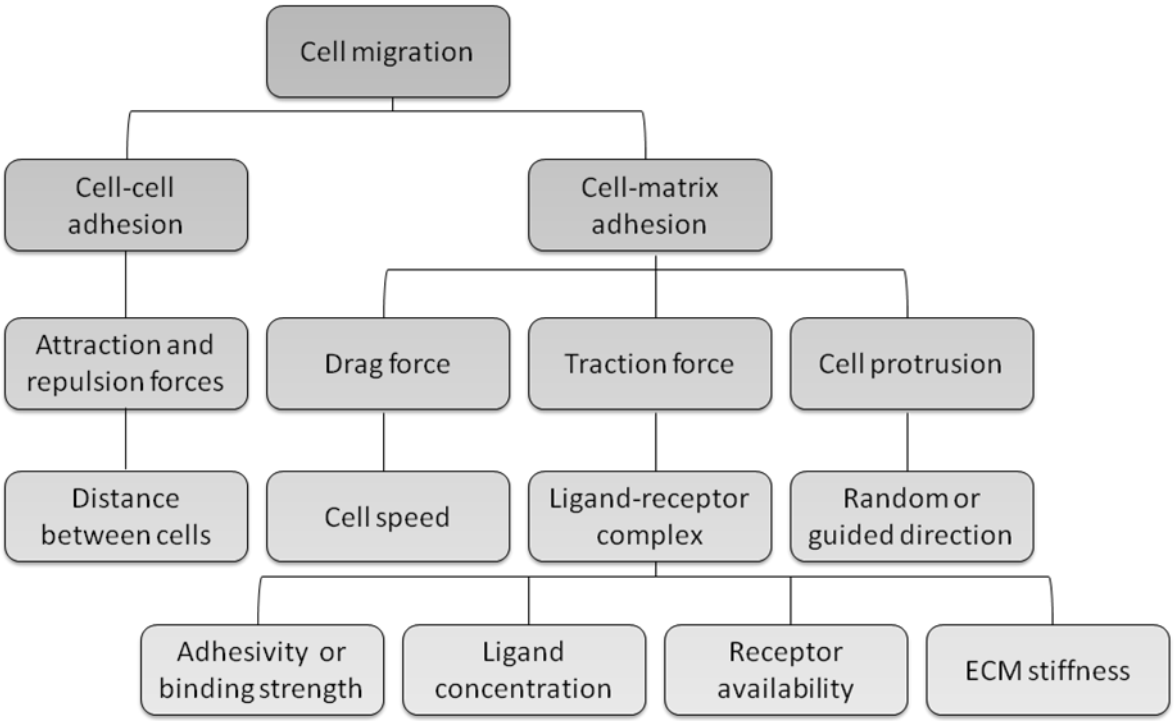

Figure 2.6: Hierarchic diagram of factors considered in mathematical models of cell adhesion and migration

2.4.1.4. Cell differentiation

The differentiation mechanism can be used to model tissue development *in vitro*. Lemon et al. [177] formulated a model based on the relation between human MSC growth, differentiation and ECM synthesis inside porous scaffolds. The model was solved analytically and could predict ECM stimulation of cell proliferation and down-regulation of cell differentiation as observed in experimental data under hypoxia (with lower secretion of ECM). The increased cell differentiation under normoxia, characterized by higher secretion of ECM was also captured by the model. In order to reduce the model complexity, cell division and differentiation were treated as independent processes and it was assumed that all cells divide and differentiate at the same rate. This model could be used in cases where it is important to predict the number of undifferentiated cells and where cell activity is mainly regulated by or could be associated with ECM synthesis.

MSC differentiation has also been modeled as a function of strain magnitudes and fluid velocities. Stops et al. [178] used a CFD model of cell proliferation and differentiation to describe cell response in scaffolds subjected to mechanical strain and flow perfusion. The combination of different strains and inlet velocities was studied, suggesting operational

regions that could favor the expression of a specific cell phenotype for cell culture in perfusion bioreactors with mechanical loading.

2.4.1.5. Cell death

Regarding cell death, Broome and Coleman [179] studied the process of apoptosis in multiple sclerosis using the biochemical systems theory, a method that generates mathematical models with mechanisms and initial values from the literature. The model was based on inflammatory response activation (T-cells and macrophages activation) and calcium accumulation, which stimulates the production of reactive oxygen and nitrogen species and the release of caspases, and on death complex formation, which opens the permeability transition pore (PTP), releasing apoptotic factors into the cytoplasm and activating the caspase cascade. The model was used to study disease and treatment scenarios, and showed that by manipulating the levels of T-cells cytokines production and the opening/closing of the PTP, the cell death could be avoided by the regulation of reactive oxygen and nitrogen species formation, DNA/RN, mtDNA amd/or protein damage, lipid peroxidation, caspase activation and apoptotic factors release.

Jin and Lei [180] proposed a starvation induced autophagy model considering the logistic growth kinetics and nutrient transport. At low nutrient levels, normal cells were considered to enter the autophagy phase, where each autophagic cell generates monomeric units that serve as nutrients for the normal cells. The model predicted that cell autophagy could regulate and maintain the cell number in cultures with extremely low nutrient conditions by secretion of nutrients and inhibition of cell death. The model can be used to determine appropriate levels of autophagy and avoid the decrease of cell numbers as a result of excessive cell death.

Tavassoly et al. [181] developed a model of the interaction of autophagic and apoptotic processes in mammalian cells. The model was based on mechanisms that regulate the expression of BCL-2 proteins and the calcium signaling in the endoplasmatic reticulum and mitochondria to account for the crosstalk between the two types of cell death. Besides the direct induction of apoptosis by the upregulation of proapoptotic proteins, cytoplasmatic calcium ions were considered to inhibit mTOR and lead to the cleavage of autophagic proteins, mechanisms that downregulate the autophagosome formation. The expression of BCL-2 proteins in the endoplasmatic reticulum and the activation of caspases were considered to inhibit and cleave Beclin-1, respectively, a protein required for autophagosome formation. On the other hand, BLC-2 in the endoplasmatic reticulum inhibited the inositol-1,4,5-

trisphosphate receptor (IP3R) release of calcium ions. The model could predict the cell response to a cytotoxic drug exposure, and could be used to optimize therapeutic protocols and to predict the balance between cell death and survival in clinically relevant scenarios.

2.4.1.6. Vascularization

Recently, Bookholt et al. [183] simulated early stages of angiogenesis by modeling endothelial cell motility due to chemotaxis and durotaxis (migration directed by the matrix stiffness gradient). The model was composed of reaction-diffusion equations for several proteins that regulate the basement membrane, the fibrin matrix and cell migration. Lemon et al. [182] proposed a model of the vascularization of a porous scaffold seeded with stem cells, considering the infiltration of macrophages, fibroblasts and pericytes from the vascular tissue after implantation *in vivo*. Stem cell division and death was modeled as a function of oxygen concentration; cell proliferation was dependent on the availability of free space inside the scaffold. Macrophages were treated as infiltrating cells with no proliferation inside the scaffold, the death of which occurs in the absence of oxygen. Fibroblasts infiltration was considered to be stimulated by the presence of macrophages due to the production of the chemoattractant PDGF-BB, while their division and death were a function of oxygen concentration. Immature capillary formation and apoptosis were modeled, taking into consideration the endothelial cells infiltration, angiogenic growth factor concentration, ECM volume fraction, and pericytes association and disassociation with the vessel wall (related to vessel maturation). Pericytes death was modeled as the other cells, but their infiltration and proliferation were dependent on the immature capillary volume fraction due to their secretion of PDGF-B. The ECM secretion was a function of oxygen concentration, and also, as with the ECM degradation, of the volume fraction of stem cells, fibroblasts and pericytes. With this model it was shown that the scaffold could be prevascularized by seeding both stem cells and vascular cells to avoid cell loss due to slow *in vivo* infiltration.

2.4.2. Mass transport analysis

Modeling of mass transport inside porous scaffolds and its interaction with cell growth constitutes another important subject in the understanding and control of cell growth in scaffolds. Nutrient availability inside three-dimensional scaffolds affects cell activity directly (migration, proliferation, death and ECM synthesis) and indirectly (differentiation and angiogenesis), and its interaction with biological processes is summarized in Figure 2.7.

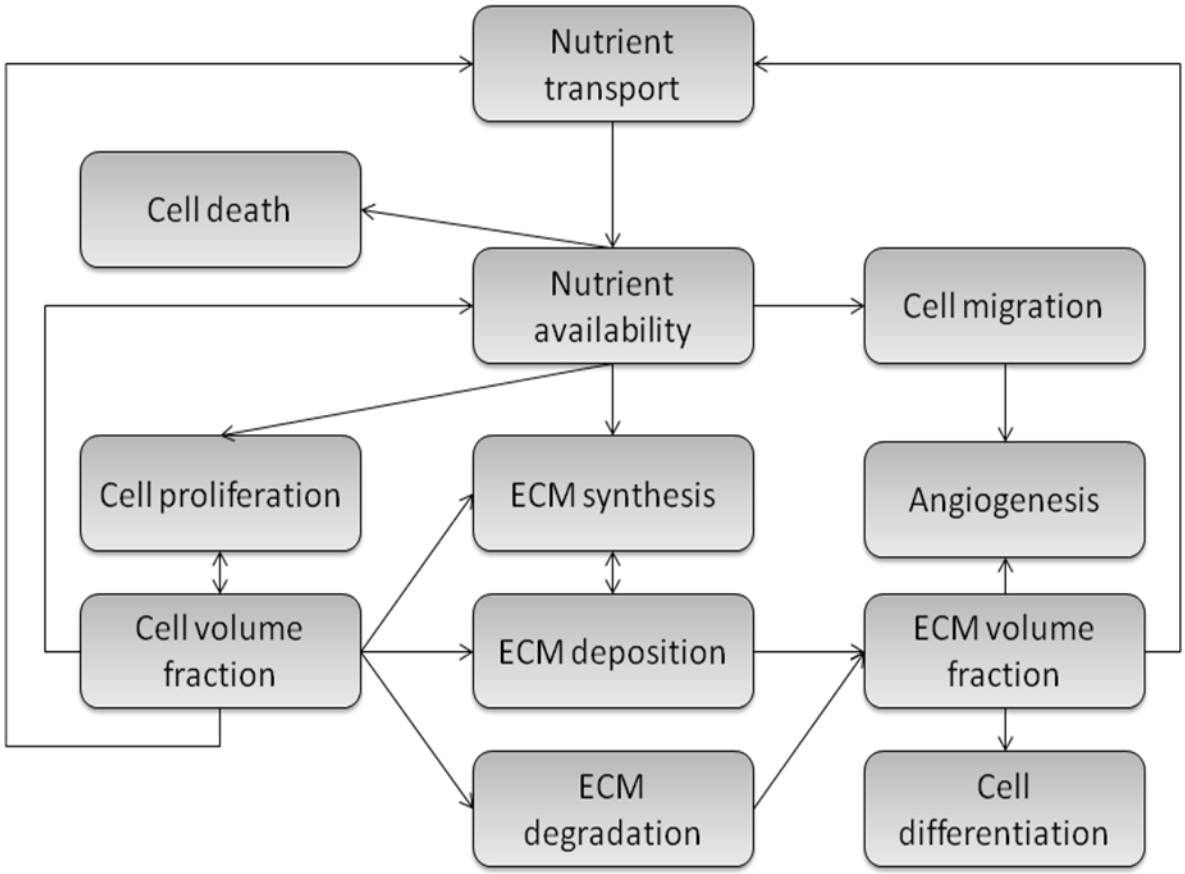

Figure 2.7: Scheme of the interconnections between different biological processes and nutrient availability that have been transcribed in mathematical modeling

Many studies consider oxygen as the cell growth limiting nutrient due to its low solubility in polymeric porous matrixes [185–189]. According to Freed et al. [190], oxygen diffusion in 3D cultures can be insufficient to allow relevant cell growth inside the scaffold. Thus, modeling of oxygen transport can help the study of alternatives to ensure an appropriate oxygen supply in thick scaffolds. On the other hand, Lin, Lin and Chung [191] performed a computational study of glucose and oxygen transport in cartilage scaffolds and observed that glucose was the nutrient responsible for low cell density inside thick scaffolds in static cultures. Glucose acts as a direct source of carbon and is a nutrient required for energy production and cell proliferation in mammalian cells [192]. Consequently, many studies include glucose transport in cell proliferation kinetic [193–204].

In order to produce energy through a glycolytic metabolism, cells degrade glucose into pyruvate, which is further converted in lactate, and this process can occur with parallel consumption of oxygen (aerobic glycolysis) or not (anaerobic glycolysis). Because lactate production provokes the acidification of the culture medium and can be harmful to the cells

[205], several studies consider the lactate production effect on cell growth model [199,201,204].

Nutrient transport modeling in scaffolds usually considers the consumption rate of differentiated cells such as chondrocytes [185,187,191,204,206], cardiomyocytes [207], hepatocytes [208], and osteoblasts [189]. In addition, most modeling studies of cell growth and nutrient transport employ kinetic parameters from literature for differentiated cells – chondrocytes [170,194,196,209–211], fibroblasts [212] and immortalized cells [213] – or for a generic cell type [214].

Human mesenchymal stem cell growth *in vitro* has been analyzed with a mathematical model based on mass balance of viable cells, glucose, lactate, glutamine and glutamate [199]. However, since the cells were cultivated statically in monolayers and not in scaffolds, the model considered average reaction and degradation rates. Another model was used to simulate the shear stress, hematopoietic cells growth and glucose and oxygen transport inside the scaffolds in a perfusion rotating wall bioreactor [200]. In this case, several cell types were considered in proliferation kinetics but no validation with experimental data was presented.

In order to predict oxygen distribution in regular scaffolds seeded with embryonic stem cells in a perfusion bioreactor, a one-dimensional model can be used [189]. However, model validation with experimental data is not always presented. Mesenchymal stem cells growth and nutrient distribution in 3D scaffolds were modeled and validated in a perfusion bioreactor for cell differentiation to obtain bone grafts [186,193]. However, nutrient consumption rates were based on chondrocyte data [186] or on average values [193], without the consideration of the spatial influence of nutrient concentration on metabolic kinetics. Because of the gradient formation in 3D scaffolds, the availability and distribution of nutrients affect cell metabolism. Thus, it is more appropriate to use a kinetic model of nutrient consumption that includes the effect of spatial nutrient concentration [184].

2.5 Conclusions

The main biological processes in tissue development are related to cell behavior (proliferation, adhesion, migration, differentiation and death) and to the interaction of cells with the scaffold for tissue remodeling (vascularization, ECM synthesis). Although significant progress has been achieved in the last decades regarding the understanding and modeling of each of these processes separately, the development of a complete model for tissue growth in scaffolds still constitutes a major scientific challenge. One of the main challenges of tissue

engineering is to optimize mass transport inside the scaffolds as this process can regulate and affect several biological phenomena. Some phenomenological models presented in the literature show great potential to be applied to study and/or control the interaction between these different processes. However, more definitive evaluations of the relative potential of these models will always require experimental measurements for the specific cell type of interest, due to the kinetic parameters and behavior variations from one cell type to another. This is especially true to the case of tissue development with stem cells, where the amount and type of experimental data available is still limited. Therefore, future progress in this area will depend strongly on an intimate and interdisciplinary interplay between modeling experts and experimentalists, aiming the development of new measurement techniques and the generation of greater amount of experimental data to be as basis for model selection and validation.

2.6 Acknowledgments

The authors would like to thank CAPES (Coordination for the Improvement of Higher Education Personnel), National Council for Scientific and Technological Development (CNPq), FINEP (Financing Agency for Studies and Projects) and Stem Cell Research Institute for their financial support.

2.7 References

[1] A.D. Theocharis, S.S. Skandalis, C. Gialeli, N.K. Karamanos, Extracellular matrix structure, Adv. Drug Deliv. Rev. 97 (2016) 4–27. doi:10.1016/j.addr.2015.11.001.

[2] E.S. Place, N.D. Evans, M.M. Stevens, Complexity in biomaterials for tissue engineering, Nat. Mater. 8 (2009) 457–470. doi:10.1038/nmat2441.

[3] S.C. Baker, G. Rohman, J. Southgate, N.R. Cameron, The relationship between the mechanical properties and cell behaviour on PLGA and PCL scaffolds for bladder tissue engineering, Biomaterials. 30 (2009) 1321–1328. doi:10.1016/j.biomaterials.2008.11.033.

[4] J.L. Olson, A. Atala, J.J. Yoo, Tissue Engineering: Current Strategies and Future Directions, © Chonnam Med. J. Chonnam Med J. 47 (2011) 1–13. doi:10.4068/cmj.2011.47.1.1.

[5] A. Chatterjea, G. Meijer, C. van Blitterswijk, J. de Boer, Clinical application of human mesenchymal stromal cells for bone tissue engineering., Stem Cells Int. 2010 (2010) 215625. doi:10.4061/2010/215625.

[6] C.J. Koh, A. Atala, Tissue Engineering, Stem Cells, and Cloning: Opportunities for Regenerative Medicine, J. Am. Soc. Nephrol. 15 (2004) 1113–1125. doi:10.1097/01.ASN.0000119683.59068.F0.

[7] L.X. Tay, R.E. Ahmad, H. Dashtdar, K.W. Tay, T. Masjuddin, S. Ab-Rahim, P.P. Chong, L. Selvaratnam, T. Kamarul, Treatment outcomes of alginate-embedded allogenic mesenchymal stem cells versus autologous chondrocytes for the repair of

focal articular cartilage defects in a rabbit model., Am. J. Sports Med. 40 (2012) 83–90. doi:10.1177/0363546511420819.

[8] K.L. Wong, K.B.L. Lee, B.C. Tai, P. Law, E.H. Lee, J.H.P. Hui, Injectable cultured bone marrow-derived mesenchymal stem cells in varus knees with cartilage defects undergoing high tibial osteotomy: A prospective, randomized controlled clinical trial with 2 years' follow-up, Arthrosc. - J. Arthrosc. Relat. Surg. 29 (2013) 2020–2028. doi:10.1016/j.arthro.2013.09.074.

[9] J. Shao, W. Zhang, T. Yang, Using mesenchymal stem cells as a therapy for bone regeneration and repairing, Biol. Res. 48 (2015) 1–7. doi:10.1186/s40659-015-0053-4.

[10] M. a. Haider, J.E. Olander, R.F. Arnold, D.R. Marous, A.J. McLamb, K.C. Thompson, W.R. Woodruff, J.M. Haugh, A phenomenological mixture model for biosynthesis and linking of cartilage extracellular matrix in scaffolds seeded with chondrocytes, Biomech. Model. Mechanobiol. 10 (2011) 915–924. doi:10.1007/s10237-010-0282-y.

[11] X. Meng, P. Leslie, Y. Zhang, J. Dong, Stem cells in a three-dimensional scaffold environment., Springerplus. 3 (2014) 80. doi:10.1186/2193-1801-3-80.

[12] B. Ben Yahia, L. Malphettes, E. Heinzle, Macroscopic modeling of mammalian cell growth and metabolism, Appl. Microbiol. Biotechnol. 99 (2015) 7009–7024. doi:10.1007/s00253-015-6743-6.

[13] S. Jung, J. Kleinheinz, Adult Mesenchymal Stem Cells in Current Tissue Engineering Concepts, in: D. Eberli (Ed.), Cells Biomater. Regen. Med., InTech, 2014. doi:10.5772/59219.

[14] J. Yu, J.A. Thomson, Pluripotent stem cell lines, Genes Dev. 22 (2008) 1987–1997. doi:10.1101/gad.1689808.

[15] K. Turksen, T.-C. Troy, Human Embryonic Stem Cells: Isolation, Maintenance, and Differentiation, in: K. Turksen (Ed.), Hum. Embryonic Stem Cell Protoc., Humana Press, New Jersey, 2011: pp. 1–12. doi:10.1385/1-59745-046-4:1.

[16] P. Andrews, D. Baker, N. Benvinisty, B. Miranda, K. Bruce, O. Brüstle, M. Choi, Y.-M. Choi, J. Crook, P. de Sousa, P. Dvorak, C. Freund, M. Firpo, M. Furue, P. Gokhale, H.-Y. Ha, E. Han, S. Haupt, L. Healy, D. Hei, O. Hovatta, C. Hunt, S.-M. Hwang, M. Inamdar, R. Isasi, M. Jaconi, V. Jekerle, P. Kamthorn, M. Kibbey, I. Knezevic, B. Knowles, S.-K. Koo, Y. Laabi, L. Leopoldo, P. Liu, G. Lomax, J. Loring, T. Ludwig, K. Montgomery, C. Mummery, A. Nagy, Y. Nakamura, N. Nakatsuji, S.-K. Oh, S.-K. Oh, T. Otonkoski, M. Pera, M. Peschanski, P. Pranke, K. Rajala, M. Rao, R. Ruttachuk, B. Reubinoff, L. Ricco, H. Rooke, D. Sipp, G. Stacey, H. Suemori, T. Takahashi, K. Takada, S. Talib, S. Tannenbaum, B.-Z. Yuan, F. Zeng, Q. Zhou, Points to consider in the development of seed stocks of pluripotent stem cells for clinical applications: International Stem Cell Banking Initiative (ISCBI), Regen. Med. 10 (2015) 1–44. doi:10.2217/rme.14.93.

[17] P. Pranke, P. Chagastelles, L.E. Sperling, The Current State of Research with Human Pluripotent Stem Cells in Brazil, Stem Cells Dev. 23 (2014) 20–23. doi:10.1089/scd.2014.0320.

[18] W.M. Botes, M. Nöthling Slabbert, M. Alessandrini, M.S. Pepper, Stem Cell Therapy: Accepted Therapies, Managing the Hope of Society, and a Legal Perspective, in: P. Van Pham (Ed.), Springer International Publishing, Cham, 2016: pp. 1–35. doi:10.1007/978-3-319-40073-0_1.

[19] A.S. Boyd, K.J. Wood, Characteristics of the early immune response following transplantation of mouse ES cell derived insulin-producing cell clusters, PLoS One. 5 (2010). doi:10.1371/journal.pone.0010965.

[20] K. Takahashi, S. Yamanaka, Induction of Pluripotent Stem Cells from Mouse Embryonic and Adult Fibroblast Cultures by Defined Factors, Cell. 126 (2006) 663–

676. doi:10.1016/j.cell.2006.07.024.
[21] K. Takahashi, K. Tanabe, M. Ohnuki, M. Narita, T. Ichisaka, K. Tomoda, S. Yamanaka, Induction of Pluripotent Stem Cells from Adult Human Fibroblasts by Defined Factors, Cell. 131 (2007) 861–872. doi:10.1016/j.cell.2007.11.019.
[22] Y. Jung, G. Bauer, J.A. Nolta, Induced Pluripotent Stem Cell - Derived Mesenchymal Stem Cells: Progress Toward Safe Clinical Products, Stem Cells. 30 (2011) 42–47. http://www.ncbi.nlm.nih.gov/entrez/query.fcgi?cmd=Retrieve&db=PubMed&dopt=Citation&list_uids=21898694.
[23] T. Zhao, Z.-N. Zhang, Z. Rong, Y. Xu, Immunogenicity of induced pluripotent stem cells., Nature. 474 (2011) 212–5. doi:10.1038/nature10135.
[24] G. Itakura, Y. Kobayashi, S. Nishimura, H. Iwai, M. Takano, A. Iwanami, Y. Toyama, H. Okano, M. Nakamura, Controlling immune rejection is a fail-safe system against potential tumorigenicity after human iPSC-derived neural stem cell transplantation, PLoS One. 10 (2015) 1–18. doi:10.1371/journal.pone.0116413.
[25] M. Gao, H. Yao, Q. Dong, H. Zhang, Z. Yang, Y. Yang, J. Zhu, M. Xu, R. Xu, Tumourigenicity and Immunogenicity of Induced Neural Stem Cell Grafts Versus Induced Pluripotent Stem Cell Grafts in Syngeneic Mouse Brain., Sci. Rep. 6 (2016) 29955. doi:10.1038/srep29955.
[26] N. Zech, Adult stem cell manipulation and possible clinical perspectives, J. Reproduktionsmed. Endokrinol. 1 (2004) 91–99. http://www.kup.at/kup/pdf/4425.pdf.
[27] B. Park, K.H. Yoo, C. Kim, Hematopoietic stem cell expansion and generation: the ways to make a breakthrough, Blood Res. 50 (2015) 194. doi:10.5045/br.2015.50.4.194.
[28] L.D. Shoemaker, H.I. Kornblum, Neural Stem Cells (NSCs) and Proteomics., Mol. Cell. Proteomics. 15 (2016) 344–54. doi:10.1074/mcp.O115.052704.
[29] M. Robert, Safety in mesenchymal stem cell transplantation, Biomed. Res. Ther. 1 (2014) 4. doi:10.7603/s40730-014-0004-7.
[30] G. Paul, I. Özen, N.S. Christophersen, T. Reinbothe, J. Bengzon, E. Visse, K. Jansson, K. Dannaeus, C. Henriques-Oliveira, L. Roybon, S. V. Anisimov, E. Renström, M. Svensson, A. Haegerstrand, P. Brundin, The adult human brain harbors multipotent perivascular mesenchymal stem cells, PLoS One. 7 (2012). doi:10.1371/journal.pone.0035577.
[31] Y. Hu, L. Liao, Q. Wang, L. Ma, G. Ma, X. Jiang, R.C. Zhao, Isolation and identification of mesenchymal stem cells from human fetal pancreas, J. Lab. Clin. Med. 141 (2003) 342–349. doi:10.1016/S0022-2143(03)00022-2.
[32] H. El-Kehdy, G. Pourcher, W. Zhang, Z. Hamidouche, S. Goulinet-Mainot, E. Sokal, P. Charbord, M. Najimi, A. Dubart-Kupperschmitt, Hepatocytic Differentiation Potential of Human Fetal Liver Mesenchymal Stem Cells: In Vitro and In Vivo Evaluation, Stem Cells Int. 2016 (2016) 1–12. doi:10.1155/2016/6323486.
[33] A.M. Hoffman, J.A. Paxson, M.R. Mazan, A.M. Davis, S. Tyagi, S. Murthy, E.P. Ingenito, Lung-Derived Mesenchymal Stromal Cell Post-Transplantation Survival, Persistence, Paracrine Expression, and Repair of Elastase-Injured Lung, Stem Cells Dev. 20 (2011) 1779–1792. doi:10.1089/scd.2011.0105.
[34] J.R. Park, E. Kim, J. Yang, H. Lee, S.H. Hong, H.M. Woo, S.M. Park, S. Na, S.R. Yang, Isolation of human dermis derived mesenchymal stem cells using explants culture method: expansion and phenotypical characterization, Cell Tissue Bank. 16 (2015) 209–218. doi:10.1007/s10561-014-9471-8.
[35] N.E. Timmins, M. Kiel, M. Günther, C. Heazlewood, M.R. Doran, G. Brooke, K. Atkinson, Closed system isolation and scalable expansion of human placental mesenchymal stem cells, Biotechnol. Bioeng. 109 (2012) 1817–1826.

doi:10.1002/bit.24425.
[36] S. Huang, L. Xu, Y. Sun, T. Wu, K. Wang, G. Li, An improved protocol for isolation and culture of mesenchymal stem cells from mouse bone marrow, J. Orthop. Transl. 3 (2015) 26–33. doi:10.1016/j.jot.2014.07.005.
[37] W.C. Pereira, I. Khushnooma, M. Madkaikar, K. Ghosh, Reproducible methodology for the isolation of mesenchymal stem cells from human umbilical cord and its potential for cardiomyocyte generation, J. Tissue Eng. Regen. Med. 2 (2008) 394–399. doi:10.1002/term.107.
[38] X.F. Yang, X. He, J. He, L.H. Zhang, X.J. Su, Z.Y. Dong, Y.J. Xu, Y. Li, Y.L. Li, High efficient isolation and systematic identification of human adipose-derived mesenchymal stem cells 1890, J Biomed.Sci. 18 (2011) 59. doi:10.1186/1423-0127-18-59.
[39] S.H. Jin, J.E. Lee, J.-H. Yun, I. Kim, Y. Ko, J.B. Park, Isolation and characterization of human mesenchymal stem cells from gingival connective tissue., J. Periodontal Res. 50 (2015) 461–7. doi:10.1111/jre.12228.
[40] M. Miletic, S. Mojsilovic, I. Okic-Djordjevic, T. Kukolj, A. Jaukovic, J.F. Santibacez, G. Jovcic, D. Bugarski, Mesenchymal stem cells isolated from human periodontal ligament, Arch. Biol. Sci. 66 (2014) 261–271. doi:10.2298/ABS1401261M.
[41] C.C. Brizuela, S.G. Galleguillos, F.A. Carrión, C.P. Cabrera, P.C. Luz, C.S. Inostroza, Aislación y Caracterización de Células Madre Mesenquimales Provenientes de Pulpa y Folículo Dentario Humano, Int. J. Morphol. 31 (2013) 739–746. doi:10.4067/S0717-95022013000200063.
[42] G.T.-J. Huang, S. Gronthos, S. Shi, Mesenchymal Stem Cells Derived from Dental Tissues vs . Those from Other Sources: Their Biology and Role in Regenerative Medicine, J. Dent. Res. 88 (2009) 792–806. doi:10.1177/0022034509340867.
[43] M. Dominici, K. Le Blanc, I. Mueller, I. Slaper-Cortenbach, F. Marini, D. Krause, R. Deans, A. Keating, D. Prockop, E. Horwitz, Minimal criteria for defining multipotent mesenchymal stromal cells. The International Society for Cellular Therapy position statement., Cytotherapy. 8 (2006) 315–7. doi:10.1080/14653240600855905.
[44] D. Jarocha, E. Lukasiewicz, M. Majka, Adventage of Mesenchymal Stem Cells (MSC) expansion directly from purified bone marrow CD105+ and CD271+ cells, Folia Histochem. Cytobiol. 46 (2008) 307–314. doi:10.2478/v10042-008-0046-z.
[45] J. Nehlin, A. Isa, T. Baringto, Immunogenicity and Immune-Modulating Properties of Human Stem Cells, in: A. Gholamrezanezhad (Ed.), Stem Cells Clin. Res., InTech, 2011: pp. 105–144. doi:10.5772/17868.
[46] J.A. Ankrum, J.F. Ong, J.M. Karp, Mesenchymal stem cells: immune evasive, not immune privileged, Nat. Biotechnol. 32 (2014) 252–260. doi:10.1038/nbt.2816.
[47] R.L. Oliveira, P.C. Chagastelles, P. Sesterheim, P. Pranke, In Vivo Immunogenic Response to Allogeneic Mesenchymal Stem Cells and the Role of Preactivated Mesenchymal Stem Cells Cotransplanted with Allogeneic Islets, Stem Cells Int. 2017 (2017) 1–12. doi:10.1155/2017/9824698.
[48] R. Sanz-Ruiz, A. Villa, E. Gutierrez, M.E. Fernandez Santos, P.L. Sanchez Fernandez, F. Fernandez-Aviles, Randomized Clinical Trials in Stem Cell Therapy for the Heart - Old and New Types of Cells for Cardiovascular Repair, in: A. Gholamrezanezhad (Ed.), Stem Cells Clin. Res., InTech, 2011: pp. 259–282. doi:10.5772/22377.
[49] K.A. Al-Anazi, A.M. Al-Jasser, Mesenchymal Stem Cells — Their Antimicrobial Effects and Their Promising Future Role as Novel Therapies of Infectious Complications in High Risk Patients, in: T. Demirer (Ed.), Prog. Stem Cell Transplant., InTech, 2015. doi:10.5772/60640.
[50] P. Semedo, M. Burgos-Silva, C. Donizetti-Oliveira, N.O. Saraiva Camar, How do

Mesenchymal Stem Cells Repair?, in: A. Gholamrezanezhad (Ed.), Stem Cells Clin. Res., InTech, 2011: pp. 83–104. doi:10.5772/17574.
[51] R.S. Cherry, E.T. Papoutsakis, Growth on Flat Surfaces and Spheres, Biotechnol. Bioeng. 33 (1989) 300–305.
[52] R.G. Ham, W.L. Mckeehan, Media and Growth Requirements, in: W.B. Jakoby, I.H. Pastan (Eds.), Methods Enzymol. Vol. 58 Cell Cult., Academic Press, New York, 1979: pp. 47–93.
[53] D.S. Gray, W.F. Liu, C.J. Shen, K. Bhadriraju, C.M. Nelson, C.S. Chen, Engineering amount of cell-cell contact demonstrates biphasic proliferative regulation through RhoA and the actin cytoskeleton, Exp. Cell Res. 314 (2008) 2846–2854. doi:10.1016/j.yexcr.2008.06.023.
[54] F. Ferro, R. Spelat, A.P. Beltrami, D. Cesselli, F. Curcio, Isolation and Characterization of Human Dental Pulp Derived Stem Cells by Using Media Containing Low Human Serum Percentage as Clinical Grade Substitutes for Bovine Serum, PLoS One. 7 (2012) 1–10. doi:10.1371/journal.pone.0048945.
[55] L. Ponchio, L. Duma, B. Oliviero, N. Gibelli, P. Pedrazzoli, G. Robustelli della Cuna, Mitomycin C as an alternative to irradiation to inhibit the feeder layer growth in long-term culture assays., Cytotherapy. 2 (2000) 281–6. http://www.ncbi.nlm.nih.gov/pubmed/12042037.
[56] Q. Wen, L. Zhou, C. Zhou, M. Zhou, W. Luo, L. Ma, Change in hepatocyte growth factor concentration promote mesenchymal stem cell-mediated osteogenic regeneration, J. Cell. Mol. Med. 16 (2012) 1260–1273. doi:10.1111/j.1582-4934.2011.01407.x.
[57] K. Tamama, V.H. Fan, L.G. Griffith, H.C. Blair, A. Wells, Epidermal Growth Factor as a Candidate for Ex Vivo Expansion of Bone Marrow-Derived Mesenchymal Stem Cells, Stem Cells. 24 (2006) 686–695. doi:10.1634/stemcells.2005-0176.
[58] Q.-B. Zeng, F.-J. Cheng, W.-G. Zhang, J.-M. Tang, L. Chen, Q.-H. Liu, Q.-P. Gao, J.-N. Wang, [Erythropoietin promotes proliferation of human bone marrow mesenchymal stem cells in vitro]., Zhongguo Shi Yan Xue Ye Xue Za Zhi. 16 (2008) 1392–7. http://www.ncbi.nlm.nih.gov/pubmed/19099651.
[59] Y. Huang, R. Qiu, W. Mai, J. Kuang, X. Cai, Y. Dong, Y. Hu, Y. Song, A. Cai, Z. Jiang, Effects of insulin-like growth factor-1 on the properties of mesenchymal stem cells in vitro., J. Zhejiang Univ. Sci. B. 13 (2012) 20–8. doi:10.1631/jzus.B1100117.
[60] A. Li, X. Xia, J. Yeh, H. Kua, H. Liu, Y. Mishina, A. Hao, B. Li, PDGF-AA Promotes Osteogenic Differentiation and Migration of Mesenchymal Stem Cell by Down-Regulating PDGFRα and Derepressing BMP-Smad1/5/8 Signaling, PLoS One. 9 (2014) e113785. doi:10.1371/journal.pone.0113785.
[61] J.C. Zhang, G.F. Zheng, L. Wu, L.Y.O. Yang, W.X. Li, Bone marrow mesenchymal stem cells overexpressing human basic fibroblast growth factor increase vasculogenesis in ischemic rats, Brazilian J. Med. Biol. Res. 47 (2014) 886–894.
[62] R. Ramasamy, C.K. Tong, W.K. Yip, S. Vellasamy, B.C. Tan, H.F. Seow, Basic fibroblast growth factor modulates cell cycle of human umbilical cord-derived mesenchymal stem cells, Cell Prolif. 45 (2012) 132–139. doi:10.1111/j.1365-2184.2012.00808.x.
[63] S. Hagmann, B. Moradi, S. Frank, T. Dreher, P.W. Kämmerer, W. Richter, T. Gotterbarm, FGF-2 addition during expansion of human bone marrow-derived stromal cells alters MSC surface marker distribution and chondrogenic differentiation potential, Cell Prolif. 46 (2013) 396–407. doi:10.1111/cpr.12046.
[64] W. Wang, X. Hu, X. Xie, X. Liu, R. Wu, Y. Wang, F. Gao, J. Wang, Nerve growth factor induces cord formation of mesenchymal stem cell by promoting proliferation and

activating the PI3K/Akt signaling pathway., Acta Pharmacol. Sin. 32 (2011) 1483–90. doi:10.1038/aps.2011.141.

[65] G. Catapano, Bioreactors for Bioartificial Organs, in: R. Eibl, D. Eibl, R. Portner, G. Catapano, P. Czermak (Eds.), Cell Tissue React. Eng., Springer, Heidelberg, 2009: p. 283.

[66] A. Allaire, M.X. Luong, K.P. Smith, Reagent Preparation, in: G.S. Stein, M. Borowski, M.X. Luong, M.-J. Shi, K.P. Smith, P. Vazquez (Eds.), Hum. Stem Cell Technol. Biol., John Wiley & Sons, Inc., Hoboken, NJ, USA, 2010: pp. 41–58. doi:10.1002/9780470889909.ch5.

[67] B. Alberts, A. Johnson, J. Lewis, M. Raff, K. Roberts, P. Walter, The Extracellular Matrix of Animals, in: Mol. Biol. Cell, 4th ed., Garland Science, New York, 2002: pp. 1–19. https://www.ncbi.nlm.nih.gov/books/NBK26810.

[68] M. Hayashi, Y. Ninomiya, K. Hayashi, T.F. Linsenmayer, B.R. Olsen, R.L. Trelstad, Secretion of collagen types I and II by epithelial and endothelial cells in the developing chick cornea demonstrated by in situ hybridization and immunohistochemistry., Development. 103 (1988) 27–36.

[69] T. Kaji, A. Yamada, S. Miyajima, C. Yamamoto, Cell density-dependent regulation of proteoglycan synthesis by transforming growth factor-β1 in cultured bovine aortic endothelial cells, J. Biol. Chem. 275 (2000) 1463–1470. http://www.jbc.org/content/275/2/1463.abstract%5Cnfile:///Users/fujimoto/Dropbox/Library.papers3/Articles/2000/Kaji/Journal of Biological … 2000 Kaji.pdf%5Cnpapers3://publication/uuid/440238D9-F017-4D13-B257-A0838727C43B.

[70] M.J. Spiro, Q. He, M.L.D. D'Autilia, Effect of high glucose on formation of extracellular matrix components by cultured rat heart endothelial cells, Diabetologia. 38 (1995) 430–436.

[71] R.L. Beach, W. V Burton, W.J. Hendricks, B.W. Festoff, Extracellular Matrix Synthesis by Skeletal Muscle in Culture, J. Biol. Chem. 257 (1982) 11437–11442.

[72] D.C. MacLeod, B.H. Strauss, M. de Jong, J. Escaned, V.A. Umans, R.J. van Suylen, A. Verkerk, P.J. de Feyter, P.W. Serruys, Proliferation and extracellular matrix synthesis of smooth muscle cells cultured from human coronary atherosclerotic and restenotic lesions, J. Am. Coll. Cardiol. 23 (1994) 59–65. doi:10.1016/0735-1097(94)90502-9.

[73] E.R. Deutsch, R.E. Guldberg, Stem cell-synthesized extracellular matrix for bone repair, J. Mater. Chem. 20 (2010) 8942. doi:10.1039/c0jm01070g.

[74] J.J. Creely, S.J. DiMari, A.M. Howe, M.A. Haralson, Effects of transforming growth factor-beta on collagen synthesis by normal rat kidney epithelial cells., Am. J. Pathol. 140 (1992) 45–55. http://www.pubmedcentral.nih.gov/articlerender.fcgi?artid=1886252&tool=pmcentrez&rendertype=abstract%5Cnhttp://www.ncbi.nlm.nih.gov/pubmed/1731530%5Cnhttp://www.pubmedcentral.nih.gov/articlerender.fcgi?artid=PMC1886252.

[75] C.P. Chen, Y.C. Yang, T.H. Su, C.Y. Chen, J.D. Aplin, Hypoxia and transforming growth factor-β1 act independently to increase extracellular matrix production by placental fibroblasts, J. Clin. Endocrinol. Metab. 90 (2005) 1083–1090. doi:10.1210/jc.2004-0803.

[76] K.A. Zimmerman, L. V. Graham, M.A. Pallero, J.E. Murphy-Ullrich, Calreticulin regulates transforming growth factor-beta-stimulated extracellular matrix production, J. Biol. Chem. 288 (2013) 14584–14598. doi:10.1074/jbc.M112.447243.

[77] X. Hu, H. Wang, J. Liu, X. Fang, K. Tao, Y. Wang, N. Li, J. Shi, Y. Wang, P. Ji, W. Cai, X. Bai, X. Zhu, J. Han, D. Hu, The role of ERK and JNK signaling in connective tissue growth factor induced extracellular matrix protein production and scar formation,

Arch. Dermatol. Res. 305 (2013) 433–445. doi:10.1007/s00403-013-1334-9.
[78] O. Yamanaka, S. Saika, K. Ikeda, K. Miyazaki, A. Kitano, Y. Ohnishi, Connective tissue growth factor modulates extracellular matrix production in human subconjunctival fibroblasts and their proliferation and migration in vitro, Jpn J Ophthalmol. 52 (2008) 8–15. doi:10.1007/s10384-007-0497-3 [doi].
[79] S. Hirano, D. Bless, D. Heisey, C. Ford, Roles of hepatocyte growth factor and transforming growth factor beta1 in production of extracellular matrix by canine vocal fold fibroblasts, Laryngoscope. 113 (2003) 144–148. doi:10.1097/00005537-200301000-00027.
[80] P.S. Howard, U. Kucich, R. Taliwal, J.M. Korostoff, Mechanical forces alter extracellular matrix synthesis by human periodontal ligament fibroblasts, J. Periodontal Res. 33 (1998) 500–508. doi:10.1111/j.1600-0765.1998.tb02350.x.
[81] C. Aulin, F. Foroughi, R. Brown, J. Hilborn, Extracellular matrix-polymer hybrid materials produced in a pulsed-flow bioreactor system, J. Tissue Eng. Regen. Med. 3 (2009) 188–195. doi:10.1002/term.152.
[82] P.M. Fong, J. Park, C.K. Breuer, Heart Valves, in: R. ANZA, R. LANGER, J. VACANTI (Eds.), Princ. Tissue Eng., Academic Press, San Diego, 2007: p. 593.
[83] S. Lin, A. Sahai, S.S. Chugh, X. Pan, E.I. Wallner, F.R. Danesh, J.W. Lomasney, Y.S. Kanwar, High glucose stimulates synthesis of fibronectin via a novel protein kinase C, Rap1b, and B-Raf signaling pathway, J. Biol. Chem. 277 (2002) 41725–41735. doi:10.1074/jbc.M203957200.
[84] K. Deschene, C. Céleste, D. Boerboom, C.L. Theoret, Hypoxia regulates the expression of extracellular matrix associated proteins in equine dermal fibroblasts via HIF1, J. Dermatol. Sci. 65 (2012) 12–18. doi:10.1016/j.jdermsci.2011.09.006.
[85] J.H.W. Distler, A. Jüngel, M. Pileckyte, J. Zwerina, B.A. Michel, R.E. Gay, O. Kowal-Bielecka, M. Matucci-Cerinic, G. Schett, H.H. Marti, S. Gay, O. Distler, Hypoxia-induced increase in the production of extracellular matrix proteins in systemic sclerosis., Arthritis Rheum. 56 (2007) 4203–15. doi:10.1002/art.23074.
[86] S.M. Naqvi, C.T. Buckley, Extracellular matrix production by nucleus pulposus and bone marrow stem cells in response to altered oxygen and glucose microenvironments, J. Anat. 227 (2015) 757–766. doi:10.1111/joa.12305.
[87] S.H. Kim, J.E. Song, D. Lee, G. Khang, Development of poly(lactide-co-glycolide) scaffold-impregnated small intestinal submucosa with pores that stimulate extracellular matrix production in disc regeneration, J. Tissue Eng. Regen. Med. 8 (2014) 279–290. doi:10.1002/term.1520.
[88] W. Mark Saltzman, T.R. Kyriakides, Cell Interactions with Polymers, in: Princ. Tissue Eng., Elsevier, 2007: pp. 279–296. doi:10.1016/B978-012370615-7/50024-X.
[89] B.M. Gumbiner, Cell adhesion: The molecular basis of tissue architecture and morphogenesis, Cell. 84 (1996) 345–357. doi:10.1016/S0092-8674(00)81279-9.
[90] M.A. Schwartz, R.K. Assoian, Integrins and cell proliferation, J. Cell Sci. 114 (2001) 2553–2560.
[91] M. Lotfi, M. Nejib, M. Naceur, Cell Adhesion to Biomaterials : Concept of Biocompatibility, Adv. Biomater. Sci. Biomed. Appl. (2013) 207–240. doi:10.5772/53542.
[92] J.K. Van Tam, K. Uto, M. Ebara, S. Pagliari, G. Forte, T. Aoyagi, Mesenchymal stem cell adhesion but not plasticity is affected by high substrate stiffness, Sci. Technol. Adv. Mater. 13 (2012) 64205. doi:10.1088/1468-6996/13/6/064205.
[93] A.C. Taylor, C.H. González, B.S. Miller, R.J. Edgington, P. Ferretti, R.B. Jackman, Surface functionalisation of nanodiamonds for human neural stem cell adhesion and proliferation, Sci. Rep. 7 (2017) 7307. doi:10.1038/s41598-017-07361-y.

[94] S. Dånmark, a Finne-Wistrand, a-C. Albertsson, M. Patarroyo, K. Mustafa, Integrin-mediated adhesion of human mesenchymal stem cells to extracellular matrix proteins adsorbed to polymer surfaces, Biomed. Mater. 7 (2012) 35011. doi:10.1088/1748-6041/7/3/035011.
[95] J.T. Parsons, A.R. Horwitz, M. a Schwartz, Cell adhesion: integrating cytoskeletal dynamics and cellular tension, Nat. Rev. Mol. Cell Biol. 11 (2010) 633–643. doi:10.1038/nrm2957.
[96] M.R. Morgan, M.J. Humphries, M.D. Bass, Synergistic control of cell adhesion by integrins and syndecans., Nat. Rev. Mol. Cell Biol. 8 (2007) 957–69. doi:10.1038/nrm2289.
[97] M.J. Kwon, B. Jang, J.Y. Yi, I.O. Han, E.S. Oh, Syndecans play dual roles as cell adhesion receptors and docking receptors, FEBS Lett. 586 (2012) 2207–2211. doi:10.1016/j.febslet.2012.05.037.
[98] N. V. Menon, Y.J. Chuah, S. Phey, Y. Zhang, Y. Wu, V. Chan, Y. Kang, Microfluidic Assay To Study the Combinatorial Impact of Substrate Properties on Mesenchymal Stem Cell Migration, ACS Appl. Mater. Interfaces. 7 (2015) 17095–17103. doi:10.1021/acsami.5b03753.
[99] L. Yuan, N. Sakamoto, G. Song, M. Sato, Low-level shear stress induces human mesenchymal stem cell migration through the SDF-1/CXCR4 axis via MAPK signaling pathways., Stem Cells Dev. 22 (2013) 2384–93. doi:10.1089/scd.2012.0717.
[100] C. Gamell, N. Osses, R. Bartrons, T. Rückle, M. Camps, J.L. Rosa, F. Ventura, BMP2 induction of actin cytoskeleton reorganization and cell migration requires PI3-kinase and Cdc42 activity., J. Cell Sci. 121 (2008) 3960–70. doi:10.1242/jcs.031286.
[101] G. Forte, M. Minieri, P. Cossa, D. Antenucci, M. Sala, V. Gnocchi, R. Fiaccavento, F. Carotenuto, P. De Vito, P.M. Baldini, M. Prat, P. Di Nardo, Hepatocyte Growth Factor Effects on Mesenchymal Stem Cells: Proliferation, Migration, and Differentiation, Stem Cells. 24 (2006) 23–33. doi:10.1634/stemcells.2004-0176.
[102] X. Liu, B. Duan, Z. Cheng, X. Jia, L. Mao, H. Fu, Y. Che, L. Ou, L. Liu, D. Kong, SDF-1/CXCR4 axis modulates bone marrow mesenchymal stem cell apoptosis, migration and cytokine secretion., Protein Cell. 2 (2011) 845–54. doi:10.1007/s13238-011-1097-z.
[103] W. Ji, F. Yang, J. Ma, M.J. Bouma, O.C. Boerman, Z. Chen, J.J.J.P. van den Beucken, J.A. Jansen, Incorporation of stromal cell-derived factor-1 alfa in PCL/gelatin electrospun membranes for guided bone regeneration, Biomaterials. 34 (2013) 735–745. doi:10.1016/j.biomaterials.2012.10.016.
[104] A. Barhanpurkar-Naik, S.T. Mhaske, S.T. Pote, K. Singh, M.R. Wani, Interleukin-3 enhances the migration of human mesenchymal stem cells by regulating expression of CXCR4, Stem Cell Res. Ther. 8 (2017) 168. doi:10.1186/s13287-017-0618-y.
[105] L. Shi, S. Fu, S. Fahim, S. Pan, H. Lina, X. Mu, Y. Niu, TNF-alpha stimulation increases dental pulp stem cell migration in vitro through integrin alpha-6 subunit upregulation, Arch. Oral Biol. 75 (2017) 48–54. doi:10.1016/j.archoralbio.2016.12.005.
[106] J. Veevers-Lowe, S.G. Ball, A. Shuttleworth, C.M. Kielty, Mesenchymal stem cell migration is regulated by fibronectin through 5 1-integrin-mediated activation of PDGFR- and potentiation of growth factor signals, J. Cell Sci. 124 (2011) 1288–1300. doi:10.1242/jcs.076935.
[107] A.G. Ardakani, U. Cheema, R.A. Brown, R.J. Shipley, Quantifying the correlation between spatially defined oxygen gradients and cell fate in an engineered three-dimensional culture model, J. R. Soc. Interface. 11 (2014) 20140501–20140501. doi:10.1098/rsif.2014.0501.
[108] R.K. Paradise, M.J. Whitfield, D. a. Lauffenburger, K.J. Van Vliet, Directional cell

migration in an extracellular pH gradient: A model study with an engineered cell line and primary microvascular endothelial cells, Exp. Cell Res. 319 (2013) 487–497. doi:10.1016/j.yexcr.2012.11.006.
[109] S.R. Peyton, Z.I. Kalcioglu, J.C. Cohen, A.P. Runkle, K.J. Van Vliet, D. a. Lauffenburger, L.G. Griffith, Marrow-Derived stem cell motility in 3D synthetic scaffold is governed by geometry along with adhesivity and stiffness, Biotechnol. Bioeng. 108 (2011) 1181–1193. doi:10.1002/bit.23027.
[110] W.M. Saltzman, Cell Migration, in: Tissue Eng. Eng. Princ. Des. Replace. Organs Tissues, Oxford University Press, New York, 2004.
[111] M. Girlovanu, S. Susman, O. Soritau, D. Rus-Ciuca, C. Melincovici, A.-M. Constantin, C.M. Mihu, Stem cells - biological update and cell therapy progress, Clujul Med. 88 (2015) 265–271. doi:10.15386/cjmed-483.
[112] M.Z. Heydarabad, M. Vatanmakanian, M. Nikasa, M.F. Hagh, Epigenetic regulation of specific transcription factors in osteogenicdifferentiation of mesenchymal stem cells, TURKISH J. Biol. 40 (2016) 1040–1049. doi:10.3906/biy-1507-6.
[113] K. Hino, A. Saito, M. Kido, S. Kanemoto, R. Asada, T. Takai, M. Cui, X. Cui, K. Imaizumi, Master regulator for chondrogenesis, Sox9, regulates transcriptional activation of the endoplasmic reticulum stress transducer BBF2H7/CREB3L2 in chondrocytes, J. Biol. Chem. 289 (2014) 13810–13820. doi:10.1074/jbc.M113.543322.
[114] J.-E. Lee, K. Ge, Transcriptional and epigenetic regulation of PPARγ expression during adipogenesis, Cell Biosci. 4 (2014) 29. doi:10.1186/2045-3701-4-29.
[115] M.L. Alves da Silva, A.R. Costa-Pinto, A. Martins, V.M. Correlo, P. Sol, M. Bhattacharya, S. Faria, R.L. Reis, N.M. Neves, Conditioned medium as a strategy for human stem cells chondrogenic differentiation, J. Tissue Eng. Regen. Med. 9 (2015) 714–723. doi:10.1002/term.1812.
[116] C.L. Korecki, J.M. Taboas, R.S. Tuan, J.C. Iatridis, Notochordal cell conditioned medium stimulates mesenchymal stem cell differentiation toward a young nucleus pulposus phenotype, Stem Cell Res. Ther. 1 (2010) 18. doi:10.1186/scrt18.
[117] C. Huang, J. Zhang, M. Ao, Y. Li, C. Zhang, Y. Xu, X. Li, W. Wang, Combination of retinal pigment epithelium cell-conditioned medium and photoreceptor outer segments stimulate mesenchymal stem cell differentiation toward a functional retinal pigment epithelium cell phenotype, J. Cell. Biochem. 113 (2012) 590–598. doi:10.1002/jcb.23383.
[118] R. Ghaem Maghami, T. Mirzapour, A. Bayrami, Differentiation of mesenchymal stem cells to germ-like cells under induction of Sertoli cell-conditioned medium and retinoic acid, Andrologia. (2017) e12887. doi:10.1111/and.12887.
[119] P. Müller, A. Langenbach, A. Kaminski, J. Rychly, Modulating the Actin Cytoskeleton Affects Mechanically Induced Signal Transduction and Differentiation in Mesenchymal Stem Cells, PLoS One. 8 (2013) 1–8. doi:10.1371/journal.pone.0071283.
[120] G. Yourek, M.A. Hussain, J.J. Mao, Cytoskeletal changes of mesenchymal stem cells during differentiation., ASAIO J. 53 (2014) 219–28. doi:10.1097/MAT.0b013e31802deb2d.
[121] L. Gao, R. McBeath, C.S. Chen, Stem Cell Shape Regulates a Chondrogenic Versus Myogenic Fate Through Rac1 and N-Cadherin, Stem Cells. 28 (2010) 564–572. doi:10.1002/stem.308.
[122] T. Popielarczyk, A. Nain, J. Barrett, Aligned Nanofiber Topography Directs the Tenogenic Differentiation of Mesenchymal Stem Cells, Appl. Sci. 7 (2017) 59. doi:10.3390/app7010059.
[123] A.J. Engler, S. Sen, H.L. Sweeney, D.E. Discher, Matrix Elasticity Directs Stem Cell

Lineage Specification, Cell. 126 (2006) 677–689. doi:10.1016/j.cell.2006.06.044.
[124] G. Kumar, M.S. Waters, T.M. Farooque, M.F. Young, C.G. Simon, Freeform fabricated scaffolds with roughened struts that enhance both stem cell proliferation and differentiation by controlling cell shape, Biomaterials. 33 (2012) 4022–4030. doi:10.1016/j.biomaterials.2012.02.048.
[125] D. Yu, J. Han, B. Kim, Stimulation of Chondrogenic Differentiation of Mesenchymal Stem Cells, Int. J. Stem Cells. 5 (2012) 16–22.
[126] S. Li, Y. Liu, Q. Zhou, R. Lue, L. Song, S.-W. Dong, P. Guo, B. Kopjar, A Novel Axial-Stress Bioreactor System Combined with a Substance Exchanger for Tissue Engineering of 3D Constructs., Tissue Eng. Part C. Methods. 20 (2014) 205–14. doi:10.1089/ten.TEC.2013.0173.
[127] S.P. Sheehy, K.K. Parker, The Role of Mechanical Forces in Guiding Tissue Differentiation, in: H.S. Bernstein (Ed.), Tissue Eng. Regen. Med., Springer, Hoboken, 2011: pp. 77–97.
[128] X. Song, Y. Li, X. Chen, G. Yin, Q. Huang, Y. Chen, G. Xu, L. Wang, bFGF promotes adipocyte differentiation in human mesenchymal stem cells derived from embryonic stem cells, Genet. Mol. Biol. 37 (2014) 127–134. doi:10.1590/S1415-47572014000100019.
[129] M. Yokoyama, H. Miwa, S. Maeda, S. Wakitani, M. Takagi, Influence of fetal calf serum on differentiation of mesenchymal stem cells to chondrocytes during expansion., J. Biosci. Bioeng. 106 (2008) 46–50. doi:10.1263/jbb.106.46.
[130] K.H. Chua, F. Raduan, W.K.Z. Wan Safwani, N.F.M. Manzor, B. Pingguan-Murphy, S. Sathapan, Effects of serum reduction and VEGF supplementation on angiogenic potential of human adipose stromal cells in vitro, Cell Prolif. 46 (2013) 300–311. doi:10.1111/cpr.12029.
[131] B.Y.K. Binder, J.E. Sagun, J.K. Leach, Reduced Serum and Hypoxic Culture Conditions Enhance the Osteogenic Potential of Human Mesenchymal Stem Cells, Stem Cell Rev. Reports. 11 (2015) 387–393. doi:10.1007/s12015-014-9555-7.
[132] H. Abdollahi, L.J. Harris, P. Zhang, S. McIlhenny, V. Srinivas, T. Tulenko, P.J. DiMuzio, The Role of Hypoxia in Stem Cell Differentiation and Therapeutics, J. Surg. Res. 165 (2011) 112–117. doi:10.1016/j.jss.2009.09.057.
[133] B. Alberts, A. Johnson, J. Lewis, M. Raff, K. Roberts, P. Walter, Programmed Cell Death (Apoptosis), in: Mol. Biol. Cell, 4th ed., Garland Science, New York, 2002. https://www.ncbi.nlm.nih.gov/books/NBK26873/.
[134] M.L. Escobar, O.M. Echeverría, G.H. Vázquez-Nin, Necrosis as Programmed Cell Death, in: T.M. Ntuli (Ed.), Cell Death - Autophagy, Apoptosis Necrosis, InTech, 2015: pp. 419–434. doi:10.5772/61483.
[135] M. Suzanne, H. Steller, Shaping organisms with apoptosis, Cell Death Differ. 20 (2013) 669–675. doi:10.1038/cdd.2013.11.
[136] H.-H. Cheung, X. Liu, O.M. Rennert, Apoptosis: Reprogramming and the Fate of Mature Cells, ISRN Cell Biol. 2012 (2012) 1–8. doi:10.5402/2012/685852.
[137] B. Cai, X. Li, Y. Wang, Y. Liu, F. Yang, H. Chen, K. Yin, X. Tan, J. Zhu, Z. Pan, B. Wang, Y. Lu, Apoptosis of Bone Marrow Mesenchymal Stem Cells Caused by Homocysteine via Activating JNK Signal, PLoS One. 8 (2013) 1–9. doi:10.1371/journal.pone.0063561.
[138] H. Wei, Z. Li, S. Hu, X. Chen, X. Cong, Apoptosis of mesenchymal stem cells induced by hydrogen peroxide concerns both endoplasmic reticulum stress and mitochondrial death pathway through regulation of caspases, p38 and JNK, J. Cell. Biochem. 111 (2010) 967–978. doi:10.1002/jcb.22785.
[139] G. Ertaş, E. Ural, D. Ural, A. Aksoy, G. Kozdağ, G. Gacar, E. Karaöz, Comparative

Analysis of Apoptotic Resistance of Mesenchymal Stem Cells Isolated from Human Bone Marrow and Adipose Tissue, Sci. World J. 2012 (2012) 1–8. doi:10.1100/2012/105698.
[140] W. Zhu, J. Chen, X. Cong, S. Hu, X. Chen, Hypoxia and Serum Deprivation-Induced Apoptosis in Mesenchymal Stem Cells, Stem Cells. 24 (2006) 416–425. doi:10.1634/stemcells.2005-0121.
[141] P. Engbers-Buijtenhuijs, M. Kamphuis, G. Van Der Sluijs Veer, C. Haanen, A.A. Poot, J. Feijen, I. Vermes, A novel time resolved fluorometric assay of anoikis using Europium-labelled Annexin V in cultured adherent cells, Apoptosis. 10 (2005) 429–437. doi:10.1007/s10495-005-0816-4.
[142] S.L. Fink, B.T. Cookson, S.L. Fink, B.T. Cookson, Eukaryotic Cells MINIREVIEW Apoptosis , Pyroptosis , and Necrosis : Mechanistic Description of Dead and Dying Eukaryotic Cells, Infect. Immun. 73 (2005) 1907–1916. doi:10.1128/IAI.73.4.1907.
[143] N. Li, Q. Zhang, H.Y. Qian, C. Jin, Y.J. Yang, R.L. Gao, Atorvastatin induces autophagy of mesenchymal stem cells under hypoxia and serum deprivation conditions by activating the mitogen- activated protein kinase/extracellular signal-regulated kinase pathway, Chin. Med. J. (Engl). 127 (2014) 1046–1051. doi:10.3760/cma.j.issn.0366-6999.20132638.
[144] J. Wu, J. Niu, X. Li, Y. Li, X. Wang, J. Lin, F. Zhang, Hypoxia induces autophagy of bone marrow-derived mesenchymal stem cells via activation of ERK1/2., Cell. Physiol. Biochem. 33 (2014) 1467–74. doi:10.1159/000358711.
[145] T. Chang, M. Hsu, K.K. Wu, High glucose induces bone marrow-derived mesenchymal stem cell senescence by upregulating autophagy., PLoS One. 10 (2015) e0126537. doi:10.1371/journal.pone.0126537.
[146] V. Turinetto, E. Vitale, C. Giachino, Senescence in Human Mesenchymal Stem Cells: Functional Changes and Implications in Stem Cell-Based Therapy, Int. J. Mol. Sci. 17 (2016) 1164. doi:10.3390/ijms17071164.
[147] W. Zong, C.B. Thompson, Necrotic death as a cell fate, Genes Dev. 20 (2006) 1–15. doi:10.1101/gad.1376506.contrast.
[148] J. Karch, J.D. Molkentin, Regulated necrotic cell death: The passive aggressive side of bax and bak, Circ. Res. 116 (2015) 1800–1809. doi:10.1161/CIRCRESAHA.116.305421.
[149] M. Lovett, K. Lee, A. Edwards, D.L. Kaplan, Vascularization strategies for tissue engineering., Tissue Eng. Part B. Rev. 15 (2009) 353–70. doi:10.1089/ten.TEB.2009.0085.
[150] R. Largo, V. Ramakrishnan, M. Ehrbar, A. Ziogas, J.A. Plock, D. Eberli, Angiogenesis and vascularity for tissue engineering, in: D. Eberli (Ed.), Regen. Med. Tissue Eng. - Cells Biomater., InTech, Rijeka, 2011: pp. 433–448.
[151] A. Kampmann, D. Lindhorst, P. Schumann, R. Zimmerer, H. Kokemüller, M. Rücker, N. Gellrich, F. Tavassol, Additive effect of mesenchymal stem cells and VEGF to vascularization of PLGA scaffolds, Microvasc. Res. 90 (2013) 71–79. doi:10.1016/j.mvr.2013.07.006.
[152] E. Quinlan, A. López-Noriega, E.M. Thompson, A. Hibbitts, S.A. Cryan, F.J. O'Brien, Controlled release of vascular endothelial growth factor from spray-dried alginate microparticles in collagen-hydroxyapatite scaffolds for promoting vascularization and bone repair, J. Tissue Eng. Regen. Med. 11 (2017) 1097–1109. doi:10.1002/term.2013.
[153] D. Kaigler, P.H. Krebsbach, P.J. Polverini, D.J. Mooney, Role of vascular endothelial growth factor in bone marrow stromal cell modulation of endothelial cells., Tissue Eng. 9 (2003) 95–103. doi:10.1089/107632703762687573.
[154] S. Strassburg, H. Nienhueser, G. Björn Stark, G. Finkenzeller, N. Torio-Padron, Co-

culture of adipose-derived stem cells and endothelial cells in fibrin induces angiogenesis and vasculogenesis in a chorioallantoic membrane model, J. Tissue Eng. Regen. Med. 10 (2016) 496–506. doi:10.1002/term.1769.

[155] X.L. Ma, K.D. Liu, F.C. Li, X.M. Jiang, L. Jiang, H.L. Li, Human mesenchymal stem cells increases expression of alpha-tubulin and angiopoietin 1 and 2 in focal cerebral ischemia and reperfusion, Curr. Neurovasc. Res. 10 (2013) 103–111. doi:CNR-EPUB-20130304-2 [pii].

[156] A. Mizukami, A. Fernandes-Platzgummer, J.G. Carmelo, K. Swiech, D.T. Covas, J.M.S. Cabral, C.L. da Silva, Stirred tank bioreactor culture combined with serum-/xenogeneic-free culture medium enables an efficient expansion of umbilical cord-derived mesenchymal stem/stromal cells, Biotechnol. J. 11 (2016) 1048–1059. doi:10.1002/biot.201500532.

[157] F. Lu, X. Zhao, J. Wu, Y. Cui, Y. Mao, K. Chen, Y. Yuan, D. Gong, Z. Xu, S. Huang, MSCs transfected with hepatocyte growth factor or vascular endothelial growth factor improve cardiac function in the infarcted porcine heart by increasing angiogenesis and reducing fibrosis, Int. J. Cardiol. 167 (2013) 2524–2532. doi:10.1016/j.ijcard.2012.06.052.

[158] F. Bussolino, Hepatocyte growth factor is a potent angiogenic factor which stimulates endothelial cell motility and growth, J. Cell Biol. 119 (1992) 629–641. doi:10.1083/jcb.119.3.629.

[159] H. Haller, C. Christel, L. Dannenberg, P. Thiele, C. Lindschau, F.C. Luft, Signal transduction of erythropoietin in endothelial cells., Kidney Int. 50 (1996) 481–8. doi:10.1038/ki.1996.339.

[160] M.J. Cross, L. Claesson-Welsh, FGF and VEGF function in angiogenesis: Signalling pathways, biological responses and therapeutic inhibition, Trends Pharmacol. Sci. 22 (2001) 201–207. doi:10.1016/S0165-6147(00)01676-X.

[161] M. Jeltsch, V.-M. Leppänen, P. Saharinen, K. Alitalo, Receptor tyrosine kinase-mediated angiogenesis., Cold Spring Harb. Perspect. Biol. 5 (2013). doi:10.1101/cshperspect.a009183.

[162] Y. Liu, S.R. Cox, T. Morita, S. Kourembanas, Hypoxia regulates vascular endothelial growth factor gene expression in endothelial cells. Identification of a 5′ enhancer, Circ. Res. 77 (1995) 638–643.

[163] V. Razban, A.S. Lotfi, M. Soleimani, H. Ahmadi, M. Massumi, S. Khajeh, M. Ghaedi, S. Arjmand, S. Najavand, A. Khoshdel, HIF-1α Overexpression Induces Angiogenesis in Mesenchymal Stem Cells, Biores. Open Access. 1 (2012) 174–183. doi:10.1089/biores.2012.9905.

[164] a Kiparissides, S.S. Kucherenko, a Mantalaris, E.N. Pistikopoulos, Global Sensitivity Analysis Challenges in Biological Systems Modeling, Ind. Eng. Chem. Res. 28 (2009) 7168–7180. doi:10.1021/ie900139x.

[165] S.K. Dasika, Reaction-Diffusion Processes in Muscle Metabolism Parametric and Sensitivity Analysis, Florida State University, 2010.

[166] T.E. Tan, G.S.L. Peh, B.L. George, H.Y. Cajucom-Uy, D. Dong, E.A. Finkelstein, J.S. Mehta, A cost-minimization analysis of tissue-engineered constructs for corneal endothelial transplantation, PLoS One. 9 (2014). doi:10.1371/journal.pone.0100563.

[167] C.J. Galban, B.R. Locke, Analysis of cell growth kinetics and substrate diffusion in a polymer scaffold, Biotechnol. Bioeng. 65 (1999) 121–132. doi:10.1002/(SICI)1097-0290(19991020)65:2<121::AID-BIT1>3.0.CO;2-6.

[168] L. Mancuso, M.I. Liuzzo, S. Fadda, M. Pisu, A. Cincotti, M. Arras, E. Desogus, F. Piras, G. Piga, G. Nasa, A. Concas, G. Cao, Experimental analysis and modelling of in vitro proliferation of mesenchymal stem cells, Cell Prolif. 42 (2009) 602–616.

[169] a K. Saha, J.N. Mazumdar, Dynamics of the cell and its extracellular matrix--a simple mathematical approach., IEEE Trans. Nanobioscience. 2 (2003) 89–93. doi:10.1109/TNB.2003.813921.
[170] P. Causin, R. Sacco, M. Verri, A multiscale approach in the computational modeling of the biophysical environment in artificial cartilage tissue regeneration, Biomech. Model. Mechanobiol. 12 (2013) 763–780. doi:10.1007/s10237-012-0440-5.
[171] U. Akalp, S.J. Bryant, F.J. Vernerey, Tuning tissue growth with scaffold degradation in enzyme-sensitive hydrogels: a mathematical model, Soft Matter. 12 (2016) 7505–7520. doi:10.1039/c6sm00583g.
[172] M.C. Lewis, B.D. MacArthur, R.S. Tare, R.O.C. Oreffo, C.P. Please, Extracellular matrix deposition in engineered micromass cartilage pellet cultures: Measurements and modelling, PLoS One. 11 (2016) 1–12. doi:10.1371/journal.pone.0147302.
[173] F. Frascoli, B.D. Hughes, M.H. Zaman, K.A. Landman, A Computational Model for Collective Cellular Motion in Three Dimensions: General Framework and Case Study for Cell Pair Dynamics, PLoS One. 8 (2013). doi:10.1371/journal.pone.0059249.
[174] K.J. Painter, Continuous Models for Cell Migration in Tissues and Applications to Cell Sorting via Differential Chemotaxis, Bull. Math. Biol. 71 (2009) 1117–1147. doi:10.1007/s11538-009-9396-8.
[175] R. Rey, J.M. García-Aznar, A phenomenological approach to modelling collective cell movement in 2D, Biomech. Model. Mechanobiol. 12 (2013) 1089–1100. doi:10.1007/s10237-012-0465-9.
[176] M.H. Zaman, R.D. Kamm, P. Matsudaira, D.A. Lauffenburger, Computational Model for Cell Migration in Three-Dimensional Matrices, Biophys. J. 89 (2005) 1389–1397. doi:10.1529/biophysj.105.060723.
[177] G. Lemon, S.L. Waters, F.R. a J. Rose, J.R. King, Mathematical modelling of human mesenchymal stem cell proliferation and differentiation inside artificial porous scaffolds, J. Theor. Biol. 249 (2007) 543–553. doi:10.1016/j.jtbi.2007.08.015.
[178] a. J.F. Stops, K.B. Heraty, M. Browne, F.J. O'Brien, P.E. McHugh, A prediction of cell differentiation and proliferation within a collagen-glycosaminoglycan scaffold subjected to mechanical strain and perfusive fluid flow, J. Biomech. 43 (2010) 618–626. doi:10.1016/j.jbiomech.2009.10.037.
[179] T.M. Broome, R.A. Coleman, A mathematical model of cell death in multiple sclerosis, J. Neurosci. Methods. 201 (2011) 420–425. doi:10.1016/j.jneumeth.2011.08.008.
[180] H. Jin, J. Lei, A mathematical model of cell population dynamics with autophagy response to starvation, Math. Biosci. 258 (2014) 1–10. doi:10.1016/j.mbs.2014.08.014.
[181] I. Tavassoly, J. Parmar, A.N. Shajahan-Haq, R. Clarke, W.T. Baumann, J.J. Tyson, Dynamic Modeling of the Interaction Between Autophagy and Apoptosis in Mammalian Cells., CPT Pharmacometrics Syst. Pharmacol. 4 (2015) 263–72. doi:10.1002/psp4.29.
[182] G. Lemon, D. Howard, M.J. Tomlinson, L.D. Buttery, F.R. a J. Rose, S.L. Waters, J.R. King, Mathematical modelling of tissue-engineered angiogenesis, Math. Biosci. 221 (2009) 101–120. doi:10.1016/j.mbs.2009.07.003.
[183] F.D. Bookholt, H.N. Monsuur, S. Gibbs, F.J. Vermolen, Mathematical modelling of angiogenesis using continuous cell-based models, Biomech. Model. Mechanobiol. 15 (2016) 1–24. doi:10.1007/s10237-016-0784-3.
[184] C.J. Galban, B.R. Locke, Effects of spatial variation of cells and nutrient and product concentrations coupled with product inhibition on cell growth in a polymer scaffold, Biotechnol. Bioeng. 64 (1999) 633–643. doi:10.1002/(SICI)1097-0290(19990920)64:6<633::AID-BIT1>3.0.CO;2-6.
[185] M. Cioffi, J. Küffer, S. Ströbel, G. Dubini, I. Martin, D. Wendt, Computational

evaluation of oxygen and shear stress distributions in 3D perfusion culture systems: Macro-scale and micro-structured models, J. Biomech. 41 (2008) 2918–2925. doi:10.1016/j.jbiomech.2008.07.023.

[186] W.L. Grayson, D. Marolt, S. Bhumiratana, M. Fröhlich, X.E. Guo, G. Vunjak-Novakovic, Optimizing the medium perfusion rate in bone tissue engineering bioreactors, Biotechnol. Bioeng. 108 (2011) 1159–1170. doi:10.1002/bit.23024.

[187] J. Malda, J. Rouwkema, D.E. Martens, E.P. Le Comte, F.K. Kooy, J. Tramper, C. a. Van Blitterswijk, J. Riesle, Oxygen Gradients in Tissue-Engineered PEGT/PBT Cartilaginous Constructs: Measurement and Modeling, Biotechnol. Bioeng. 86 (2004) 9–18. doi:10.1002/bit.20038.

[188] M. Radisic, W. Deen, R. Langer, G. Vunjak-Novakovic, Mathematical model of oxygen distribution in engineered cardiac tissue with parallel channel array perfused with culture medium containing oxygen carriers., Am. J. Physiol. Heart Circ. Physiol. 288 (2005) H1278–H1289. doi:10.1152/ajpheart.00787.2004.

[189] S. Truscello, G. Kerckhofs, S. Van Bael, G. Pyka, J. Schrooten, H. Van Oosterwyck, Prediction of permeability of regular scaffolds for skeletal tissue engineering: A combined computational and experimental study, Acta Biomater. 8 (2012) 1648–1658. doi:10.1016/j.actbio.2011.12.021.

[190] L.E. Freed, F. Guilak, X.E. Guo, M.L. Gray, R. Tranquillo, J.W. Holmes, M. Radisic, M. V Sefton, D. Kaplan, G. Vunjak-Novakovic, Advanced tools for tissue engineering: scaffolds, bioreactors, and signaling., Tissue Eng. 12 (2006) 3285–3305. doi:10.1089/ten.2006.12.3285.

[191] T.-H. Lin, C.-H. Lin, C.A. Chung, Comutational Study of Oxygen and Glucose Transport in Engineered Cartilage Constructs, J. Mech. 27 (2011) 337–346. doi:10.1017/jmech.2011.36.

[192] K.E. Wellen, C. Lu, A. Mancuso, J.M.S. Lemons, M. Ryczko, J.W. Dennis, J.D. Rabinowitz, H.A. Coller, C.B. Thompson, The hexosamine biosynthetic pathway couples growth factor-induced glutamine uptake to glucose metabolism, Genes Dev. 24 (2010) 2784–2799. doi:10.1101/gad.1985910.

[193] M. Campolo, F. Curcio, A. Soldati, Minimal perfusion flow for osteogenic growth of mesenchymal stem cells on lattice scaffolds, AIChE J. 59 (2013) 3131–3144. doi:10.1002/aic.14084.

[194] P. Causin, R. Sacco, A computational model for biomass growth simulation in tissue engineering, Commun. Appl. Ind. Math. 2 (2011). doi:10.1685/journal.caim.370.

[195] C.A. Chung, C.P. Chen, T.H. Lin, C.S. Tseng, A compact computational model for cell construct development in perfusion culture, Biotechnol. Bioeng. 99 (2008) 1535–1541. doi:10.1002/bit.21701.

[196] C.A. Chung, C.W. Chen, C.P. Chen, C.S. Tseng, Enhancement of cell growth in tissue-engineering constructs under direct perfusion: Modeling and simulation, Biotechnol. Bioeng. 97 (2007) 1603–1616. doi:10.1002/bit.21378.

[197] C.A. Chung, S.Y. Ho, Analysis of collagen and glucose modulated cell growth within tissue engineered scaffolds, Ann. Biomed. Eng. 38 (2010) 1655–1663. doi:10.1007/s10439-010-9909-5.

[198] M. Devarapalli, B.J. Lawrence, S. V. Madihally, Modeling nutrient consumptions in large flow-through bioreactors for tissue engineering, Biotechnol. Bioeng. 103 (2009) 1003–1015. doi:10.1002/bit.22333.

[199] G. Higuera, D. Schop, F. Janssen, R. van Dijkhuizen-Radersma, T. van Boxtel, C. a van Blitterswijk, Quantifying in vitro growth and metabolism kinetics of human mesenchymal stem cells using a mathematical model., Tissue Eng. Part A. 15 (2009) 2653–2663. doi:10.1089/ten.TEA.2008.0328.

[200] C.Y.J. Ma, R. Kumar, X.Y. Xu, A. Mantalaris, A combined fluid dynamics, mass transport and cell growth model for a three-dimensional perfused biorector for tissue engineering of haematopoietic cells, Biochem. Eng. J. 35 (2007) 1–11. doi:10.1016/j.bej.2006.11.024.
[201] C. Schirmaier, V. Jossen, S.C. Kaiser, F. Jüngerkes, S. Brill, A. Safavi-Nab, A. Siehoff, C. van den Bos, D. Eibl, R. Eibl, Scale-up of adipose tissue-derived mesenchymal stem cell production in stirred single-use bioreactors under low-serum conditions, Eng. Life Sci. 14 (2014) 292–303. doi:10.1002/elsc.201300134.
[202] B.G. Sengers, C.W. Oomens, F.P. Baaijens, An integrated finite-element approach to mechanics, transport and biosynthesis in tissue engineering, J Biomech Eng. 126 (2004) 82–91. doi:10.1115/1.1645526.
[203] X. Yan, D.J. Bergstrom, X.B. Chen, Modeling of cell cultures in perfusion bioreactors, IEEE Trans. Biomed. Eng. 59 (2012) 2568–2575. doi:10.1109/TBME.2012.2206077.
[204] S. Zhou, Z. Cui, J.P.G. Urban, Nutrient gradients in engineered cartilage: Metabolic kinetics measurement and mass transfer modelings, Biotechnol. Bioeng. 101 (2008) 408–421. doi:10.1002/bit.21887.
[205] R.J. Whittaker, R. Booth, R. Dyson, C. Bailey, L. Parsons Chini, S. Naire, S. Payvandi, Z. Rong, H. Woollard, L.J. Cummings, S.L. Waters, L. Mawasse, J.B. Chaudhuri, M.J. Ellis, V. Michael, N.J. Kuiper, S. Cartmell, Mathematical modelling of fibre-enhanced perfusion inside a tissue-engineering bioreactor, J. Theor. Biol. 256 (2009) 533–546. doi:10.1016/j.jtbi.2008.10.013.
[206] B. Obradovic, J.H. Meldon, L.E. Freed, G. Vunjak-Novakovic, Glycosaminoglycan deposition in engineered cartilage: Experiments and mathematical model, AIChE J. 46 (2000) 1860–1871. doi:10.1002/aic.690460914.
[207] M. Radisic, J. Malda, E. Epping, W. Geng, R. Langer, G. Vunjak-Novakovic, Oxygen gradients correlate with cell density and cell viability in engineered cardiac tissue, Biotechnol. Bioeng. 93 (2006) 332–343. doi:10.1002/bit.20722.
[208] G.D.S. Tan, G.W. Toh, E. Birgersson, J. Robens, D. van Noort, H.L. Leo, A thin-walled polydimethylsiloxane bioreactor for high-density hepatocyte sandwich culture, Biotechnol. Bioeng. 110 (2013) 1663–1673. doi:10.1002/bit.24822.
[209] M. Flaibani, E. Magrofuoco, N. Elvassore, Computational modeling of cell growth heterogeneity in a perfused 3D scaffold, Ind. Eng. Chem. Res. 49 (2010) 859–869. doi:10.1021/ie900418g.
[210] M.M. Nava, M.T. Raimondi, R. Pietrabissa, A multiphysics 3D model of tissue growth under interstitial perfusion in a tissue-engineering bioreactor, Biomech. Model. Mechanobiol. 12 (2013) 1169–1179. doi:10.1007/s10237-013-0473-4.
[211] R. Sacco, P. Causin, P. Zunino, M.T. Raimondi, A multiphysics/multiscale 2D numerical simulation of scaffold-based cartilage regeneration under interstitial perfusion in a bioreactor, Biomech. Model. Mechanobiol. 10 (2011) 577–589. doi:10.1007/s10237-010-0257-z.
[212] T.Y. Kang, H.W. Kang, C.M. Hwang, S.J. Lee, J. Park, J.J. Yoo, D.W. Cho, The realistic prediction of oxygen transport in a tissue-engineered scaffold by introducing time-varying effective diffusion coefficients, Acta Biomater. 7 (2011) 3345–3353. doi:10.1016/j.actbio.2011.05.015.
[213] M. Shakeel, P.C. Matthews, R.S. Graham, S.L. Waters, A continuum model of cell proliferation and nutrient transport in a perfusion bioreactor., Math. Med. Biol. 30 (2013) 21–44. doi:10.1093/imammb/dqr022.
[214] T.I. Croll, S. Gentz, K. Mueller, M. Davidson, A.J. O'Connor, G.W. Stevens, J.J. Cooper-White, Modelling oxygen diffusion and cell growth in a porous, vascularising scaffold for soft tissue engineering applications, Chem. Eng. Sci. 60 (2005) 4924–

4934. doi:10.1016/j.ces.2005.03.051.

Capítulo 3

Condições de cultivo e propriedades do *scaffold* relevantes para o cultivo de células e modelagem fenomenológica

A pesquisa na área de engenharia de tecidos cresceu muito na última década, a qual foi caracterizada por inúmeros avanços na tecnologia de biomateriais e na obtenção de células-tronco. Este capítulo tem o objetivo de esclarecer a importância das condições de cultivo e das propriedades dos *scaffolds* no desenvolvimento de tecidos *in vitro*. Inicialmente, é feita uma breve discussão acerca dos tipos de *scaffolds* e da importância de utilizar a técnica de *electrospinnig* nessa área. Na sequência, é discutida a aplicação de diferentes técnicas de semeadura e cultivo. Por fim, é discutida a importância da modelagem na engenharia de tecidos. Este capítulo está na forma de artigo de revisão, na língua inglesa, o qual foi submetido para a revista *Journal of Biological Physics* e está sob revisão.

Artigo 2

RELEVANT CULTURE CONDITIONS AND 3D ARCHITECTURE FEATURES AND THEIR MECHANISTIC MODELING FOR MESENCHYMAL STEM CELL GROWTH IN ELECTROSPUN SCAFFOLDS

Ágata Paim [*,1,2], Isabel C. Tessaro[1], Nilo S. M. Cardozo[1], Patricia Pranke[2,3]

[1]Department of Chemical Engineering, Universidade Federal do Rio Grande do Sul (UFRGS), R. Eng. Luis Englert, s/n. Porto Alegre, Rio Grande do Sul 90040-040, Brazil.

[2]Faculty of Pharmacy, Universidade Federal do Rio Grande do Sul (UFRGS), Av. Ipiranga, 2752. Porto Alegre, Rio Grande do Sul 90610-000, Brazil.

[3]Stem Cell Research Institute, Universidade Federal do Rio Grande do Sul (UFRGS), Av. Ipiranga, 2752. Porto Alegre, Rio Grande do Sul 90610-000, Brazil.

**Corresponding author (Ágata Paim)*

Present address: Department of Chemical Engineering, Universidade Federal do Rio Grande do Sul (UFRGS), R. Eng. Luis Englert, s/n. Porto Alegre, Rio Grande do Sul 90040-040, Brazil

Phone/Fax: +55 51 33085257

E-mail address: agata@enq.ufrgs.br

Abstract

Tissue engineering is a multidisciplinary field of research, in which the cells, biomaterials and processes can be optimized to develop a tissue substitute. Three-dimensional (3D) architecture features from electrospun scaffolds such as porosity, tortuosity, fiber diameter, pore size and interconnectivity have a great impact on cell behavior. Regarding tissue development in vitro, culture conditions such as pH, osmolality, temperature, nutrient and metabolites concentrations dictate cell viability inside the constructs. The effect of different electrospun scaffold properties, bioreactor designs, mesenchymal stem cell culture parameters and seeding techniques on cell behavior can be studied individually or combined with phenomenological modeling techniques. This work reviews the main culture and scaffold factors that affect tissue development in vitro regarding the culture of cells inside 3D matrices. The mathematical modeling of the relationship between these factors and cell behavior inside 3D constructs has also been critically revised, focusing on mesenchymal stem cell culture in electrospun scaffolds.

Keywords: stem cells, tissue development, electrospun scaffolds, phenomenological modeling.

3.1 Introduction

Tissue engineering is a potential alternative for tissue transplants and applies basic principles of engineering to restore, preserve and/or enhance tissue function [1]. In tissue engineering, biomaterials can be engineered to produce scaffolds that mimic the extracellular matrix environment, considering appropriate architecture, biodegradability, biocompatibility and mechanical properties [2].

There are commercial devices available for tissue engineering but their high cost can impair the treatment of large tissue damage [3]. In addition, according to the regulated commercial products presented by Place, Evans and Stevens [4], 87 % of these products use animal derived materials (e.g. porcine, bovine, equine or rat collagen or decellularized tissue), 37% present nutrient diffusion limitations (products in sheet form), and only 25% contain cells (e.g. MACI, Hyalograft C autograft and CaRes contain chondrocytes, and TransCyte, Apligraf and Dermagraft contain human fibroblasts). In order to reduce risks of adverse immunological response and animal component contamination and pathogen transmission, many efforts are being made to develop low cost xeno-free (with no animal-derived components) devices [5,6].

The combination of different scaffold fabrication techniques – freeze-thawing [7], knitting [8], braiding [9], fused deposition modelling [10] – and biomaterials – natural [11], synthetic [7,9,10], hybrid [8] – have been explored in several commercial products. After an initial focus on the development of skin substitutes for burns treatment, the engineering and availability of devices for other tissue, such as bone [12], cartilage [13], vascular [14] and nerve [15], have become possible.

Many tissue-engineering strategies are based on the culture of autologous cells in scaffolds – BioSeed-C, CaRes, Hyalograft C autograft, MACI, Neo-bladder, VascuGel [4,13]. However, autologous cell sampling requires an invasive procedure and may not provide a sufficient cell number for expansion or transplant techniques [16,17]. Meanwhile, mesenchymal stem cells (MSCs) are a potential alternative for tissue regeneration because of their differentiation potential and highly proliferative and immune privileged characteristics [17–20].

However, the success of cell culture in three-dimensional scaffolds requires adequate culture conditions. Beyond cell viability, the culture parameters should be able to provide chemical, electrical and mechanical stimuli to induce specific cell responses and generate functional tissue [21,22]. In this review, the main scaffold architecture and culture conditions

features affecting tissue development *in vitro* are discussed with an emphasis on the culture of mesenchymal stem cells in electrospun scaffolds. Furthermore, tissue engineering applications of several bioreactor systems and seeding techniques are synthesized. Regarding these process variables, mechanistic modeling applications in tissue engineering are reviewed.

3.2 Scaffolds

Several types of biomaterials can be used as scaffolds in tissue engineering, such as films, beads and porous three-dimensional matrices (Figure 3.1).

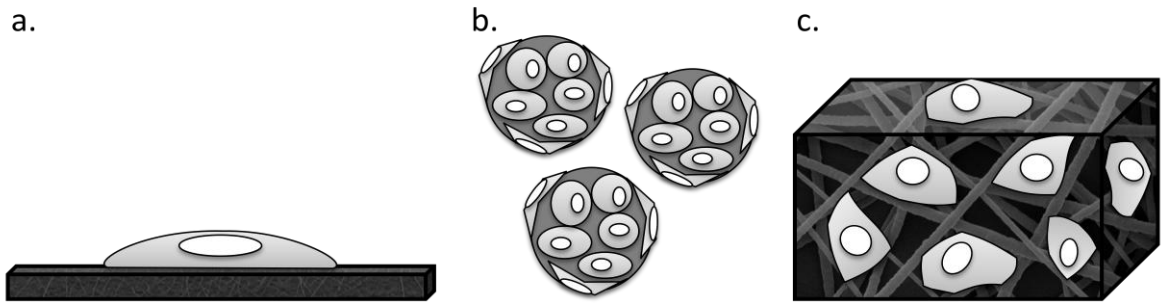

Figure 3.1: Types of structures for cell attachment and culture: film (a), beads (b), porous scaffold (c)

Films can be used as bi-dimensional (2D) scaffolds and, along with MSCs, can be employed to develop substitutes for vascular tissue [23]. However, 2D scaffolds are unable to support *in vitro* cell growth and organization in a tissue-like structure because *in vivo* the extra-cellular matrix (ECM) provides a three-dimensional (3D) microenvironment for the cells [24]. While 2D cultures are not affected by biophysical properties of the matrix, 3D scaffolds provide physical and chemical signals to guide tissue development [25]. In this context, the interaction of MSCs with biomaterials can be investigated using a 2D platform to determine suitable models for further investigation in 3D structures for bone engineering [26]. In addition, porous films seeded with cells can be stacked to engineer a 3D corneal substitute [27].

Three-dimensional scaffolds have been fabricated in the form of beads or blocks with a defined shape [28]. Beads are usually alginate [29], collagen [30], calcium phosphate – e.g. tricalcium phosphate [29] –, and polymer [31] based spherical structures designed for further molding into a 3D defined shape [30–32] or for injection for minimally invasive treatment to repair bone defects [29]. Beads and injectable hydrogels have also been used as soft tissue fillers in adipose [33] and cartilage [34] tissue engineering. Hydrogels are composed of

crosslinked hydrophilic polymer chains and can be produced in specific shapes other than microspheres. However, their application is usually limited to soft tissue due to their poor mechanical properties [35].

MSCs have been cultivated in ceramic [36], metallic [37] and polymeric [38] porous 3D solid scaffolds to develop substitutes for load-bearing tissue. However, metals are non-resorbable [37] and ceramics present low fracture toughness and brittleness [39]. On the other hand, synthetic biodegradable polymers have be used to develop 3D porous scaffolds for hard [40] and soft [41] tissue engineering due to their adequate mechanical properties and degradability.

The use of biodegradable polymer blends in tissue engineering allows for adjustment of the scaffold performance in terms of biocompatibility, processability, mechanical resistance and degradation rate [42]. Aliphatic polyesters, such as polycaprolactone (PCL), polylactic acid (PLA), polyglycolic acid (PGA) and their copolymers degrade mostly by the hydrolysis of the ester bonds in acid monomers that can be removed from the body by metabolic routes, characterizing them as bioresorbable materials [43,44]. However, degradation byproducts can affect the medium acidity, and consequently, cell viability, migration and angiogenesis [45]. The local accumulation of these byproducts can be avoided with a perfusion culture system, which can also reduce the polymer degradation rate [46].

The fabrication process can determine the architecture and mechanical properties of the scaffold. The more common techniques to produce polymeric porous 3D structures for tissue engineering are gas foaming, fiber extrusion and bonding, electrospinning, solid free-form fabrication, three-dimensional printing, phase separation, solvent casting/particulate leaching, freeze-drying and emulsion freeze-drying [41]. However, interconnectivity and pore size and shape are not always controllable with most of these methods [47].

According to Pulikkot et al.[48], when compared to non-porous and microporous polycaprolactone scaffolds, microfibrous matrices enhanced cell proliferation as a result of the higher surface roughness and area available for cell adhesion. Electrospinning is a technique capable of producing micro and nanofibrous scaffolds with interesting characteristics for tissue engineering, allowing for the use of a wide range of polymers. The self-organization process of the fibers is induced by electrostatic repulsion forces (Figure 3.2), assigning to the technique high versatility in terms of morphology, surface topology and fiber properties control [49].

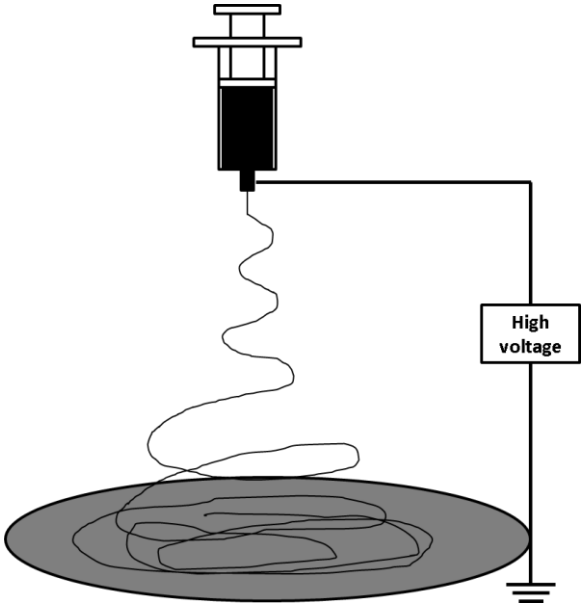

Figure 3.2: Electrospinning setup scheme

Electrospun scaffolds have high packing density (ratio of surface area to total volume), highly interconnected pore network and fibers with diameters similar to the dimensions of the extracellular matrix protein networks [50]. Besides this, electrospinning also enables the fiber thickness to be controlled through the manipulation of process variables, allowing for the study of the impact of the porous matrix spatial architecture on cell behavior [51].

Due to their unique features, the use of nanofibrous electrospun scaffolds in tissue engineering is expanding rapidly. Polycaprolactone/collagen/hydroxyapatite (PCL/col/HA) (Phipps et al., 2011), fibrinogen/polydioxanone (Fg/PDO) (Francis et al., 2016) and polycaprolactone/polylactic acid (PCL/PLA) (Yao et al., 2017) nanofibrous electrospun scaffolds have been shown to promote bone regeneration in vitro when seeded with human MSCs. In diabetic animal models, 3D poly(lactic acid-co-glycolic acid) (PLGA) electrospun scaffolds have been used for chronic wound repair [55], while poly-L-lactide acid (PLLA) electrospun devices have been able to improve insulin secretion [56]. Polymeric nanofibrous electrospun scaffolds have also been applied in clinical trials for the treatment of cutaneous leishmaniasis [57], diabetic foot ulcers [58], and for human pelvic floor reconstruction [59].

3.3 Scaffold architecture impact on cell behavior

The chemical nature and architecture of a 3D scaffold can affect cell proliferation and differentiation due to their importance in cell adhesion and migration and in mass transport within the matrix [60].

The scaffold porosity has a direct impact on the supply of nutrients to the cells, metabolite dispersion, pH local stability and cell signaling [61]. Higher porosities are known to support larger cell densities and to enhance cell proliferation and differentiation [62,63]. In addition, scaffolds with higher porosity often present higher permeability and cell infiltration [64,65]. However, a larger void fraction can lead to poor mechanical resistance [64]. Thus, the biomaterial porosity must be optimized to allow for cell interaction and provide the mechanical properties required for the intended application.

Tortuosity is another factor that has an impact on mass transport, affecting the nutrients effective diffusivity and the cell migration rate within the scaffold [61]. The tortuosity refers to the path that the culture medium has to take through the interconnected pores to get from one extremity of the scaffold to another. Thus, scaffolds with high tortuosity present high resistance to fluid passage through the porous structure, resulting in low permeability.

Pore size should also be appropriate to allow for cell spreading and network formation and its optimal value usually depends on the material of the scaffold and on the cell type [25]. According to Fu and Wang [66], the optimal mean pore diameter is the approximate diameter of the cell. This is because pore size establishes the proximity between the cells in the initial stages of the culture and the space available for their three-dimensional organization during tissue development [61]. Although large pores can enhance cell proliferation, excessively large pores can be prejudicial to the mechanical properties of the structure [67] and discourage the extracellular matrix synthesis between the fibers [68].

In fibrous scaffolds, mean fiber diameter can affect the porosity and pore size mean values and distribution. In a range from 1 to 2.5 μm, electrospun scaffolds with higher fiber diameters can be associated with higher porosity [69]. However, in a range of 1 to 10 μm, fiber thickness may not present a linear correlation with the porosity [70–72]. Elsayed et al. [69] observed the highest cell infiltration and migration through the electrospun scaffolds with the largest pore size and greatest porosity. In addition, scaffolds with smaller fiber diameters present smaller pores [71,73], which can hinder cell migration and colonization [50]. Furthermore, while electrospun scaffolds with smaller fiber diameters can present higher human MSC densities at the beginning of the *in vitro* cell culture, larger fiber diameters scaffolds can influence the cellular phenotype and differentiation [74].

Figure 3.3 presents a scheme of a porous structure where the architectural features discussed above are illustrated.

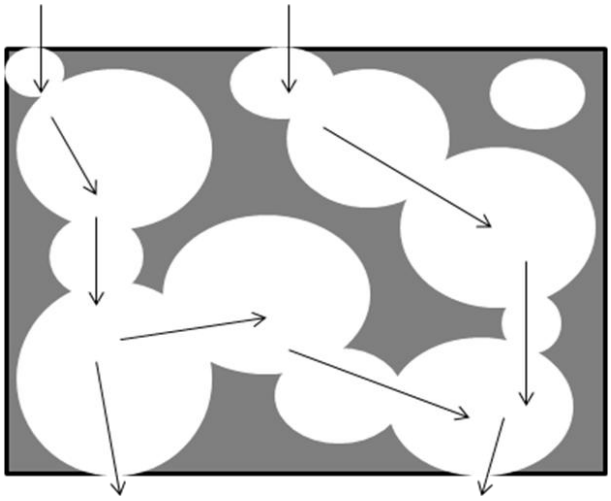

Figure 3.3: Architectural features of three-dimensional scaffolds. The porosity (void fraction) is indicated by the amount of blank space and the pore size and geometry is represented by the size and geometry of the blank spaces; the tortuosity is illustrated by the paths signaled with black arrows

3.4 Culture conditions

The culture conditions directly affect cell behavior and tissue development *in vitro*. Parameters such as pH, osmolality and temperature should be kept in an optimal operating range to ensure the viability of the cells. Other factors, like nutrient and metabolites concentrations can be used to induce a specific cell reaction. Thus, some key culture variables that influence the cell culture are discussed below.

3.4.1. pH and osmolality

The most appropriate pH for the majority of mammalian cells is between 7.2 and 7.4. The decrease of the pH of the culture medium leads to lower cell proliferation and glucose uptake rate [75]. The main reason for pH variation in the culture medium is the production of carbon dioxide by metabolic processes. A buffer of bicarbonate-carbon dioxide provides an excellent control of the pH while the cell culture remains in an incubator (usually with 5 % CO_2) [76].

Cells need an isotonic environment because of the necessity to maintain the osmotic pressure over the culture, usually between 260 e 320mOsm/kg. Hypo and hyperosmotic cultures, when compared to cultures with a physiologic osmolality, can present smaller

extracellular matrix (ECM) synthesis and reduced cell metabolism, and in extreme cases lead to cell death [77].

3.4.2. Oxygen concentration

Oxygen levels lower than the atmospheric concentration (21%, v/v) can characterize a hypoxia condition and are part of the physiologic conditions found *in vivo* in the microenvironment of several stem-cell types (1 - 8%, v/v). Under hypoxia, oxygen is not only a nutrient but becomes a signaling molecule that acts on cell development and organization [78]. Human MSCs under hypoxia initiate the exponential phase of growth earlier and have reduced nutrient uptake and inhibitory metabolite production, when compared to cell cultures in normoxia [79].

Culture of human MSCs under hypoxia can modify the conversion of glucose in lactate (gradual accumulation of lactate) and change the energy production metabolism from aerobic to anaerobic [80]. Cell expansion under this condition can also affect the differentiation potential of MSCs through the up-regulation of the transcriptional expression of hypoxia-inducible factor-2 alpha (HIF-2α) [81]. While the HIF-2α can promote the proliferation of MSC [82], HIF-1α, a similar transcription factor mediating the cellular response to hypoxia, can stimulate proliferation, migration and angiogenesis of MSC [83]. Low oxygen tensions can be used in rotating bioreactors but can lead to reduced and non-uniform ECM component deposition and, consequently, smaller tissue size [84].

3.4.3. Glucose concentration

Glucose is an important metabolic fuel and a limiting nutrient for MSC culture because their ATP production occurs mainly through glycolysis, which leads to the degradation of glucose into pyruvate [85]. According to Machado [86], glucose concentrations of approximately 5mM propitiate higher viability and proliferation of human dental stem cells. The glucose can also affect the oxygen uptake rate of chondrocytes, resulting in near anoxia region formation in scaffolds cultivated with low glucose medium [87]. Furthermore, cell viability has shown to be hindered by carbon sources and not oxygen availability in three-dimensional tumors [88].

Glucose concentration can drop drastically to 0.5 or 1.5 mM, within three days in cell cultures with low glucose medium, under hypoxia and normoxia, respectively, leading to reduced cell viability [89]. According to Deschepper et al. [80], combined low oxygen and

glucose depletion leads to cell shrinking and decreased cell viability and ATP production. Furthermore, not a single viable cell is observed after 3 days in cultures with no glucose with or without bovine fetal serum addition (which contains a small glucose concentration).

On the other hand, high glucose conditions can suppress bone-marrow MSC proliferation and migration. This condition can activate glycogen synthase kinase-3β (GSK3β), which inhibits the expression of cyclin D through the Wnt/β-catenin pathway, reducing cell proliferation. Simultaneously, the migration ability of the cells is reduced by the activation of GSK3β, which can decrease C-X-C chemokine receptor type 4 (CXCR4) expression via stromal cell-derived factor 1 (SDF-1)/CXCR4 signaling [90].

3.4.4. Toxic metabolite concentration

In glycolysis, cells convert pyruvate by lactate dehydrogenase (LDH) to lactate and can lead to lactate accumulation at high glycolytic rates due to the increase of lactate production and efflux from the cells [91]. Mammalian cells, including MSCs, can also produce energy through glutaminolysis, generating ammonia and glutamate by hydrolysis of glutamine and lactate or alanine by further conversion of pyruvate [92]. The accumulation of toxic metabolites such as lactate and ammonia can change the pH and the osmolality of the culture medium and inhibit cell growth. Lactate concentrations up to 20 mM inhibit MSC growth from the fifth day of cultivation [93]. According to Schop et al. [92], the source of the MSCs can influence cell metabolism and the capacity of the cells to tolerate high concentrations of toxic metabolites.

Metabolite concentration can also affect cell morphology, changing the fibroblast form of the MSCs to a more stretchy or cubic morphology. This can be related to the alkalinization or acidification of the cytoplasm, induced by high lactate and ammonia concentrations, respectively. However, human MSCs do not lose their differentiation potential when their growth is hindered by high amounts of lactate or ammonia in the culture medium [92].

3.5 Bioreactors

Dynamic culture systems, such as spinner flask, rotating systems and perfusion bioreactors (Figure 3.4), can be used to reduce mass transport limitations *in vitro* and/or to optimize a specific process, such as cell expansion, differentiation, extracellular matrix (ECM) synthesis or growth factor secretion. A dynamic culture more efficiently mimics the natural environment in which the scaffold will be transplanted afterward because it can

regulate the cell microenvironment and simulate different conditions of oxygen and shear stress. Furthermore, bioreactors can be designed to control time and spatial cell signaling through the incorporation of biological or physical stimuli [94].

Spinner flask and stirred tank bioreactors (Figure 3.4a) have been widely used to expand MSCs in commercial microspheres which are also called microcarriers, due to the enhanced mass transport inside the constructs and resultant higher cell growth [95]. In order to optimize MSCs growth, different microcarriers [96], culture medium [96–98] and shear stress levels [99] have been studied in stirred bioreactors. However, contrary to microcarriers, tissue substitutes require appropriate geometry and functions, usually being cultivated in dynamic systems with perfusion and rotation (Figure 3.4b-f). Regarding engineered 3D scaffolds, the use of bioreactors in tissue engineering constitutes an alternative for providing appropriate nutrient supply, residual removal, gas exchange and mechanical forces stimulus for cells [60].

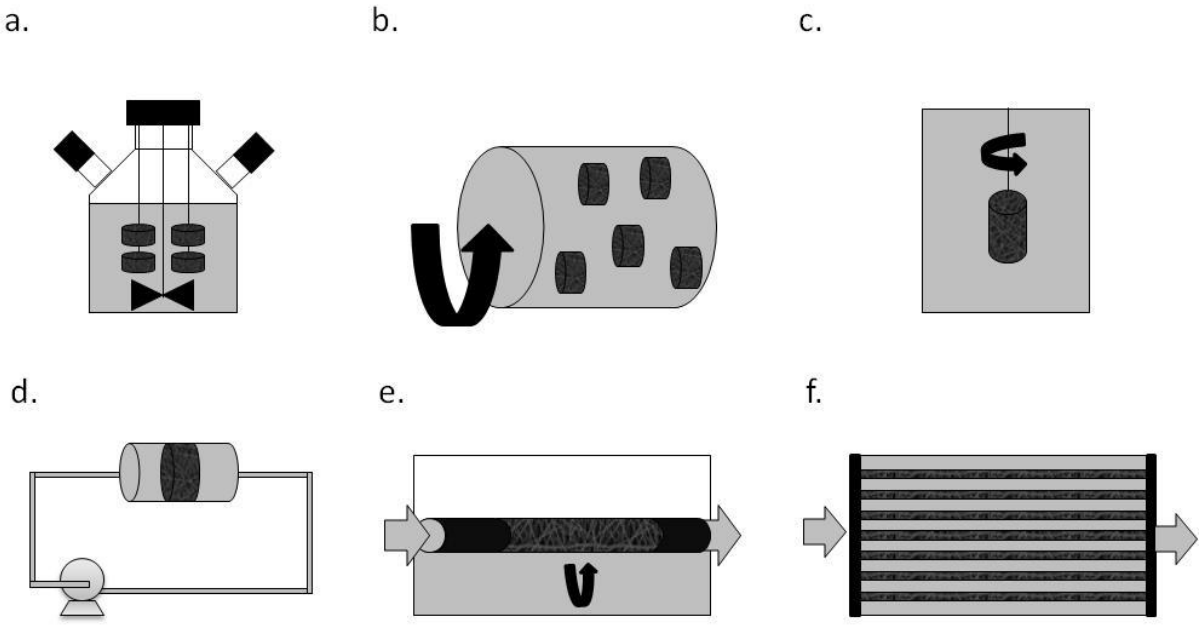

Figure 3.4: Bioreactor types for cell culture in tissue engineering (culture medium in grey, air in white): spinner flask (a), rotating wall (b), rotating bed (c), perfusion (d), rotating bed perfusion (e) and hollow fiber (f)

Rotating wall bioreactors (Figure 3.4b) provide mechanical stress stimulation, which induces osteogenic and chondrogenic differentiation [100]. This system involves lower shear stress than other dynamic culture systems, while also resulting in homogeneous cell distribution due to enhanced mass transport. In a similar way, bioreactors with a rotating bed

(Figure 3.4c), where the scaffold rotates instead of the bioreactor wall, have been used to cultivate human umbilical vein smooth muscle cells in tubular electrospun scaffolds. Elsayed et al. [69] showed that a rotation dynamic system promoted cell infiltration through the scaffold thickness and increased cell proliferation when compared to a static culture.

Other bioreactors use flow perfusion (Figure 3.4d) to provide higher nutrient transport, leading to enhanced cell viability and uniform distribution through 3D scaffolds [101]. Higher cell growth, osteoblastic differentiation induced by the shear stress [63,102–104], and cell migration [105–108] are often observed in perfusion bioreactors when compared to static culture. Furthermore, oxygen concentration gradients can be produced in perfusion bioreactors to mimic *in vivo* ECM conditions and enhance cell migration and growth [109].

Direct perfusion bioreactors have also been shown to enhance ECM deposition and distribution [104,110]. Liao et al. [111] used perfusion bioreactors to generate an ECM coated in electrospun microfibrous scaffolds by cultivating chondrocytes and then decellularizing the construct. The constructs were later used for MSC chondrogenic differentiation under serum-free conditions and with no transforming growth factor beta 1 (TGF-β1) addition. Thibault et al. [112] also used perfusion flow to induce ECM deposition by MSCs in an electrospun scaffold followed by decellularization of the construct and reseeding with MSCs, but used osteogenic medium and focused on osteogenic differentiation.

In direct perfusion systems, it is important to establish an optimal perfusion flow rate to avoid cell death due to high shear stress [103]. Small pores can also result in high shear stress levels, with bioreactor cultures being mainly performed with porous matrixes with mean pore sizes in the range of 100 to 500μm, which are not possible in electrospun scaffolds (maximum mean pores of 45μm reported by Pham et al. [71]). The perfusion culture of human MSCs seeded in electrospun nanofibers can lead to initial round-shaped morphology and may result in cell proliferation, chondrogenic differentiation and ECM synthesis similar to those obtained in static culture [113]. Gugerell et al. [114] also obtained no improvement with direct perfusion of MSCs seeded in hydrogels or on top of the bottom layer in stacked electrospun scaffolds.

One alternative to reduce shear stress inside the pores in perfusion systems is to use a bypass to release pressure build-up [115]. Fixed bed fibrous bioreactors can also allow for lower shear stress inside electrospun scaffolds [116]. Yeatts et al. [117] used an indirect perfusion system with flow through a packed bed of electrospun scaffolds seeded with human MSCs to produce tissue substitutes for further subsequent implantation into rat femoral

condyle defects. Kim and Ma [118] compared two indirect perfusion systems with parallel flow and transverse flow for growth factor secretion by human MSCs in 3D constructs. It was verified that parallel flow allowed for cell secreted basic fibroblast growth factor (FGF-2) accumulation in the scaffolds whereas transverse flow increased the mass transport through the scaffold and affected FGF-2 redistribution in the construct.

For direct perfusion, da Silva et al. [113], Grayson et al. [119], Dahlin et al.) [120], and Santoro et al. [121] used a system in which the flow split in several channels, reaching lower flow rates and reducing shear stress in electrospun scaffolds. However, the culture medium was the same for all the scaffolds and it was not possible to control the individual metabolite production, nutrient consumption and flow because each scaffold has a random geometry and consequently results in a different resistance to flow, as pointed out by Dahlin et al. [120].

On the other hand, medium perfusion and scaffold rotation can be combined in a direct perfusion bioreactor with rotating bed (Figure 3.4e). Diederichs et al. [122] compared the culture of human MSCs seeded in macroporous ceramic scaffolds in static conditions and in a direct perfusion bioreactor with rotating bed. Under the proposed dynamic conditions, high glucose consumption and lactate production indicated increased cell proliferation. In addition, the bioreactor promoted enhanced osteogenic differentiation. Neumann et al. [123] also expanded human MSCs in a perfused rotating bed (cell carrier slides), but used a disposable bioreactor. Their dynamic culture scheme provided low shear stress and high cell yields while maintaining MSC morphology and stemness characteristics (specific MSC surface markers and osteo/adipo/chondro lineages differentiation potential).

Tubular electrospun scaffolds have also been seeded with human MSCs for cultivation in rotating bed perfusion bioreactors with alternate exposure to air and culture medium phases. This dynamic culture system, when combined with appropriate growth factors and serum amounts, stimulated MSC differentiation into a smooth muscle cell phenotype. The bioreactor culture also increased the ECM synthesis and deposition and the homogeneity of cell distribution on the scaffold surface it also presented cell colonization inside the scaffold – which was not observed in static culture due to small pore size [124].

Another dynamic system that has been used to produce bone tissue substitutes with MSCs is the hollow fiber bioreactor (Figure 3.4f), in which cells are seeded in the extracapillary space and culture medium flows inside the hollow fiber lumen [125]. Furthermore, higher cell density, proliferation and osteogenic differentiation can be achieved

by 3D scaffolds seeded with MSC cultures in bioreactors with combined perfusion and cyclic compression [126]. Furthermore, in order to generate functional tissue responsive to both mechanical and electrical signaling, MSCs have been incorporated in electrospun fibers and cultivated in bioreactors with dynamic uniaxial strain and electrical stimulus [21].

3.6 Cell seeding

The seeding density of cells can influence tissue development because high cellularity increase the cell-cell contact and communication. However, its effect is not so evident when cells become confluent with culture time, which occurs with high cell concentrations in long-term cultures [127]. Cell seeding methods can be static (droplet or suspension) or dynamic (agitation, vacuum, centrifugation, stirring, rotational, and perfusion), observing that in some cases (stirred, rotational and perfusion) bioreactors can be used for cell seeding by using a cell suspension instead of the culture medium [128]. As the seeding methods affect the quantity and the distribution of viable cells adhered to the scaffolds at the beginning of the culture, the main features of these seeding methods, schematized in Figure 3.5 (except for stirring, rotational, and perfusion, already presented in Figure 3.4), are discussed below.

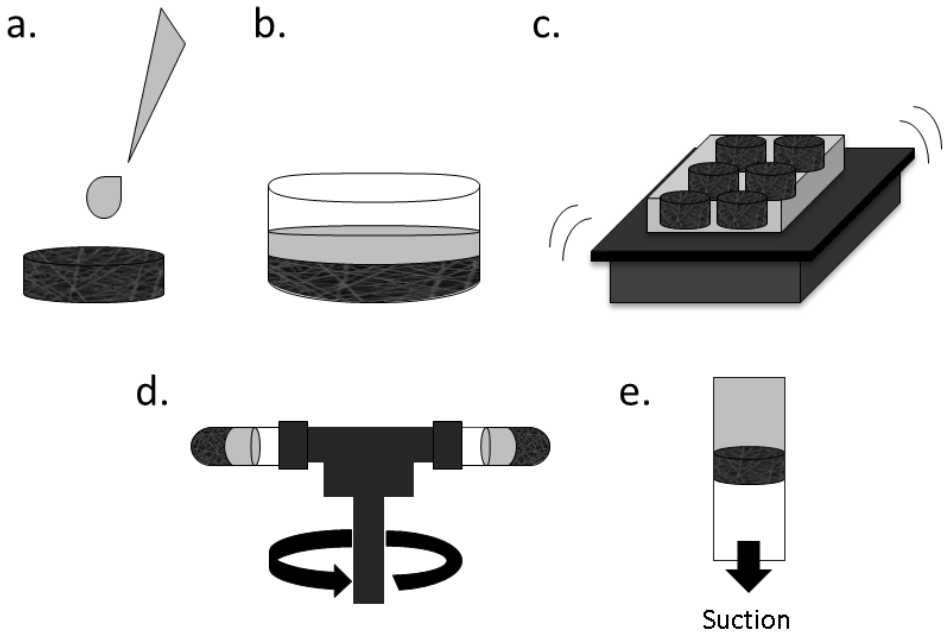

Figure 3.5: Seeding methods (cell suspension in grey): droplet (a), suspension (b), agitated (c), centrifugation (d), vacuum (e)

Static methods by droplet (Figure 3.5a) or suspension (Figure 3.5b) are simpler but have a low level of efficiency and superficial adhesion. The droplet seeding, for instance, can

lead to 20 to 50 % of cells not attached to the scaffold due to breakup of the cell suspension and further floating of the cells [68]. Yamanaka et al. [129] used an alternative droplet seeding, in which the floating of MSCs was avoided by using an absorbent surface under the scaffold to force the flow of the cell suspension from the top to the bottom of the scaffold. However, there is no evidence that this would be an effective solution for electrospun scaffolds as they used scaffolds produced by solvent casting and particulate leaching, with large and interconnected pores.

Other methods, such as vacuum seeding (Figure 3.5e) [130] and centrifugation seeding (Figure 3.5d) [131,132] require small cell quantities and can be applied to reduce the time of the procedure, increase cell infiltration and homogenize their distribution in 3D scaffolds. However, scaffold porosity and pore size may affect the results of both vacuum [133] and centrifugation [132] seeding. Accordingly, different systems and protocols result in distinct seeding efficiencies and even optimized protocols for these methods can lead to results inferior to those with static seeding [129]. Furthermore, Griffon et al. [128] studied MSC attachment with several seeding techniques and verified that the scaffold material and structure could be determinant in seeding efficiency.

Regarding electrospun scaffolds, Wanasekara et al. [134] observed that nanofiber and microfiber structures presented different fibroblast infiltration and may require distinct vacuum pressures to optimize cell distribution inside the scaffolds. In addition, epithelial cells have presented higher viability with the centrifugal method than with static seeding [135].

The most widely used dynamic methods are stirred (Figure 3.4a), agitated (Figure 3.5c) and perfusion (Figure 3.4d) seeding. The first two have higher efficiency levels than static methods, but the amount of adhered cells depends on the cell concentration in the seeding solution [136]. Perfusion systems have higher efficiency levels and lower standard deviations for the number of cells adhered to scaffolds than static seeding methods [137]. When compared to droplet or stirred seeding, perfusion presents higher cell viability and uniformity of cell distribution [138]. A rotating bed scheme (Figure 3.4e) can be used in perfusion bioreactors to increase the homogeneity of the cell distribution inside 3D scaffolds [110]. Besides this, perfusion seeding can be optimized considering the inverse correlation between flow rate and cell seeding efficiency. Due to these characteristics, perfusion bioreactors have been used for seeding in a variety of systems, including ceramic scaffolds with goat MSCs [110], fibrous scaffolds with human MSCs [139], electrospun scaffolds with human fibroblasts [137] and rat MSCs [140] for subsequent cultivation.

The thickness of electrospun scaffolds is limited by the reduction of fiber deposition efficiency caused by the insulating effect of deposited fibers and consequent reduction of electrostatic force applied on the polymeric solution [141]. For applications that require high volume of tissue, thin scaffolds can be assembled in a multilayer form to obtain the desired thickness [142–146]. According to Ardakani et al. [147], cells cannot detach from one layer and adhere to an adjacent layer naturally, especially when there is liquid between the surfaces. Thus, in multilayered configurations, the position and disposition of the seeding surfaces can be important for the final cell distribution and the drag of cells with the passage of the flow.

3.7 Modeling scaffold properties and impacts

Modeling methods are mainly used to determine 3D scaffold architectural properties or analyze their impact on nutrient transport and cell growth, adhesion, deformation and detachment [148–156]. In addition, the process of scaffold degradation can also be studied and modeled to evaluate tissue development [157–162].

Truscello et al. [155] used a computational fluid-dynamic (CFD) model to predict 3D scaffolds permeability with different pore sizes and resulting different porosities. Santamaría et al. [154] also used CFD modeling to determine permeability and wall shear stress under diverse flow rates for heterogeneous 3D structures with different pore sizes and interconnectivity. Mechanical and biological properties of electrospun nanofibrous scaffolds can also be estimated with mathematical models. Gómez-Pachón et al. [150] predicted the effective Young's modulus of scaffolds with aligned or random fiber disposition, while Decuzzi and Ferrari [149] estimated the cellular adhesion strength as a function of the scaffold roughness and surface energy. These models can be helpful in the design of scaffolds and bioreactors and in situations where experimental measurements of these parameters are not available.

Coletti et al. [148] evaluated the effect of scaffold porosity and permeability variation due to cell density on cell growth and mass transport in 3D perfusion cultures. Simulation results showed that nutrient availability and cell density decrease with time in deeper sections of the scaffold as a result of the pore volume occupation by cells as they proliferate and consequent reduction of the scaffold porosity and permeability. This could indicate that initial cell density and distribution must be optimized in accordance with the scaffold pore size in order to generate homogeneous tissue. Figure 3.6 shows different pore obstruction and size reduction as a result of cell adhesion and growth.

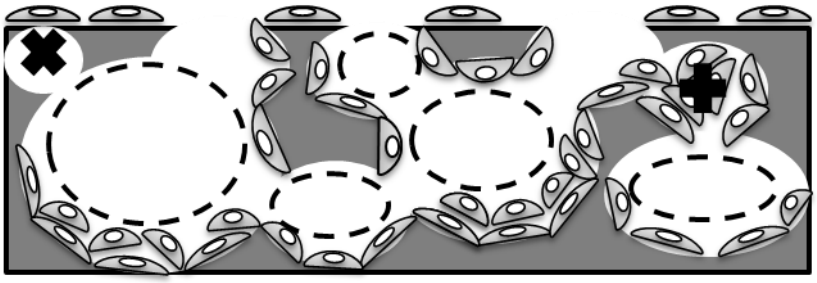

Figure 3.6: Pore obstruction with cell growth: dashed circles represent the reduction of the pore size with cell adhesion on the pore walls; the "x" symbol denotes the obstruction of superficial small pores with cell adhesion on the scaffold surface and the "+" symbol indicates pore obstruction due to cell growth and full occupation of the pore space

Jungreuthmayer et al. [151] used CFD modeling to study cell drag and shear stress through scaffolds with different pore sizes under flow perfusion. It was observed that cells with bridged morphology (adhered to more than one strut) were up to 500 times more deformed when subjected to the same shear stress than cells with a flat morphology (adhered to only one strut). Thus, cell morphology when adhered on the scaffold pore could determine its detachment under perfusion. Mccoy and O'Brien [153] studied the influence of scaffold pore size in cell attachment and detachment under different perfusion flow rates, and correlated cell deformation with cell detachment through experimental and computational techniques. The proposed model could predict cell loss under different flow perfusion as a function of the initial cell number, mean pore size and mean shear stress, and included a constant for cell growth in static cultures. Thus, their model could be used to determine the conditions that minimize the effect of pore obstruction with cell proliferation.

Ma et al. [152] evaluated the effect of porosity in perfusion flow through scaffolds, and observed that smaller porosities and pore sizes presented higher velocities due to the restriction of available space for fluid flow and consequent increase of pressure drop. In addition, low porosity scaffolds presented higher oxygen volume fraction, indicating reduced consumption and thus smaller cell growth. Yan et al. [156] studied the effect of different initial porosities and flow rates on glucose and oxygen transport and on cell growth within 3D scaffolds, taking into consideration the increase of the scaffold porosity due to polymer degradation. It was observed that high initial porosities can reduce nutrient effective diffusivity and availability with time due to the occupation of the void space by cells and, as a result, affect cell distribution inside the scaffold. This model could be useful for scaffolds with rapid degradation times and corroborates with the results of Coletti et al. [148] and Mccoy and O'Brien [153].

Scaffold degradation has also been studied using complex models. Chen et al. [157] developed a mathematical model of the hydrolysis reaction and autocatalysis and considered the effect of mass transport to evaluate the polymeric degradation of microparticles and tissue scaffolds. The stochastic hydrolysis process was described based on a pseudo first-order kinetic equation. The probability of hydrolysis of a single element was modeled as a probability density function dependent on the structural porosity and on the average molecular weight loss. The autocatalytic contribution was modeled as an exponential function of the acid catalyst. The model was able to predict the experimental behavior of degradation and erosion of bulk-erosive polymer structures and evaluated the impact of scaffold architecture and mass transfer on the degradation of porous structures.

Heljak et al. [160] modeled the aliphatic polyester hydrolytic degradation of a 3D porous scaffold using reaction-diffusion equations for the concentrations of ester bounds and monomers, and also considered the autocatalytic effect of soluble monomers. The model could predict the degradation time and changes in the molecular weight and mass of a bone scaffold. At a later date, these authors used this model to study the effect of different porosities on the degradation process of a poly(DL-lactide-*co*-glycolide) scaffold under dynamic or static conditions. Simulation results indicated that high porosity, fluid flow or periodic replacement of the medium (in static conditions) could reduce polymeric scaffold degradation [159]. The model could be used to optimize scaffold porosity and to determine when medium replacement is necessary in static culture, based on the accumulation of degradation by-products.

Shazly et al. [161] developed a computational model of bulk hydrolysis of bioresorbable vascular poly(L-lactide) scaffolds in a post-implantation *in vivo* environment. The authors studied the degradation by-product transport via diffusion and convection by considering the blood flow (in the lumen and the porous arterial wall) when the erodible scaffold is implanted within the arterial wall. The polymer degradation and autocatalysis was modeled as a first-order reaction with a system of reaction-diffusion equations that considered the systematic formation of four oligomer groups and lactic acid. The metabolism of lactic acid in a healing zone with varying diffusivity (to account for tissue remodeling) and in the arterial wall was described as a first-order reaction and incorporated in reaction-diffusion-convection equations. The model could predict the levels of lactic acid that accumulate in local tissue by coupling its production with convective and diffusive transport and metabolic elimination. It was observed that the interplay between the tissue remodeling and the

hydrolysis process regulate the levels of degradation by-products within the tissue and that mass transport is a more effective by-product clearance mechanism than metabolic elimination.This model was later used to evaluate the effect of polydispersity, initial degree of crystallinity and lactide doping in the degradation, erosion and by-product accumulation. It was observed that only the erosion process was sensitive to crystallinity and that all processes were responsive to lactide doping [158].

Akalp et al. [162] proposed a model of tissue growth, enzymatic degradation of an enzyme-sensitive hydrogel and ECM molecules transport within the hydrogel scaffold. Enzymes released by the cells were considered to diffuse through the polymer network and degrade the hydrogel through cross-link cleavage with a Michaelis-Menten kinectics. The transport and deposition of ECM molecules secreted by the cells were modeled with a convection-diffusion-reaction system, considered an inhibition term for ECM deposition. It was shown that an appropriate relationship between scaffold degradation and ECM transport and deposition is necessary to maintain the mechanical properties of the structure. The discussed degradation models could be used in scaffold design to optimize the relationship between architectural and degradation properties.

3.8 Modeling for bioreactors, seeding methods, and culture conditions analysis

Modeling can also be used as a tool for bioreactor design [163–167], seeding process analysis [143,168–170] and culture condition analysis and optimization [22,119,148,171–179].

Singh et al. [167] used CFD modeling to study the velocities and wall shear stress inside and outside a scaffold under uni-axial and bi-axial flow schemes in a rotational bioreactor. It was observed that bi-axial rotations were capable of increasing fluid velocities and shear stress within the scaffolds by combining rotational velocity vectors. This model could be useful in rotational bioreactor design and optimization in a simplified study, as nutrient transport and cell growth are not considered.

Pathi et al. [165] studied parallel perfusion bioreactors with different liquid layer thicknesses above a porous scaffold seeded with granulocyte progenitor cells. Oxygen supply was increased with a larger liquid layer thickness, due to the higher oxygen delivery through hydrodynamic flow, with little contribution of the oxygen permeability of the outer membrane. Through computational modeling it was possible to verify that convective oxygen

delivery provided by culture medium perfusion could overcome diffusion limitations and enhance cell growth.

Devarapalli et al. [163] used CFD modeling to simulate several perfusion bioreactor designs with rectangular or circular shapes and different inlet and outlet flow configurations in order to evaluate the resulting shear stress and pressure drop in porous scaffolds. Homogenous shear stress distribution could be achieved in circular bioreactors with semicircular inlet and outlets. Hidalgo-Bastida et al. [164] also performed CFD simulations to compare circular and rectangular shape perfusion bioreactors, but did not evaluate diverse inlet and outlet shapes. On the other hand, a proposal was made for a mixed design with a rectangular holder for circular scaffolds and a safe distance between the scaffold and the inlet and output to guarantee uniform flow and shear stress through the scaffold.

Schirmaier et al. [166] used mathematical models to determine optimum values for impeller speeds and local shear stress in stirred single-use bioreactors for human adipose tissue-derived MSC expansion under low-serum conditions. With the help of simulation results it was possible to scale-up microcarrier-based cell cultures from spinner flasks to large-scale stirred single-use bioreactors. Thus, CFD modeling could be used not only in the design step but also in the scale-up of bioreactors to guarantee the required conditions for cell expansion and tissue development.

The generation of homogeneous tissue can also be affected by the seeding process with an initial homogeneous cell distribution not necessarily being the best alternative in tissue engineering. Doagă et al. [169] proposed a non-linear kinetic model of cell adhesion in porous scaffolds based on the Langmuir's theory of adsorption to describe cell seeding in a stirred bioreactor. Cell attachment was considered a two-step process with initial recovery of the cell integrin function – inhibited after the trypsinization required for cell detachment from the culture flask for cell counting before cell seeding – and further integrin binding with scaffold sites available for cell attachment. The model was able to represent the experimental process of cell adhesion and reinforced the higher cell seeding efficiencies obtained in protocols with alternative cell detachment treatments other than trypsinization.

Dunn et al. [143] proposed an alternating cell seeding strategy for multilayer matrices to surpass oxygen depletion in the inner core of the scaffold, verified with computational simulations. Modeling cell growth and nutrient transport in a homogeneously seeded scaffold showed the formation of hypoxic regions with time as the cell consumption became higher than oxygen delivery through diffusion. Chung et al. [168] compared the result of various

seeding modes in cell growth in scaffolds and proposed that cell seeding in only the middle portion of the scaffold could increase nutrient availability and homogenize cell distribution and growth in tissue engineered constructs.

In addition, Jeong et al. [170] evaluated the effect of different seeding strategies on cell growth, and identified an optimal set of parameters for obtaining a homogeneous cell distribution in five stacked scaffolds through mathematical modeling. It was observed that the interplay between cell growth and nutrient consumption could be optimized by alternating seeding between unseeded and partially cell-seeded scaffolds (with cells seeded in concentric annulus) (Figure 3.7). These models could be used to develop new strategies for optimal cell seeding based on specific cell proliferation, migration and nutrient consumption.

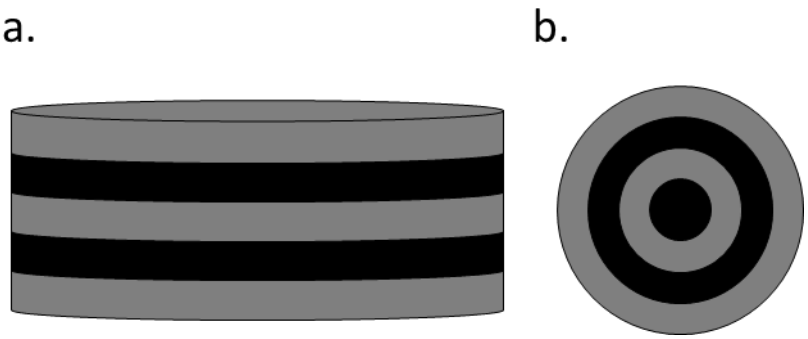

Figure 3.7: Different cell seeding strategies proposed by Jeong et al. [170]: seeded scaffold (grey) intercalated with non-seeded scaffolds (black) (a) and scaffolds seeded in alternating concentric annulus regions (b)

Several modeling applications aim to evaluate and /or identify optimal culture conditions (flow rate, shear stress, fluid velocity, oxygen tension, electrical potential) within scaffolds cultivated in bioreactors. Raimondi et al. [176] used CFD modeling to predict shear stress and fluid velocity in 3D fibrous structures under perfusion. Grayson et al. [119] optimized medium perfusion rate for a direct perfusion bioreactor by predicting the shear stress inside the scaffold. Through mathematical modeling it was possible to evaluate the oxygen transport and verify if the oxygen levels and cell viability were maintained in a range of flow rate values. These models could be used to characterize the bioreactor conditions that cannot always be experimentally measured, such as shear stress and oxygen concentration.

Flaibani et al. [172] used mathematical modeling to identify an optimum flow rate for reaching a maximum cell volume fraction inside 3D scaffolds under perfusion. To achieve this, cell growth was modeled as a function of pore size distribution and oxygen

concentration. It was observed that low flow rates could inhibit cell growth by leading to very low oxygen concentrations (hypoxia) inside pores with different diameters. On the other hand, high flow rates resulted in elevated shear stress levels that could inhibit cell growth or induce cell detachment. This model could be used to estimate cell growth and distribution inside heterogeneous porous scaffolds.

Another option to account for scaffold microorganization was reported by Porter et al. [175]. The authors used microcomputed tomography imaging to define scaffold microarchitecture. Local shear stress was then estimated at various perfusion flow rates to determine an optimal value through association with experimental data of cell growth in the literature. A peak in shear stress of 57 mPa was observed and associated with cell death within the constructs. This model could be used to define limiting and optimal values of local shear stress for cell growth as a function of scaffold microarchitecture.

Chung et al. [179] predicted shear stress levels inside a scaffold under direct perfusion as a function of pore size and its reduction with cell growth. It was observed that the macro average stresses could have a 5 fold increase and that the overall permeability could be reduced dramatically with a slight overall cell volume fraction increase. These changes were associated with the reduction of the scaffold void space with pore occupation by cell and ECM volumes. In the same context, Lesman et al. [173] developed a CFD model to predict the shear stress and pressure drop with different flow rates in 3D cultures under direct perfusion. A cell-layer thickness was considered to account for cell growth impact on the pore space reduction and on the scaffold mass transport. The simulations shows that shear stress average values increased with time due to cell growth and thickening of the cell-layer inside the pores, which corroborates with the time decrease of scaffold permeability constant obtained experimentally. These models could be used to predict permeability and shear stress values for scaffolds with high density of cells or small pore sizes.

Sacco et al. [180] proposed a model where the cells and the ECM compose a biomass phase and the maximum biomass growth rate of the Monod kinetics is a function of shear stress. However, nutrient concentration and shear stress variation in time and space were not considered. Liu et al. [174] compared static and dynamic cultures under direct perfusion with different flow rates using a CFD model that considers both nutrient availability and shear stress stimulation on cell growth kinetics. The cells and the ECM components secreted by the cells were also considered one single phase in a way whereby it is possible to use these

models to consider the shear stress effect on cell growth by stimulation of the ECM synthesis under perfusion.

Zhao et al. [178] used a mathematical model to predict shear stress and oxygen levels inside 3D poly (ethylene terephthalate) (PET) scaffolds under perfusion; three matrices were assembled in series in each perfusion chamber. The simulation results indicated that different flow rates did not yield changes in oxygen levels that could affect cell growth and metabolism. Furthermore, while increased human MSC growth and ECM deposition were observed at low flow perfusion, higher flow rates could upregulate the osteogenic differentiation potential of the cells. Thus, this model was helpful to indicate that shear stress levels could be an important factor regulating human MSC development in 3D scaffolds.

Coletti et al. [148] simulated two flow conditions in a perfusion bioreactor – partial flow (flow channelized through a gap between the scaffold and the bioreactor wall) and total flow perfusion through the scaffold. They studied their impact on oxygen transport and cell growth. The channeling of flow perfusion can occur experimentally as a result of the lack (when this bypass is required and designed to reduce shear stress levels inside the scaffold) or insufficiency of the sealing system. Simulation results were compared and showed that partial perfusion could affect oxygen delivery by reducing convection inside the scaffold and as a consequence could reduce the construct cell density. Thus, this model could be used to evaluate operational flaws and also to design bioreactor bypasses in order to optimize flow conditions and cell growth inside 3D scaffolds.

One example of a partial perfusion bioreactor is given by Campolo et al. [171], where a gap around the scaffold is designed to serve as a by-pass flow. The authors proposed a modeling approach to determine an appropriate flow rate to obtain homogeneous cell distribution in 3D scaffolds under indirect perfusion. Mass transport and reaction information was used in association with flow regime characteristics to calculate the required perfusion flow to maintain a target cell growth rate.

In addition to flow perfusion, electrical variables have also been modeled in bioreactors for tissue engineering purposes. Maidhof et al. [22] characterized the electrical potential of a perfusion bioreactor by modeling its generation and evaluating the electrical field where cardiac constructs were placed. It was observed that the electric potential drop was quite linear and constant through the scaffold length. This model was helpful in validating the generation of scaffolds as functional cardiac constructs exposed to the same electrical field.

3.9 Concluding remarks

The main tissue engineering challenges are related to scaffold design, mass transport and cell infiltration and colonization within the scaffolds. In addition, culture conditions affect cell behavior and vary from one study to another, making the comparison of different experiments difficult. In order to control and study these conditions, bioreactors and modeling techniques can be applied. Regarding the dynamic culture of mesenchymal stem cells in electrospun scaffolds, the cell proliferation and differentiation, and the secretion of growth factors and extracellular matrix components have been studied in different systems and under several culture conditions. Bioreactors with electrical and mechanical stimulation have also recently been studied for the development of functional tissue responsive to these stimuli. However, tissue vascularization, which is important for the maintenance of cell viability *in vivo* after transplantation, is not always evaluated in bioreactor studies. In addition, the co-culture of stem cells and other cell types in bioreactors could reveal important features of tissue function as shear stress and other factors present in dynamic conditions could affect the development of multicellular 3D cultures. While the bioreactor design has to be optimized according to the scaffold and cell characteristics, modeling has its own challenges. There are limitations in measurement techniques, which makes it difficult to validate the model with respect to variables that cannot be measured directly. Thus, the combination of modeling and electrospun scaffolds for stem cell culture still requires research and improvement to fulfill its potential for optimizing tissue development.

3.10 Acknowledgments

The authors wish to thank the Stem Cell Research Institute, the Coordination for the Improvement of Higher Level Personnel (CAPES), the Study and Project Financer (FINEP) for financial support.

3.11 References

[1] R. Langer, J.P. Vacanti, Tissue engineering, Science (80-.). 260 (1993) 920–926.
[2] F.J. O'Brien, Biomaterials & scaffolds for tissue engineering, Mater. Today. 14 (2011) 88–95. doi:10.1016/S1369-7021(11)70058-X.
[3] A.W.C. Chua, Y.C. Khoo, B.K. Tan, K.C. Tan, C.L. Foo, S.J. Chong, Skin tissue engineering advances in severe burns: review and therapeutic applications, Burn. Trauma. 4 (2016) 3. doi:10.1186/s41038-016-0027-y.
[4] E.S. Place, N.D. Evans, M.M. Stevens, Complexity in biomaterials for tissue engineering, Nat. Mater. 8 (2009) 457–470. doi:10.1038/nmat2441.
[5] A. Oryan, S. Alidadi, A. Moshiri, N. Maffulli, Bone regenerative medicine : classic

options , novel strategies , and future directions, (2014) 1–27.
[6] L.E. Fitzpatrick, T.C. McDevitt, Cell-derived matrices for tissue engineering and regenerative medicine applications, Biomater. Sci. 3 (2015) 12–24. doi:10.1039/C4BM00246F.
[7] D. Ku, L. Braddon, D. Wooton, Poly(Vinyl Alcohol) Cryogel, 1999.
[8] R.J. Kumar, R.M. Kimble, R. Boots, S.P. Pegg, Treatment of partial-thickness burns: A prospective, randomized trial using transcyte™, ANZ J. Surg. 74 (2004) 622–626. doi:10.1111/j.1445-1433.2004.03106.x.
[9] W.R. Walsh, N. Bertollo, P. Heuberer, C. Christou, R. Stanton, R. Poggie, Evaluation Of A PLLA Device In-vitro And In An Ovine Model Of Acute Rupture Of The Rotator Cuff, 1 (2015). prgmobileapps.com/AppUpdates/ors2015/Abstracts/abs1185.html.
[10] A. Khojasteh, H. Behnia, F.S. Hosseini, M.M. Dehghan, P. Abbasnia, F.M. Abbas, The effect of PCL-TCP scaffold loaded with mesenchymal stem cells on vertical bone augmentation in dog mandible: A preliminary report, J. Biomed. Mater. Res. - Part B Appl. Biomater. 101 B (2013) 848–854. doi:10.1002/jbm.b.32889.
[11] M. Flasza, P. Kemp, D. Shering, J. Qiao, D. Marshall, A. Bokta, P.A. Johnson, Development and manufacture of an investigational human living dermal equivalent (ICX-SKN), Regen. Med. 2 (2007) 903–918. doi:10.2217/17460751.2.6.903.
[12] D.S. Baskin, P. Ryan, V. Sonntag, R. Westmark, M.A. Widmayer, A prospective, randomized, controlled cervical fusion study using recombinant human bone morphogenetic protein-2 with the CORNERSTONE-SR allograft ring and the ATLANTIS anterior cervical plate, Spine (Phila Pa 1976). 28 (2003) 1219–24; discussion 1225. doi:10.1097/01.BRS.0000065486.22141.CA.
[13] P.C. Kreuz, S. Müller, C. Ossendorf, C. Kaps, C. Erggelet, Treatment of focal degenerative cartilage defects with polymer-based autologous chondrocyte grafts: four-year clinical results., Arthritis Res. Ther. 11 (2009) R33. doi:10.1186/ar2638.
[14] P.A. Stone, A.F. AbuRahma, A.Y. Mousa, D. Phang, S.M. Hass, A. Modak, D. Dearing, Prospective Randomized Trial of ACUSEAL Versus Vascu-Guard Patching in Carotid Endarterectomy, Ann. Vasc. Surg. 28 (2014) 1530–1538. doi:10.1016/j.avsg.2014.02.017.
[15] S. Kehoe, X.F. Zhang, D. Boyd, FDA approved guidance conduits and wraps for peripheral nerve injury: A review of materials and efficacy, Injury. 43 (2012) 553–572. doi:10.1016/j.injury.2010.12.030.
[16] J.L. Olson, A. Atala, J.J. Yoo, Tissue Engineering: Current Strategies and Future Directions, © Chonnam Med. J. Chonnam Med J. 47 (2011) 1–13. doi:10.4068/cmj.2011.47.1.1.
[17] A. Chatterjea, G. Meijer, C. van Blitterswijk, J. de Boer, Clinical application of human mesenchymal stromal cells for bone tissue engineering., Stem Cells Int. 2010 (2010) 215625. doi:10.4061/2010/215625.
[18] C.J. Koh, A. Atala, Tissue Engineering, Stem Cells, and Cloning: Opportunities for Regenerative Medicine, J. Am. Soc. Nephrol. 15 (2004) 1113–1125. doi:10.1097/01.ASN.0000119683.59068.F0.
[19] L.X. Tay, R.E. Ahmad, H. Dashtdar, K.W. Tay, T. Masjuddin, S. Ab-Rahim, P.P. Chong, L. Selvaratnam, T. Kamarul, Treatment outcomes of alginate-embedded allogenic mesenchymal stem cells versus autologous chondrocytes for the repair of focal articular cartilage defects in a rabbit model., Am. J. Sports Med. 40 (2012) 83–90. doi:10.1177/0363546511420819.
[20] K.L. Wong, K.B.L. Lee, B.C. Tai, P. Law, E.H. Lee, J.H.P. Hui, Injectable cultured bone marrow-derived mesenchymal stem cells in varus knees with cartilage defects undergoing high tibial osteotomy: A prospective, randomized controlled clinical trial

with 2 years' follow-up, Arthrosc. - J. Arthrosc. Relat. Surg. 29 (2013) 2020–2028. doi:10.1016/j.arthro.2013.09.074.

[21] C.A. Cook, P.Y. Huri, B.P. Ginn, J. Gilbert-Honick, S.M. Somers, J.P. Temple, H.Q. Mao, W.L. Grayson, Characterization of a novel bioreactor system for 3D cellular mechanobiology studies, Biotechnol. Bioeng. 113 (2016) 1825–1837. doi:10.1002/bit.25946.

[22] R. Maidhof, N. Tandon, E.J. Lee, J. Luo, Y. Duan, K. Yeager, E. Konofagou, G. Vunjak-Novakovic, Biomimetic perfusion and electrical stimulation applied in concert improved the assembly of engineered cardiac tissue, J Tissue Eng Regen Med. 6 (2012) e12–e23. doi:10.1002/term.525.Biomimetic.

[23] Z. Wang, S.H. Teoh, N.B. Johana, M.S. Khoon Chong, E.Y. Teo, M. Hong, J.K. Yen Chan, E. San Thian, Enhancing mesenchymal stem cell response using uniaxially stretched poly(ε-caprolactone) film micropatterns for vascular tissue engineering application, J. Mater. Chem. B. 2 (2014) 5898–5909. doi:10.1039/C4TB00522H.

[24] E. Knight, S. Przyborski, Advances in 3D cell culture technologies enabling tissue-like structures to be created in vitro, J. Anat. 227 (2015) 746–756. doi:10.1111/joa.12257.

[25] B.J. Lawrence, Mass Transfer in Porous Tissue Engineering Scaffolds, Oklahoma State University, 2008.

[26] C. Romagnoli, R. Zonefrati, G. Galli, D. Puppi, A. Pirosa, F. Chiellini, F.S. Martelli, A. Tanini, M.L. Brandi, In Vitro Behavior of Human Adipose Tissue-Derived Stem Cells on Poly(ε-caprolactone) Film for Bone Tissue Engineering Applications., Biomed Res. Int. 2015 (2015) 323571. doi:10.1155/2015/323571.

[27] B.J. Lawrence, M. Devarapalli, S. V Madihally, Flow dynamics in bioreactors containing tissue engineering scaffolds, Biotechnol. Bioeng. 102 (2009) 935–947. doi:10.1002/bit.22106.

[28] T. Asaoka, S. Ohtake, K.S. Furukawa, A. Tamura, T. Ushida, Development of bioactive porous α-TCP/HAp beads for bone tissue engineering, J. Biomed. Mater. Res. Part A. 101 (2013) n/a-n/a. doi:10.1002/jbm.a.34517.

[29] T. Matsuno, Y. Hashimoto, S. Adachi, K. Omata, Y. Yoshitaka, Y. Ozeki, Y. Umezu, Y. Tabata, M. Nakamura, T. Satoh, Preparation of injectable 3D-formed beta-tricalcium phosphate bead/alginate composite for bone tissue engineering., Dent. Mater. J. 27 (2008) 827–834. doi:10.4012/dmj.27.827.

[30] Y.T. Matsunaga, Y. Morimoto, S. Takeuchi, Molding cell beads for rapid construction of macroscopic 3D tissue architecture, Adv. Mater. 23 (2011) 90–94. doi:10.1002/adma.201004375.

[31] J. Wang, Porous Microbeads as Three-Dimensional Scaffolds for Tissue Engineering, in: NNIN REU Res. Accompl., 2010: pp. 32–33.

[32] S. Takeuchi, Cell-laden hydrogel beads, fibers and plates for 3D tissue construction, 2013 Transducers Eurosensors XXVII 17th Int. Conf. Solid-State Sensors, Actuators Microsystems, TRANSDUCERS EUROSENSORS 2013. (2013) 1515–1518. doi:10.1109/Transducers.2013.6627069.

[33] D.A. Young, K.L. Christman, Injectable biomaterials for adipose tissue engineering, Biomed. Mater. 7 (2012) 24104. doi:10.1088/1748-6041/7/2/024104.

[34] D. a Lee, T. Reisler, D.L. Bader, Expansion of chondrocytes for tissue engineering in alginate beads enhances chondrocytic phenotype compared to conventional monolayer techniques., Acta Orthop. Scand. 74 (2003) 6–15. doi:10.1080/00016470310013581.

[35] I. El-Sherbiny, M. Yacoub, Hydrogel scaffolds for tissue engineering: Progress and challenges, Glob. Cardiol. Sci. Pract. 2013 (2013) 316–42. doi:10.5339/gcsp.2013.38.

[36] S. Teixeira, H. Fernandes, A. Leusink, C. Van Blitterswijk, M.P. Ferraz, F.J. Monteiro, J. De Boer, In vivo evaluation of highly macroporous ceramic scaffolds for bone tissue

engineering, J. Biomed. Mater. Res. - Part A. 93 (2010) 567–575. doi:10.1002/jbm.a.32532.
[37] J.F. Blanco, F.M. Sánchez-Guijo, S. Carrancio, S. Muntion, J. García-Briñon, M.C. del Cañizo, Titanium and tantalum as mesenchymal stem cell scaffolds for spinal fusion: an in vitro comparative study, Eur. Spine J. 20 (2011) 1–8. doi:10.1007/s00586-011-1901-8.
[38] J.K. Wise, A.L. Yarin, C.M. Megaridis, M. Cho, Chondrogenic differentiation of human mesenchymal stem cells on oriented nanofibrous scaffolds: engineering the superficial zone of articular cartilage., Tissue Eng. Part A. 15 (2009) 913–21. doi:10.1089/ten.tea.2008.0109.
[39] H. Awaji, T. Matsunaga, S.-M. Choi, Relation between Strength, Fracture Toughness, and Critical Frontal Process Zone Size in Ceramics, Mater. Trans. 47 (2006) 1532–1539. doi:10.2320/matertrans.47.1532.
[40] A. Sadiasa, T.H. Nguyen, B.-T. Lee, In vitro and in vivo evaluation of porous PCL-PLLA 3D polymer scaffolds fabricated via salt leaching method for bone tissue engineering applications., J. Biomater. Sci. Polym. Ed. 25 (2014) 150–67. doi:10.1080/09205063.2013.846633.
[41] S.C. Baker, G. Rohman, J. Southgate, N.R. Cameron, The relationship between the mechanical properties and cell behaviour on PLGA and PCL scaffolds for bladder tissue engineering, Biomaterials. 30 (2009) 1321–1328. doi:10.1016/j.biomaterials.2008.11.033.
[42] A.S. Asran, K. Razghandi, N. Aggarwal, M.G. H., T. Groth, Nanofibers from Blends of Polyvinyl Alcohol and Polyhydroxy butyrate as a potensional scaffold materail.pdf, Biomacromolecules. 11 (2010) 3413–3421.
[43] G.L. Siparsky, K.J. Voorhees, F. Miao, Hydrolysis of Polylactic Acid (PLA) and Polycaprolactone (PCL) in Aqueous Acetonitrile Solutions: Autocatalysis, J. Environ. Polym. Degrad. 6 (1998) 31–41. doi:10.1023/A:1022826528673.
[44] S.H. Barbanti, C.A. Carvalho Zavaglia, E.A. De Rezende Duek, Effect of Salt Leaching on PCL and PLGA (50 / 50) Resorbable Scaffolds 2 . Material and Methods, Mater. Res. 11 (2008) 75–80. doi:10.1590/S1516-14392008000100014.
[45] H.-J. Sung, C. Meredith, C. Johnson, Z.S. Galis, The effect of scaffold degradation rate on three-dimensional cell growth and angiogenesis., Biomaterials. 25 (2004) 5735–5742. doi:10.1016/j.biomaterials.2004.01.066.
[46] J. An, S.C.G. Leeuwenburgh, J.G.C. Wolke, J.A. Jansen, Effects of Stirring and Fluid Perfusion on the In Vitro Degradation of Calcium Phosphate Cement/PLGA Composites, Tissue Eng. Part C. 21 (2015) 1171–1177. doi:10.1089/ten.tec.2015.0016.
[47] Q.L. Loh, C. Choong, Three-dimensional scaffolds for tissue engineering applications: role of porosity and pore size., Tissue Eng. Part B. Rev. 19 (2013) 485–502. doi:10.1089/ten.TEB.2012.0437.
[48] S. Pulikkot, Y.E. Greish, A.H.I. Mourad, S.M. Karam, Establishment of a three-dimensional culture system of gastric stem cells supporting mucous cell differentiation using microfibrous polycaprolactone scaffolds, Cell Prolif. 47 (2014) 553–563. doi:10.1111/cpr.12141.
[49] J.H. Wendorff, S. Agarwal, A. Greiner, Materials, Processing, and Applications von Joachim H. Wendorff, Seema Agarwal, Andreas Greiner 1., (2012).
[50] C. Vaquette, J.J. Cooper-White, Increasing electrospun scaffold pore size with tailored collectors for improved cell penetration, Acta Biomater. 7 (2011) 2544–2557. doi:10.1016/j.actbio.2011.02.036.
[51] Q.P. Pham, U. Sharma, A.G. Mikos, Electrospun Poly(ε-caprolactone) Microfiber and Multilayer Nanofiber/Microfiber Scaffolds: Characterization of Scaffolds and

Measurement of Cellular Infiltration, Biomacromolecules. 7 (2006) 2796–2805. doi:10.1021/bm060680j.

[52] M.C. Phipps, W.C. Clem, S.A. Catledge, Y. Xu, K.M. Hennessy, V. Thomas, M.J. Jablonsky, S. Chowdhury, A. V. Stanishevsky, Y.K. Vohra, S.L. Bellis, Mesenchymal stem cell responses to bone-mimetic electrospun matrices composed of polycaprolactone, collagen I and nanoparticulate hydroxyapatite, PLoS One. 6 (2011) 1–8. doi:10.1371/journal.pone.0016813.

[53] M.P. Francis, Y.M. Moghaddam-White, P.C. Sachs, M.J. Beckman, S.M. Chen, G.L. Bowlin, L.W. Elmore, S.E. Holt, Modeling early stage bone regeneration with biomimetic electrospun fibrinogen nanofibers and adipose-derived mesenchymal stem cells, Electrospinning. 1 (2016) 10–19. doi:10.1515/esp-2016-0002.

[54] Q. Yao, J.G.L. Cosme, T. Xu, J.M. Miszuk, P.H.S. Picciani, H. Fong, H. Sun, Three dimensional electrospun PCL/PLA blend nanofibrous scaffolds with significantly improved stem cells osteogenic differentiation and cranial bone formation, Biomaterials. 115 (2017) 115–127. doi:10.1016/j.biomaterials.2016.11.018.

[55] H. Chen, Y. Peng, S. Wu, L.P. Tan, Electrospun 3D fibrous scaffolds for chronic wound repair, Materials (Basel). 9 (2016) 1–12. doi:10.3390/ma9040272.

[56] A. Fazili, S. Gholami, B.M. Zangi, E. Seyedjafari, M. Gholami, In Vivo Differentiation of Mesenchymal Stem Cells into Insulin Producing Cells on Electrospun Poly-L-Lactide Acid Scaffolds Coated with, Cell J. 18 (2016) 310–321.

[57] S.Y. Silva, L.C. Rueda, M. López, I.D. Vélez, C.F. Rueda-Clausen, D.J. Smith, G. Muñoz, H. Mosquera, F.A. Silva, A. Buitrago, H. Díaz, P. López-Jaramillo, Double blind, randomized controlled trial, to evaluate the effectiveness of a controlled nitric oxide releasing patch versus meglumine antimoniate in the treatment of cutaneous leishmaniasis [NCT00317629]., Trials. 7 (2006) 14. doi:10.1186/1745-6215-7-14.

[58] S.Y. Silva, L.C. Rueda, G. a Márquez, M. López, D.J. Smith, C. a Calderón, J.C. Castillo, J. Matute, C.F. Rueda-Clausen, A. Orduz, F. a Silva, P. Kampeerapappun, M. Bhide, P. López-Jaramillo, Double blind, randomized, placebo controlled clinical trial for the treatment of diabetic foot ulcers, using a nitric oxide releasing patch: PATHON, Trials. 8 (2007) 26. doi:10.1186/1745-6215-8-26.

[59] X. Wu, Y. Wang, C. Zhu, X. Tong, M. Yang, L. Yang, Z. Liu, W. Huang, F. Wu, H. Zong, H. Li, H. He, Preclinical animal study and human clinical trial data of co-electrospun poly(L-lactide-co-caprolactone) and fibrinogen mesh for anterior pelvic floor reconstruction, Int. J. Nanomedicine. 11 (2016) 389–397. doi:10.2147/IJN.S88803.

[60] D.W. Hutmacher, H. Singh, Computational fluid dynamics for improved bioreactor design and 3D culture, Trends Biotechnol. 26 (2008) 166–172. doi:10.1016/j.tibtech.2007.11.012.

[61] H. Chang, Y. Wang, Cell Responses to Surface and Architecture of Tissue Engineering Scaffolds, in: Regen. Med. Tissue Eng. - Cells Biomater., InTech, 2011: pp. 569–588. doi:10.5772/21983.

[62] A. Aarvold, J.O. Smith, E.R. Tayton, S.A. Lanham, J.B. Chaudhuri, I.G. Turner, R.O.C. Oreffo, The effect of porosity of a biphasic ceramic scaffold on human skeletal stem cell growth and differentiation in vivo, J. Biomed. Mater. Res. - Part A. 101 (2013) 3431–3437.

[63] M.E. Gomes, H.L. Holtorf, R.L. Reis, A.G. Mikos, Influence of the porosity of starch-based fiber mesh scaffolds on the proliferation and osteogenic differentiation of bone marrow stromal cells cultured in a flow perfusion bioreactor., Tissue Eng. 12 (2006) 801–809. doi:10.1089/ten.2006.12.801.

[64] R. Ikeda, H. Fujioka, I. Nagura, T. Kokubu, N. Toyokawa, A. Inui, T. Makino, H.

Kaneko, M. Doita, M. Kurosaka, The effect of porosity and mechanical property of a synthetic polymer scaffold on repair of osteochondral defects, Int. Orthop. 33 (2008) 821–828. doi:10.1007/s00264-008-0532-0.

[65] B.L.-P. Lee, Z. Tang, A. Wang, F. Huang, Z. Yan, D. Wang, J.S. Chu, N. Dixit, L. Yang, S. Li, Synovial stem cells and their responses to the porosity of microfibrous scaffold, Acta Biomater. 9 (2013) 7264–7275. doi:10.1016/j.actbio.2013.03.009.

[66] X. Fu, H. Wang, Rapid fabrication of biomimetic nanofiber-enabled skin grafts, in: T.J. Webster (Ed.), Nanomedicine Technol. Appl., Woodhead Publishing, Cambridge, UK, 2012: p. 428.

[67] I. Sabree, J.E. Gough, B. Derby, Mechanical properties of porous ceramic scaffolds: Influence of internal dimensions, Ceram. Int. 41 (2015) 8425–8432. doi:10.1016/j.ceramint.2015.03.044.

[68] J.L. Lowery, N. Datta, G.C. Rutledge, Effect of fiber diameter, pore size and seeding method on growth of human dermal fibroblasts in electrospun poly(epsilon-caprolactone) fibrous mats., Biomaterials. 31 (2010) 491–504. doi:10.1016/j.biomaterials.2009.09.072.

[69] Y. Elsayed, C. Lekakou, F. Labeed, P. Tomlins, Smooth muscle tissue engineering in crosslinked electrospun gelatin scaffolds, J. Biomed. Mater. Res. - Part A. 104 (2016) 313–321. doi:10.1002/jbm.a.35565.

[70] H. Bergmeister, C. Schreiber, C. Grasl, I. Walter, R. Plasenzotti, M. Stoiber, D. Bernhard, H. Schima, Healing characteristics of electrospun polyurethane grafts with various porosities, Acta Biomater. 9 (2013) 6032–6040. doi:10.1016/j.actbio.2012.12.009.

[71] Q.P. Pham, U. Sharma, A.G. Mikos, Electrospinning of Polymeric Nanofibers for Tissue Engineering Applications: A Review, Tissue Eng. 12 (2006) 60509065116001. doi:10.1089/ten.2006.12.ft-65.

[72] S. Soliman, S. Pagliari, A. Rinaldi, G. Forte, R. Fiaccavento, F. Pagliari, O. Franzese, M. Minieri, P. Di Nardo, S. Licoccia, E. Traversa, Multiscale three-dimensional scaffolds for soft tissue engineering via multimodal electrospinning, Acta Biomater. 6 (2010) 1227–1237. doi:10.1016/j.actbio.2009.10.051.

[73] J.M. Gluck, Electrospun Nanofibrous Poly(ε-caprolactone) (PCL) Scaffolds for Liver Tissue Engineering, Graduate Faculty of North Carolina State University, 2007.

[74] R.D. Cardwell, L.A. Dahlgren, A.S. Goldstein, Electrospun fibre diameter, not alignment, affects mesenchymal stem cell differentiation into the tendon/ligament lineage, J. Tissue Eng. Regen. Med. 8 (2014) 937–945. doi:10.1002/term.1589.

[75] H. Aghamohseni, K. Ohadi, M. Spearman, N. Krahn, M. Moo-young, J.M. Scharer, M. Butler, H.M. Budman, Effects of nutrient levels and average culture pH on the glycosylation pattern of camelid-humanized monoclonal antibody, J. Biotechnol. 186 (2014) 98–109. doi:10.1016/j.jbiotec.2014.05.024.

[76] R.G. Ham, W.L. Mckeehan, Media and Growth Requirements, in: W.B. Jakoby, I.H. Pastan (Eds.), Methods Enzymol. Vol. 58 Cell Cult., Academic Press, New York, 1979: pp. 47–93.

[77] K. Negoro, S. Kobayashi, K. Takeno, K. Uchida, H. Baba, Effect of osmolarity on glycosaminoglycan production and cell metabolism of articular chondrocyte under three-dimensional culture system, Clin. Exp. Rheumatol. 26 (2008) 534–541.

[78] T. Ma, W.L. Grayson, M. Fröhlich, G. Vunjak-Novakovic, Hypoxia and stem cell-based engineering of mesenchymal tissues, Biotechnol. Prog. 25 (2009) 32–42. doi:10.1002/btpr.128.

[79] F. Dos Santos, P.Z. Andrade, J.S. Boura, M.M. Abecasis, C.L. Da Silva, J.M.S. Cabral, Ex vivo expansion of human mesenchymal stem cells: A more effective cell

proliferation kinetics and metabolism under hypoxia, J. Cell. Physiol. 223 (2010) 27–35. doi:10.1002/jcp.21987.

[80] M. Deschepper, K. Oudina, B. David, V. Myrtil, C. Collet, M. Bensidhoum, D. Logeart-Avramoglou, H. Petite, Survival and function of mesenchymal stem cells (MSCs) depend on glucose to overcome exposure to long-term, severe and continuous hypoxia, J. Cell. Mol. Med. 15 (2011) 1505–1514. doi:10.1111/j.1582-4934.2010.01138.x.

[81] A.B. Adesida, A. Mulet-sierra, N.M. Jomha, Hypoxia mediated isolation and expansion enhances the chondrogenic capacity of bone marrow mesenchymal stromal cells, Stem Cell Res. Ther. 3 (2012) 9. doi:10.1186/scrt100.

[82] C. Zhu, J. Yu, Q. Pan, J. Yang, G. Hao, Y. Wang, L. Li, H. Cao, Hypoxia-inducible factor-2 alpha promotes the proliferation of human placenta-derived mesenchymal stem cells through the MAPK/ERK signaling pathway, Sci. Rep. 6 (2016) 35489. doi:10.1038/srep35489.

[83] F.M. Lampert, C. Kütscher, G.B. Stark, G. Finkenzeller, Overexpression of Hif-1α in Mesenchymal Stem Cells Affects Cell-Autonomous Angiogenic and Osteogenic Parameters, J. Cell. Biochem. 117 (2016) 760–768. doi:10.1002/jcb.25361.

[84] R.I. Freshney, B. Obradovic, W. Grayson, C. Cannizzaro, G. Vunjak-Novakovic, Principles of tissue culture and bioreactor design, in: R. LANZA, R. LANGER, J. VACANTI (Eds.), Princ. Tissue Eng., Academic Press, San Diego, 2007: pp. 155–183. doi:10.1016/B978-012370615-7/50016-0.

[85] A. Nuschke, M. Rodrigues, A.W. Wells, K. Sylakowski, A. Wells, Mesenchymal stem cells / multipotent stromal cells (MSCs) are glycolytic and thus glucose is a limiting factor of in vitro models of MSC starvation, Stem Cell Res. Ther. (2016) 1–9. doi:10.1186/s13287-016-0436-7.

[86] N.M. Machado, Glicose e Glutamina na Proliferação e Viabilidade de Células-Tronco Dentais Humanas, Universidade Federal de São Paulo, 2014.

[87] H.K. Heywood, D.L. Bader, D. a. Lee, Rate of oxygen consumption by isolated articular chondrocytes is sensitive to medium glucose concentration, J. Cell. Physiol. 206 (2006) 402–410. doi:10.1002/jcp.20491.

[88] R.W. Kasinskas, R. Venkatasubramanian, N.S. Forbes, Rapid uptake of glucose and lactate, and not hypoxia, induces apoptosis in three-dimensional tumor tissue culture., Integr. Biol. (Camb). 6 (2014) 399–410. doi:10.1039/c4ib00001c.

[89] M.J. Farrell, J.I. Shin, L.J. Smith, R.L. Mauck, Functional consequences of glucose and oxygen deprivation on engineered mesenchymal stem cell-based cartilage constructs, Osteoarthr. Cartil. 23 (2015) 134–142. doi:10.1016/j.joca.2014.09.012.

[90] B. Zhang, N. Liu, H. Shi, H. Wu, Y. Gao, H. He, B. Gu, H. Liu, High glucose microenvironments inhibit the proliferation and migration of bone mesenchymal stem cells by activating GSK3β, J. Bone Miner. Metab. 34 (2016) 140–150. doi:10.1007/s00774-015-0662-6.

[91] M.J. Rogatzki, B.S. Ferguson, M.L. Goodwin, L.B. Gladden, Lactate is always the end product of glycolysis, Front. Neurosci. 9 (2015) 1–7. doi:10.3389/fnins.2015.00022.

[92] D. Schop, F.W. Janssen, L.D.S. van Rijn, H. Fernandes, R.M. Bloem, J.D. de Bruijn, R. van Dijkhuizen-Radersma, Growth, Metabolism, and Growth Inhibitors of Mesenchymal Stem Cells, Tissue Eng. Part A. 15 (2009) 1877–1886. doi:10.1089/ten.tea.2008.0345.

[93] T. Chen, Y. Zhou, W. Tan, Effects of low temperature and lactate on osteogenic differentiation of human amniotic mesenchymal stem cells, Biotechnol. Bioprocess Eng. 14 (2009) 708–715. doi:10.1007/s12257-009-0034-y.

[94] J. a Burdick, G. Vunjak-Novakovic, Engineered microenvironments for controlled stem

cell differentiation., Tissue Eng. Part A. 15 (2009) 205–219. doi:10.1089/ten.tea.2008.0131.

[95] C. Ferrari, E. Olmos, F. Balandras, N. Tran, I. Chevalot, E. Guedon, A. Marc, Investigation of growth conditions for the expansion of porcine mesenchymal stem cells on microcarriers in stirred cultures, Appl. Biochem. Biotechnol. 172 (2014) 1004–1017. doi:10.1007/s12010-013-0586-3.

[96] S. Sart, A. Errachid, Y.-J. Schneider, S.N. Agathos, Modulation of mesenchymal stem cell actin organization on conventional microcarriers for proliferation and differentiation in stirred bioreactors, J. Tissue Eng. Regen. Med. 7 (2013) 537–551. doi:10.1002/term.545.

[97] A. Mizukami, A. Fernandes-Platzgummer, J.G. Carmelo, K. Swiech, D.T. Covas, J.M.S. Cabral, C.L. da Silva, Stirred tank bioreactor culture combined with serum-/xenogeneic-free culture medium enables an efficient expansion of umbilical cord-derived mesenchymal stem/stromal cells, Biotechnol. J. 11 (2016) 1048–1059. doi:10.1002/biot.201500532.

[98] F. Rosa, K.C. Sales, J.G. Carmelo, A. Fernandes-Platzgummer, C.L. da Silva, M.B. Lopes, C.R.C. Calado, Monitoring the ex-vivo expansion of human mesenchymal stem/stromal cells in xeno-free microcarrier-based reactor systems by MIR spectroscopy, Biotechnol. Prog. 32 (2016) 447–455. doi:10.1002/btpr.2215.

[99] T.A. Grein, J. Leber, M. Blumenstock, F. Petry, T. Weidner, D. Salzig, P. Czermak, Multiphase mixing characteristics in a microcarrier-based stirred tank bioreactor suitable for human mesenchymal stem cell expansion, Process Biochem. 51 (2016) 1109–1119. doi:10.1016/j.procbio.2016.05.010.

[100] X. Wu, S. Li, L. Lou, Z. Chen, The Effect of the Microgravity Rotating Culture System on the Chondrogenic Differentiation of Bone Marrow Mesenchymal Stem Cells, Mol. Biotechnol. 54 (2013) 331–336. doi:10.1007/s12033-012-9568-x.

[101] G.N. Bancroft, V.I. Sikavitsas, A.G. Mikos, Design of a flow perfusion bioreactor system for bone tissue-engineering applications., Tissue Eng. 9 (2003) 549–554. doi:10.1089/107632703322066723.

[102] A.B. Yeatts, TUBULAR PERFUSION SYSTEM BIOREACTOR FOR THE DYNAMIC CULTURE OF HUMAN MESENCHYMAL STEM CELLS, College Park, 2012.

[103] S.H. Cartmell, B.D. Porter, A.J. García, R.E. Guldberg, Effects of medium perfusion rate on cell-seeded three-dimensional bone constructs in vitro., Tissue Eng. 9 (2003) 1197–1203. doi:10.1089/10763270360728107.

[104] G.M. de Peppo, M. Sladkova, P. Sjövall, A. Palmquist, K. Oudina, J. Hyllner, P. Thomsen, H. Petite, C. Karlsson, Human Embryonic Stem Cell-Derived Mesodermal Progenitors Display Substantially Increased Tissue Formation Compared to Human Mesenchymal Stem Cells Under Dynamic Culture Conditions in a Packed Bed/Column Bioreactor, Tissue Eng. Part A. 19 (2013) 175–187. doi:10.1089/ten.tea.2011.0412.

[105] Y. Ban, Y. Wu, T. Yu, N. Geng, Y. Wang, X. Liu, P. Gong, Response of osteoblasts to low fluid shear stress is time dependent, Tissue Cell. 43 (2011) 311–317. doi:10.1016/j.tice.2011.06.003.

[106] J. Markhoff, J. Wieding, V. Weissmann, J. Pasold, A. Jonitz-Heincke, R. Bader, Influence of Different Three-Dimensional Open Porous Titanium Scaffold Designs on Human Osteoblasts Behavior in Static and Dynamic Cell Investigations, Materials (Basel). 8 (2015) 5490–5507. doi:10.3390/ma8085259.

[107] Z. Yang, Y. Tang, J. Li, Y. Zhang, X. Hu, Facile synthesis of tetragonal columnar-shaped TiO2 nanorods for the construction of sensitive electrochemical glucose biosensor, Biosens. Bioelectron. 54 (2014) 528–533. doi:10.1016/j.bios.2013.11.043.

[108] Z. Zhang, L. Yuan, P.D. Lee, E. Jones, J.R. Jones, Modeling of time dependent localized flow shear stress and its impact on cellular growth within additive manufactured titanium implants, J. Biomed. Mater. Res. Part B Appl. Biomater. 102 (2014) 1689–1699. doi:10.1002/jbm.b.33146.
[109] M. Moore, R. Moore, P.S. McFetridge, Directed oxygen gradients initiate a robust early remodeling response in engineered vascular grafts., Tissue Eng. Part A. 19 (2013) 2005–13. doi:10.1089/ten.TEA.2012.0592.
[110] F.W. Janssen, J. Oostra, A. Van Oorschot, C. a. Van Blitterswijk, A perfusion bioreactor system capable of producing clinically relevant volumes of tissue-engineered bone: In vivo bone formation showing proof of concept, Biomaterials. 27 (2006) 315–323. doi:10.1016/j.biomaterials.2005.07.044.
[111] J. Liao, X. Guo, K.J. Grande-Allen, F.K. Kasper, A.G. Mikos, Bioactive polymer/extracellular matrix scaffolds fabricated with a flow perfusion bioreactor for cartilage tissue engineering, Biomaterials. 31 (2010) 8911–8920. doi:10.1016/j.biomaterials.2010.07.110.
[112] R.A. Thibault, A.G. Mikos, F.K. Kasper, Protein and mineral composition of osteogenic extracellular matrix constructs generated with a flow perfusion bioreactor, Biomacromolecules. 12 (2011) 4204–4212. doi:10.1021/bm200975a.
[113] M.L. Alves da Silva, A. Martins, A.R. Costa-Pinto, P. Costa, S. Faria, M. Gomes, R.L. Reis, N.M. Neves, Cartilage Tissue Engineering Using Electrospun PCL Nanofiber Meshes and MSCs, Biomacromolecules. 11 (2010) 3228–3236. doi:10.1021/bm100476r.
[114] A. Gugerell, A. Neumann, J. Kober, L. Tammaro, E. Hoch, M. Schnabelrauch, L. Kamolz, C. Kasper, M. Keck, Adipose-derived stem cells cultivated on electrospun l-lactide/glycolide copolymer fleece and gelatin hydrogels under flow conditions – aiming physiological reality in hypodermis tissue engineering, Burns. 41 (2015) 163–171. doi:10.1016/j.burns.2014.06.010.
[115] B. Weyand, C. Kasper, M. Israelowitz, C. Gille, H.P. von Schroeder, K. Reimers, P.M. Vogt, A differential pressure laminar flow reactor supports osteogenic differentiation and extracellular matrix formation from adipose mesenchymal stem cells in a macroporous ceramic scaffold., Biores. Open Access. 1 (2012) 145–56. doi:10.1089/biores.2012.9901.
[116] A.-C. Tsai, Y. Liu, T. Ma, Expansion of human mesenchymal stem cells in fibrous bed bioreactor, Biochem. Eng. J. 108 (2016) 51–57. doi:10.1016/j.bej.2015.09.002.
[117] A.B. Yeatts, S.K. Both, W. Yang, H.S. Alghamdi, F. Yang, J.P. Fisher, J. a Jansen, In Vivo Bone Regeneration Using Tubular Perfusion System Bioreactor Cultured Nanofibrous Scaffolds, Tissue Eng. Part A. 20 (2014) 139–146. doi:10.1089/ten.tea.2013.0168.
[118] J. Kim, T. Ma, Perfusion regulation of hMSC microenvironment and osteogenic differentiation in 3D scaffold, Biotechnol. Bioeng. 109 (2012) 252–261. doi:10.1002/bit.23290.
[119] W.L. Grayson, D. Marolt, S. Bhumiratana, M. Fröhlich, X.E. Guo, G. Vunjak-Novakovic, Optimizing the medium perfusion rate in bone tissue engineering bioreactors, Biotechnol. Bioeng. 108 (2011) 1159–1170. doi:10.1002/bit.23024.
[120] R.L. Dahlin, V. V. Meretoja, M. Ni, F.K. Kasper, A.G. Mikos, Design of a High-Throughput Flow Perfusion Bioreactor System for Tissue Engineering, Tissue Eng. Part C Methods. 18 (2012) 817–820. doi:10.1089/ten.tec.2012.0037.
[121] M. Santoro, S.-E. Lamhamedi-Cherradi, B. a Menegaz, J. a Ludwig, A.G. Mikos, Flow perfusion effects on three-dimensional culture and drug sensitivity of Ewing sarcoma, Proc. Natl. Acad. Sci. 112 (2015) 10304–10309. doi:10.1073/pnas.1506684112.

[122] S. Diederichs, S. Röker, D. Marten, A. Peterbauer, T. Scheper, M. van Griensven, C. Kasper, Dynamic cultivation of human mesenchymal stem cells in a rotating bed bioreactor system based on the Z®RP platform, Biotechnol. Prog. 25 (2009) 1762–1771. doi:10.1002/btpr.258.
[123] A. Neumann, A. Lavrentieva, A. Heilkenbrinker, M. Loenne, C. Kasper, Characterization and Application of a Disposable Rotating BedBioreactor for Mesenchymal Stem Cell Expansion, Bioengineering. 1 (2014) 231–245. doi:10.3390/bioengineering1040231.
[124] I. Stefani, M.A. Asnaghi, J.J. Cooper-White, S. Mantero, A double chamber rotating bioreactor for enhanced tubular tissue generation from human mesenchymal stem cells, J. Tissue Eng. Regen. Med. (2016). doi:10.1002/term.2341.
[125] I.E. De Napoli, S. Scaglione, P. Giannoni, R. Quarto, G. Catapano, Mesenchymal stem cell culture in convection-enhanced hollow fibre membrane bioreactors for bone tissue engineering, J. Memb. Sci. 379 (2011) 341–352. doi:10.1016/j.memsci.2011.06.001.
[126] S. Li, Y. Liu, Q. Zhou, R. Lue, L. Song, S.-W. Dong, P. Guo, B. Kopjar, A Novel Axial-Stress Bioreactor System Combined with a Substance Exchanger for Tissue Engineering of 3D Constructs., Tissue Eng. Part C. Methods. 20 (2014) 205–14. doi:10.1089/ten.TEC.2013.0173.
[127] C.E. Holy, M.S. Shoichet, J.E. Davies, Engineering three-dimensional bone tissuein vitro using biodegradable scaffolds: Investigating initial cell-seeding density and culture period, J. Biomed. Mater. Res. 51 (2000) 376–382. doi:10.1002/1097.
[128] D.J. Griffon, J.P. Abulencia, G.R. Ragetly, L.P. Fredericks, S. Chaieb, A comparative study of seeding techniques and three-dimensional matrices for mesenchymal cell attachment, J. Tissue Eng. Regen. Med. 5 (2011) 169–179. doi:10.1002/term.302.
[129] K. Yamanaka, K. Yamamoto, Y. Sakai, Y. Suda, Y. Shigemitsu, T. Kaneko, K. Kato, T. Kumagai, Y. Kato, Seeding of mesenchymal stem cells into inner part of interconnected porous biodegradable scaffold by a new method with a filter paper., Dent. Mater. J. 34 (2015) 78–85. doi:10.4012/dmj.2013-330.
[130] L.A. Solchaga, E. Tognana, K. Penick, H. Baskaran, V.M. Goldberg, A.I. Caplan, J.F. Welter, A rapid seeding technique for the assembly of large cell/scaffold composite constructs., Tissue Eng. 12 (2006) 1851–63. doi:10.1089/ten.2006.12.1851.
[131] W.T. Godbey, B.S. Stacey Hindy, M.E. Sherman, A. Atala, A novel use of centrifugal force for cell seeding into porous scaffolds, Biomaterials. 25 (2004) 2799–2805. doi:10.1016/j.biomaterials.2003.09.056.
[132] R. Ng, J.S. Gurm, S.-T. Yang, Centrifugal seeding of mammalian cells in nonwoven fibrous matrices, Biotechnol. Prog. 26 (2009) n/a-n/a. doi:10.1002/btpr.317.
[133] A.T. Buizer, A.G. Veldhuizen, S.K. Bulstra, R. Kuijer, Static versus vacuum cell seeding on high and low porosity ceramic scaffolds, J. Biomater. Appl. 29 (2014) 3–13. doi:10.1177/0885328213512171.
[134] N.D. Wanasekara, S. Ghosh, M. Chen, V.B. Chalivendra, S. Bhowmick, Effect of stiffness of micron/sub-micron electrospun fibers in cell seeding, J. Biomed. Mater. Res. - Part A. 103 (2015) 2289–2299. doi:10.1002/jbm.a.35362.
[135] W.-J. Fu, Y.-D. Xu, Z.-X. Wang, G. Li, J.-G. Shi, F.-Z. Cui, Y. Zhang, X. Zhang, New ureteral scaffold constructed with composite poly(L-lactic acid)-collagen and urothelial cells by new centrifugal seeding system, J. Biomed. Mater. Res. Part A. 100A (2012) 1725–1733. doi:10.1002/jbm.a.34134.
[136] B.-S. Kim, A.J. Putnam, T.J. Kulik, D.J. Mooney, Optimizing seeding and culture methods to engineer smooth muscle tissue on biodegradable polymer matrices, Biotechnol. Bioeng. 57 (1998) 46–54. doi:10.1002/(SICI)1097-0290(19980105)57:1<46::AID-BIT6>3.0.CO;2-V.

[137] J.L. Lowery, N. Datta, G.C. Rutledge, Effect of fiber diameter, pore size and seeding method on growth of human dermal fibroblasts in electrospun poly(ε-caprolactone) fibrous mats, Biomaterials. 31 (2010) 491–504. doi:10.1016/j.biomaterials.2009.09.072.
[138] D. Wendt, A. Marsano, M. Jakob, M. Heberer, I. Martin, Oscillating perfusion of cell suspensions through three-dimensional scaffolds enhances cell seeding efficiency and uniformity, Biotechnol. Bioeng. 84 (2003) 205–214. doi:10.1002/bit.10759.
[139] F. Zhao, T. Ma, Perfusion bioreactor system for human mesenchymal stem cell tissue engineering: Dynamic cell seeding and construct development, Biotechnol. Bioeng. 91 (2005) 482–493. doi:10.1002/bit.20532.
[140] F. Ajalloueian, M.L. Lim, G. Lemon, J.C. Haag, Y. Gustafsson, S. Sjöqvist, A. Beltrán-Rodríguez, C. Del Gaudio, S. Baiguera, A. Bianco, P. Jungebluth, P. Macchiarini, Biomechanical and biocompatibility characteristics of electrospun polymeric tracheal scaffolds, Biomaterials. 35 (2014) 5307–5315. doi:10.1016/j.biomaterials.2014.03.015.
[141] M.R. LADD, T.K. HILL, J.J. YOO, S.J. LEE, Electrospun Nanofibers, in: T. Lin (Ed.), Tissue Eng. Nanofibers - Prod. Prop. Funct. Appl., InTech, 2011.
[142] D. a Barker, D.T. Bowers, B. Hughley, E.W. Chance, K.J. Klembczyk, K.L. Brayman, S.S. Park, E. a Botchwey, Multilayer cell-seeded polymer nanofiber constructs for soft-tissue reconstruction., JAMA Otolaryngol. Head Neck Surg. 139 (2013) 914–22. doi:10.1001/jamaoto.2013.4119.
[143] J.C.Y. Dunn, W.-Y. Chan, V. Cristini, J.S. Kim, J. Lowengrub, S. Singh, B.M. Wu, Analysis of cell growth in three-dimensional scaffolds., Tissue Eng. 12 (2006) 705–716. doi:10.1089/ten.2006.12.705.
[144] B.J. Papenburg, J. Liu, G. a. Higuera, A.M.C. Barradas, J. de Boer, C. a. van Blitterswijk, M. Wessling, D. Stamatialis, Development and analysis of multi-layer scaffolds for tissue engineering, Biomaterials. 30 (2009) 6228–6239. doi:10.1016/j.biomaterials.2009.07.057.
[145] S. Srouji, T. Kizhner, E. Suss-Tobi, E. Livne, E. Zussman, 3-D Nanofibrous electrospun multilayered construct is an alternative ECM mimicking scaffold, J. Mater. Sci. Mater. Med. 19 (2008) 1249–1255. doi:10.1007/s10856-007-3218-z.
[146] A. Gugerell, A. Neumann, J. Kober, L. Tammaro, E. Hoch, M. Schnabelrauch, L. Kamolz, C. Kasper, M. Keck, Adipose-derived stem cells cultivated on electrospun l-lactide/glycolide copolymer fleece and gelatin hydrogels under flow conditions – aiming physiological reality in hypodermis tissue engineering, Burns. 41 (2014) 163–171. doi:10.1016/j.burns.2014.06.010.
[147] A.G. Ardakani, U. Cheema, R.A. Brown, R.J. Shipley, Quantifying the correlation between spatially defined oxygen gradients and cell fate in an engineered three-dimensional culture model, J. R. Soc. Interface. 11 (2014) 20140501–20140501. doi:10.1098/rsif.2014.0501.
[148] F. Coletti, S. Macchietto, N. Elvassore, Mathematical Modeling of Three-Dimensional Cell Cultures in Perfusion Bioreactors, Ind. Eng. Chem. Res. 45 (2006) 8158–8169. doi:10.1021/ie051144v.
[149] P. Decuzzi, M. Ferrari, Modulating cellular adhesion through nanotopography, Biomaterials. 31 (2010) 173–179. doi:10.1016/j.biomaterials.2009.09.018.
[150] E.Y. Gómez-Pachón, F.M. Sánchez-Arévalo, F.J. Sabina, A. Maciel-Cerda, R.M. Campos, N. Batina, I. Morales-Reyes, R. Vera-Graziano, Characterisation and modelling of the elastic properties of poly(lactic acid) nanofibre scaffolds, J. Mater. Sci. 48 (2013) 8308–8319. doi:10.1007/s10853-013-7644-7.
[151] C. Jungreuthmayer, S.W. Donahue, M.J. Jaasma, A. a Al-Munajjed, J. Zanghellini, D.J. Kelly, F.J. O'Brien, A comparative study of shear stresses in collagen-

glycosaminoglycan and calcium phosphate scaffolds in bone tissue-engineering bioreactors., Tissue Eng. Part A. 15 (2009) 1141–1149. doi:10.1089/ten.tea.2008.0204.
[152] C.Y.J. Ma, R. Kumar, X.Y. Xu, A. Mantalaris, A combined fluid dynamics, mass transport and cell growth model for a three-dimensional perfused biorector for tissue engineering of haematopoietic cells, Biochem. Eng. J. 35 (2007) 1–11. doi:10.1016/j.bej.2006.11.024.
[153] R.J. Mccoy, F.J. O'Brien, Visualizing feasible operating ranges within tissue engineering systems using a "windows of operation" approach: A perfusion-scaffold bioreactor case study, Biotechnol. Bioeng. 109 (2012) 3161–3171. doi:10.1002/bit.24566.
[154] V.A.A. Santamaría, M. Malvè, a. Duizabo, a. Mena Tobar, G. Gallego Ferrer, J.M. García Aznar, M. Doblaré, I. Ochoa, Computational methodology to determine fluid related parameters of non regular three-dimensional scaffolds, Ann. Biomed. Eng. 41 (2013) 2367–2380. doi:10.1007/s10439-013-0849-8.
[155] S. Truscello, G. Kerckhofs, S. Van Bael, G. Pyka, J. Schrooten, H. Van Oosterwyck, Prediction of permeability of regular scaffolds for skeletal tissue engineering: A combined computational and experimental study, Acta Biomater. 8 (2012) 1648–1658. doi:10.1016/j.actbio.2011.12.021.
[156] X. Yan, D.J. Bergstrom, X.B. Chen, Modeling of cell cultures in perfusion bioreactors, IEEE Trans. Biomed. Eng. 59 (2012) 2568–2575. doi:10.1109/TBME.2012.2206077.
[157] Y. Chen, S. Zhou, Q. Li, Mathematical modeling of degradation for bulk-erosive polymers: Applications in tissue engineering scaffolds and drug delivery systems, Acta Biomater. 7 (2011) 1140–1149. doi:10.1016/j.actbio.2010.09.038.
[158] J. Ferdous, V.B. Kolachalama, T. Shazly, Impact of polymer structure and composition on fully resorbable endovascular scaffold performance, Acta Biomater. 9 (2013) 6052–6061. doi:10.1016/j.actbio.2012.12.011.
[159] M. Heljak, W. Swieszkowski, K.J. Kurzydlowski, Modeling of the degradation kinetics of biodegradable scaffolds: The effects of the environmental conditions, J. Appl. Polym. Sci. 131 (2014) 1–7. doi:10.1002/app.40280.
[160] M. Heljak, W. Swieszkowski, K.J. Kurzydlowski, A phenomenological model for the degradation of polymeric tissue engineering scaffolds, (2011).
[161] T. Shazly, V.B. Kolachalama, J. Ferdous, J.P. Oberhauser, S. Hossainy, E.R. Edelman, Assessment of material by-product fate from bioresorbable vascular scaffolds, Ann. Biomed. Eng. 40 (2012) 955–965. doi:10.1007/s10439-011-0445-8.
[162] U. Akalp, S.J. Bryant, F.J. Vernerey, Tuning tissue growth with scaffold degradation in enzyme-sensitive hydrogels: a mathematical model, Soft Matter. 12 (2016) 7505–7520. doi:10.1039/c6sm00583g.
[163] M. Devarapalli, B.J. Lawrence, S. V. Madihally, Modeling nutrient consumptions in large flow-through bioreactors for tissue engineering, Biotechnol. Bioeng. 103 (2009) 1003–1015. doi:10.1002/bit.22333.
[164] L.A. Hidalgo-Bastida, S. Thirunavukkarasu, S. Griffiths, S.H. Cartmell, S. Naire, Modeling and design of optimal flow perfusion bioreactors for tissue engineering applications, Biotechnol. Bioeng. 109 (2012) 1095–1099. doi:10.1002/bit.24368.
[165] P. Pathi, T. Ma, B.R. Locke, Role of nutrient supply on cell growth in bioreactor design for tissue engineering of hematopoietic cells, Biotechnol. Bioeng. 89 (2005) 743–758. doi:10.1002/bit.20367.
[166] C. Schirmaier, V. Jossen, S.C. Kaiser, F. Jüngerkes, S. Brill, A. Safavi-Nab, A. Siehoff, C. van den Bos, D. Eibl, R. Eibl, Scale-up of adipose tissue-derived mesenchymal stem cell production in stirred single-use bioreactors under low-serum conditions, Eng. Life Sci. 14 (2014) 292–303. doi:10.1002/elsc.201300134.

[167] H. Singh, S.H. Teoh, H.T. Low, D.W. Hutmacher, Flow modelling within a scaffold under the influence of uni-axial and bi-axial bioreactor rotation, J. Biotechnol. 119 (2005) 181–196. doi:10.1016/j.jbiotec.2005.03.021.
[168] C.A. Chung, T.-H. Lin, S.-D. Chen, H.-I. Huang, Hybrid cellular automaton modeling of nutrient modulated cell growth in tissue engineering constructs, J. Theor. Biol. 262 (2010) 267–278. doi:10.1016/j.jtbi.2009.09.031.
[169] I.O. Doagă, T. Savopol, M. Neagu, a. Neagu, E. Kovács, The kinetics of cell adhesion to solid scaffolds: An experimental and theoretical approach, J. Biol. Phys. 34 (2008) 495–509. doi:10.1007/s10867-008-9108-x.
[170] D. Jeong, A. Yun, J. Kim, Mathematical model and numerical simulation of the cell growth in scaffolds, Biomech. Model. Mechanobiol. 11 (2012) 677–688. doi:10.1007/s10237-011-0342-y.
[171] M. Campolo, F. Curcio, A. Soldati, Minimal perfusion flow for osteogenic growth of mesenchymal stem cells on lattice scaffolds, AIChE J. 59 (2013) 3131–3144. doi:10.1002/aic.14084.
[172] M. Flaibani, E. Magrofuoco, N. Elvassore, Computational modeling of cell growth heterogeneity in a perfused 3D scaffold, Ind. Eng. Chem. Res. 49 (2010) 859–869. doi:10.1021/ie900418g.
[173] A. Lesman, Y. Blinder, S. Levenberg, Modeling of flow-induced shear stress applied on 3D cellular scaffolds: Implications for vascular tissue engineering, Biotechnol. Bioeng. 105 (2010) 645–654. doi:10.1002/bit.22555.
[174] D. Liu, C.K. Chua, K.F. Leong, A mathematical model for fluid shear-sensitive 3D tissue construct development, Biomech. Model. Mechanobiol. 12 (2013) 19–31. doi:10.1007/s10237-012-0378-7.
[175] B. Porter, R. Zauel, H. Stockman, R. Guldberg, D. Fyhrie, 3-D computational modeling of media flow through scaffolds in a perfusion bioreactor, J. Biomech. 38 (2005) 543–549. doi:10.1016/j.jbiomech.2004.04.011.
[176] M.T. Raimondi, F. Boschetti, L. Falcone, G.B. Fiore, a. Remuzzi, E. Marinoni, M. Marazzi, R. Pietrabissa, Mechanobiology of engineered cartilage cultured under a quantified fluid-dynamic environment, Biomech. Model. Mechanobiol. 1 (2002) 69–82. doi:10.1007/s10237-002-0007-y.
[177] P. Causin, R. Sacco, A computational model for biomass growth simulation in tissue engineering, Commun. Appl. Ind. Math. 2 (2011). doi:10.1685/journal.caim.370.
[178] F. Zhao, R. Chella, T. Ma, Effects of shear stress on 3-D human mesenchymal stem cell construct development in a perfusion bioreactor system: Experiments and hydrodynamic modeling, Biotechnol. Bioeng. 96 (2007) 584–595. doi:10.1002/bit.21184.
[179] C.A. Chung, C.W. Chen, C.P. Chen, C.S. Tseng, Enhancement of cell growth in tissue-engineering constructs under direct perfusion: Modeling and simulation, Biotechnol. Bioeng. 97 (2007) 1603–1616. doi:10.1002/bit.21378.
[180] R. Sacco, P. Causin, P. Zunino, M.T. Raimondi, A multiphysics/multiscale 2D numerical simulation of scaffold-based cartilage regeneration under interstitial perfusion in a bioreactor, Biomech. Model. Mechanobiol. 10 (2011) 577–589. doi:10.1007/s10237-010-0257-z.

Capítulo 4

Crescimento, metabolismo e infiltração celular em *scaffolds* eletrofiados de PCL com diferentes tamanhos de poro

A técnica de *electrospinning* é geralmente utilizada para a produção de nanofibras, embora possa ser utilizada para produzir *scaffolds* com microfibras dependendo do polímero e dos solventes utilizados. De modo a determinar a composição de solvente adequada e os parâmetros de eletrofiação, as seguintes questões de pesquisa foram respondidas neste capítulo:

→ É possível eletrofiar scaffolds de PCL com poros de diâmetro adequado para a infiltração de DPSCs?

→ O cultivo tridimensional afeta o crescimento, o consumo de nutrientes e produção de metabólitos das células?

Neste capítulo, é apresentado o estudo relacionado com a determinação dos parâmetros de eletrofiação e do sistema de solvente para obtenção de *scaffolds* com fibras micrométricas com poros adequados para a infiltração de células-tronco da polpa de dente decíduo. Além disto, também é exibida a influência do substrato no metabolismo e no crescimento celular. Este capítulo está na forma de artigo científico, na língua inglesa, e ainda está sob revisão dos autores.

Artigo 3

DENTAL PULP STEM CELL GROWTH, METABOLISM AND INFILTRATION IN ELECTROSPUN POLYCAPROLACTONE SCAFFOLDS WITH DIFFERENT PORE SIZE AND DISTRIBUTION

Ágata Paim[1,2,3], Nilo S. M. Cardozo[2], Patricia Pranke[3], Isabel C. Tessaro[1]

[1]Laboratory of Membrane Separation Processes (LASEM)

[2]Simulation Laboratory (LASIM)

[3]Hematology and Stem-cells Laboratory (LHCT)

[1,2]Department of Chemical Engineering, Universidade Federal do Rio Grande do Sul (UFRGS)

[3]Faculty of Pharmacy, Universidade Federal do Rio Grande do Sul (UFRGS)

[1,2] R. Eng. Luis Englert, s/n. Porto Alegre, Rio Grande do Sul 90040-040, Brazil.

[3] Av. Ipiranga, 2752. Porto Alegre, Rio Grande do Sul 90610-000, Brazil.

**Corresponding author (Ágata Paim)*

Present address: Department of Chemical Engineering, Universidade Federal do Rio Grande do Sul (UFRGS), R. Eng. Luis Englert, s/n. Porto Alegre, Rio Grande do Sul 90040-040, Brazil

Phone/Fax: +55 51 33085257

E-mail address: agata@enq.ufrgs.br

Abstract

Electrospinning is an attractive alternative to mimic the extracellular matrix. However, the performance of electrospun scaffolds depends strongly on its pore size distribution, which is dictated by the diameter of the fibers. The aim of this work has been to study dental pulp stem cell growth, distribution and metabolism (glucose uptake, lactate production) in electrospun polycaprolactone (PCL) scaffolds with different fiber diameters. Pure chloroform (Solution I) and chloroform/methanol mixtures in the proportions of 9:1 (Solution II) and 5:1 (Solutions III and IV) were used to prepare the PCL electrospinning solutions. Dental pulp stem cells were seeded on each scaffold and the cell number was determined with a Cell Counting Kit-8 (WST-8, Sigma–Aldrich) after 1, 4 and 7 days of culture. Glucose uptake and lactate production were quantified by enzymatic methods (K082 and K084-2, Bioclin), and cell distribution was analyzed through cell nuclei staining with DAPI. All scaffolds presented similar results for cell growth, at all times smaller than that found for the well group, possibly due to reduced cell adhesion and doubling time. Regarding cell energy metabolism, the pore size did not seem to affect glucose uptake and lactate production in the range of fiber diameters studied. Even though these rates were higher in scaffolds than in the well group (control), the lactate/glucose ratio was similar among all groups. Furthermore, it was observed that only Solution II was capable of producing scaffolds with fiber and pore diameters appropriated for infiltration and three-dimensional culture of mesenchymal stem cells.

Keywords: electrospinning, tissue engineering, scaffold, pore diameter, dental pulp stem cell.

4.1 Introduction

Electrospun scaffolds have high packing density, interconnected pore network and fibers with diameters comparable to the dimension of the protein network present in the extracellular matrix [1]. Besides, electrospinning is a technique that makes it possible to control fiber thickness through manipulation of the process variables, being useful to study the impact of the porous matrix spatial architecture on cellular behavior [2].

Pore size must be appropriate to allow cell spreading and network formation, the optimal size being dependent on the scaffold material and cell type [3]. The optimal mean pore diameter is generally close to the diameter of the cells in suspension [4], because the pore size establishes the proximity between cells in the initial stages of culture and the space the cells will have to organize themselves three-dimensionally during tissue development [5]. Oversized pores lead to structures with low mechanical resistance and can discourage extracellular matrix synthesis between the fibers, despite the positive effect on cell growth [6].

In fibrous scaffolds, the average fiber diameter can affect porosity and pore size, with a non-linear correlation between fiber thickness and porosity being reported in the range 1-10 μm of diameter [2,7,8]. Furthermore, the smaller the fiber diameter, the smaller the pores in the scaffolds [2,9], which can hinder cell migration [1]. There are strategies that can be used to increase the pore size in electrospun scaffolds, such as selective fiber removal [10], addition of microparticles[11] and low temperature electrospinning (crioelectrospinning) [12]. However, depending on the polymeric solution properties and on the electrospinning parameters, it is also possible to electrospin microfibers and to obtain a mesoporous matrix.

Synthetic polymers have been widely applied in tissue engineering as biomaterials, because their mechanical properties and degradation can be controlled to attend specific needs of a certain application[13]. The choice of the appropriate polymer must take into account chemical, physical and biological properties of the material. Polycaprolactone (PCL) is an biodegradable polyester, commonly used in tissue engineering due to its mechanical properties (strength and elasticity) [14]. Furthermore, it has FDA (Food and Drug Administration) approval for biomedical applications and its degradation products are non-toxic [9].

Chloroform is a solvent widely used to electrospin PCL microfibers, due to its low dielectric constant. Pham et al. [2] used a non-standard electrospinning setup to produce PCL scaffolds from methanol solutions. Their electrospinning setup employed a copper wire ring between the capillary tip and the collector, characterizing a variation with a dual electrode

setup. They combined different volume ratios of chloroform and methanol with PCL concentrations from 80 to 140 $kg \cdot m^{-3}$ to electrospin microfibers with diameters from 2 to 10 μm (pore diameters ranging from 10 to 45 μm) by varying the collector distance, voltage, flow rate and needle gauge.

Concerning the production of electrospun PCL fibers using the conventional single electrode mode, Van der Schueren et al. [15] and Del Gaudio et al. [16] used chloroform solutions with PCL concentrations of 100 and 140 $kg \cdot m^{-3}$, respectively, producing fibers with a mean diameter of approximately 4 μm, corresponding to a mean pore diameter of nearly 12 μm. Luo et al. [17] verified that the addition of methanol to a 100 $kg \cdot m^{-3}$ solution of PCL in chloroform at methanol:chloroform volumetric ratios of 1:1, 1:3 and 1:5 reduced the mean fiber diameter from 6.67 μm to 1.19, 2.28 and 3.65 μm, respectively. However, the results presented by these authors only include fibers collected for 10 s after stabilizing the jet for 60 s, resulting in a small number of fibers that does not characterize a three-dimensional scaffold. Therefore, the effect of the non-solvent ratio on the fiber morphology has still not been studied for three-dimensional PCL scaffolds produced from chloroform solutions with the standard electrospinning setup.

Regarding cell growth kinetics in electrospun scaffolds, the effect of pore size on growth rate depends on the capability of the structure to allow for proper cell infiltration. Soliman et al. [8] observed increase of the cell growth rate with the fiber diameter in three scaffolds of different mean fiber diameter (0.3 μm, 2.6 μm and 5.2 μm), but the small pores (0.2 μm, 5.1 μm, 14.9 μm, respectively) of the scaffolds did not allowed the infiltration of the mTERT mesenchymal stem cell (diameter between 50 and 70 μm). On the other hand, cell infiltration through the inside of microfiber three-dimensional scaffolds may not always be maximized with larger pores [18]. Furthermore, since the pore size affects the permeability and diffusion phenomena inside three-dimensional scaffolds, it is also interesting to investigate if this design parameter has influence on glucose uptake and lactate production. Thus, in order to optimize scaffold design and tissue development, it is important to study how the fiber and pore diameter influence mesenchymal stem cell growth, infiltration and metabolism in PCL scaffolds electrospun with a single electrode system.

4.2 Experimental

Scaffold fabrication

Four PCL solutions were prepared using pure chloroform or chloroform/methanol mixtures as solvent, using the PCL concentrations and volumetric ratios of chloroform/methanol described in Table 4.1. For the preparation of the solutions polycaprolactone (with a number average molecular weight of 70-90 kDa, 440744, Sigma-Aldrich, USA) was added to the corresponding solvent mixture and stirred at room temperature for 24 h.

Table 4.1: Composition of the PCL solutions in chloroform

PCL Solution	I	II	III	IV
PCL concentration ($kg \cdot m^{-3}$)	130	160	160	140
Non solvent (methanol)	no	Yes	Yes	yes
Chloroform/methanol volumetric ratio	---	9:1	5:1	5:1

The scaffolds were electrospun under a controlled humidity and temperature environment, using a single electrode electrospinning apparatus (EC-CLI, IME Technologies, Netherlands). The solution concentration and the electrospinning parameters (flow rate, distance between needle and collector, voltage, humidity and temperature) used for each solution were specified in a preliminary set of tests. These preliminary tests were performed to identify adequate electrospinning conditions, i.e, conditions in which no instabilities in the fiber and scaffold formation (such as beading, electrospraying, dripping from the syringe tip, oscillating streaming jet, small deposition area) occur. The parameters used to electrospin the fibers, which were selected based on a battery of previous tests, are presented in Table 4.2.

Table 4.2: Experimental parameters used to electrospin the scaffolds

Solution	I	II	III	IV
Flow rate ($\times 10^{10}$ $m^3 s^{-1}$)	2.8	16.7	13.3	13.3
Distance (cm)	30	35	15	15
Voltage (kV)	29	17	25	25
Relative humidity (%)	38.5	38.5	38.5	38.5
Temperature (K)	298.15	292.15	292.15	292.15
Needle inner diameter ($\times 10^4$ m)	8	8	8	8

Scaffold characterization

The morphology and diameter of the fibers were estimated using a scanning electron microscope (SEM; JEOL - JSM 6060, JEOL Ltd., Japan). The samples were prepared by collection of the fibers on 15 mm glass coverslips, coated with platinum, and then mounted on aluminum stubs for SEM analysis using an accelerating voltage of 10 kV. For each of the four forming solutions under considerations, 3 samples were produced (in different days), and 3 images (different regions of the sample) were acquired by sample, resulting in a total of 9 images for each system. The resulting scanning electron microscopy images were analyzed with the open source software ImageJ. The diameter of each fiber in the image (at least 10 fibers per image) was determined manually using the "Measure" tool of ImageJ. Pore diameters were determined according to the following steps: (i) visual identification of individual pores, specified as closed polygons whose sides are fibers contained in adjacent layers; (ii) determination of the area of the respective polygon using the "Polygon Selection" and "Measure" tools of ImageJ; (iii) estimation of the pore diameter as the diameter of a circle with equivalent area, as proposed by McHugh et al. [19].

Cell culture

Dental pulp stem cells were obtained from human deciduous teeth with physiologic root resorption with the approval (project number33177214.1.3001.5330) of the Ethics Committee of the Universidade Federal do Rio Grande do Sul. After dental pulp tissue removal, thecells were isolated using mechanic and enzymatic digestion with 0.2 % type I collagenase (Gibco, Grand Island, NY) and then incubated for 60 min in a 37° C bath. Non-adherent cells were removed by medium exchange and the cells were cultured at 37 °C and 5 % CO_2 in Dulbecco's modified Eagle's culture medium (DMEM) supplemented with 10 % fetal bovine serum (FBS) (Gibco, Grand Island, NY) and 100 U/mL penicillin and 100 mg/mL streptomycin (Gibco, Grand Island, NY). The medium was exchanged every 4 days. The cells were trypsinized until reaching a confluence of 90 %.

In order to determine the cell number, the cell metabolic activity was evaluated by a water-soluble tetrazolium salts assay (WST-8, 2-(2-methoxy-4-nitrophenyl)-3-(4-nitrophenyl)-5-(2,4-disulfophenyl)-2H-tetrazolium]). Therefore, after culture medium removal, the samples were incubated (at 5 % CO_2 and 37°C) with 180 µL of fresh medium and 20 µL of Cell Counting Kit-8 solution (CCK-8, Sigma–Aldrich, USA) for 1 h. Then, a microplate reader (Multiskan FC, Thermo Scientific, USA) was used for absorbance (450 nm)

detection and a calibration curve was used for each culture to estimate the cell number (three primary culture cells were used).

Glucose uptake and lactate production

Glucose concentrations were quantified by an enzymatic colorimetric assay based on the glucose oxidation by glucose oxidase (K082, Bioclin, Quibasa, Brazil), whereas lactate concentrations were determined with an UV enzymatic assay based on lactate oxidation by dehydrogenase lactate (K084, Bioclin, Quibasa, Brazil). Culture medium samples were collected at the days 1, 4 and 7, mixed with the respective monoreagent containing the enzymatic reagent of each assay according to the manufacturer's instructions. Glucose and lactate concentrations were calculated based on absorbance detection with a microplate reader (Multiskan FC, Thermo Scientific, USA) at 340 nm and 570 nm, respectively.

Cell distribution

After 7 days of culture, the samples were fixed in 4 % (w/v) paraformaldehyde (Sigma-Aldrich, USA) for 30 min, washed with phosphate buffered saline (PBS) and stained with 5 mg mL^{-1} 4',6-diamidino-2-phenylindole (DAPI) for 5 minutes. After washed again with PBS, sections of 30 µm were obtained in a cryostat for further imaging with an optical microscope Eclipse Ti-S (Nikon).

Statistical analysis

Statistical analysis was performed using Gnu PSPP statistical software (version 0.10.5). Normal distribution was verified with the combination of Shapiro–Wilk test and visual inspection of Q-Q plots. Statistical comparison between samples was performed using either the one-way ANOVA with post-hoc Tukey test or the Mann-Whitney-Wilcoxon test, depending on the samples distribution.

4.3 Results and Discussion

Aiming to facilitate the understanding and visualization of the results that will be discussed in this section, only one of the nine scanning electron microscope images collected for fibers obtained from Solutions I, II, III and IV are depicted in Figures 4.1, 4.2, 4.3 and 4.4, respectively. Their respective fiber and pore size distribution are given in Figures 4.5 and 4.6,

followed by the results regarding cell growth, distribution and metabolism, presented in Figures 4.7, 4.8, 4.9, 4.10 and 4.11.

Scaffold characterization

It was experimentally observed that the addition of methanol improved the electrospinnability of the PCL solution, increasing the spreading of the fibers throughout the collector and reducing the heterogeneity of the fiber diameters. The latter is clearly observed in Figures 4.2-4.4, where the fibers are notably more homogeneous in diameter than those obtained with Solution I (Figure 4.1).

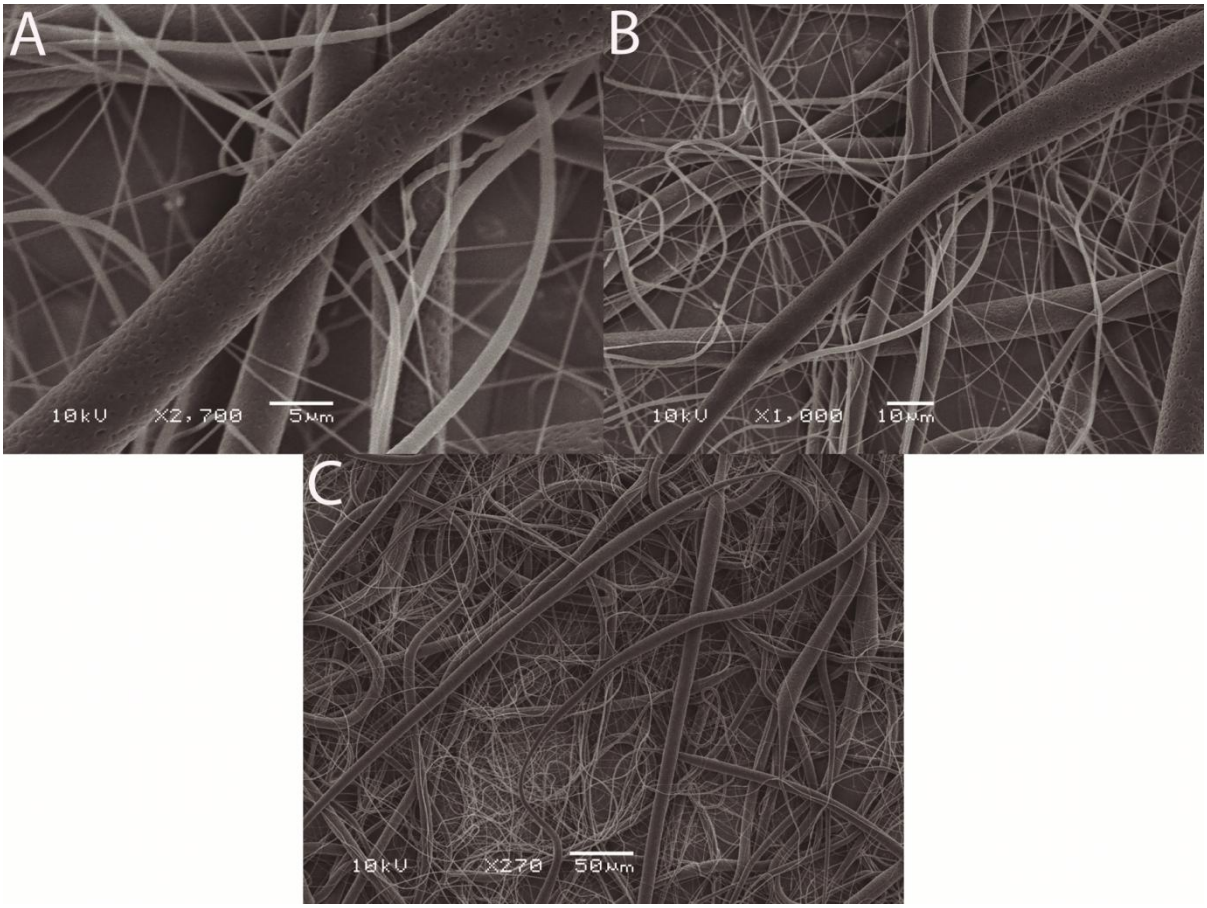

Figure 4.1: Scanning electron microscope images of the scaffolds produced from Solution I: chloroform and polycaprolactone (130 kg·m^{-3}). Images with decreasing magnification A: x2700 magnification, B: x1000 magnification, C: x270 magnification

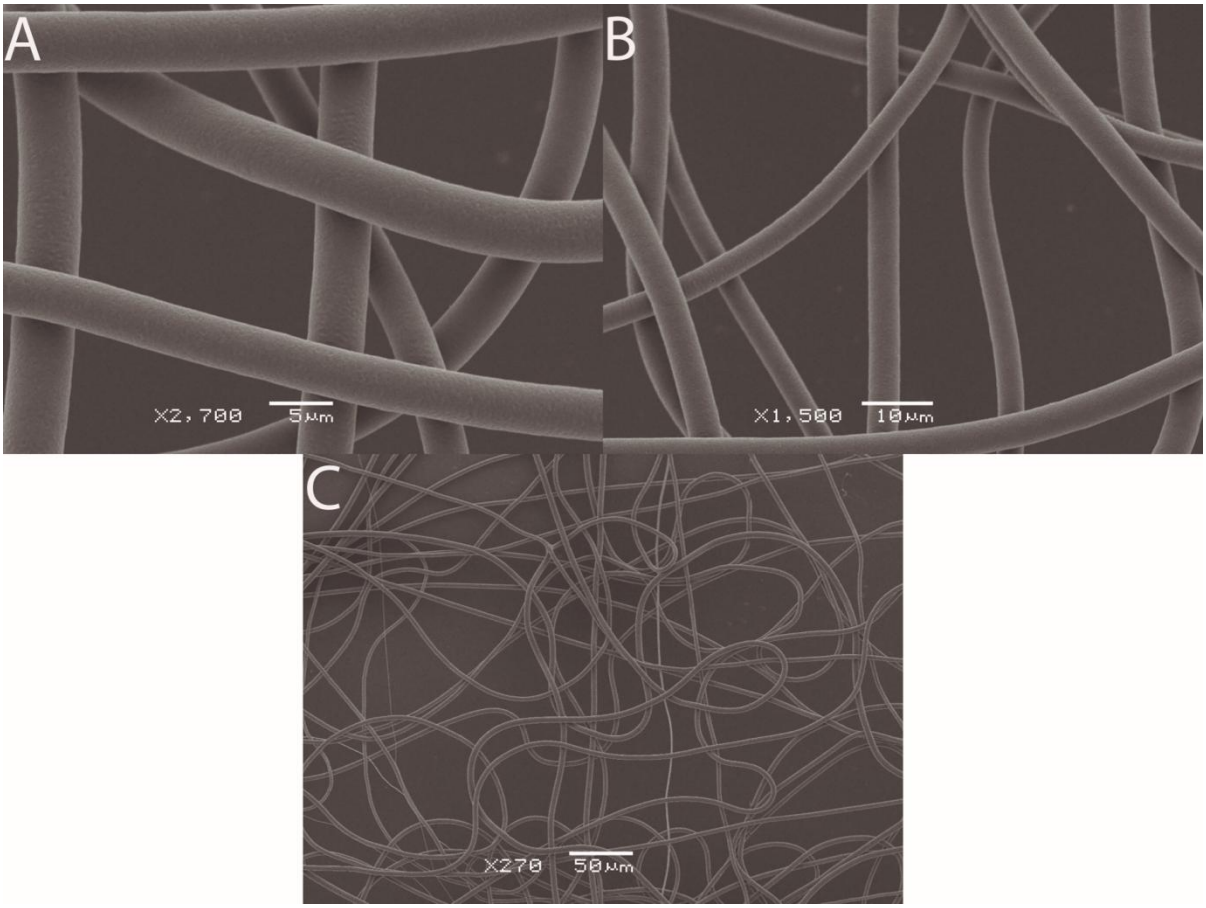

Figure 4.2: Scanning electron microscope images of the scaffolds produced from Solution II: chloroform:methanol (9:1) and polycaprolactone (160 $kg \cdot m^{-3}$). Images with decreasing magnification A: x2700 magnification, B: x1000 magnification, C: x270 magnification

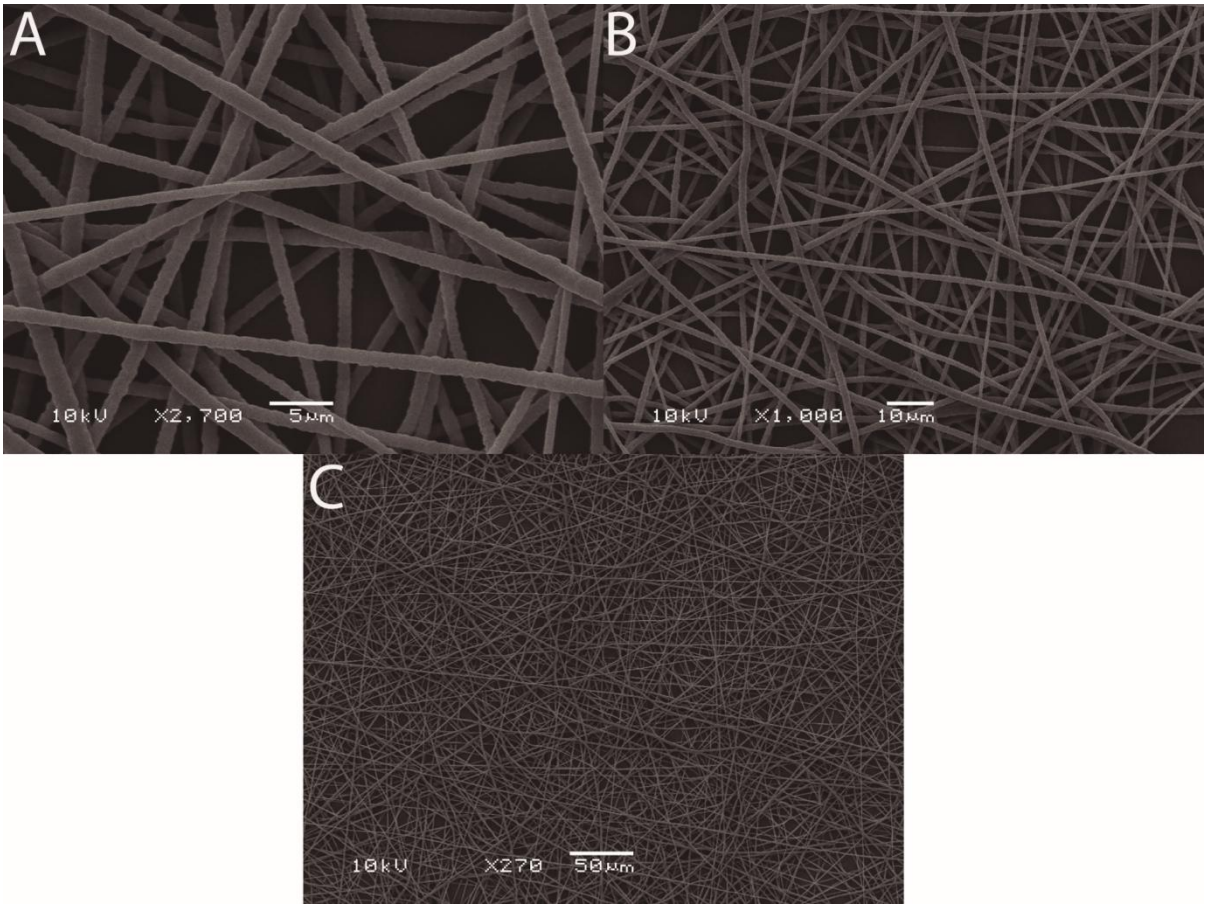

Figure 4.3: Scanning electron microscope images of the scaffolds produced from Solution III: chloroform:methanol (5:1) and polycaprolactone (160 kg·m^{-3}). Images with decreasing magnification A: x2700 magnification, B: x1500 magnification, C: x270 magnification

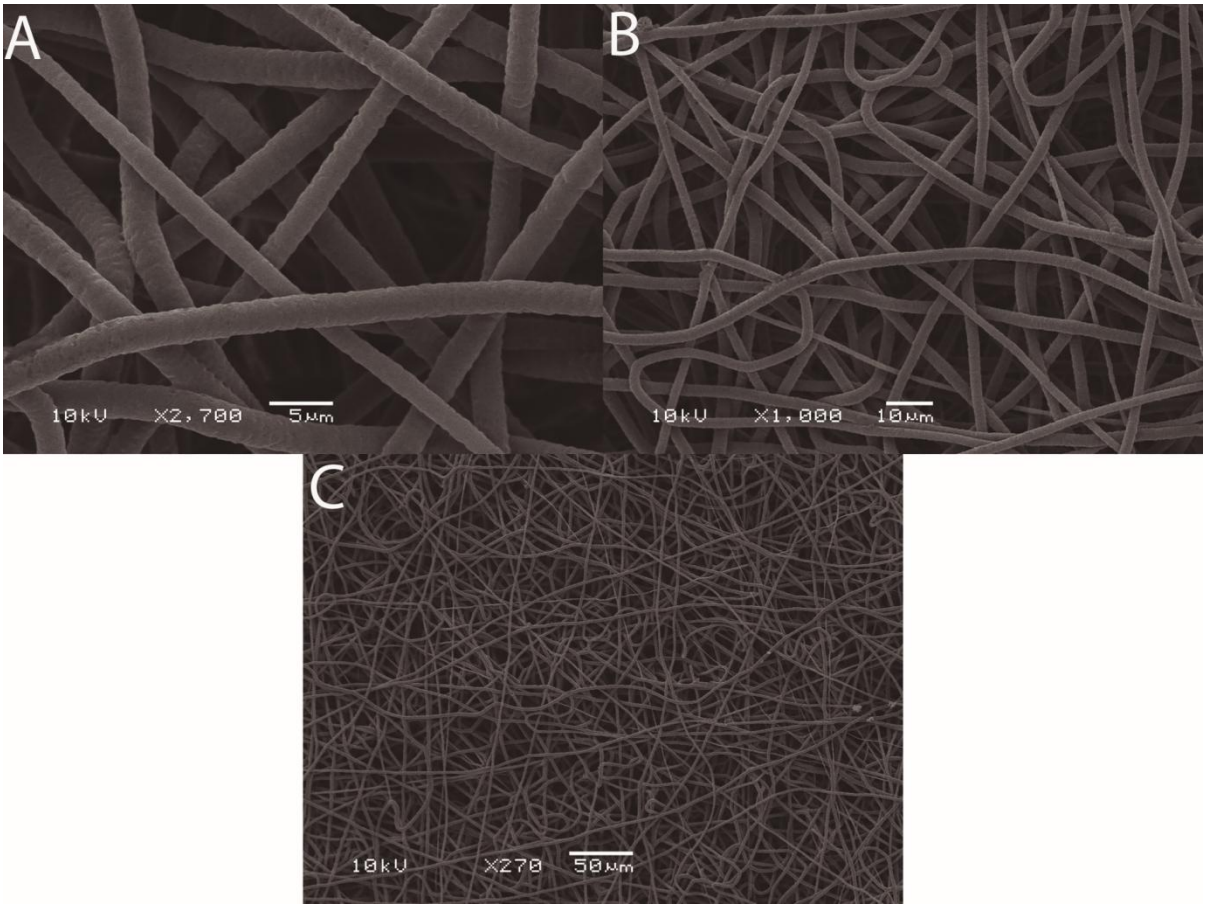

Figure 4.4: Scanning electron microscope images of the scaffolds produced from Solution IV: chloroform:methanol (5:1) and polycaprolactone (140 $kg \cdot m^{-3}$). Images with decreasing magnification A: x2700 magnification, B: x1000 magnification, C: x270 magnification

The fiber size distributions obtained with the Solutions I, II, III and IV are shown in Figure 4.5, where the frequencies are given as a percentile of the total number of fibers measured for each solution, and are plotted at the midpoint of each interval of fiber diameter.

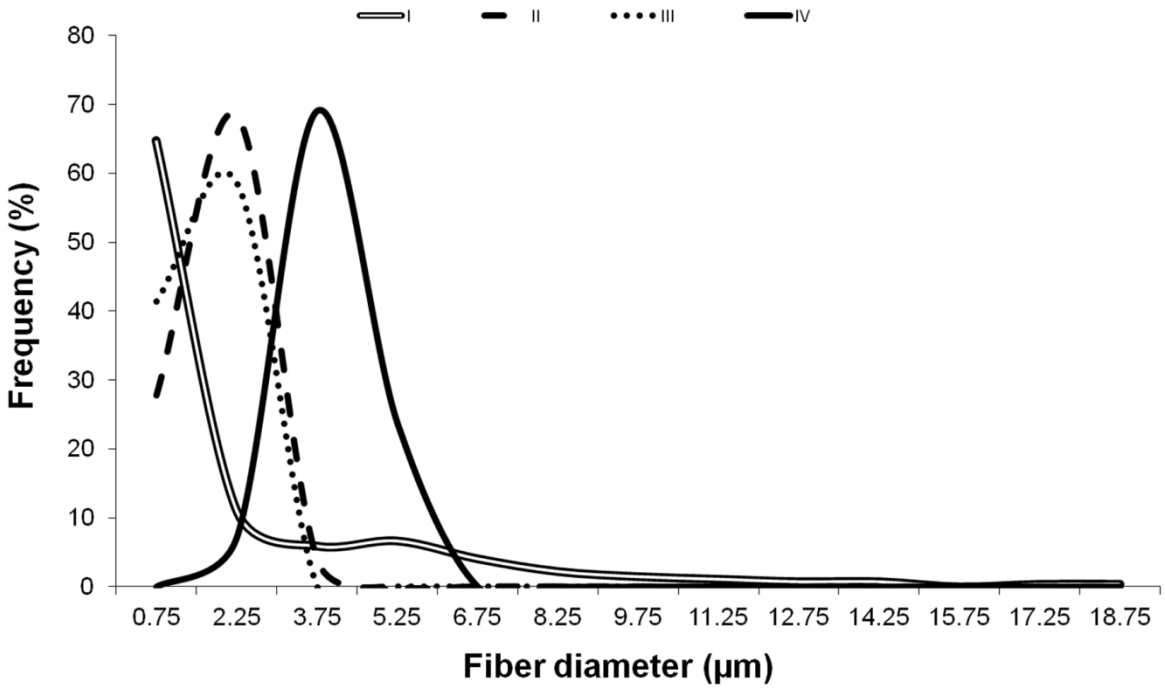

Figure 4.5: Scaffold fiber diameter distribution obtained using Solutions I, II, III and IV

In Figure 4.5, it can be observed a very heterogeneous distribution of fiber diameter obtained with the Solution I, where 65 % of the fibers had a diameter from 0 to 1.5 μm, 24 % within 1.5 and 6 μm, and 11 % within 6 to 21 μm. The PCL solutions with both chloroform and methanol (II, III and IV) presented narrower normal-like fiber diameter distributions, with 68 %, 59 % and 69 % frequency within the intervals 1.5 and 3 μm, 1.5 and 3 μm and 3 and 4.5 μm, respectively. The decrease of the distribution width with the increase of the methanol amount and of the concentration (Solution III) can be explained by the increase in electrospinnability due to higher electrical conductivities [20].

According to the Shapiro–Wilk test and visual inspection of Q-Q plots, only the fibers obtained with Solution I presented a non-normal distribution of diameters. Besides, using the Mann-Whitney-Wilcoxon test, it was observed that the mean fiber diameter obtained with Solution I was significantly different from the ones obtained with Solutions II, III and IV ($p<0.0001$). With the Student's t-test, it was observed that the mean fiber diameters obtained with the Solutions II, III and IV were significantly different from each other ($p<0.0001$).

The fiber size distribution parameters obtained with the fiber-forming solutions used are shown in Table 4.3.

Table 4.3: Fiber diameter obtained for each polymeric solution

Solution	I	II	III	IV
Mean (μm)	1.96	3.95	1.59	1.83
Standard deviation (μm)	2.67	0.73	0.45	0.65
Minimum (μm)	0.02	1.98	0.47	0.30
Maximum (μm)	20.15	5.62	2.69	3.55

The scaffold mean fiber diameter obtained from Solution II was higher than that from Solution I, which could be expected as the former had a higher polymer concentration and, consequently, higher viscosity. However, the maximum fiber diameter was higher for Solution I, which can be related to the poor electrospinnability of the solution using only chloroform, leading to a very heterogeneous fiber distribution.

As can be seen in Table 4.3, the mean diameter of fibers obtained from Solution III, with higher PCL concentration (160 $kg \cdot m^{-3}$) and methanol addition, is smaller than the one from Solution I (130 $kg \cdot m^{-3}$), with pure chloroform. This indicates that in the studied system the decrease of diameter resulting from the addition of non-solvent overcomes the effect of the increase of viscosity due to the increase in polymer concentration. These results are in agreement with those presented by Luo et al. [17] for the electrospinning of PCL, who showed that the higher the addition of non-solvents with high dielectric constant, such as methanol, to solvents with low dielectric constant, like chloroform, the smaller the fiber diameter obtained. Accordingly, Solution II, with lower methanol content in the solvent mixture, led to higher values of the fiber diameter (minimum, maximum and mean) than Solution III, which had the same polymer concentration. On the other hand, the reduction of the polymer concentration (Solution IV) led to thicker fibers in comparison to those obtained with Solution III, which can also be explained based on the effect of the polymer concentration on the forming-solution conductivity, as discussed earlier. Similar behavior effect has been reported for several fiber-forming solutions, including polyvinyl butyral (PVB) in ethanol[20], PVB in isopropanol[21], polyethylene glycol in a 2:1 chloroform:methanol mixture[22], and polycaprolactone/gelatin in formic acid[23]. Yalcinkaya[20] suggested that the presence of a polar group promotes increase of the electrical conductivity with the increase of the polymer concentration and that this effect overcomes the effect of the simultaneous increase of viscosity, resulting in smaller fiber diameters.

Besides the effect on the fiber diameter distribution, the addition of methanol to the forming solution also affected the morphology of the produced fibers, mainly with relation to the characteristics of the fiber surface and to the fiber shape (straight or curled).

In accordance with Figure 4.1, the scaffolds obtained with pure chloroform (Solution I) presented voids on fiber surface. This morphology can be explained by the high volatility of chloroform as solvents that evaporate rapidly lead to more porous fibers [24]. Besides, a curly morphology and presence of thick microfibers among the nanofibers can be observed, suggesting a bimodal fiber size distribution. This can be caused by an irregular jet-like ejection, as verified by Gomez-Sanchez et al. [25] in the electrospinning of poly(lactic acid)/polyhedral oligomeric silsesquioxane nanocomposites at a low feeding rate and with a large distance between the electrodes

The effect of the addition of methanol on the characteristics of the surface is evident when comparing Figure 4.1A to Figures 4.2A and 4.3A. This comparison shows a gradual evolution of a smooth surface with voids (Figures 4.1A and 4.2A) to a rough surface (Figure 4.3A). This behavior may be related to a change in the phase separation process due to the addition of the non-solvent. The higher polymer concentration and lower temperature used to electrospin Solutions II and III, when compared to the correspondent values used to electrospin Solution I, could also have affected phase separation.

Regarding the shape of the formed fibers, a reduction of curliness is observed even with the addition of small proportion of methanol the sequence of the fibers, as indicates the comparison of Figure 4.1C and 4.2C. Then, the fibers obtained with Solution III (Figure 4.3C), i.e, with higher content of methanol, are nearly straight. This effect is probably due to the increase of electrical conductivity with the increase of the content of methanol in the forming solution, since methanol is drastically more conductive than chloroform. This behavior was also verified by Xue et al. [26] for gelatin dissolved in a mixture of acetic acid and ethyl acetate, where a high conductivity polymeric solution leads to whipping instability, forming curly fibers.

In Figure 4.4, the images show that the fibers obtained with Solution IV are also curlier than the ones obtained with Solution III. This is probably related to the decrease of the fiber-forming solution conductivity due to the lower PCL concentration of Solution IV in comparison to Solution III. Poly(vinyl butyral) (PVB) nanofibers produced with different solvents have shown increased solution conductivities with the increase of the polymer concentration from 80 to 100 $kg \cdot m^{-3}$ [27].

The pore diameters distributions of each PCL solution are shown in Figure 4.6, where the frequencies are given as a percentile of the total number of pores measured for each solution, and are plotted at the midpoint of each interval of pore diameter.

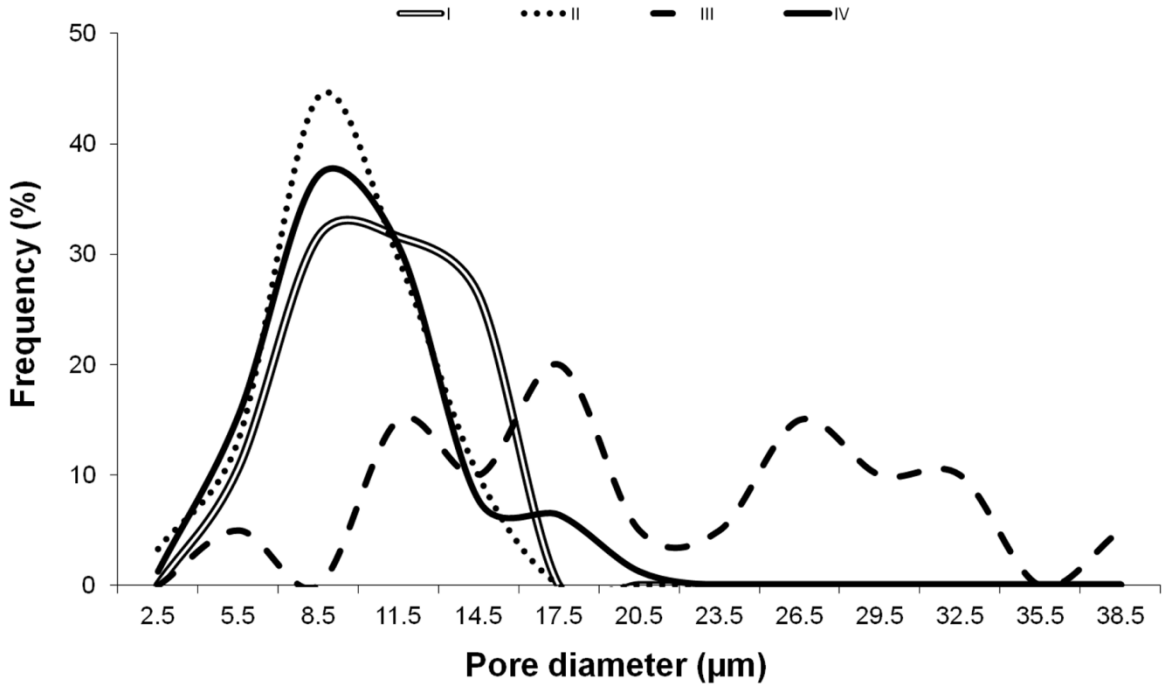

Figure 4.6: Scaffold pore diameter distribution obtained using Solutions I, II, III and IV

In accordance with Figure 4.6, the homogeneity of the pore size distribution is enhanced with a lower PCL concentration, since the Solution IV (5:1 chloroform:methanol, 140 $kg \cdot m^{-3}$) produced scaffolds with a pore diameter distribution more homogeneous than the Solution III (5:1 chloroform:methanol, 160 $kg \cdot m^{-3}$). An increased homogeneity was also observed with a smaller proportion of methanol, given that Solution II presented a more homogeneous pore diameter distribution than Solution III (5:1 chloroform:methanol, 160 $kg \cdot m^{-3}$). The Solution III produced scaffolds with a more heterogeneous distribution of pore diameter.

By visual inspection of Q-Q plots, it was verified that the pore diameters obtained with the Solutions I and II were not normally distributed. Using the Student's t-test, it was observed that the mean pore diameters obtained with the Solutions III and IV were not significantly different from each other. According the Mann-Whitney-Wilcoxon test, it was observed that only the mean pore diameter obtained with Solution II was significantly different from the ones obtained with Solutions I, III and IV ($p<0.0001$).

Table 4.4 presents the results regarding the pore size and the ratio between the fiber and pore diameters for the Solutions I, II, III and IV.

Table 4.4: Pore diameter and ratio between the fiber and the pore sizes

Solution	I	II	III	IV
Mean pore diameter (μm)	10.89	21.35	9.38	10.01
Pore diameter standard deviation (μm)	3.31	8.89	2.76	3.49
Maximum pore diameter (μm)	15.92	38.06	14.77	19.97
Minimum pore diameter (μm)	5.64	5.78	2.05	1.62
Mean ratio fiber diameter/pore diameter	5.54	5.40	5.89	5.48

As it can be seen in Table 4.4, the values of mean pore diameter followed the same trend as values of the mean fiber diameter presented in the Table 4.3, with scaffolds obtained from Solutions II, I, IV and III appearing in descending order of mean pore size. On the other hand, the pore diameter standard deviation was lower for Solution I (around 30 % of the mean pore size), when compared to the ones obtained for the fiber diameter (around 130 % of the mean value). This can be attributed to the wide fiber diameter distribution obtained for this system, since the nanofibers produced with Solution I end up accommodating in the network formed by the microfibers, reducing the pore diameters. In addition, the scaffolds produced without the addition of methanol (Solution I) resulted in a ratio fiber diameter/pore diameter close to the value of 6.0 found by Hussain et al. [28] for an electrospun scaffold of polyacrylonitrile (PAN) and N,N-dimethylformamide (DMF) with bimodal fiber diameter distribution.

With the addition of methanol to the forming solution (Solutions II, III and IV), presented ratios of fiber diameter and pore diameter close to the value of 5.0 reported by Hussain et al. [28] for mean capillary pore size of a nonwoven scaffold with unimodal fiber diameter distribution obtained from a PAN and DMF spinning solution.

Cell growth and infiltration

The cell growth in the scaffolds produced with each PCL solution is shown in Figure 4.7A. It can be observed that is a similar cell number in all scaffold types studied (no statistical difference was observed between the groups) at the initial days of culture (days 1-4). Regarding the scaffolds, statistical difference ($p<0.05$) was only observed between the number of cells at day 7 in scaffolds produced with the Solution I and the ones produced with

the Solution IV. This could be associated with the smaller fibers present in the scaffolds produced with the first solution, which can provide a higher surface area for cell spreading and proliferation. Chen et al. [29] also obtained higher growth kinetics in PCL scaffolds with smaller fiber diameter than with larger fibers. Furthermore, the cell numbers in the wells (control group) were statistically higher than in the scaffolds at all time points, what was expected since the well's polystyrene surface can be considered a gold standard for adherent cell culture [30]. In addition to the smaller adhesion of the cells on the PCL surface of the electrospun scaffolds, the scaffolds (considering the results obtained with the four PCL solutions) presented a statistically different doubling time – 7.06 ± 2.07 days – when compared to the well – 3.18 ± 0.41 days ($p<0.05$), even though no statistical difference between the groups was observed when each scaffold group was compared individually (Figure 4.7B). Brennan et al. [31] also obtained a smaller growth rate for human mesenchymal stem cells in a PCL electrospun scaffold than in the control group (well). According to Liu et al. [32], a smaller human mesenchymal stem cell density can lead to a reduced doubling time, what can explain the smaller doubling time in the scaffold groups. The Figures 4.7C, 4.7D and 4.7E show similar cell growth for Culture I, II and III, with a behavior analogous to the one depicted in Figure 4.7A.

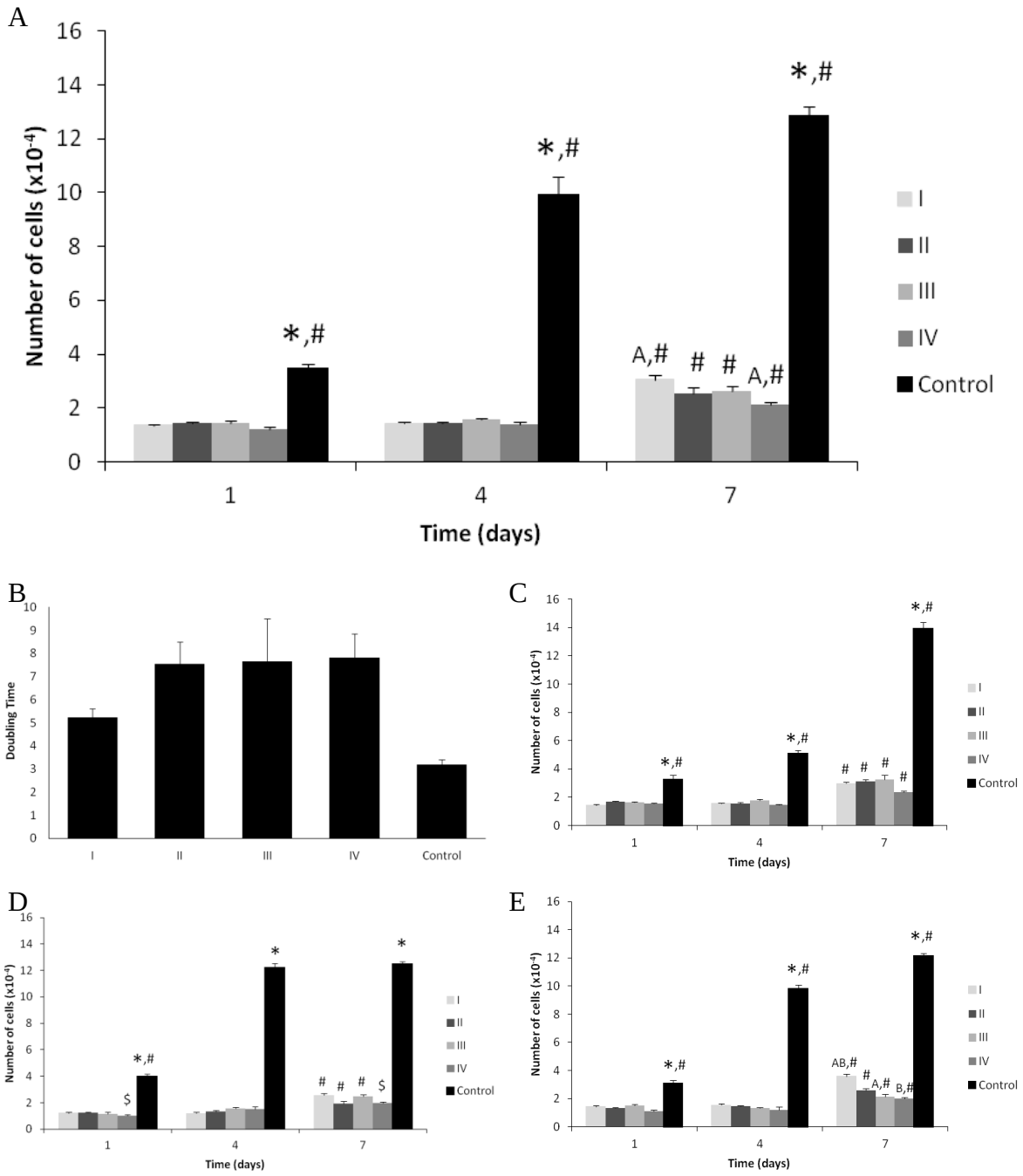

Figure 4.7: Cell growth in the scaffolds obtained with the Solutions I, II, III and IV, with the well as the control group (well). A: mean cell number between cultures over time, B: mean doubling time between cultures for each group, C, D and E: cell number for Culture I, II and III over time, respectively. Results expressed as mean ± standard error of the mean and compared by one-way ANOVA with Tukey post-hoc test. The symbols * and # represents significant difference ($p<0.05$) with all the other groups within the same time point and with all the other time points within the same group, whereas capital letters and $ indicate significant difference between two groups within the same time point and two time points within the same group, respectively

Figure 4.8 presents the images of the cell nuclei staining, through which it can be observed the cell distribution along the scaffold thickness. It can be seen that the higher and smaller cell infiltration occurred in the scaffold with the higher and smaller mean pore size (given in Table 4.4), produced with the Solution II and III, respectively. Regarding cell culture requirements, the pore size should be small enough to allow cell adhesion among the fibers, and sufficiently large to promote cell infiltration. Since solution III formed mostly small pores, with nearly 70 % of them smaller than 10.5 μm, it could be more favorable for tissue engineering applications that admit a two-dimensional cell growth. As it can be observed in Figure 4.8C, the cells remained only on the surface of the scaffold. Scaffolds produced with Solutions I and IV, with 58 % and 40 % of the pores within 10.5 and 16.5 μm, respectively, could be suitable for the culture of bovine chondrocytes (average cell diameters of 10.8 μm) [33,34], human placenta and umbilical cord cells (cell diameters between 10 and 15 μm) [35]. The diameter of mesenchymal stem cells (MSCs) have been reported between 14 and 16 μm for human dental pulp stem cells (hDPSCs) [36] and human bone-marrow derived stem cells (hBMSCs) [37,38], with higher values for human (21.59 μm) [39], mouse (28 μm) [40] and whale (29 μm) [39] stem cells derived from adipose tissues. With only 16 % and 13 % of the pores with diameters higher than 14 μm, the scaffolds produced Solutions I and IV did not present a relevant cell infiltration, as presented in Figures 4.8A and 4.8D. However, these scaffolds could be applied for wound healing and skin tissue engineering, since they allow cell adherence and growth on the surface [41]. Wang et al. [42] also did not observed the infiltration of NIH3T3 cells, which have a diameter in the range of 10-18 μm [43], in electrospun PCL scaffolds with pore sizes from 13 to 16 μm. With 35 % of the pore diameters between 15 and 25 μm and 40 % higher than 25 μm, the scaffolds produced with Solution II allowed human MSCs infiltration, as shown in Figure 4.8B. Furthermore, it is possible these scaffolds could also support the growth of MSCs derived from animal adipose tissues at some extent, given that 20 % of the pore diameters obtained with Solution II were between 30 and 38 μm. Wang et al. [42] could only observe cells infiltration in electrospun scaffolds with poly(ethylene oxide) microparticles as porogen, in which the pore diameter was higher than 31 μm [43].

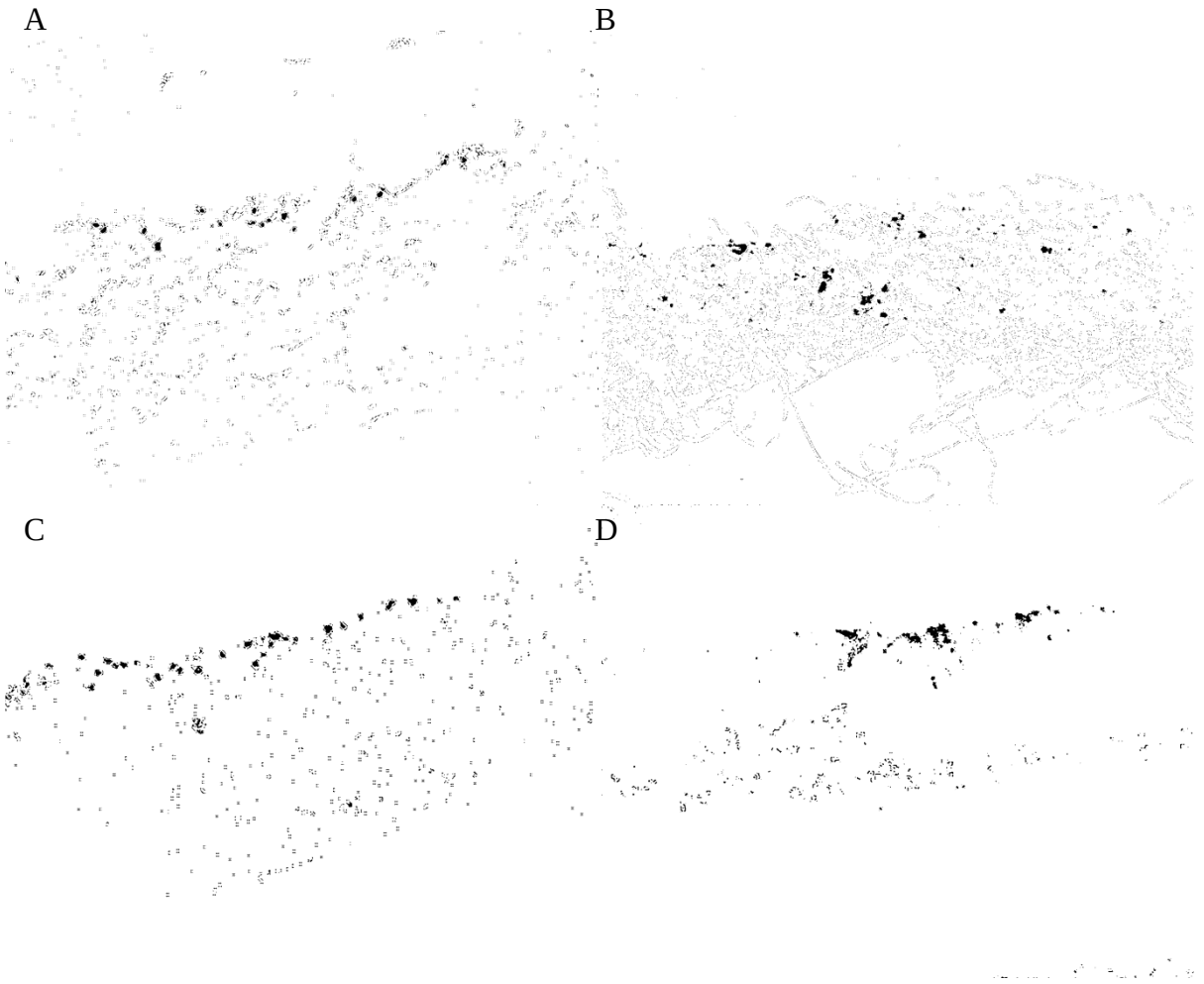

Figure 4.8: Cell nuclei staining with DAPI (filled rounded shapes) indicating cell distribution in the scaffolds (background lines) obtained with the Solutions I (A), II (B), III (C) and IV (D) after 7 days. Magnification 100x

Glucose uptake and lactate production

Figure 4.9 shows the data of glucose uptake in the scaffolds groups and in the control group (well). There was a significant difference between all the scaffold groups and the control in the time intervals 0-1 and 1-4 days. In the time interval 4-7 days only the scaffolds produced with Solutions I and IV presented significant difference with the control group (well). Also, the scaffolds from Solution II and the control group presented a significant smaller glucose uptake in the time intervals 1-4 and 4-7 days when compared to the initial time interval. Despite the discrepancies among the cultures (Figures 4.9B, 4.C and 4.D), the tendencies and behavior of the cells were depicted in Figure 4.9A.

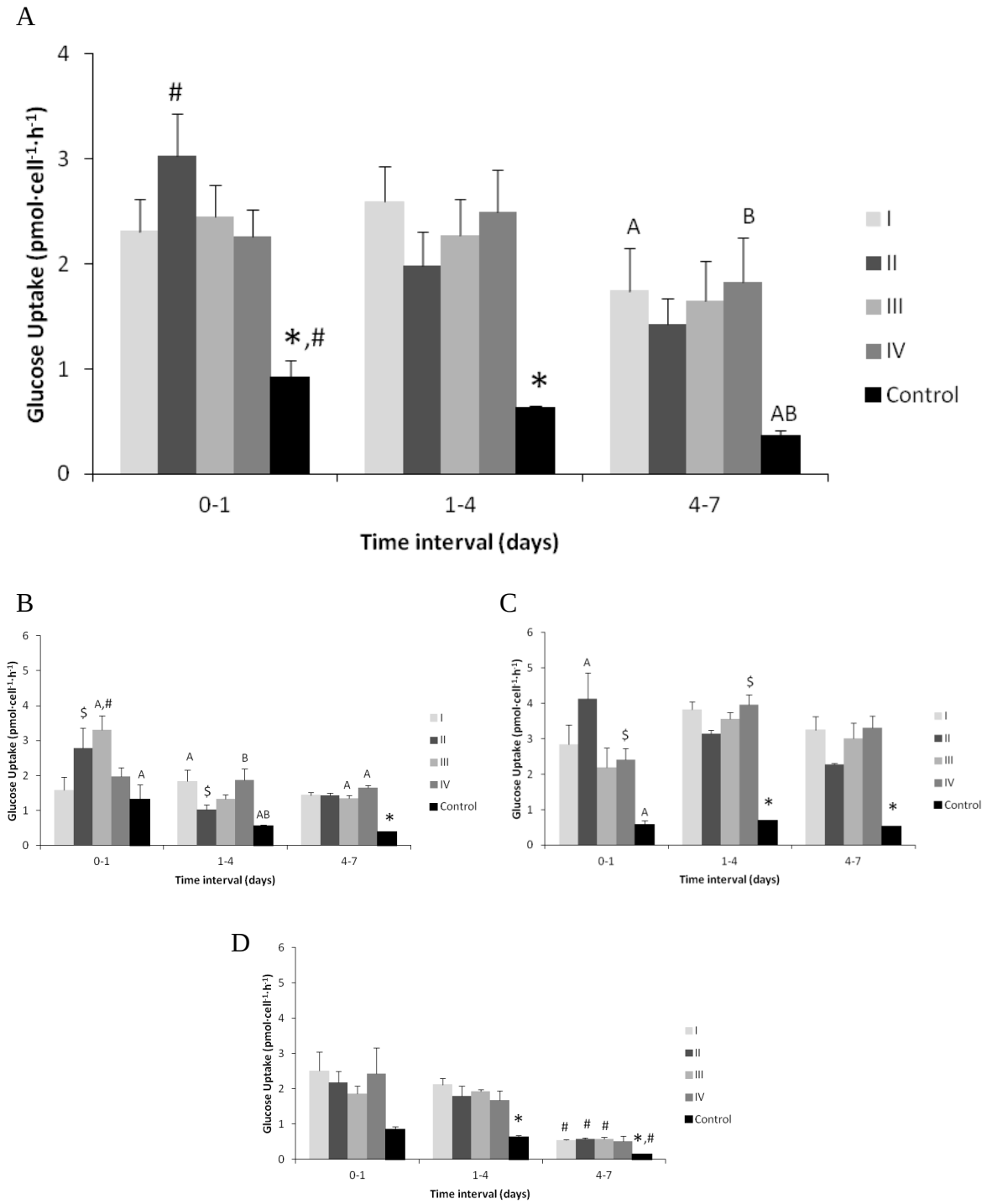

Figure 4.9: Glucose uptake in the scaffolds obtained with the Solutions I, II, III and IV, with the well as the control group. A: mean glucose uptake between cultures, B, C and D: glucose uptake for Culture I, II and III, respectively. Results expressed as mean ± standard error of the mean and compared by one-way ANOVA with Tukey post-hoc test. The symbols * and # represents significant difference ($p<0.05$) with all the other groups within the same time point and with all the other time points within the same group, whereas capital letters and $ indicate significant difference between two groups within the same time point and two time points within the same group, respectively

The lactate production was also higher in some of the scaffold groups – Solution I, in all time intervals, and Solutions II and III, in the interval 1-4 days – than in the control (well) (Figure 4.10). Furthermore, there was a significant reduction in the lactate production in all groups with time (Figure 4.10A), what can be also observed in the different cell cultures individually (Figured 4.10B, 4.C and 4.D). Murphy et al. [44] observed decreased glucose uptake and lactate production with increasing number of MSC per spheroids, possibly due to reduced extracellular matrix (ECM) synthesis. This could explain the results observed in the present study, since the scaffold groups presented reduced cell number.

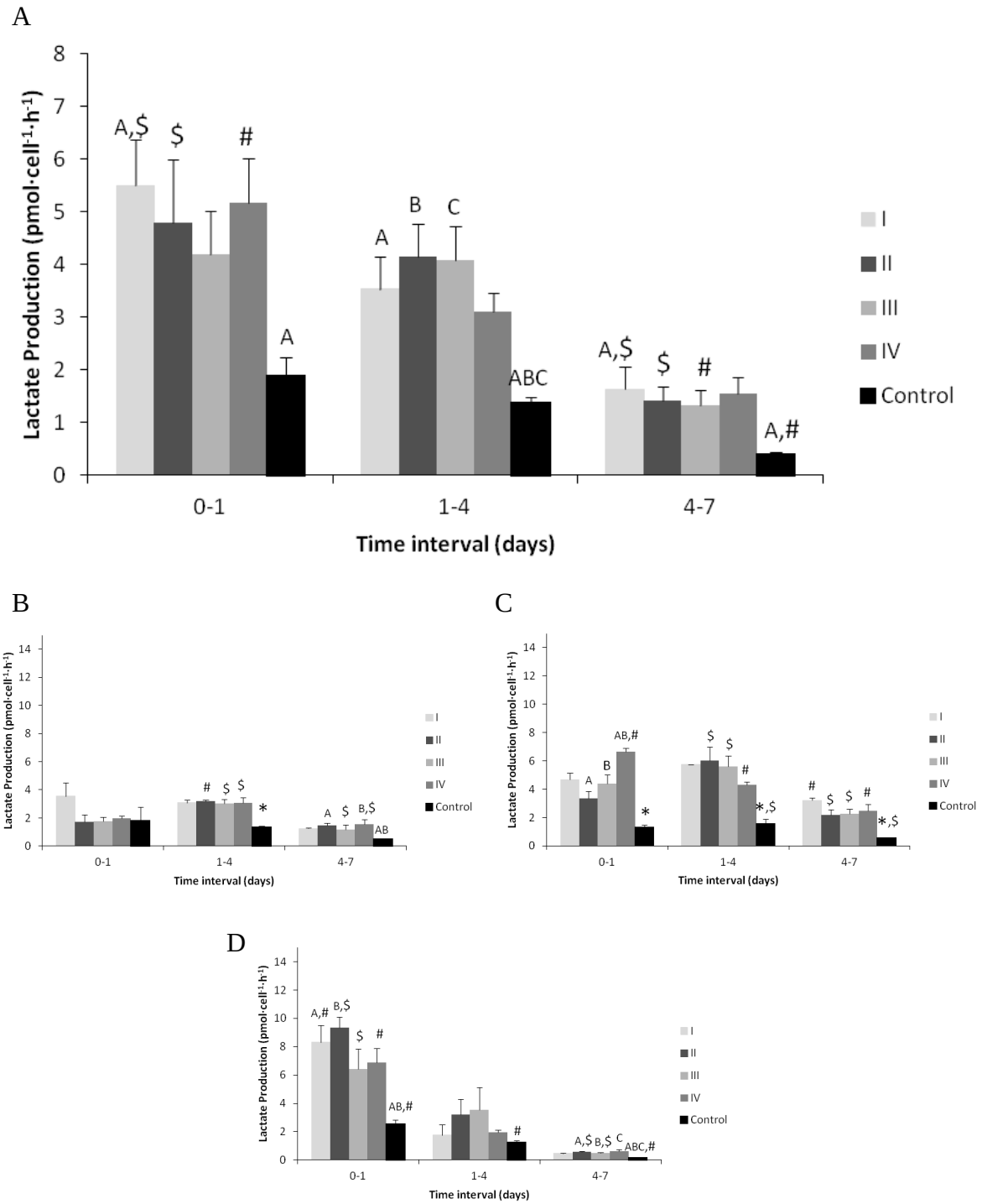

Figure 4.10: Lactate production in the scaffolds obtained with the Solutions I, II, III and IV, with the well as the control group. A: mean lactate production between cultures, B, C and D: lactate production for Culture I, II and III, respectively. Results expressed as mean ± standard error of the mean and compared by one-way ANOVA with Tukey post-hoc test. The symbols * and # represents significant difference ($p<0.05$) with all the other groups within the same time point and with all the other time points within the same group, whereas capital letters and $ indicate significant difference between two groups within the same time point and two time points within the same group, respectively

As presented in Figure 4.11, the resultant lactate/glucose ratios presented no significant difference between the scaffold groups and the well, indicating anaerobic glycolysis. In addition, there was significant difference between the ratios in the initial and final intervals for the scaffolds produced with the Solution I and IV and for the control group (well). Hamon et al. [45], also observed an anaerobic metabolism with a decrease in lactate/glucose ratio from day 4 to 14 of culture of fetal liver cells in polydimethylsiloxane membranes. Due to the small pore size of the scaffolds produced with Solutions I and IV, the cell growth occurred only on the surface of these scaffolds, similar to the bidimensional growth of the control group and of the Hamon et al. [45] membranes. Liu et al. [32] observed a smaller lactate/glucose ratio for a high density culture of human mesenchymal stem cells when compared to a low density culture. It is possible that these groups (Solutions I and IV and control) presented a higher cell-cell contact, and thus, a behavior similar to the one of a high density population on the day 7.

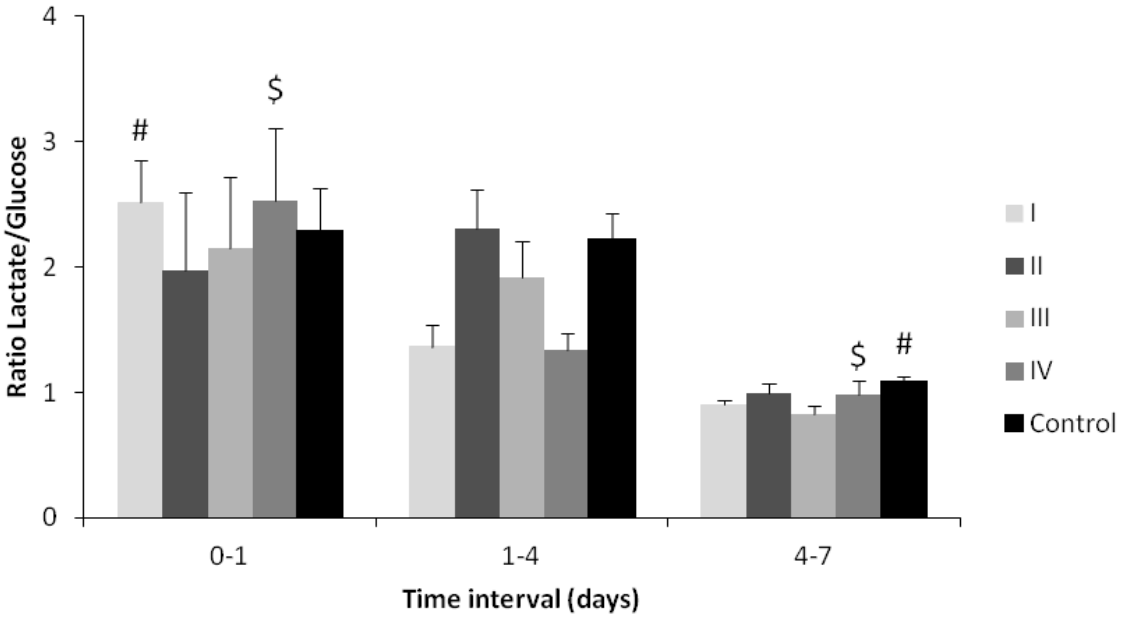

Figure 4.11: Mean lactate/glucose ratio between cultures in the scaffolds obtained with the Solutions I, II, III and IV, with the well as the control group. Results expressed as mean ± standard error of the mean and compared by one-way ANOVA with Tukey post-hoc test. The symbols * and # represents significant difference ($p<0.05$) with all the other groups within the same time point and with all the other time points within the same group, whereas capital letters and $ indicate significant difference between two groups within the same time point and two time points within the same group, respectively

4.4 Conclusions

The effect of the addition of a non-solvent on the fiber diameter of the polycaprolactone (PCL) scaffolds resulted in a more homogeneous fiber diameter distribution and improved electrospinnability of the solution. In addition, the solution with higher methanol content in the solvent mixture resulted in lower values of fiber diameter and straighter fibers. Therefore, the addition of methanol as a non-solvent in the PCL solution decreases the mean value and the width of the fiber diameter distribution of PCL electrospun scaffolds. The pore size did not affected cell growth, glucose uptake or lactate production in scaffolds. However, the scaffolds presented reduced cell adhesion and doubling time, and higher glucose uptake and lactate production than the control group (well). Finally, it was observed that the combination of methanol and chloroform at a rate of 9:1 in a 16 % PCL solution is capable to produce scaffolds with fiber and pore diameters appropriated for the infiltration and three-dimensional culture of mesenchymal stem cells.

4.5 Acknowledgments

The authors would like to thank CAPES (Coordination for the Improvement of Higher Education Personnel), FINEP (Financing Agency for Studies and Projects) and Stem Cell Research Institute for their financial support.

4.6 References

[1] C. Vaquette, J.J. Cooper-White, Increasing electrospun scaffold pore size with tailored collectors for improved cell penetration, Acta Biomater. 7 (2011) 2544–2557. doi:10.1016/j.actbio.2011.02.036.

[2] Q.P. Pham, U. Sharma, A.G. Mikos, Electrospun Poly(ε-caprolactone) Microfiber and Multilayer Nanofiber/Microfiber Scaffolds: Characterization of Scaffolds and Measurement of Cellular Infiltration, Biomacromolecules. 7 (2006) 2796–2805. doi:10.1021/bm060680j.

[3] B.J. Lawrence, Mass Transfer in Porous Tissue Engineering Scaffolds, Oklahoma State University, 2008.

[4] X. Fu, H. Wang, Rapid fabrication of biomimetic nanofiber-enabled skin grafts, in: T.J. Webster (Ed.), Nanomedicine Technol. Appl., Woodhead Publishing, Cambridge, UK, 2012: p. 428.

[5] H. Chang, Y. Wang, Cell Responses to Surface and Architecture of Tissue Engineering Scaffolds, in: Regen. Med. Tissue Eng. - Cells Biomater., InTech, 2011: pp. 569–588. doi:10.5772/21983.

[6] J.L. Lowery, N. Datta, G.C. Rutledge, Effect of fiber diameter, pore size and seeding method on growth of human dermal fibroblasts in electrospun poly(ε-caprolactone) fibrous mats, Biomaterials. 31 (2010) 491–504. doi:10.1016/j.biomaterials.2009.09.072.

[7] H. Bergmeister, C. Schreiber, C. Grasl, I. Walter, R. Plasenzotti, M. Stoiber, D. Bernhard, H. Schima, Healing characteristics of electrospun polyurethane grafts with various porosities, Acta Biomater. 9 (2013) 6032–6040. doi:10.1016/j.actbio.2012.12.009.

[8] S. Soliman, S. Pagliari, A. Rinaldi, G. Forte, R. Fiaccavento, F. Pagliari, O. Franzese, M. Minieri, P. Di Nardo, S. Licoccia, E. Traversa, Multiscale three-dimensional scaffolds for soft tissue engineering via multimodal electrospinning, Acta Biomater. 6 (2010) 1227–1237. doi:10.1016/j.actbio.2009.10.051.

[9] J.M. Gluck, Electrospun Nanofibrous Poly(ε-caprolactone) (PCL) Scaffolds for Liver Tissue Engineering, Graduate Faculty of North Carolina State University, 2007.

[10] A. Guimarães, A. Martins, E.D. Pinho, S. Faria, R.L. Reis, N.M. Neves, Solving cell infiltration limitations of electrospun nanofiber meshes for tissue engineering applications, Nanomedicine. 5 (2010) 539–554.

[11] K. Wang, M. Xu, M. Zhu, H. Su, H. Wang, D. Kong, L. Wang, Creation of macropores in electrospun silk fibroin scaffolds using sacrificial PEO-microparticles to enhance cellular infiltration, J. Biomed. Mater. Res. - Part A. 101 (2013) 3474–3481. doi:10.1002/jbm.a.34656.

[12] M.F. Leong, M.Z. Rasheed, T.C. Lim, K.S. Chian, In vitro cell infiltration and in vivo cell infiltration and vascularization in a fibrous, highly porous poly(D,L-lactide) scaffold fabricated by cryogenic electrospinning technique, J. Biomed. Mater. Res. - Part A. 91 (2009) 231–240. doi:10.1002/jbm.a.32208.

[13] B. Dhandayuthapani, Y. Yoshida, T. Maekawa, D.S. Kumar, Polymeric scaffolds in tissue engineering application: A review, Int. J. Polym. Sci. 2011 (2011). doi:10.1155/2011/290602.

[14] M. Abedalwafa, F. Wang, L. Wang, C. Li, Biodegradable poly-epsilon-caprolactone (pcl) for tissue engineering applications: a review, Rev Adv Mater Sci. 34 (2013) 123–140.

[15] L. Van Der Schueren, B. De Schoenmaker, Ö.I. Kalaoglu, K. De Clerck, An alternative solvent system for the steady state electrospinning of polycaprolactone, Eur. Polym. J. 47 (2011) 1256–1263. doi:10.1016/j.eurpolymj.2011.02.025.

[16] C. Del Gaudio, S. Baiguera, P. Macchiarini, A. Bianco, Microscopic assessment of scaffold ultrastructure for tissue engineering applications, Curr. Microsc. Contrib. to Adv. Sci. Technol. (2012) 406–413. http://www.formatex.info/microscopy5/book/406-413.pdf.

[17] C.J. Luo, E. Stride, M. Edirisinghe, Mapping the influence of solubility and dielectric constant on electrospinning polycaprolactone solutions, Macromolecules. 45 (2012) 4669–4680. doi:10.1021/ma300656u.

[18] S.R. Peyton, Z.I. Kalcioglu, J.C. Cohen, A.P. Runkle, K.J. Van Vliet, D. a. Lauffenburger, L.G. Griffith, Marrow-Derived stem cell motility in 3D synthetic scaffold is governed by geometry along with adhesivity and stiffness, Biotechnol. Bioeng. 108 (2011) 1181–1193. doi:10.1002/bit.23027.

[19] K.J. McHugh, S.L. Tao, M. Saint-Geniez, A novel porous scaffold fabrication technique for epithelial and endothelial tissue engineering, J. Mater. Sci. Mater. Med. 24 (2013) 1659–1670. doi:10.1007/s10856-013-4934-1.

[20] F. Yalcinkaya, Experimental study on electrospun polyvinyl butyral nanofibers using a non-solvent system, Fibers Polym. 16 (2015) 2544–2551. doi:10.1007/s12221-015-5525-1.

[21] F. Yener, O. Jirsak, R. Gemci, Effect of Polymer Concentration on Electrospinning System, in: Fiber Soc., Bursa, Turkey, 2010.

[22] H.J. Haroosh, D.S. Chaudhary, G.D. Ingram, Effect of Solution Concentration and Co-

solvent Ratio on Electrospun PEG Fibers, in: Chemeca, Sydney, Australia, 2011.
[23] M.M. Lim, N. Sultana, A. Bin Yahya, Fabrication and Characterization of Polycaprolactone (PCL)/Gelatin Electrospun Fibers, Appl. Mech. Mater. 554 (2014) 52–56. doi:10.4028/www.scientific.net/AMM.554.52.
[24] A. Celebioglu, T. Uyar, Electrospun porous cellulose acetate fibers from volatile solvent mixture, Mater. Lett. 65 (2011) 2291–2294. doi:10.1016/j.matlet.2011.04.039.
[25] C. Gomez-Sanchez, T. Kowalczyk, G. Ruiz De Eguino, A. Lopez-Arraiza, A. Infante, C.I. Rodriguez, T.A. Kowalewski, M. Sarrionandia, J. Aurrekoetxea, Electrospinning of poly(lactic acid)/polyhedral oligomeric silsesquioxane nanocomposites and their potential in chondrogenic tissue regeneration, J. Biomater. Sci. Polym. Ed. 25 (2014) 802–825. doi:10.1080/09205063.2014.910151.
[26] N. Xue, X. Li, C. Bertulli, Z. Li, A. Patharagulpong, A. Sadok, Y.Y.S. Huang, Rapid Patterning of 1-D Collagenous Topography as an ECM Protein Fibril Platform for Image Cytometry, PLoS One. 9 (2014) e93590. doi:10.1371/journal.pone.0093590.
[27] F. Yener, B. Yalcinkaya, Electrospinning of polyvinyl butyral in different solvents, E-Polymers. 13 (2013). doi:10.1515/epoly-2013-0121.
[28] D. Hussain, F. Loyal, A. Greiner, J.H. Wendorff, Structure property correlations for electrospun nanofiber nonwovens, Polymer (Guildf). 51 (2010) 3989–3997. doi:10.1016/j.polymer.2010.06.036.
[29] M. Chen, P.K. Patra, S.B. Warner, S. Bhowmick, Role of Fiber Diameter in Adhesion and Proliferation of NIH 3T3 Fibroblast on Electrospun Polycaprolactone Scaffolds, Tissue Eng. 13 (2007) 579–587. doi:10.1089/ten.2006.0205.
[30] K.M. Ferlin, M.E. Prendergast, M.L. Miller, D.S. Kaplan, J.P. Fisher, Influence of 3D printed porous architecture on mesenchymal stem cell enrichment and differentiation, Acta Biomater. 32 (2016) 161–169. doi:10.1016/j.actbio.2016.01.007.
[31] M.Á. Brennan, A. Renaud, A. Gamblin, C. D'Arros, S. Nedellec, V. Trichet, P. Layrolle, 3D cell culture and osteogenic differentiation of human bone marrow stromal cells plated onto jet-sprayed or electrospun micro-fiber scaffolds, Biomed. Mater. 10 (2015) 45019. doi:10.1088/1748-6041/10/4/045019.
[32] Y. Liu, N. Muñoz, B.A. Bunnell, T.M. Logan, T. Ma, Density-Dependent Metabolic Heterogeneity in Human Mesenchymal Stem Cells, Stem Cells. 33 (2015) 3368–3381. doi:10.1002/stem.2097.
[33] E.J. Vanderploeg, C.G. Wilson, M.E. Levenston, Articular chondrocytes derived from distinct tissue zones differentially respond to in vitro oscillatory tensile loading, Osteoarthr. Cartil. 16 (2008) 1228–1236. doi:10.1016/j.joca.2008.02.016.
[34] Z. Wang, J. Irianto, S. Kazun, W. Wang, M.M. Knight, The rate of hypo-osmotic challenge influences regulatory volume decrease (RVD) and mechanical properties of articular chondrocytes, Osteoarthr. Cartil. 23 (2015) 289–299. doi:10.1016/j.joca.2014.11.003.
[35] D.M. Anastasiu, A. Cean, M.F. Bojin, A. Gluhovschi, C. Panaitescu, V. Păunescu, G. Tănăsie, Explants-isolated human placenta and umbilical cord cells share characteristics of both epithelial and mesenchymal stem cells., Rom. J. Morphol. Embryol. 57 (2016) 383–90. http://www.ncbi.nlm.nih.gov/pubmed/27516009.
[36] J. Suchanek, T. Soukup, B. Visek, R. Ivancakova, L. Kucerova, J. Mokry, Dental pulp stem cells and their characterization., Biomed. Pap. Med. Fac. Univ. Palacky. Olomouc. Czech. Repub. 153 (2009) 31–5. http://www.ncbi.nlm.nih.gov/pubmed/19365523.
[37] T.R.J. Heathman, V.A.M. Glyn, A. Picken, Q.A. Rafiq, K. Coopman, A.W. Nienow, B. Kara, C.J. Hewitt, Expansion, harvest and cryopreservation of human mesenchymal stem cells in a serum-free microcarrier process, Biotechnol. Bioeng. 112 (2015) 1696–

1707. doi:10.1002/bit.25582.
[38] J. Lo Surdo, S.R. Bauer, Quantitative Approaches to Detect Donor and Passage Differences in Adipogenic Potential and Clonogenicity in Human Bone Marrow-Derived Mesenchymal Stem Cells, Tissue Eng. Part C Methods. 18 (2012) 877–889. doi:10.1089/ten.tec.2011.0736.
[39] A. Faroni, R.J.P. Smith, L. Lu, A.J. Reid, Human Schwann-like cells derived from adipose-derived mesenchymal stem cells rapidly de-differentiate in the absence of stimulating medium, Eur. J. Neurosci. 43 (2016) 417–430. doi:10.1111/ejn.13055.
[40] M.J. Hoogduijn, J.C. van den Beukel, L.C.M. Wiersma, J. Ijzer, Morphology and size of stem cells from mouse and whale: observational study, BMJ. 347 (2013) f6833–f6833. doi:10.1136/bmj.f6833.
[41] Y. Pilehvar-Soltanahmadi, A. Akbarzadeh, N. Moazzez-Lalaklo, N. Zarghami, An update on clinical applications of electrospun nanofibers for skin bioengineering, Artif. Cells, Nanomedicine, Biotechnol. (2015) 1–15. doi:10.3109/21691401.2015.1036999.
[42] K. Wang, M. Zhu, T. Li, W. Zheng, L.L. Xu, Q. Zhao, D. Kong, L. Wang, Improvement of Cell Infiltration in Electrospun Polycaprolactone Scaffolds for the Construction of Vascular Grafts, J. Biomed. Nanotechnol. 10 (2014) 1588–1598. doi:10.1166/jbn.2014.1849.
[43] K. Zhang, M. Gao, Z. Chong, Y. Li, X. Han, R. Chen, L. Qin, Single-cell isolation by a modular single-cell pipette for RNA-sequencing, Lab Chip. 16 (2016) 4742–4748. doi:10.1039/C6LC01241H.
[44] K.C. Murphy, B.P. Hung, S. Browne-Bourne, D. Zhou, J. Yeung, D.C. Genetos, J.K. Leach, Measurement of oxygen tension within mesenchymal stem cell spheroids, J. R. Soc. Interface. 14 (2017) 20160851. doi:10.1098/rsif.2016.0851.
[45] M. Hamon, S. Hanada, T. Fujii, Y. Sakai, Direct Oxygen Supply with Polydimethylsiloxane (PDMS) Membranes Induces a Spontaneous Organization of Thick Heterogeneous Liver Tissues from Rat Fetal Liver Cells in Vitro, Cell Transplant. 21 (2012) 401–410. doi:10.3727/096368911X605303.

Capítulo 5

Adesão e arraste celular em *scaffolds* sob perfusão direta

De acordo com a revisão da literatura realizada, existe um limite crítico de tensão de cisalhamento com a passagem de fluxo pelo *scaffold* em que as células se desprendem da superfície em que estão aderidas. A fim de determinar a vazão máxima de operação do sistema em que seja minimizado o arraste das células com a perfusão de meio, este capítulo buscou responder às seguintes questões de pesquisa:

→ É possível minimizar o arraste de DPSCs de um *scaffold* eletrofiado de PCL sob perfusão diminuindo a vazão?

→ Qual a vazão máxima ou ótima de operação?

Com o andamento dos experimentos, verificou-se que a tensão de cisalhamento não era a única variável que influenciava o arraste das células, de forma que foi formulada a seguinte questão de pesquisa:

→ O tempo de semeadura e a densidade das células afetam o processo de adesão e o posterior arraste das células?

Com o trabalho apresentado neste capítulo, visou-se a determinação de limites operacionais para viabilizar o estabelecimento do protocolo de cultivo dinâmico. O texto está estruturado na forma de artigo científico, na língua inglesa. Este artigo foi submetido e aceito pela revista *Brazilian Journal of Medical and Biological Research*, mas ainda não foi publicado.

Artigo 4

HUMAN DENTAL PULP STEM CELL ADHESION AND DETACHMENT IN POLYCAPROLACTONE ELECTROSPUN SCAFFOLDS UNDER DIRECT PERFUSION

Ágata Paim [*,1,2,3], Daikelly I. Braghirolli[3], Nilo S. M. Cardozo[2], Patricia Pranke[3,4], Isabel C. Tessaro[1]

[1]Laboratório de Separação por Membranas, Departamento de Engenharia Química, Universidade Federal do Rio Grande do Sul, Porto Alegre, RS, Brasil

[2]Laboratório de Simulação, Departamento de Engenharia Química, Universidade Federal do Rio Grande do Sul, Porto Alegre, RS, Brasil

[3]Laboratório de Hematologia e Células-Tronco, Faculdade de Farmácia, Universidade Federal do Rio Grande do Sul, Porto Alegre, RS, Brasil

[4]Instituto de Pesquisas com Células-Tronco, Universidade Federal do Rio Grande do Sul, Porto Alegre, RS, Brasil

Corresponding author (Ágata Paim)

Present address: Department of Chemical Engineering, Universidade Federal do Rio Grande do Sul (UFRGS), R. Eng. Luis Englert, s/n. Porto Alegre, Rio Grande do Sul 90040-040, Brazil

Phone/Fax: +55 51 33083622

E-mail address: agata@enq.ufrgs.br

Abstract

Cell adhesion in three-dimensional scaffolds plays a key role in tissue development. However, stem cell behavior in electrospun scaffolds under perfusion is not fully understood. Thus, an investigation was made on the effect of flow rate and shear stress, adhesion time and seeding density under direct perfusion in polycaprolactone electrospun scaffolds on human dental pulp stem cell detachment. Polycaprolactone scaffolds were electrospun using a solvent mixture of chloroform and methanol. The viable cell number was determined at each tested condition. Cell morphology was analyzed by confocal microscopy after various incubation times for static cell adhesion with a high seeding density. Scanning electron microscopy images were obtained before and after perfusion for the highest flow rate tested. The wall pore shear stress was calculated for all tested flow rates (0.005 - 3 mL/min). An inversely proportional relation between adhesion time with cell detachment under perfusion was observed. Lower flow rates and lower seeding densities reduced the drag of cells by shear stress. However, there is an operational limit for the lowest flow rate that can be used without compromising cell viability, indicating that a flow rate of 0.05 mL/min may be more suitable for the tested cell cultures in electrospun scaffolds under direct perfusion.

Keywords: Cell adhesion; Perfusion; Shear stress; Stem cell; Electrospun scaffolds.

5.1 Introduction

In tissue engineering, scaffolds are used as substitutes for damaged tissue and act as a support for cell proliferation, differentiation and migration. In order to promote the formation of natural extracellular-matrix, a scaffold must be designed with appropriate biocompatibility, biodegradability, architecture and mechanical properties [1].

An important class of scaffolds for tissue engineering is based on electrospun polymer-based structures comprising solid microfibers or nanofibers, which can present high packing density and interconnected pore network [2]. Nanofiber scaffolds favor higher mesenchymal stem cell viability than smooth surfaces [3]. However, nanofiber scaffolds usually present small pores [4] that can hinder cell infiltration through three-dimensional structures [2]. On the other side, microfiber scaffolds can provide structures with bigger pores, allowing the cell migration and colonization inside the matrix [5].

Perfusion culture systems enhance mass transfer in scaffold-containing bioreactors and provide increased nutrient transport and cell viability [6], migration [7], growth and differentiation [8]. In addition, perfusion bioreactors can reduce the accumulation of toxic metabolites and degradation byproducts and the polymer degradation rate [9]. Nevertheless, high shear stress can provoke cell detachment followed by cell death [10]. Consequently, the cell number in three-dimensional (3D) scaffolds under perfusion is influenced by the cell detachment provoked by shear stress [11] and the capability of the cells to remain adhered to the scaffold and to proliferate, differentiate, and migrate is strongly dependent on the flow rate and the pore size employed. This is important because in order to obtain a homogeneous and effective regeneration of damaged tissue, it is essential to produce a biomaterial with an adequate cell number for implantation. Therefore, it is necessary to quantify the cell drag and the final cell number in perfusion bioreactors to produce tissue substitutes that fit the quality standard required in a medical environment. Despite this, many studies on perfusion systems based on 3D scaffolds focus on the flow rate and shear stress effect on nutrient transport and stem cell proliferation and differentiation [12–14], without evaluating the cell detachment from the scaffold.

This work addresses the reduction of the shear stress effects inside the scaffold pores under perfusion, in order to produce cellularized electrospun structures for clinical application. An investigation was made of flow rate and shear stress under direct perfusion in polycaprolactone electrospun scaffolds on human dental pulp stem cell detachment. The influence of the adhesion time on cell adhesion and detachment under static conditions was

also evaluated. Different seeding densities were tested under perfusion to evaluate the detachment.

5.2 Materials and Methods

Scaffold production

The scaffolds were produced in an electrospinning apparatus with temperature and humidity control (EC-CLI, IME Technologies, Netherlands). A 16 % w/w solution of polycaprolactone (Sigma-Aldrich, Mw 70-90 kDa) in a chloroform:methanol 9:1 vol% mixture was electrospun at 38 % humidity, 19 °C, 35 cm distance between the needle and the collector, flow rate of 0.1 mL/min, and voltage of 17 kV. The scaffolds were cut into 16 mm diameter disks and sterilized by ultraviolet radiation (UV) for 1 h.

Cell isolation and expansion

Human deciduous teeth pulp was used to obtain dental pulp stem cells with the approval of the Research Committee and the Ethics Committee of the Universidade Federal do Rio Grande do Sul (project number33177214.1.3001.5330), according to the methodology described by Werle et al. [15]. Human deciduous teeth with physiologic root resorption were extracted and immersed in DMEM (Dulbecco's modified Eagle's culture medium)/Hepes (Sigma-Aldrich, St. Louis, MO) supplemented with 10 % fetal bovine serum (FBS) (Gibco, Grand Island, NY), 100 U/mL penicillin and 100 mg/mL streptomycin (Gibco, Grand Island, NY), for transportation. The dental pulp tissue was removed with the use of endodontic instruments and the cells were isolated from the pulp by mechanic and enzymatic process. The isolated cells were incubated for 24 h at 37 °C and 5 % CO_2. The primary cultures and further passages were subcultivated when a confluence of 90 % was reached, with medium exchange every 3 or 4 days. Five primary culture cells (between the third to eighth passage) were used in this work. The cells were characterized as mesenchymal stem cells in terms of immunophenotypic profile and differentiation potential, as presented in the supplementary material (Table 5.S1 and Figure 5,S1, respectively).

Cell viability

A colorimetric assay with water-soluble tetrazolium salts (WST-8, [2-(2-methoxy-4-nitrophenyl)-3-(4-nitrophenyl)-5-(2,4-disulfophenyl)-2H-tetrazolium]) was used to determine the number of viable cells. As opposed to other common colorimetric assays, the WST-8

assay does not kill the cells, which allows continuous culturing of the cells, performing other assays with the living cells and preserving the samples after the measurements. For this test, the culture medium was removed and the scaffolds were incubated with 20 µL of Cell Counting Kit-8 solution (CCK-8, Sigma–Aldrich, USA) and 180 µL of fresh culture medium at 5 % CO_2 and 37°C for 1 h. The absorbance was read in 450 nm in a microplate reader (Multiskan FC, Thermo Scientific, USA). Standard curves relating absorbance readings (450 nm) with cell number were constructed for each cell culture for the determination of the viable cell number.

Cell morphology

After the viability assay, the scaffolds were washed with phosphate-buffered saline solution (PBS) and fixed with 4 % (w/v) paraformaldehyde (PFA) (Sigma-Aldrich, USA) for 30 minutes. The PFA was then removed and the scaffolds were washed again with PBS. Cytoskeleton and nuclei cells were stained with 50 µg/mL rhodamine-phalloidin (Molecular Probes, USA) for 40 minutes and 0.5 µg/mL 4',6-diamidino-2-phenylindole (DAPI) for 5 minutes, respectively, for further imaging using a confocal microscope (Olympus FV1000, Japan). For scanning electron microscopy (SEM) (JEOL JSM 6060, Japan), the scaffolds were washed with PBS, fixed with 3 % glutaraldehyde and dehydrated in graded ethanol baths before being sputtered with gold and imaged.

Scaffold properties

The porosity of the scaffolds was calculated from the volume of fibers and the total volume of the scaffold. The volume of the fibers (V_{fibers}) of the scaffold was determined by dividing the weight of the scaffold by the PCL density, and the total volume of the scaffold (V_{total}) was determined taking into account its geometry. The total porous fraction (θ) is given by Equation 5.1.

$$\theta = \frac{V_{total} - V_{fibers}}{V_{total}} \tag{5.1}$$

The average shear stress on the wall of the pores was calculated considering a cylindrical pore approximation [16], using the Equation 5.2.

$$\sigma = \frac{8\mu Q}{d_p \theta \pi \left(\frac{D}{2}\right)^2} \tag{5.2}$$

where μ is the medium viscosity (Pa.s) (similar to that of water at 37 °C), d_p is the pore diameter (m) (measured through analysis of SEM images of the scaffolds with the software ImageJ), Q is the flow rate (m^3/s) , and D is the scaffold diameter (m).

Cell adhesion and drag

Initially, 1.5×10^5 or 0.5×10^5 cells were seeded in each scaffold and the volume was completed to 1 mL with culture medium in each well. Different adhesion times – 3 h [17], 6 h [18] and 24 h [19,20] – were used for mesenchymal stem cell attachment in the 3D scaffolds. In order to evaluate the impact of the adhesion time on cell adhesion and morphology, the cells were then incubated at 5 % CO_2 and 37°C for 3, 6 and 24 h for cell adhesion. Three cell cultures were used in this experiment and the number of scaffolds analyzed for each adhesion time was 3 per culture.

Firstly, the scaffolds seeded with 0.5×10^5 cells and incubated for 3, 6 and 24 h were perfused with culture medium for 18 h at 0.05 mL/min, in order to evaluate the adhesion strength of each adhesion time group. Two scaffolds per culture were analyzed for each adhesion time under flow and three cell cultures were used. The bioreactor system used for the culture medium perfusion is shown in Figure 5.1.

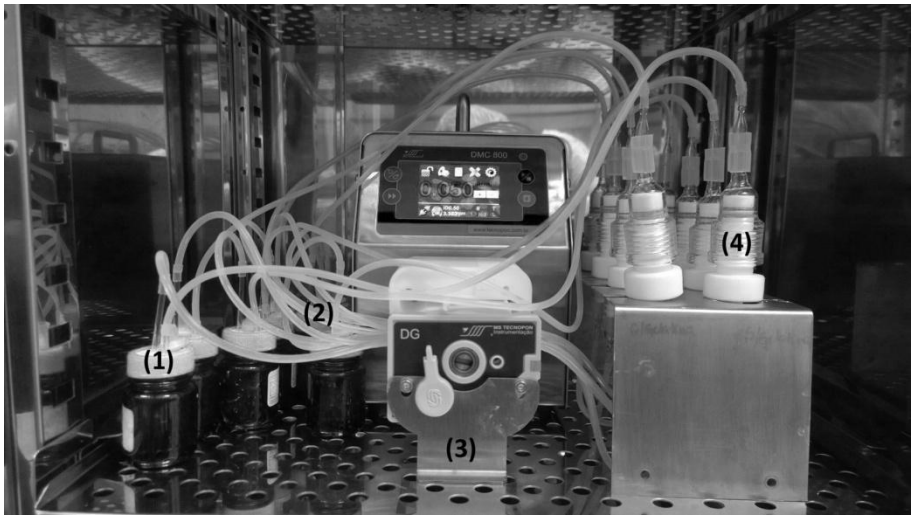

Figure 5.1: Perfusion bioreactor system: medium reservoir (1), silicon tubing (2), peristaltic pump (3), perfusion chamber (4)

Taking into consideration that increased cell adhesion and spreading have been reported in the literature with longer adhesion times [19–21], the effect of the flow rate in cell detachment was evaluated following an adhesion time of 24 h under static conditions, in order to guarantee that the cells were fully adhered and would not be detached with flow perfusion due to poor adhesion. In addition, the perfusion time used in further experiments was changed from 18 to 24 h to guarantee that maximum cell drag was achieved. Therefore, the scaffolds with 24 h cell adhesion were transferred to the bioreactor chambers (Figure 5.1) and incubated at 5 % CO_2 and 37°C for 24 h of perfusion in a bioreactor system.

As the cell drag was expected to increase with the flow rate, the scaffolds with high and low cell densities were perfused at high and low flow rates, respectively, to guarantee that the viability measurements remained above the detection limit. Thus, the scaffolds seeded with 0.5×10^5 cells were perfused with culture medium at the flow rates of 0.005, 0.01, 0.05 and 0.1 mL/min (as presented in Figure 5.2), while those seeded with 1.5×10^5 cells were perfused at 0.75, 1.5 and 3 mL/min (as presented in Figure 5.3). Two cell cultures were used in these experiments and the number of scaffolds analyzed for each flow rate was 4 per culture.

The schemes of the experimental procedure for cell adhesion and perfusion experiments are presented in Figures 5.2 and 5.3, with an indication of the steps in which cell viability and morphological characteristics were determined.

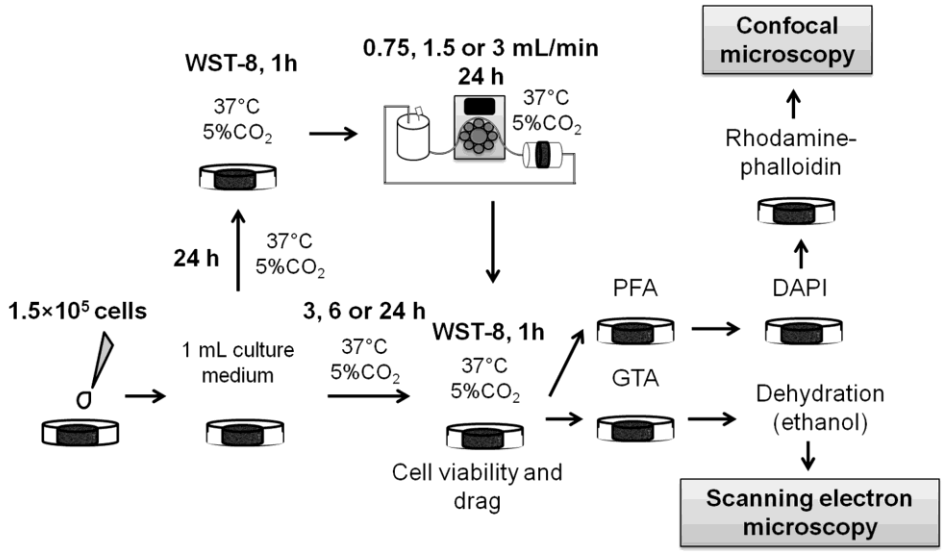

Figure 5.2: Scheme of the experimental procedure for cell culture with seeding density of 1.5×10^5 cells/scaffold (WST-8, PFA, GTA and DAPI are the viability assay, paraformaldehyde, glutaraldehyde, and 4',6-diamidino-2-phenylindole, respectively)

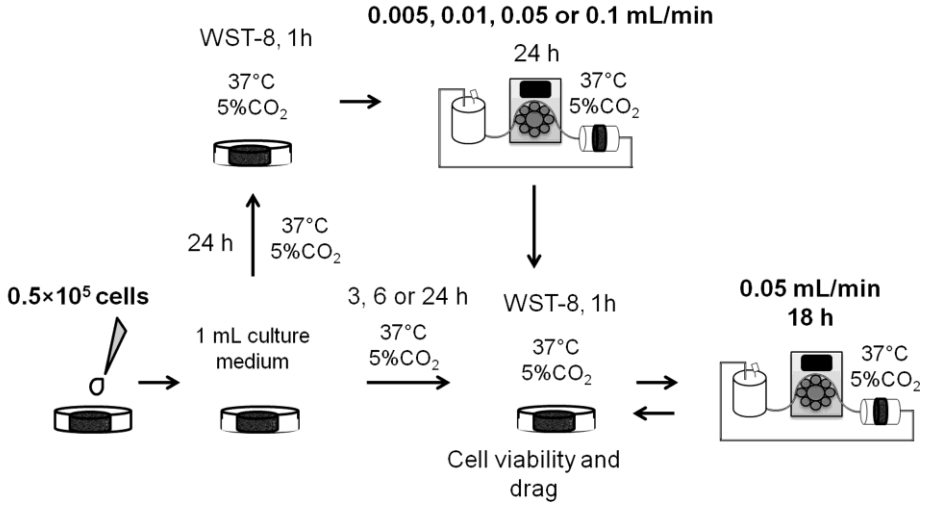

Figure 5.3: Scheme of the experimental procedure for cell culture with seeding density of 0.5×10^5 cells/scaffold (WST-8 is the viability assay)

It was also considered that with the reduction of the flow rate, the time required to fill the perfusion system increased. Hence, if the culture medium arrival to the scaffold occurs with an increased delay, the cells could starve due to the lack of nutrients. Thus, at low flow rates (0.005 – 0.1 mL/min), the perfusion chambers were at first partially filled with culture medium at a higher flow rate (0.5 mL/min). The flow rate was then decreased to 0.005, 0.01, 0.05 or 0.1 mL/min before the fluid reached the scaffold in any of the chambers.

The average drag ratio was calculated by subtracting the average cell number (determined with the CCK-8 kit) after perfusion from the control average cell number (non perfused scaffolds), normalizing this difference with the control average cell number.

Statistical analysis

Normal distribution was verified with the combination of the Shapiro–Wilk test and visual inspection of Q-Q plots. Statistical analyses were performed using one-way ANOVA followed by Tukey's post hoc test, and were carried out with R Statistical Software (version 3.3.2; R Foundation for Statistical Computing, Vienna, Austria).

5.3 Results and Discussion

Cell morphology

Figure 5.4 presents the confocal images of scaffolds seeded with 1.5×10^5 cells and incubated for 3, 6 and 24 h. Additionally, a similar set of images with smaller magnification were supplied as supplementary material (Figure 5.S2) to show the effects observed in Figure 5.4 do not depend on the specific focused region. By reference to the images in Figure 5.4, it can be observed that the cell shape is still round after 3 h of adhesion (Figure 5.4A). At 6 h (Figure 5.4B), the area of actin fibers stained with phalloidin is higher and after 24 h of adhesion, a spread morphology can be observed (Figure 5.4C). These results indicate that cytoskeleton spreading is increased with longer adhesion times. As larger cell spreading has been associated with increased focal adhesion size [22] and strength [23], it can be expected that after 24 h adhesion, the cells are more strongly attached to the fibers of the scaffold.

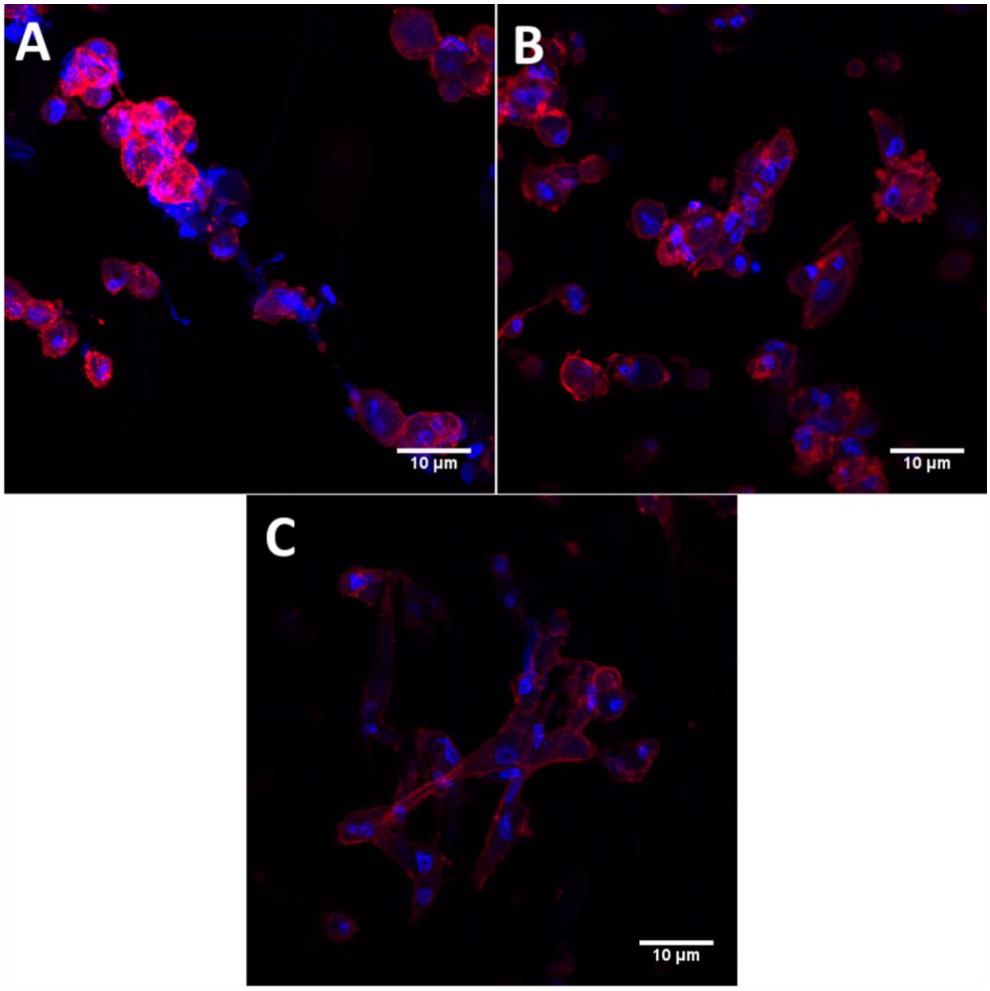

Figure 5.4: Confocal images of stem cells from Culture I in scaffolds seeded with 1.5×10^5 cells and stained with rhodamine-phalloidin (cell cytoskeleton in red) and DAPI (cell nuclei in blue) after 3 (A), 6 (B) and 24 h (C) cell adhesion. Magnification x40

In order to evaluate the cell distribution on the scaffold surface, SEM analysis was performed before and after perfusion. Figure 5.5 presents the SEM images of the scaffolds seeded with 1.5×10^5 cells after 24 h cell adhesion and after 24 h cell adhesion followed by 24 h perfusion. As can be seen in Figure 5.5A, after 24 h adhesion, the cells organize themselves in agglomerates, forming regions containing a layer of cells on the matrix surface, obstructing the pores. Several studies support that the pore size is responsible for cell infiltration and shear stress is applied to the cells due to the passage of flow in perfusion bioreactors [24,25]. In this study, the porosity (93 ±1 %) and pore diameter of the scaffolds (11.97±4.36 µm) does not necessarily limit cell penetration into the scaffold, if the cell diameter range of 12.2-16.6 µm is considered, as suggested by Suchanek et al.[26]. However, with the static seeding, the cells adhered on the fibers covering the scaffold surface and

occupying the pore spaces (as shown in Figure 5.5A). Due to fluid flow, the cells obstructing large pores were detached and dragged with the culture medium under high velocities (Figure 5.5B), and eventually detached because of the shear stress applied, even under low flow rates.

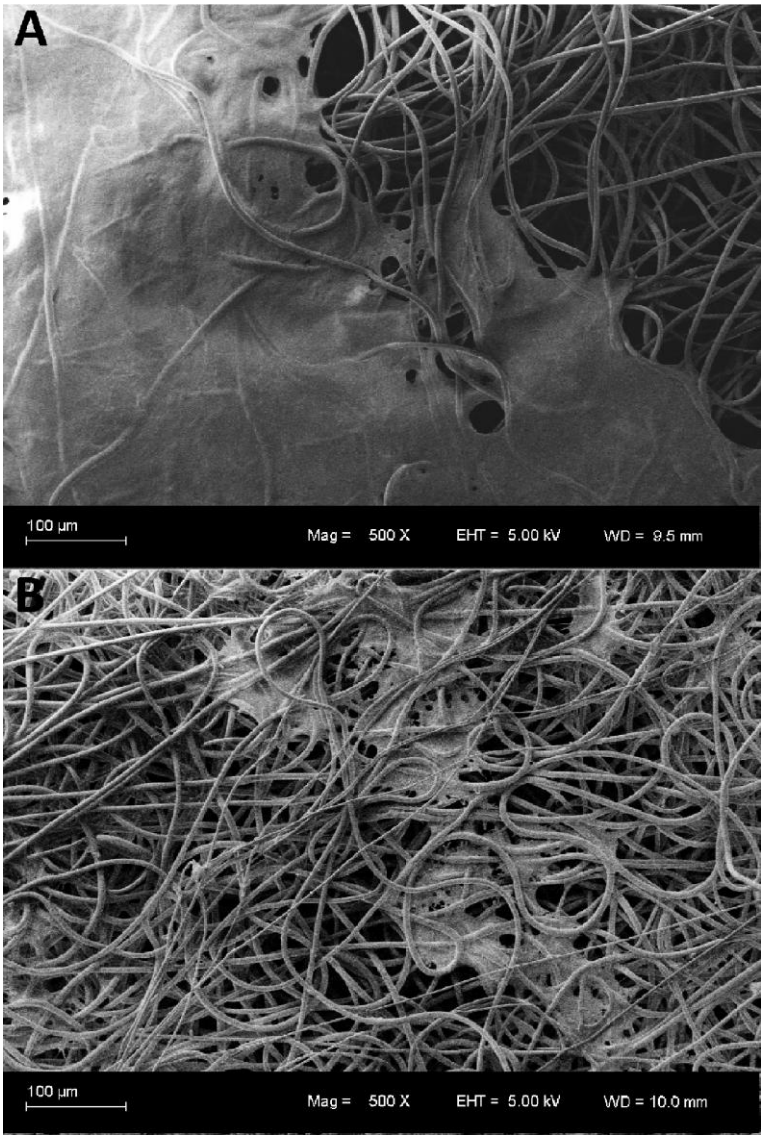

Figure 5.5: SEM images of scaffolds seeded with 1.5×10^5 cells for 24 h with cell culture V before (A) and after (B) culture medium perfusion for 24 h with a flow rate of 1.5 mL/min. Magnification x500

Cell adhesion and drag

Figure 5.6 presents the results of the cell number, determined by WST-8, for the adhesion times of 3, 6 and 24 h, for the scaffolds seeded with a low seeding density (0.5×10^5 cells/scaffold) with the cell cultures I, III and IV (Figure 5.6A) and with a high seeding density (1.5×10^5 cells/scaffold) with the cell cultures I and II (Figure 5.6B). For low seeding

density (Figure 5.6A), there was no significant effect of adhesion time on the cell number determined by cell viability for cultures III and IV, while for culture I a significant ($p < 0.05$) decrease of mean cell number occurred after 24 h adhesion when compared to the lower adhesion times (3 and 6 h). For high seeding density (Figure 5.6B), there was no significant difference between the values of the mean cell number obtained at the different adhesion times for Culture I, while for Culture II a decrease of this parameter was also observed between 6 and 24 h, after an initial increase between the adhesion times of 3 and 6 h. However, these results are probably exhibiting a behavior related to the intrinsic characteristics of this specific cell culture, what can be an outcome with primary cell cultures due to the variability between donors. Donor-to-donor variability can occur due to several factors such as donor age and gender, and it has been reported in several studies with primary cultures of human mesenchymal stem cells [27–31]. Harumi Miyagi et al. [31] observed donor-to-donor variation of the expression of extracellular matrix proteins with different human dental pulp stem cells from deciduous teeth, what could justify the different adhesion behavior between the cultures presented in Figure 5.6.This is in agreement with the fact that mesenchymal stem cells, as anchorage-dependent cells, can undergo cell death by the lack of appropriated attachment to a substrate [32].

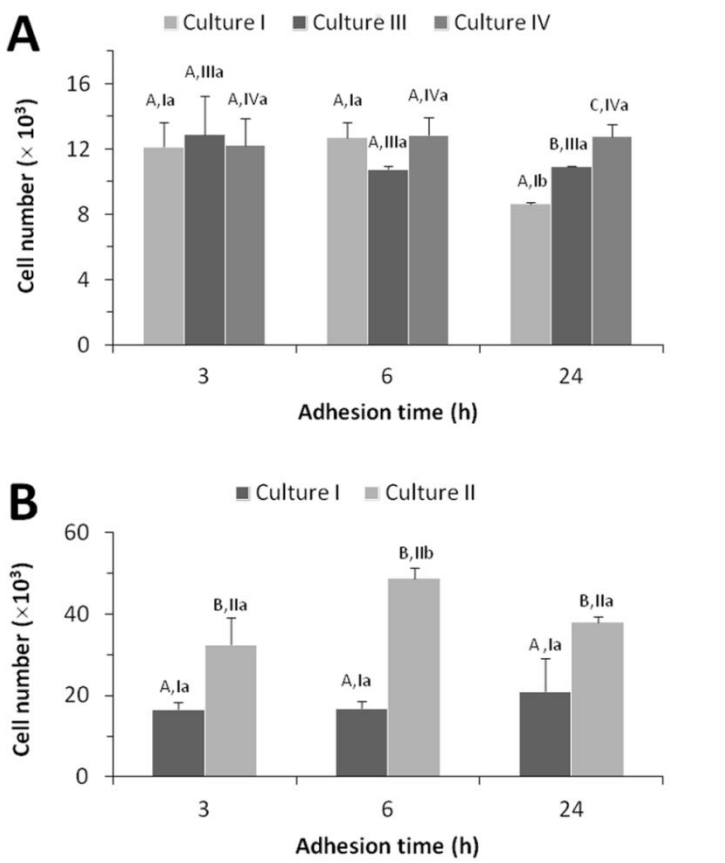

Figure 5.6: Cell number for different adhesion times for cell cultures I, III and IV seeded with 0.5×10^5 cells (A) and for cell cultures I and II seeded with 1.5×10^5 cells (B). The different capital letters represent significantly different means for the groups with the same adhesion time. The different lowercase letters preceded by the culture number represent significantly different means for the groups of the same culture with different adhesion times (One-way ANOVA with post-hoc Tukey test, $p<0.05$)

A further aspect to mention in relation to Figure 5.6 is that both at low and high seeding density, significant differences between the cultures regarding the number of cells were observed. This can be as a result of the use of cells derived from different individuals, as already discussed before.

Figure 5.7 presents the cell drag percentage calculated from the viable cell numbers (determined by WST-8) obtained for the scaffolds seeded with 0.5×10^5 cells and perfused at a flow rate of 0.05 mL/min for 18 h. As can be seen, there is no effect of adhesion time in cell loss under perfusion at 0.05 mL/min for cultures I and IV because no significant difference was observed for the different adhesion time groups. In addition, mean cell drag, calculated as the average drag from the three cultures, presented no significant difference between the

different adhesion time groups (mean cell drag of 17±11, 20±28 and 5±6 % for scaffolds with 3, 6 and 24 h of adhesion time, respectively). However, culture III presented significantly different cell drag when seeded with 6 h adhesion when compared to the other cultures with the same adhesion time ($p < 0.001$), and to the same culture with other adhesion times ($p < 0.001$). Furthermore, culture I presented no cell loss for 6 and 24 h (0 % cell drag). These reduced cell losses can be related to a higher cell spreading observed at 6 and 24 h adhesion, observed in Figure 5.4. Similar results to those obtained for cultures I and IV were observed by van Kooten et al.[33] in bi-dimensional studies using parallel-plate flow chambers, where tangential flow was used to induce shear stress and detach a cell population from a surface. The authors observed that cell adhesion strength, determined as the shear stress level that promotes 50 % of cell detachment, was not sensitive to the adhesion time. However, a three-dimensional (3D) attachment results in different cell morphology (bridged form) than cell adhesion in 2D structures (flat shape) [34]. Furthermore, reduced cell adhesion strength and resistance to shear stress can be observed in 3D scaffolds under perfusion conditions because the cells can adhere in an orientation normal for the flow and lead to increased cell detachment under low flow rates [35]. However, cell attachment in bi-dimensional structures result in flat form morphology [34]. In this study, with the increase of adhesion time, the cells, initially adhered to the fibers (Figure 5.4A), stretched through the fibers and the pore space to adhere to other cells and fibers (Figure 5.4C). This is in accordance with the bridged form morphology (cells attached to more than one fiber) obtained by Binulal et al. [34] for cell attachment in three-dimensional (3D) electrospun scaffolds. Furthermore, since the cells adhered, filling the pore space (Figure 5.5), the main orientation to cell attachment in the studied system is expected to be perpendicular to the flow direction, which differs from the parallel flow used by van Kooten et al. [33]. According to McCoy and O'Brien [35], reduced cell adhesion strength and resistance to shear stress can be observed in 3D scaffolds under perfusion conditions, because cells can adhere in an orientation normal for the flow and lead to increased cell detachment under low flow rates. This could explain the mechanism of cell drag in a direct perfusion system and the distribution of the cells after perfusion, observed in Figure 5.5B. Thus, it can be that cultures I and IV presented no enhancement in adhesion strength, with larger adhesion times due to this relation between cell morphology and flow direction.

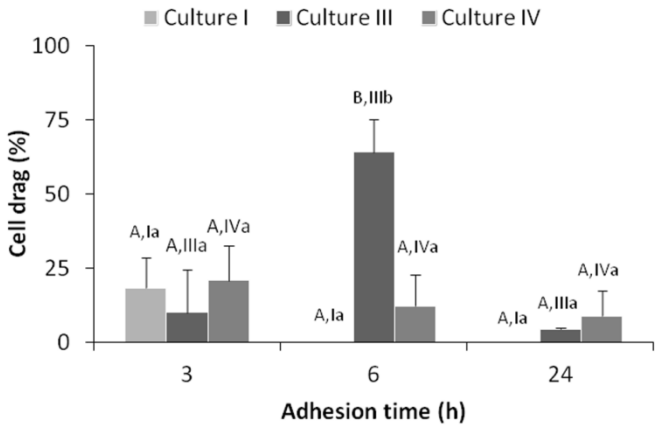

Figure 5.7: Cell drag in scaffolds seeded with 0.5×10^5 cells with different adhesion times and perfused with a flow rate of 0.05 mL/min (shear stress of 2.1 mPa) for 18 h. The different capital letters represent significantly different means for the groups with the same adhesion time. The different lowercase letters preceded by the culture number represent significantly different means for the groups of the same culture with different adhesion times (One-way ANOVA with post-hoc Tukey test, $p<0.05$)

Figure 5.8 presents the values of cell drag percentage calculated from the viable cell numbers (determined with WST-8) in the scaffolds from cell cultures I, III and IV, seeded with 0.5×10^5 cells and perfused with flow rates varying from 0.005 to 0.1 mL/min (Figure 5.8A) and from cultures I, II, III and V, seeded with 1.5×10^5 cells and perfused with flow rates from 0.75 to 3 mL/min (Figure 5.8B). In all cases, the cell drag percentages were determined after 24 h adhesion followed by 24 h perfusion. As can be seen in Figure 5.8A, at low seeding density, higher flow rates lead to a significant increase in cell loss for Culture IV ($p < 0.001$). This was also observed for the scaffolds seeded (0.5×10^5 cells) with Cultures I and III ($p < 0.01$), when compared to the results with flow rates of 0.05 and 0.1 mL/min. On the other hand, Culture I, when seeded at a low density, presented higher cell loss for the flow rate of 0.005 mL/min, when compared to the flow rate of 0.05 mL/min ($p < 0.0001$). For very low flow rates as 0.005 mL/min, the loss of cell viability (observed for Culture I) is probably not provoked by shear stress but by the reduction of oxygen delivery inside the perfusion chamber, as a result of the decreased convection. Decreased oxygen concentrations have already been reported with reduced convection in perfusion bioreactors [36,37]. Furthermore, the cell drag differences observed between the cultures can be a result of the use of cells derived from different individuals, as previously mentioned. Interestingly, at higher flow rates

and seeding density there was no significant difference in cell loss between the different groups with different flow rates and/or cultures (Figure 5.8B). This can be due to the higher seeding density, which results in higher cell number at the beginning of the perfusion and in an initial reduction of the permeability of the scaffold due to superficial pore obstruction. With less free space for fluid flow, the pore diameter and porosity of the scaffold are reduced, increasing shear stress levels (as in accordance with Equation 5.2) and cell drag. Additionally, it was observed that as cells are detached by the passage of flow through the pores, the amount of cells and debris in suspension is increased (results not shown). It is possible that, with a high flow rate, the high quantity of cellular particles in suspension affected the viscosity of the culture medium, also increasing the shear stress levels (as in accordance with Equation 5.2). The combination of these factors with the variability in seeding efficiency between the cultures with high seeding density (observed in Figure 5.6B) could have homogenized the cell drag with different flow rates.

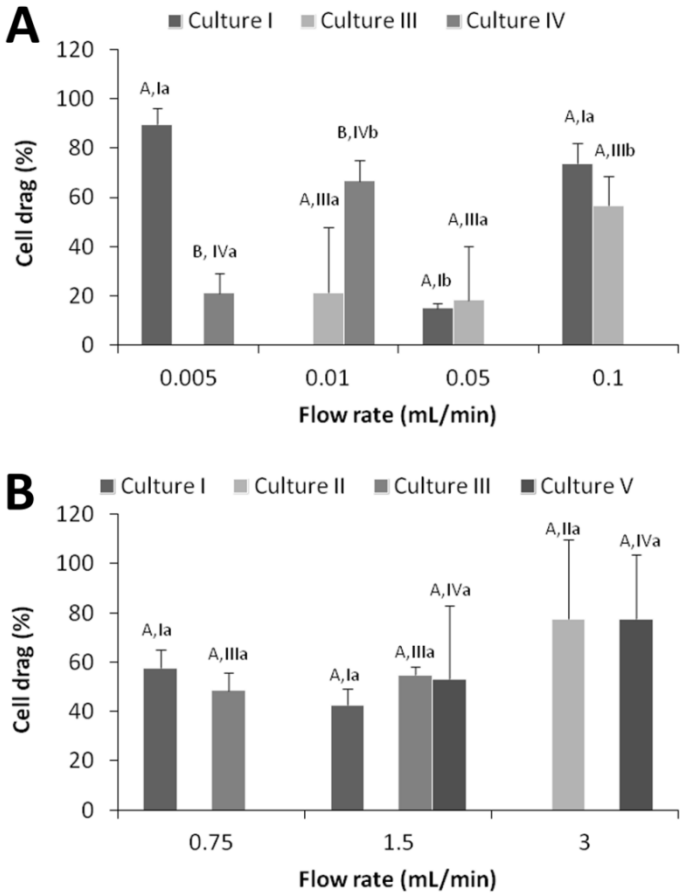

Figure 5.8: Cell drag percentage in scaffolds seeded with 0.5×10^5 cells from cell cultures I, III and IV, perfused with flow rates varying from 0.005 to 0.1 mL/min (a), and in scaffolds seeded with 1.5×10^5 cells from cultures I, II, III and V, perfused with flow rates from 0.75 to 3 mL/min (b), with 24 h of adhesion and perfused for 24 h. The different capital letters represent significantly different means for the groups with the same adhesion time. The different lowercase letters preceded by the culture number represent significantly different means for the groups of the same culture with different adhesion times (One-way ANOVA with post-hoc Tukey test, $p < 0.05$)

Table 5.1 shows the values of mean cell drag percentage and shear stress (Equation 5.2) obtained with the scaffolds seeded with 0.5 and 1.5×10^5 cells for 24 h adhesion and perfused with flow rates from 0.005 to 3 mL/min for 24 h. The lowest cell drag (24 %) was obtained with a flow rate of 0.05 mL/min, which results in a shear stress of 2.1 mPa on the pore walls. This result indicates that there is an optimal flow rate value for each system, providing this flow rate does not provoke cell starvation or high cell detachment. However, no significant difference was observed for mean cell drag with different flow rates, what can be

due to the high standard deviation of each group and donor-to-donor variability. Fibrous (but not electrospun) scaffolds with fiber diameters of 20 µm presented cell detachment values (62 % and 69 %) at flow rates of 0.5 and 1 mL/min [38] similar to those presented in Table 5.1 at flow rates of 0.75 and 1.5 mL/min. On the other hand, high shear stresses – values up to 56 and 57 mPa, which are close to those that calculated in this work for a flow rate of 1.5 mL/min, have been proved to provoke cell wash out and apoptosis [10,39]. This could justify the high cell loss presented in Table 5.1 at high flow rates, as cell drag was calculated based on cell viability, being the possible reason for the general trend reported in direct perfusion systems (i.e., increase in cell detachment with the increase of the flow rate) [40] was not observed in the present work.

Table 5.1: Mean cell drag and shear stress in scaffolds seeded with 0.5 and 1.5×10^5 cells with 24 h of cell adhesion and perfused for 24 h

Seeding density ($\times10^5$ cells)	0.5				1.5		
Flow rate (mL/min)	0.005	0.01	0.05	0.1	0.75	1.5	3
Shear stress (mPa)	0.2	0.4	2.1	4.1	30.9	61.9	123.7
Mean cell drag (%)	63	44	24	65	54	50	78
Standard deviation (%)	35	30	29	13	9	18	26
Cultures	I, IV	III, IV	I, III	I, III	I, III	I, III, V	II, V

The detachment of human dental pulp stem cells from polycaprolactone electrospun scaffolds under direct perfusion was studied for different flow rates, adhesion time and seeding densities. Higher adhesion time lead to higher cell spreading in static conditions and reduced cell detachment under perfusion. The seeding density was revealed to affect cell distribution on the scaffold surface and the sensibility of the cells to the flow rate. High shear stress and flow rate values resulted in high cell detachments, but too low flow rates were closer to operational constraints that could result in loss of cell viability. Thus, the lowest flow rate within a safe operating range may be more suitable for the culture of human dental pulp stem cells in electrospun scaffolds.

5.4 Acknowledgments

The authors wish to thank the Stem Cell Research Institute (Instituto de Pesquisa com Células-tronco), the Coordination for the Improvement of Higher Level Personnel (CAPES), the Study and Project Financer (FINEP) for financial support.

5.5 References

[1] S. Khorshidi, A. Solouk, H. Mirzadeh, S. Mazinani, J.M. Lagaron, S. Sharifi, S. Ramakrishna, A review of key challenges of electrospun scaffolds for tissue-engineering applications, J. Tissue Eng. Regen. Med. 10 (2016) 715–738. doi:10.1002/term.1978.

[2] C. Vaquette, J.J. Cooper-White, Increasing electrospun scaffold pore size with tailored collectors for improved cell penetration, Acta Biomater. 7 (2011) 2544–2557. doi:10.1016/j.actbio.2011.02.036.

[3] T.T. Ruckh, K. Kumar, M.J. Kipper, K.C. Popat, Osteogenic differentiation of bone marrow stromal cells on poly(ε-caprolactone) nanofiber scaffolds, Acta Biomater. 6 (2010) 2949–2959. doi:10.1016/j.actbio.2010.02.006.

[4] J.M. Gluck, Electrospun Nanofibrous Poly(ε-caprolactone) (PCL) Scaffolds for Liver Tissue Engineering, Graduate Faculty of North Carolina State University, 2007.

[5] Q.P. Pham, U. Sharma, A.G. Mikos, Electrospun Poly(ε-caprolactone) Microfiber and Multilayer Nanofiber/Microfiber Scaffolds: Characterization of Scaffolds and Measurement of Cellular Infiltration, Biomacromolecules. 7 (2006) 2796–2805. doi:10.1021/bm060680j.

[6] G.N. Bancroft, V.I. Sikavitsas, A.G. Mikos, Design of a Flow Perfusion Bioreactor System for Bone Tissue-Engineering Applications, Tissue Eng. 9 (2003) 549–554. doi:10.1089/107632703322066723.

[7] Y. Ban, Y. Wu, T. Yu, N. Geng, Y. Wang, X. Liu, P. Gong, Response of osteoblasts to low fluid shear stress is time dependent, Tissue Cell. 43 (2011) 311–317. doi:10.1016/j.tice.2011.06.003.

[8] A.B. Yeatts, TUBULAR PERFUSION SYSTEM BIOREACTOR FOR THE DYNAMIC CULTURE OF HUMAN MESENCHYMAL STEM CELLS, College Park, 2012.

[9] J. An, S.C.G. Leeuwenburgh, J.G.C. Wolke, J.A. Jansen, Effects of Stirring and Fluid Perfusion on the In Vitro Degradation of Calcium Phosphate Cement/PLGA Composites, Tissue Eng. Part C Methods. 21 (2015) 1171–1177. doi:10.1089/ten.tec.2015.0016.

[10] S.H. Cartmell, B.D. Porter, A.J. García, R.E. Guldberg, Effects of Medium Perfusion Rate on Cell-Seeded Three-Dimensional Bone Constructs in Vitro, Tissue Eng. 9 (2003) 1197–1203. doi:10.1089/10763270360728107.

[11] S. Sinlapabodin, P. Amornsudthiwat, S. Damrongsakkul, S. Kanokpanont, An axial distribution of seeding, proliferation, and osteogenic differentiation of MC3T3-E1 cells and rat bone marrow-derived mesenchymal stem cells across a 3D Thai silk fibroin/gelatin/hydroxyapatite scaffold in a perfusion bioreactor, Mater. Sci. Eng. C. 58 (2016) 960–970. doi:10.1016/j.msec.2015.09.034.

[12] N. Datta, Q.P. Pham, U. Sharma, V.I. Sikavitsas, J.A. Jansen, A.G. Mikos, In vitro generated extracellular matrix and fluid shear stress synergistically enhance 3D osteoblastic differentiation, Proc. Natl. Acad. Sci. 103 (2006) 2488–2493. doi:10.1073/pnas.0505661103.

[13] W.L. Grayson, S. Bhumiratana, C. Cannizzaro, P.-H.G. Chao, D.P. Lennon, A.I. Caplan, G. Vunjak-Novakovic, Effects of Initial Seeding Density and Fluid Perfusion Rate on Formation of Tissue-Engineered Bone, Tissue Eng. Part A. 14 (2008) 1809–1820. doi:10.1089/ten.tea.2007.0255.

[14] M. Jagodzinski, A. Breitbart, M. Wehmeier, E. Hesse, C. Haasper, C. Krettek, J. Zeichen, S. Hankemeier, Influence of perfusion and cyclic compression on proliferation and differentiation of bone marrow stromal cells in 3-dimensional culture,

J. Biomech. 41 (2008) 1885–1891. doi:10.1016/j.jbiomech.2008.04.001.

[15] S.B. Werle, D. Lindemann, D. Steffens, F.F. Demarco, F.B. de Araujo, P. Pranke, L. Casagrande, Carious deciduous teeth are a potential source for dental pulp stem cells, Clin. Oral Investig. 20 (2016) 75–81. doi:10.1007/s00784-015-1477-5.

[16] M. Santoro, S.-E. Lamhamedi-Cherradi, B.A. Menegaz, J.A. Ludwig, A.G. Mikos, Flow perfusion effects on three-dimensional culture and drug sensitivity of Ewing sarcoma, Proc. Natl. Acad. Sci. 112 (2015) 10304–10309. doi:10.1073/pnas.1506684112.

[17] M.A. Yassin, K.N. Leknes, T.O. Pedersen, Z. Xing, Y. Sun, S.A. Lie, A. Finne-Wistrand, K. Mustafa, Cell seeding density is a critical determinant for copolymer scaffolds-induced bone regeneration, J. Biomed. Mater. Res. Part A. 103 (2015) 3649–3658. doi:10.1002/jbm.a.35505.

[18] Y.-L. Cheng, Y.-W. Chen, K. Wang, M.-Y. Shie, Enhanced adhesion and differentiation of human mesenchymal stem cell inside apatite-mineralized/poly(dopamine)-coated poly(ε-caprolactone) scaffolds by stereolithography, J. Mater. Chem. B. 4 (2016) 6307–6315. doi:10.1039/C6TB01377E.

[19] M.A. Kafi, Y. Phanny, Y. Nakamuta, M. Todo, Proliferation Behavior of Mesenchymal Stem Cells in Peptide Functionalized Chitosan Scaffolds, in: J. Goh (Ed.), 15th Int. Conf. Biomed. Eng. ICBME 2013, 4th to 7th December 2013, Singapore, Springer International Publishing, Cham, 2014: pp. 279–282. doi:10.1007/978-3-319-02913-9_71.

[20] T. Serra, Development of 3d-printed biodegradable composite scaffolds for tissue engineering applications, Universitat Politècnica de Cataluny, 2014.

[21] B.L. Banik, T.R. Riley, C.J. Platt, J.L. Brown, Human Mesenchymal Stem Cell Morphology and Migration on Microtextured Titanium, Front. Bioeng. Biotechnol. 4 (2016). doi:10.3389/fbioe.2016.00041.

[22] D.-H. Kim, D. Wirtz, Predicting how cells spread and migrate, Cell Adh. Migr. 7 (2013) 293–296. doi:10.4161/cam.24804.

[23] C. Christophis, M. Grunze, A. Rosenhahn, Quantification of the adhesion strength of fibroblast cells on ethylene glycol terminated self-assembled monolayers by a microfluidic shear force assay, Phys. Chem. Chem. Phys. 12 (2010) 4498. doi:10.1039/b924304f.

[24] A. Balguid, A. Mol, M.H. van Marion, R.A. Bank, C.V.C. Bouten, F.P.T. Baaijens, Tailoring Fiber Diameter in Electrospun Poly(ε-Caprolactone) Scaffolds for Optimal Cellular Infiltration in Cardiovascular Tissue Engineering, Tissue Eng. Part A. 15 (2009) 437–444. doi:10.1089/ten.tea.2007.0294.

[25] M.E. Lynch, C. Fischbach, Biomechanical forces in the skeleton and their relevance to bone metastasis: Biology and engineering considerations, Adv. Drug Deliv. Rev. 79–80 (2014) 119–134. doi:10.1016/j.addr.2014.08.009.

[26] J. Suchanek, T. Soukup, B. Visek, R. Ivancakova, L. Kucerova, J. Mokry, Dental pulp stem cells and their characterization., Biomed. Pap. Med. Fac. Univ. Palacky. Olomouc. Czech. Repub. 153 (2009) 31–5. http://www.ncbi.nlm.nih.gov/pubmed/19365523.

[27] E. Capra, R. Beretta, V. Parazzi, M. Viganò, L. Lazzari, A. Baldi, R. Giordano, Changes in the proteomic profile of adipose tissue-derived mesenchymal stem cells during passages, Proteome Sci. 10 (2012) 46. doi:10.1186/1477-5956-10-46.

[28] R. Siddappa, R. Licht, C. van Blitterswijk, J. de Boer, Donor variation and loss of multipotency during in vitro expansion of human mesenchymal stem cells for bone tissue engineering, J. Orthop. Res. 25 (2007) 1029–1041. doi:10.1002/jor.20402.

[29] T.R.J. Heathman, Q.A. Rafiq, A.K.C. Chan, K. Coopman, A.W. Nienow, B. Kara, C.J.

Hewitt, Characterization of human mesenchymal stem cells from multiple donors and the implications for large scale bioprocess development, Biochem. Eng. J. 108 (2016) 14–23. doi:10.1016/j.bej.2015.06.018.

[30] S. Sundelacruz, M. Levin, D.L. Kaplan, Comparison of the depolarization response of human mesenchymal stem cells from different donors., Sci. Rep. 5 (2015) 18279. doi:10.1038/srep18279.

[31] S.P. Harumi Miyagi, I. Kerkis, C.M. da Costa Maranduba, C.M. Gomes, M.D. Martins, M.M. Marques, Expression of Extracellular Matrix Proteins in Human Dental Pulp Stem Cells Depends on the Donor Tooth Conditions, J. Endod. 36 (2010) 826–831. doi:10.1016/j.joen.2010.02.020.

[32] P. Engbers-Buijtenhuijs, M. Kamphuis, G. van der Sluijs Veer, C. Haanen, A.A. Poot, J. Feijen, I. Vermes, A novel time resolved fluorometric assay of anoikis using Europium-labelled Annexin V in cultured adherent cells, Apoptosis. 10 (2005) 429–437. doi:10.1007/s10495-005-0816-4.

[33] T.G. van Kooten, J.M. Schakenraad, H.C. van der Mei, A. Dekker, C.J. Kirkpatrick, H.J. Busscher, Fluid shear induced endothelial cell detachment from glass - influence of adhesion time and shear stress, Med. Eng. Phys. 16 (1994) 506–512. doi:10.1016/1350-4533(94)90077-9.

[34] N.S. Binulal, M. Deepthy, N. Selvamurugan, K.T. Shalumon, S. Suja, U. Mony, R. Jayakumar, S.V. Nair, Role of Nanofibrous Poly(Caprolactone) Scaffolds in Human Mesenchymal Stem Cell Attachment and Spreading for In Vitro Bone Tissue Engineering—Response to Osteogenic Regulators, Tissue Eng. Part A. 16 (2010) 393–404. doi:10.1089/ten.tea.2009.0242.

[35] R.J. McCoy, F.J. O'Brien, Influence of Shear Stress in Perfusion Bioreactor Cultures for the Development of Three-Dimensional Bone Tissue Constructs: A Review, Tissue Eng. Part B Rev. 16 (2010) 587–601. doi:10.1089/ten.teb.2010.0370.

[36] F. Coletti, S. Macchietto, N. Elvassore, Mathematical Modeling of Three-Dimensional Cell Cultures in Perfusion Bioreactors, Ind. Eng. Chem. Res. 45 (2006) 8158–8169. doi:10.1021/ie051144v.

[37] P. Pathi, T. Ma, B.R. Locke, Role of nutrient supply on cell growth in bioreactor design for tissue engineering of hematopoietic cells, Biotechnol. Bioeng. 89 (2005) 743–758. doi:10.1002/bit.20367.

[38] J.F. Alvarez-Barreto, S.M. Linehan, R.L. Shambaugh, V.I. Sikavitsas, Flow Perfusion Improves Seeding of Tissue Engineering Scaffolds with Different Architectures, Ann. Biomed. Eng. 35 (2007) 429–442. doi:10.1007/s10439-006-9244-z.

[39] M.T. Raimondi, M. Moretti, M. Cioffi, C. Giordano, F. Boschetti, K. Laganà, R. Pietrabissa, The effect of hydrodynamic shear on 3D engineered chondrocyte systems subject to direct perfusion., Biorheology. 43 (2006) 215–22. http://www.ncbi.nlm.nih.gov/pubmed/16912395.

[40] M.T. Raimondi, S. Bertoldi, S. Caddeo, S. Farè, C. Arrigoni, M. Moretti, The effect of polyurethane scaffold surface treatments on the adhesion of chondrocytes subjected to interstitial perfusion culture, Tissue Eng. Regen. Med. 13 (2016) 364–374. doi:10.1007/s13770-016-9047-8.

5.6 Supplementary material

Table 5.S1: Flow cytometric immunophenotyping analysis of human dental pulp stem cells (data are expressed as mean ± standard error, n=3)

Surface Marker	Positive Percentage (%)
CD90	98 ± 3
CD29	98 ± 2
CD73	99 ± 0.5
CD14	< 0.5
CD34	< 0.5
HLA-DR	< 0.5
CD45	< 0.5

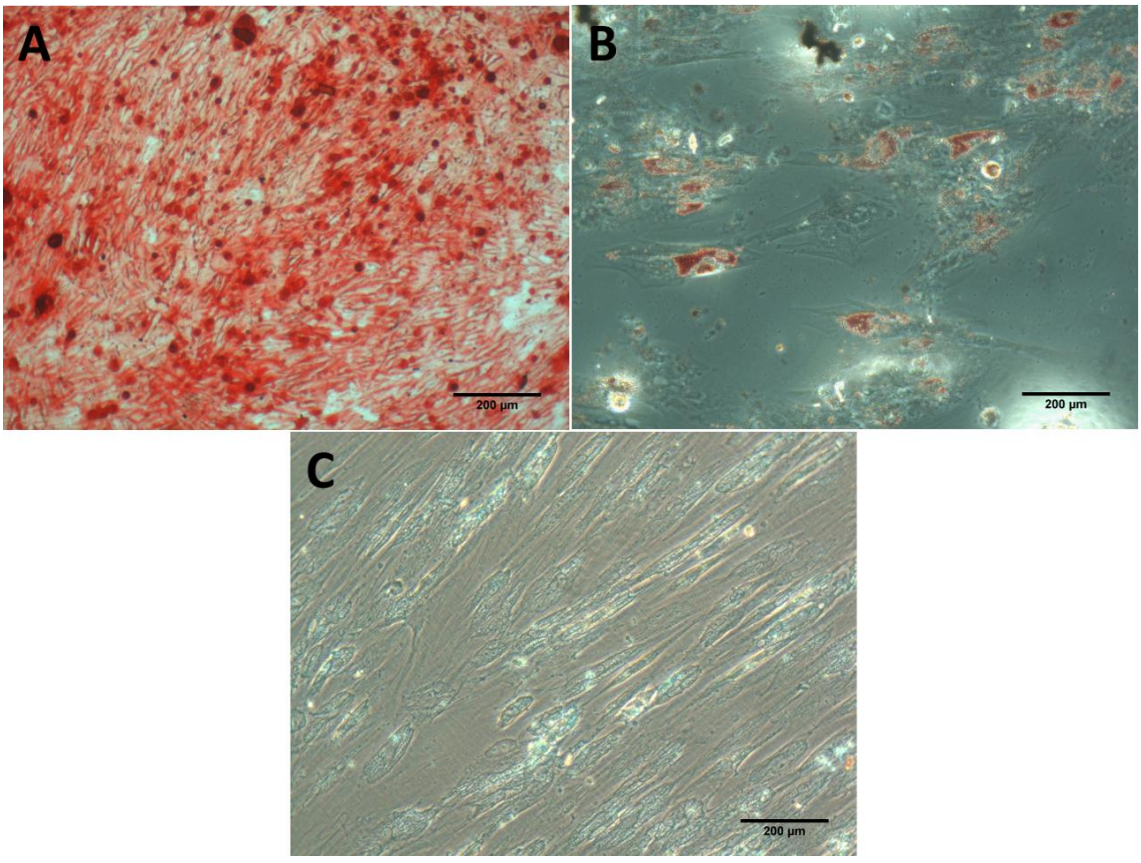

Figure 5.S1: Differentiation of human dental pulp stem cells in osteogenic (A) – Alizarin red staining –, adipogenic (B) – Oil red O staining – and chondrogenic (C) – Alcian blue staining – lineages. Magnification x200

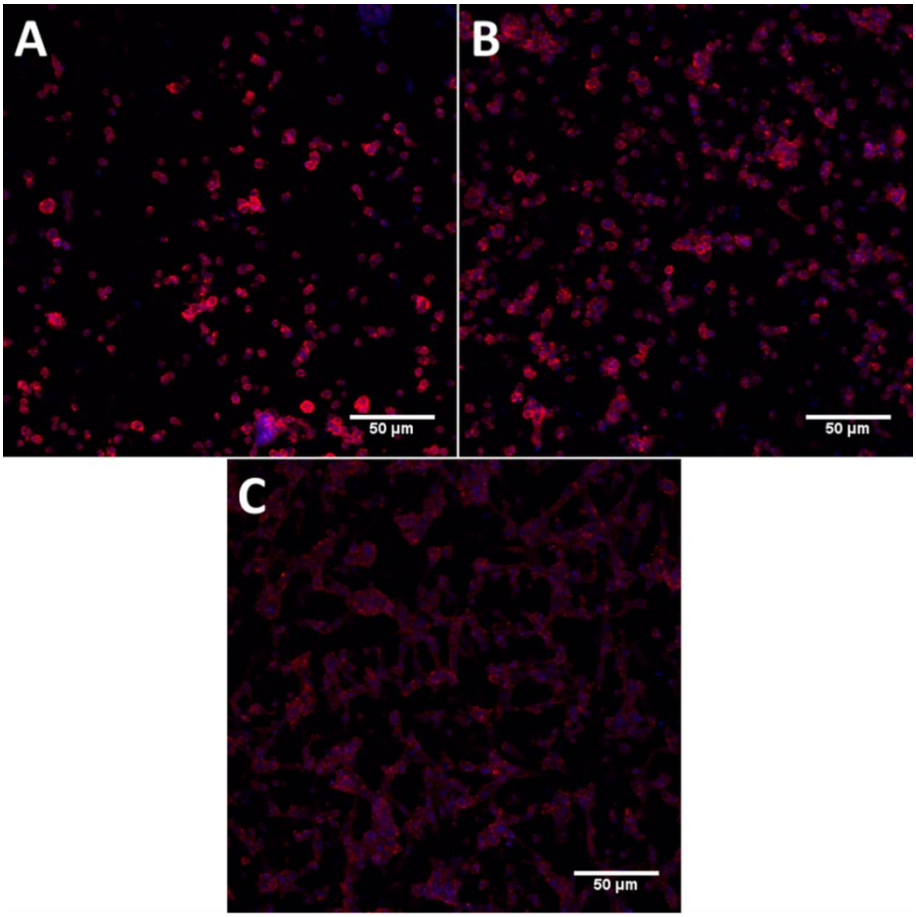

Figure 5.S2: Confocal images of stem cells from Culture I in scaffolds seeded with 1.5×10^5 cells and stained with rhodamine-phalloidin (cell cytoskeleton in red) and DAPI (cell nuclei in blue) after 3 (A), 6 (B) and 24 h (C) cell adhesion. Magnification x10

Capítulo 6

Análise de um modelo do desenvolvimento de tecidos

A fim de determinar os parâmetros e as variáveis significativas de um modelo amplamente estudado na engenharia de tecidos, foi realizada uma análise de sensibilidade com relação aos parâmetros e às variáveis de entrada, respondendo as seguintes questões de pesquisa:

→ Qual o efeito dos parâmetros e das variáveis de entrada nas variáveis de saída do modelo?

→ O modelo estudado é adequado para representar o sistema experimental deste estudo?

Neste capítulo, está apresentado o estudo sobre modelagem da proliferação celular e do transporte de massa em *scaffolds* porosos, e a realização de análise de sensibilidade para determinar os parâmetros e as variáveis de entrada significativos do modelo. O capítulo está estruturado na forma de artigo científico, na língua inglesa, o qual foi submetido para a revista *The Canadian Journal of Chemical Engineering* e está sob revisão.

Artigo 5

A SENSITIVITY ANALYSIS FOR TISSUE DEVELOPMENT BY VARYING MODEL PARAMETERS AND INPUT VARIABLES

Ágata Paim [*,1,2], Isabel C. Tessaro[1], Patricia Pranke[3], Nilo S. M. Cardozo [2]

[1,2]Department of Chemical Engineering, Universidade Federal do Rio Grande do Sul (UFRGS), R. Eng. Luis Englert, s/n. Porto Alegre, Rio Grande do Sul 90040-040, Brazil.
[3]Faculty of Pharmacy, Universidade Federal do Rio Grande do Sul (UFRGS), Av. Ipiranga, 2752. Porto Alegre, Rio Grande do Sul 90610-000, Brazil.

*Corresponding author (Ágata Paim)
Present address: Department of Chemical Engineering, Universidade Federal do Rio Grande do Sul (UFRGS), R. Eng. Luis Englert, s/n. Porto Alegre, Rio Grande do Sul 90040-040, Brazil
Phone/Fax: +55 51 33085257
E-mail address: agata@enq.ufrgs.br

Abstract

Phenomenological models can help in the study of the relation between mass transport and cell growth in three-dimensional porous scaffolds, which is one of the main challenges of tissue engineering. Thus, using a model for cell proliferation and glucose diffusion and consumption, the dimensionless parameters and input variables were varied to determinate those which affect the model output the most. The simulations were performed with the software OpenFOAM, and the results were compared through a sensitivity analysis for the parameters. It was observed that the model is more sensitive to the dimensionless parameters related to cell proliferation, death and nutrient uptake, and that dimensionless initial glucose concentration and scaffold porosity had a higher impact on cell volume fraction and on dimensionless glucose concentration. When compared to data from experimental studies, the computational results showed that the studied model is capable of represent the phenomena involved in tissue development in vitro.

Keywords: computational model, tissue engineering, sensitivity analysis, mass transport, cell growth.

Symbols

A scaffold area perpendicular to nutrient transport

C_G dimensionless glucose concentration

C_G' glucose concentration in the fluid phase

$C_{G,0}$ initial nutrient concentration in the ambient culture medium

$C_{G,0,max}$ maximum value used for the average glucose concentration in the fluid

D_α, dimensionless diffusivity in the cell phase

D_α' glucose diffusivity in the cell phase

D_β, dimensionless diffusivity in the fluid phase

D_β' glucose diffusivity in the fluid phase

D_{cell} cell diffusion coefficient

H scaffold thickness

H_{max} maximum value used for the scaffold thickness

K_c Contois saturation coefficient

K_{eq} cellular and fluid phases equilibrium partition coefficient

R_d cell death rate

R_g maximum cell growth rate

R_m dimensionless glucose uptake parameter

R_m' glucose uptake rate

Greek letters

α dimensionless cell diffusion parameter

ε scaffold porosity

ε_β fluid phase volume fraction

ε_{cell} cell phase volume fraction

$\varepsilon_{cell,0}$ initial volumetric fraction of cells

$\varepsilon_{cell,0,max}$ maximum value used for the initial number of cells

ε_{max} maximum value used for the scaffold porosity

$\varepsilon_{scaffold}$ volume fraction occupied by the scaffold

η dimensionless Contois parameter

λ dimensionless cell death parameter

ρ_{cell} average mass density of the cell phase

6.1 Introduction

The application of phenomenological models in tissue engineering allows to describe highly interconnected phenomena as mass transport [1–7], cell growth [8–20], and extracellular matrix synthesis [21]. Computational modeling can assist in the study of physical [22–27], chemical [28–32] and biological [33] mechanisms of tissue development. It can also contribute to the estimation of parameters and variables that cannot be measured experimentally and in hypothesis tests [34].

The main challenges in tissue engineering are related to mass transport limitations that occur both, in cultures *in vitro* and in the integration of the implant *in vivo*. Since diffusion is commonly the main mechanism of mass transport into the tissue, nutrient distribution is heterogeneous and leads to the spatial variation of cell density and viability, according to nutrient gradients [35]. Chung et al. [10] developed a mathematical model to describe nutrient consumption and chondrocytes growth and diffusion on polyglycolic acid (PGA) scaffolds under static conditions. They used the experimental data from Freed et al. [36] for estimation of parameters and model validation [10]. However, only the effect of the dimensionless parameter related to cell diffusion coefficient in the growth equation was evaluated by Chung et al. [10].

The model of Chung et al. [10] is one of the simplest models of tissue development and has served as a basis for several other works, which include other terms related to nutrient transport in the fluid phase [37–39], description of the nutrient uptake by the Michaelis-Menten model [12,37,38], extracellular matrix synthesis [37,38], oxygen uptake [38,40] or lactate production [12]. Liu, Chua and Leong [40] and Chung et al. [12] used a similar equation derivation (volume averaging) for a perfusion instead of a static culture system. Izadifar [41] proposed a numerical solution for a cylindrical scaffold and performed a sensitivity analysis of cell proliferation with relation to the inputs scaffold dimension and initial glucose concentration, but the effect of the model parameters was not evaluated.

Although experimental validation is actually the best way of evaluating the ability of a model to represent the real system, it is sometimes a hard task, due to experimental limitations and cost. In this sense, also due to the complexity of the models used in tissue engineering, sensitivity analysis is an interesting tool for use in this field, since it may provide a computational evaluation of the predictive capacity and robustness of computational models and identification of the critical parameters of a model [42,43]. Sensitivity analysis can be used to study the role of each parameter variation in tissue development [44], to clarify the

mechanisms that most affect the studied phenomenon [45], to optimize the computational mesh [17], to analyze the effect of different culture conditions [46], and to evaluate the influence of additional factors and processes to the model [47]. In addition, it can be used for the simplification of a model through the identification of input variables whose variation does not result in a significant change on the outputs of the model.

A complete sensitivity analysis, contemplating both input variables and parameters, is not currently available for the model proposed by Chung et al. [10]. Nevertheless, before incorporating a new phenomenon in this model and/or sophisticating the description of a particular mechanism, it is important to study the impact of different porosities and parameters values on the model, and evaluate the effect of the input variables on the output variables.

In the present work, a new dimensionless arrangement of the model proposed by Chung et al. [10] is used as basis for a sensitivity analysis aiming to identify which of the considered dimensionless parameters and input variables (namely, initial cell density and glucose concentration, scaffold thickness and porosity) have more pronounced effect on the outputs of the model (cell volume fraction and glucose concentration).

6.2 Methodology

Modeling

Chung and colleagues' model was based on the volume average method proposed by Wood, Quintard and Whitaker [48], considering a biphasic porous medium with a cell and a fluid phase. Thus, the nutrient concentration in the fluid phase is given by the following equation.

$$\frac{\partial[\varepsilon_\beta+\varepsilon_{cell}K_{eq}]C_G{}'}{\partial t'} = \nabla\left[\left(\varepsilon_\beta D_\beta{}' + \varepsilon_{cell}K_{eq}D_\alpha{}'\right)\nabla C_G{}'\right] - K_{eq}R_m{}'C_G{}'\varepsilon_{cell} \qquad (6.1)$$

where ε_{cell} and ε_β are the cell and fluid volume fraction, respectively, $C_G{}'$ is the glucose concentration in the fluid phase, K_{eq} is the cellular and fluid phases equilibrium partition coefficient, $D_\beta{}'$ is the glucose diffusivity in the fluid phase, $D_\alpha{}'$ is the glucose diffusivity in the cell phase, and $R_m{}'$ is the glucose uptake rate.

For the cell mass conservation, Chung et al. [10] assumed a constant average mass density of the cell phase (ρ_{cell}). Thus, the cell volume fraction time derivative is given by the following equation.

$$\frac{\partial \varepsilon_{cell}}{\partial t} = \nabla(D_{cell}\nabla\varepsilon_{cell}) + \frac{\mathrm{R_g} C_G}{K_c \rho_{cell} K_{eq}{}^{-1} \varepsilon_{cell} + C_G} - R_d \varepsilon_{cell} \tag{6.2}$$

The first term on the right-hand side of the Equation 6.2 represents the cell flux, where D_{cell} is the cell diffusion coefficient, assuming that cells have mobility due to random walking [10]. The second term on the right-hand side describes cell growth with the Modified Contois kinetics [49], which considers the effect of nutrient saturation and the cell amount dependence. In this term, R_g is the maximum cell growth rate and K_c is the Contois saturation coefficient. The third term on the right-hand side represents cell death and R_d is the cell death rate.

Adopting the inverse growth rate Rg^{-1}, the scaffold thickness H, and the initial nutrient concentration in the ambient culture medium $C_{G,0}$ as characteristic scales for time, length, and nutrient concentration, respectively, Chung et al. [10] proposed the following dimensionless expression for cell mass conservation Equation 6.2:

$$\frac{\partial \varepsilon_{cell}}{\partial t} = \nabla(\alpha\nabla\varepsilon_{cell}) + \frac{C_G}{\eta\varepsilon_{cell} + C_G} - \lambda\varepsilon_{cell} \tag{6.3}$$

where C_G is the dimensionless glucose concentration ($C_G^{'}/\ C_{G,0}$), and the dimensionless parameters α, η, and λ, are given by Equations 6.4, 6.5, and 6.6, representing the cell movement, the cell growth kinetics and the cell death, respectively.

$$\alpha = \frac{D_{cell}}{AR_g} \tag{6.4}$$

$$\eta = \frac{K_c \rho_{cell}}{K_{eq} C_{G,0}} \tag{6.5}$$

$$\lambda = \frac{R_d}{R_g} \tag{6.6}$$

where A is the scaffold area perpendicular to nutrient transport [10], given by the Equation 6.7.

$$A = H^2 \tag{6.7}$$

To consider scaffold porosities other than 100 %, the volume fraction occupied by the scaffold ($\varepsilon_{scaffold}$) must be included in the model ($\varepsilon = 1 - \varepsilon_{scaffold}$) [40]. Thus, the volume fraction of the fluid phase (ε_β) is given by the following equation:

$$\varepsilon_\beta = \varepsilon - \varepsilon_{cell} \tag{6.8}$$

Chung et al. [10] proposed a dimensionless form for nutrient equation (Eq. (6.1)) where all the dimensionless parameters were dependent on the glucose diffusivity in the fluid phase. In order to analyze separately the effects of the nutrient uptake and of the nutrient diffusion, we rearranged the dimensionless form of the nutrient transport equation as follows:

$$\frac{\partial[\varepsilon_\beta+\varepsilon_{cell}K_{eq}]C_G}{\partial t} = \nabla\left[\left(\varepsilon_\beta D_\beta + \varepsilon_{cell}K_{eq}D_\alpha\right)\nabla C_G\right] - R_m C_G \varepsilon_{cell} \tag{6.9}$$

where the dimensionless parameters D_β, D_α, and R_m are given by Equations 6.10, 6.11, and 6.12, representing the glucose transport in the fluid and in the cell phase, and the glucose consumption, respectively.

$$D_\beta = \frac{D_\beta{}'}{AR_g} \tag{6.10}$$

$$D_\alpha = \frac{D_\alpha{}'}{AR_g} \tag{6.11}$$

$$R_m = \frac{K_{eq}R_m{}'}{R_g} \tag{6.12}$$

The boundary conditions are the same as those proposed by Chung et al. [10]: zero cell mass flux on the boundaries, and nutrient concentration at the extremities of the scaffold surface equal to the bulk concentration of the medium surrounding the scaffold. Thus, the nutrient transport occurs from the extremities to the center of the scaffold.

Model implementation and sensitivity analysis

The model equations were implemented in a finite volume code using the open source CFD *package* OpenFOAM and the algorithm PIMPLE [50] for the solution of the transient process. The reference values of the dimensionless parameters are presented in Table 6.1.

Table 6.1: Dimensionless parameters, based on the parametric values proposed by Chung et al. [10]

Parameter	Value	Equations involved
K_{eq}	0.1	6.1, 6.3, 6.7, 6.10
η	62	6.3, 6.5
α	0.00011	6.1, 6.2, 6.5
λ	0.021	6.1, 6.4
D_β	6.67	6.5, 6.7, 6.8
D_α	0.67	6.5, 6.7, 6.9
R_m	196	6.7, 6.10

Four bi-dimensional rectangular geometries corresponding to the cases with thickness of 0.307 cm, 0.169 cm, 0.116 cm, and 0.088 cm were employed. The proportions between the dimensionless values of *x* and *y* in each of these geometries were of 3.26 × 1, 5.95 × 1, 8.62 × 1, and 11.36 × 1, respectively. The 2 meshes presented in Table 6.2, generated with the blockMesh tool of the OpenFOAM *package*, were studied.

Table 6.2: Mesh analysis

Refinement	Number of cells in each direction	
	X	*Y*
I	163	50
II	82	25

The sensitivity analysis was made by varying one of the dimensionless parameters values at a time by 25 % and 50 % positively and negatively, while maintaining the all the other parameters constant. The model sensitivity to each parameter was then calculated as the ratio of the change in the output variables to the normalized variation of the parameters (- 0.5 to + 0.5).

The relation between the inputs (initial volumetric fraction of cells ($\varepsilon_{cell,0}$), scaffold porosity (ε), scaffold thickness (H), and initial average glucose concentration in the fluid phase ($C_{G,0}$)) and the output variables (volumetric fraction of cells and glucose concentration in the scaffold) was studied with the set of input values shown in Table 6.3, expressed in terms of percentage of the maximum value used for each input. The sensitivity was not calculated using the dimensionless ratio defined in the previous paragraph for the analysis of

the parameters, due to the variation of more than one variable at the same time in most of the studied cases (G to U).

Table 6.3: Percentile input values for the different studied cases

Case	$\varepsilon_{cell,0}/\varepsilon_{cell,0,max}$ (%)	$\varepsilon/\varepsilon_{max}$ (%)	H/H_{max} (%)	$C_{G,0}/C_{G,0,max}$ (%)
A	40	100	100	100
B	10	100	100	100
C	100	100	100	100
D	40	100	100	22.22
E	40	80	100	100
F	40	60	100	100
G	20	100	28.95	100
H	20	100	38.16	100
I	20	100	55.26	100
J	20	80	28.95	100
K	20	80	38.16	100
L	20	80	55.26	100
M	20	60	28.95	100
N	20	60	38.16	100
O	20	60	55.26	100
P	20	80	28.95	22.22
Q	20	80	38.16	22.22
R	20	80	55.26	22.22
S	20	60	28.95	22.22
T	20	60	38.16	22.22
U	20	60	55.26	22.22

The maximum values used for the initial number of cells, scaffold porosity, scaffold thickness and average glucose concentration in the fluid ($\varepsilon_{cell,0,max}$, ε_{max}, H_{max} and $C_{G,0,max}$, respectively) are given in Table 6.4.

Table 6.4: Maximum input values and the equations involved

Input	Maximum value	Equations involved
$\varepsilon_{cell,0}$ (cells)	1×10^{7}	6.1, 6.6, 6.7

ε (%)	100	6.6, 6.7
H (cm)	0.304	6.1, 6.2, 6.5, 6.7, 6.8, 6.9
$C_{G,0}$ (g·cm^{-3})	4.5×10^{-3}	6.1, 6.3, 6.7

6.3 Results and Discussion

Table 6.5 presents the maximum and minimum values of cell volume fraction and dimensionless glucose concentration at the final time for case A with meshes I and II.

Table 6.5: Output values at the final time for meshes I and II

Mesh	$\varepsilon_{cell,\,min}$	$\varepsilon_{cell,\,max}$	$C_{G,min}$	$C_{G,max}$
I	0.234	0.448	0.358	1
II	0.235	0.448	0.358	1

According to the results presented in Table 6.5, a higher refinement on the directions x and y (I) did not change radically the maximum and minimum values of cell volume fraction and dimensionless glucose concentration at the final time. These results indicate that for Mesh II the convergence was already achieved. Thus, the sensitivity analysis was conducted with Mesh II.

Figures 6.1 and 6.2 present the time evolution of mean cell volume fraction and dimensionless glucose concentration sensitivities to the dimensionless parameter η. It can be seen that η has a significant impact on cell volume fraction and glucose concentration over the entire culture time. This could be because the parameter η is related to growth kinetics (Contois saturation coefficient) and to initial conditions (glucose concentration in the media).

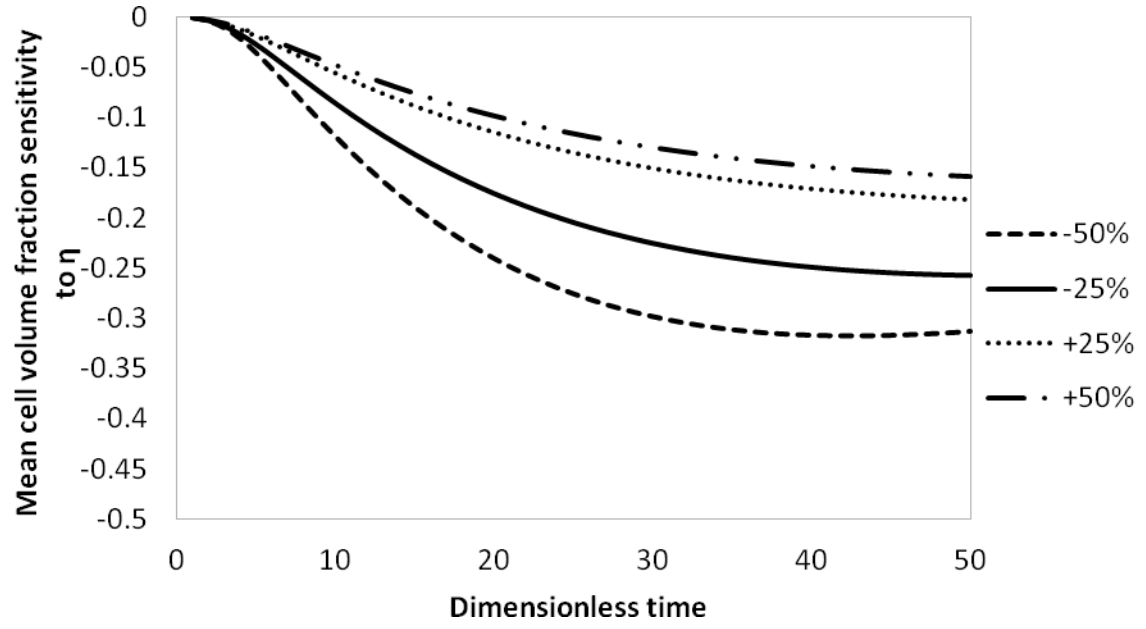

Figure 6.1: Time evolution of mean cell volume fraction sensitivity to dimensionless parameter η

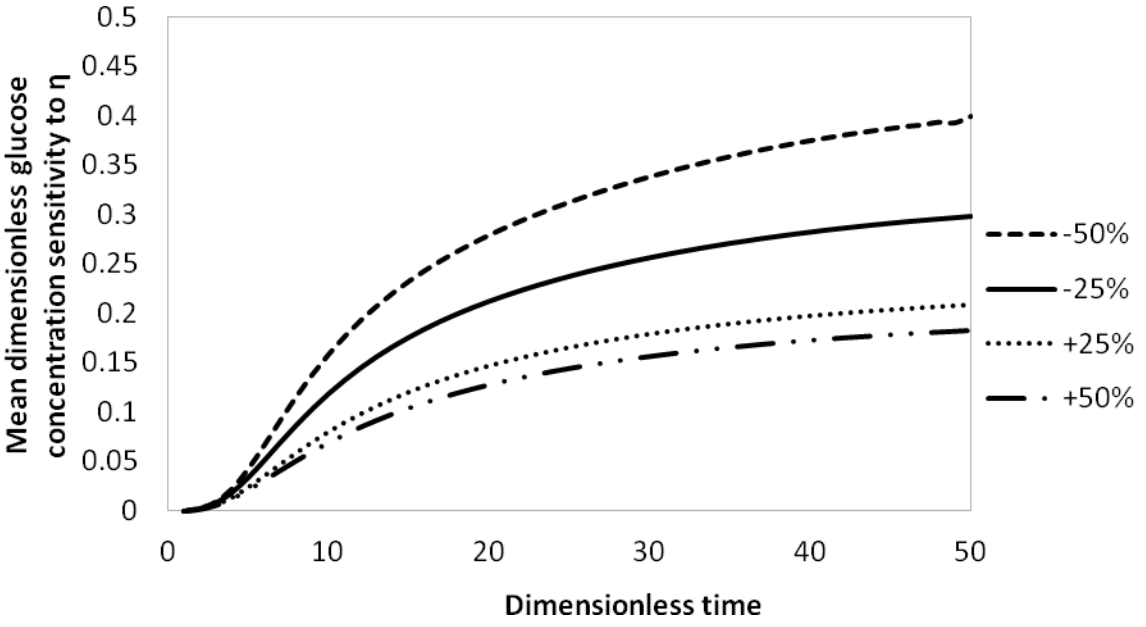

Figure 6.2: Time evolution of mean dimensionless glucose concentration sensitivity to dimensionless parameter η

Figures 6.3 and 6.4 present the sensitivity of the maximum absolute value of mean cell volume fraction and dimensionless glucose concentration to the model parameters. According to these figures, the model is not very sensitive to the parameters α, D_α and K_{eq} in the studied range (absolute values of sensitivity smaller than 0.005). It can be noticed that the absolute

values of mean cell volume fraction sensitivity to all parameters, except to η, were smaller than 0.15, with the same applying to the sensitivity of the mean dimensionless glucose concentration to D_α, λ, α and K_{eq}.

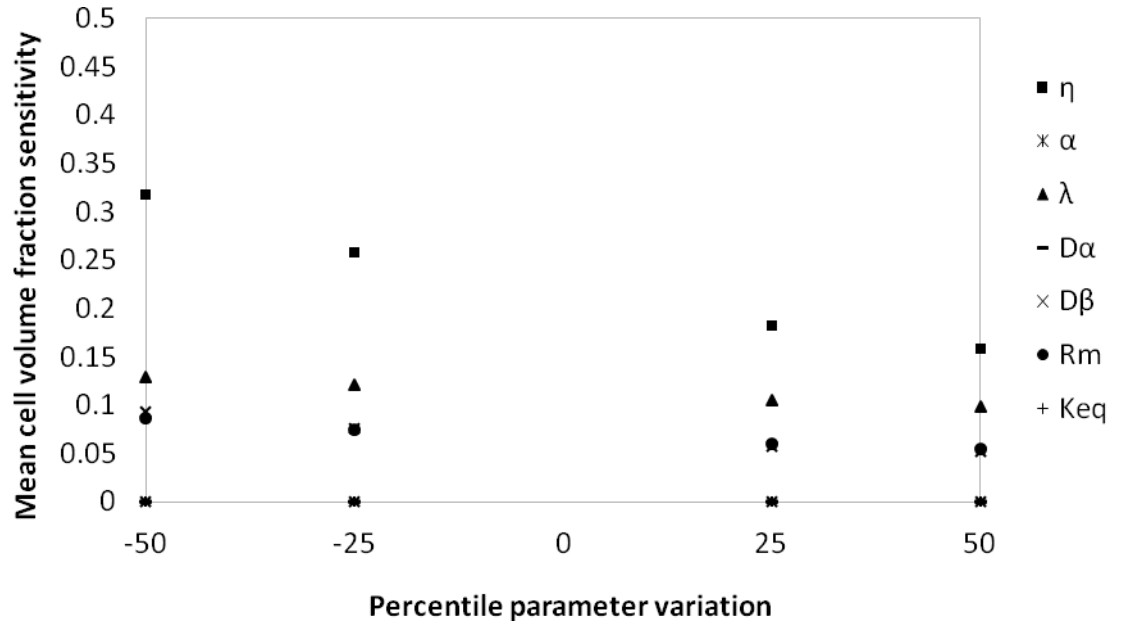

Figure 6.3: Maximum absolute value of mean cell volume fraction sensitivity to the model parameters

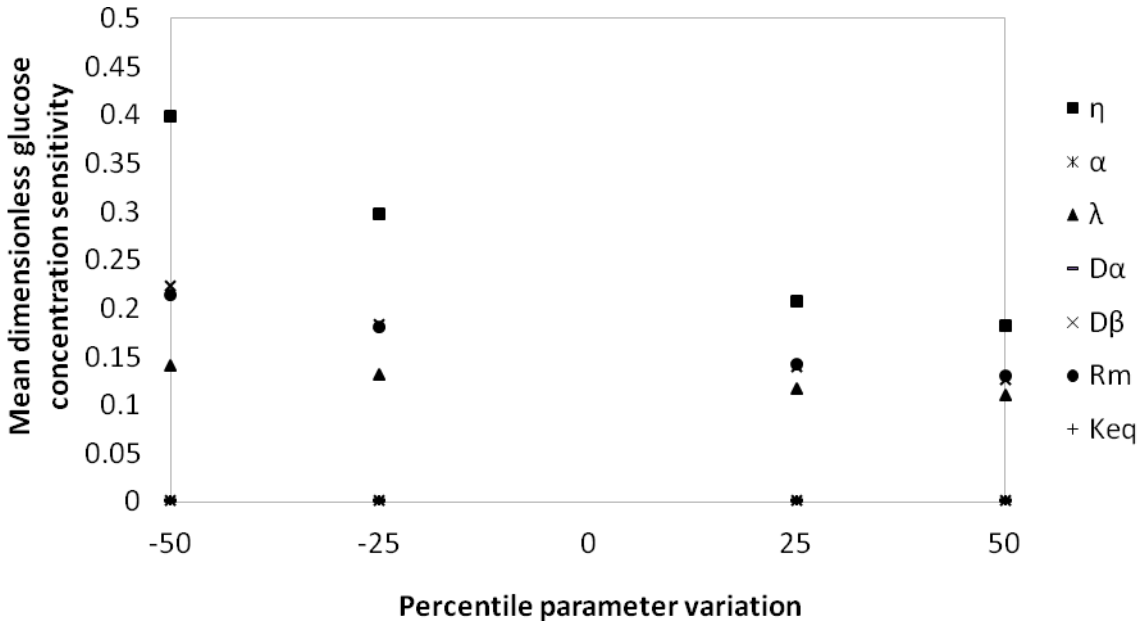

Figure 6.4: Maximum absolute value of mean dimensionless glucose concentration sensitivity to the model parameters

Moreover, glucose concentration showed a higher sensitivity to D_β than cell volume fraction, which can be attributed to the fact that D_β is the dimensionless parameter that represents the nutrient transport in the model. This parameter could be varied by changing the culture media conditions or the nutrient considered in the model, altering the diffusivity of the nutrient on the fluid phase. On the other hand, D_β can also be influenced by modifications on the cross-sectional area for nutrient transport (or scaffold thickness) and on the cell growth kinetics.

The model has a certain sensitivity to R_m, being all the sensitivities negative in the studied range. This parameter can be modified by a change in the equilibrium of the cellular and fluid phases (K_{eq}), on cell metabolism (maximum nutrient consumption rate), or on the growth kinetics (R_g).

Also, the model presents higher sensitivity to smaller values of λ, since negative variations of 50 and 25% (in this order), resulted in higher sensitivity values than positive variations of λ (Figures 6.3 and 6.4). It can be implied that an increase in λ has a negative effect on cell volume fraction and a higher positive effect on glucose concentration. The higher cell death or smaller cell proliferation, the smaller the cell volume fraction and the uptake of glucose and the higher the glucose concentration. Since the cell death rate and the maximum cell growth rate are associated to cell kinetics, λ could be varied by changes in the culture conditions.

Figure 6.5 presents the distribution of mean cell volume fraction and dimensionless glucose concentration for the case A (0.307 cm of thickness). The effect of transport limitation on cell volume fraction distribution (Figure 6.5a) follows the glucose concentration behavior (Figure 6.5b), with smaller values at the center of the scaffold. This trend was similar for all cases (results not shown).

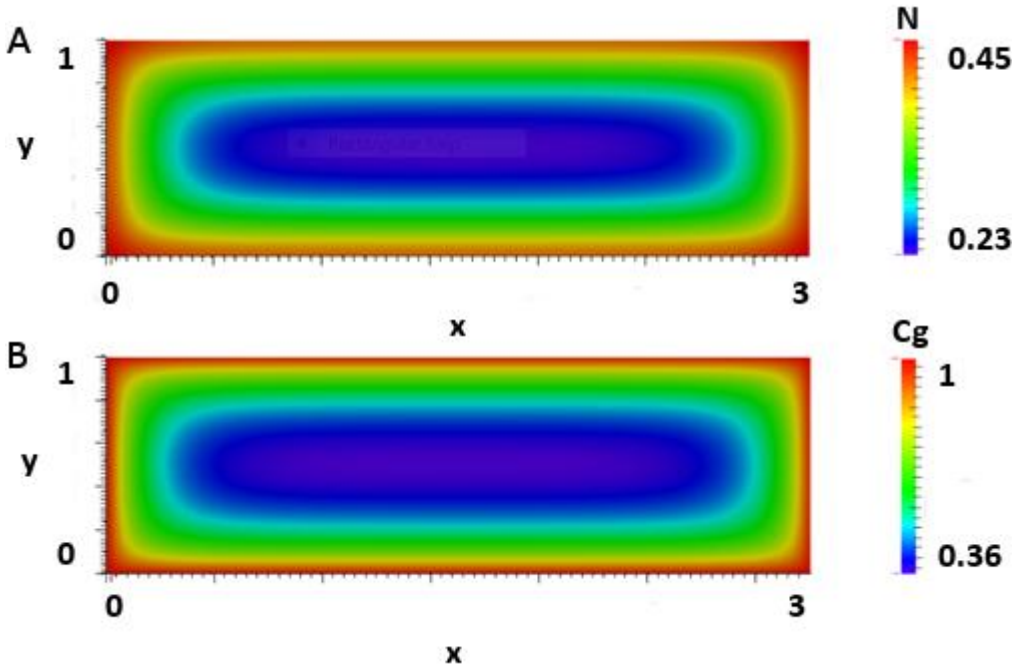

Figure 6.5: Distribution of mean cell volume fraction and dimensionless glucose concentration at the final time for a scaffold thickness of 0.307 cm

Figures 6.6 and 6.7 present the time evolution of mean cell volume fraction and the dimensionless glucose concentration for the cases A to F (0.307 cm of thickness). It can be seen that lower initial glucose concentration led to reduced cell growth and consequent smaller glucose consumption (case D when compared to case A). Besides this, the initial cell volume fraction did not present a significant impact on the model, since the curves of cell volume fraction and dimensionless glucose concentration corresponding to the cases A, B and C are overlapped at the final time. Also, lower porosities presented lower mean cell volume fractions and lower mean glucose concentration over time (cases E and F when compared to case A), what could be due to higher transport limitation.

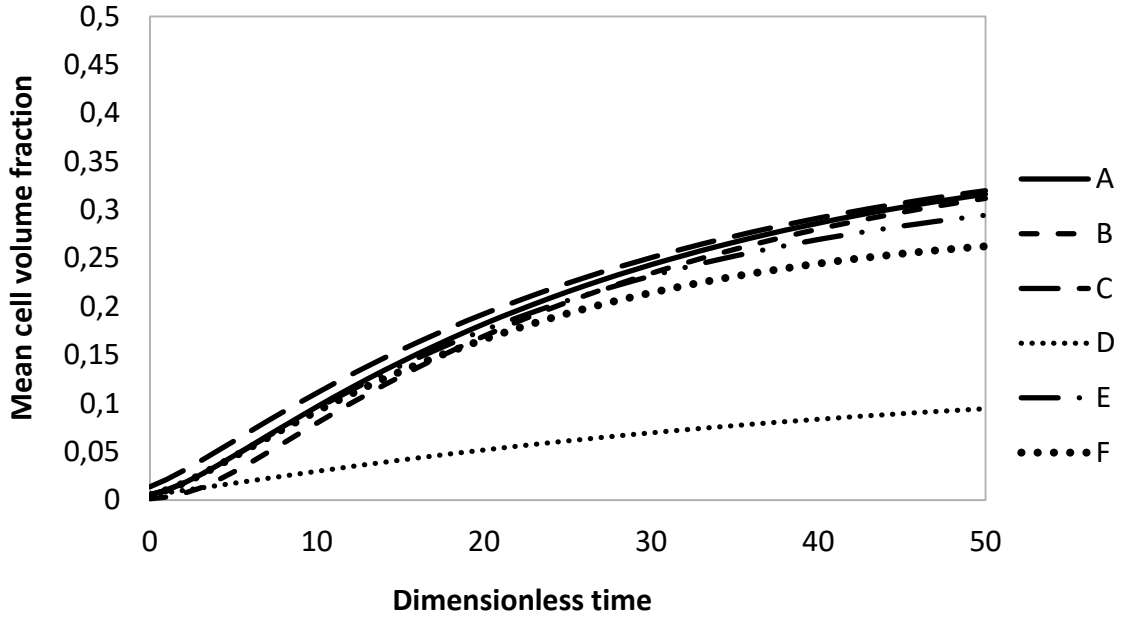

Figure 6.6: Time evolution of mean cell volume fraction for scaffold thickness of 0.307 cm. A: $[\varepsilon_{cell,0}/\varepsilon_{cell,0,max}\ \ \varepsilon/\varepsilon_{max}\ \ C_{G,0}/C_{G,0,max}] = [40\ 100\ 100]$, B: $[\varepsilon_{cell,0}/\varepsilon_{cell,0,max}\ \ \varepsilon/\varepsilon_{max}\ \ C_{G,0}/C_{G,0,max}] = [10\ 100\ 100]$, C: $[\varepsilon_{cell,0}/\varepsilon_{cell,0,max}\ \ \varepsilon/\varepsilon_{max}\ \ C_{G,0}/C_{G,0,max}] = [100\ 100\ 100]$, D: $[\varepsilon_{cell,0}/\varepsilon_{cell,0,max}\ \ \varepsilon/\varepsilon_{max}\ \ C_{G,0}/C_{G,0,max}] = [40\ 100\ 22.22]$, E: $[\varepsilon_{cell,0}/\varepsilon_{cell,0,max}\ \ \varepsilon/\varepsilon_{max}\ \ C_{G,0}/C_{G,0,max}] = [40\ 80\ 100]$, F: $[\varepsilon_{cell,0}/\varepsilon_{cell,0,max}\ \ \varepsilon/\varepsilon_{max}\ \ C_{G,0}/C_{G,0,max}] = [40\ 60\ 100]$

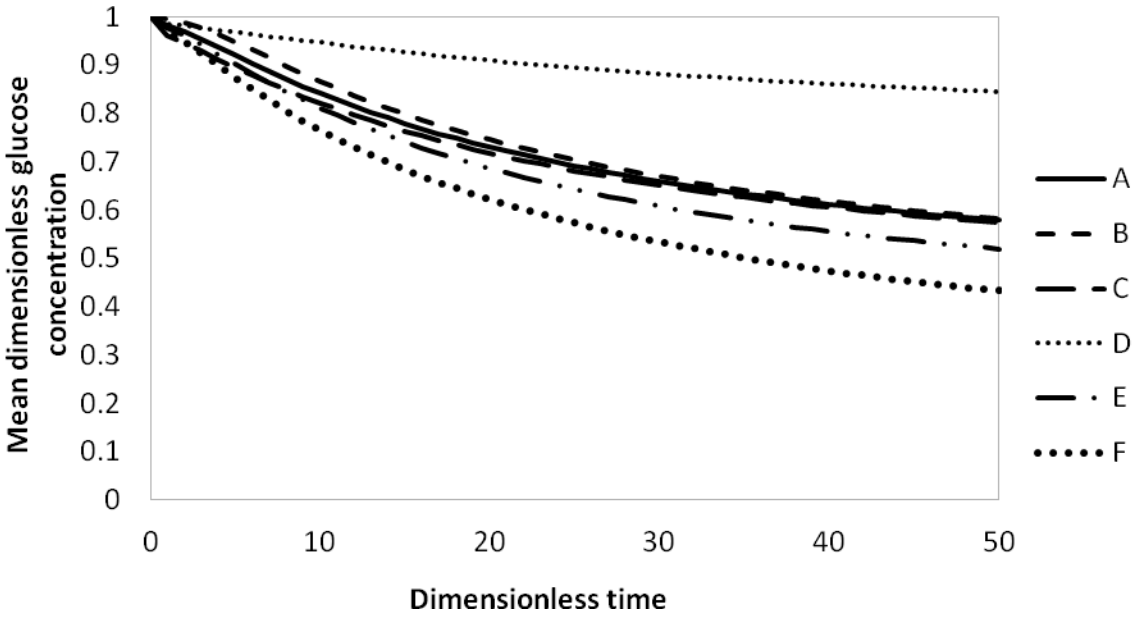

Figure 6.7: Time evolution of mean dimensionless glucose concentration for a scaffold thickness of 0.307 cm. A: [$\varepsilon_{cell,0}/\varepsilon_{cell,0,max}$ $\varepsilon/\varepsilon_{max}$ $C_{G,0}/C_{G,0,max}$] = [40 100 100], B: [$\varepsilon_{cell,0}/\varepsilon_{cell,0,max}$ $\varepsilon/\varepsilon_{max}$ $C_{G,0}/C_{G,0,max}$] = [10 100 100], C: [$\varepsilon_{cell,0}/\varepsilon_{cell,0,max}$ $\varepsilon/\varepsilon_{max}$ $C_{G,0}/C_{G,0,max}$] = [100 100 100], D: [$\varepsilon_{cell,0}/\varepsilon_{cell,0,max}$ $\varepsilon/\varepsilon_{max}$ $C_{G,0}/C_{G,0,max}$] = [40 100 22.22], E: [$\varepsilon_{cell,0}/\varepsilon_{cell,0,max}$ $\varepsilon/\varepsilon_{max}$ $C_{G,0}/C_{G,0,max}$] = [40 80 100], F: [$\varepsilon_{cell,0}/\varepsilon_{cell,0,max}$ $\varepsilon/\varepsilon_{max}$ $C_{G,0}/C_{G,0,max}$] = [40 60 100]

Figures 6.8 and 6.9 present the time evolution of mean cell volume fraction and dimensionless glucose concentration for the cases G to O (0.088, 0.116 and 0.168 cm of thickness, with high initial glucose concentration). The same trend was observed for thickness of 0.088 (cases G, J and M), 0.116 (cases H, K and N) and 0.168 (cases I, L and O), but the profiles of mean cell volume fraction and dimensionless glucose concentration over time were further away from reaching the plateau with the increase of the scaffold thickness (cases I, L and O did not reach the plateau in the studied time). In addition, the increase of the mean cell volume fraction and the decrease of the mean glucose dimensionless concentration over time were smaller with thicker scaffolds (cases I, L and O). This can be due to the reduction in cell volume fraction with the increase of scaffold volume and no variation on initial cell number, what results in smaller local nutrient consumption (smoother profiles) and higher mean glucose concentration at the final time. It can also be observed that the profiles of both output variables were steepest for smaller porosities (cases M, N and O), what could be due to higher nutrient diffusion limitation.

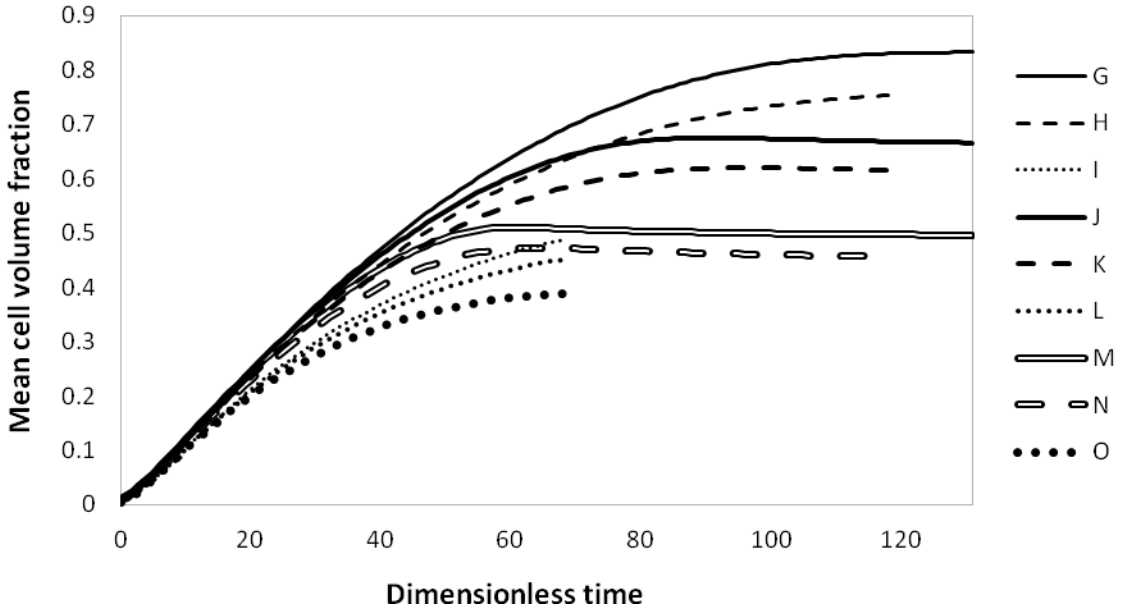

Figure 6.8: Time evolution of mean cell volume fraction for scaffold thickness of 0.088, 0.116 and 0.168 cm, with high initial glucose concentration. G: [$\varepsilon/\varepsilon_{max}$ H/H_{max}] = [100 28.95], H: [$\varepsilon/\varepsilon_{max}$ H/H_{max}] = [100 38.16], I: [$\varepsilon/\varepsilon_{max}$ H/H_{max}] = [100 55.26], J: [$\varepsilon/\varepsilon_{max}$ H/H_{max}] = [80 28.95], K: [$\varepsilon/\varepsilon_{max}$ H/H_{max}] = [80 38.16], L: [$\varepsilon/\varepsilon_{max}$ H/H_{max}] = [80 55.26], M: [$\varepsilon/\varepsilon_{max}$ H/H_{max}] = [60 28.95], N: [$\varepsilon/\varepsilon_{max}$ H/H_{max}] = [60 38.16], O: [$\varepsilon/\varepsilon_{max}$ H/H_{max}] = [60 55.26]

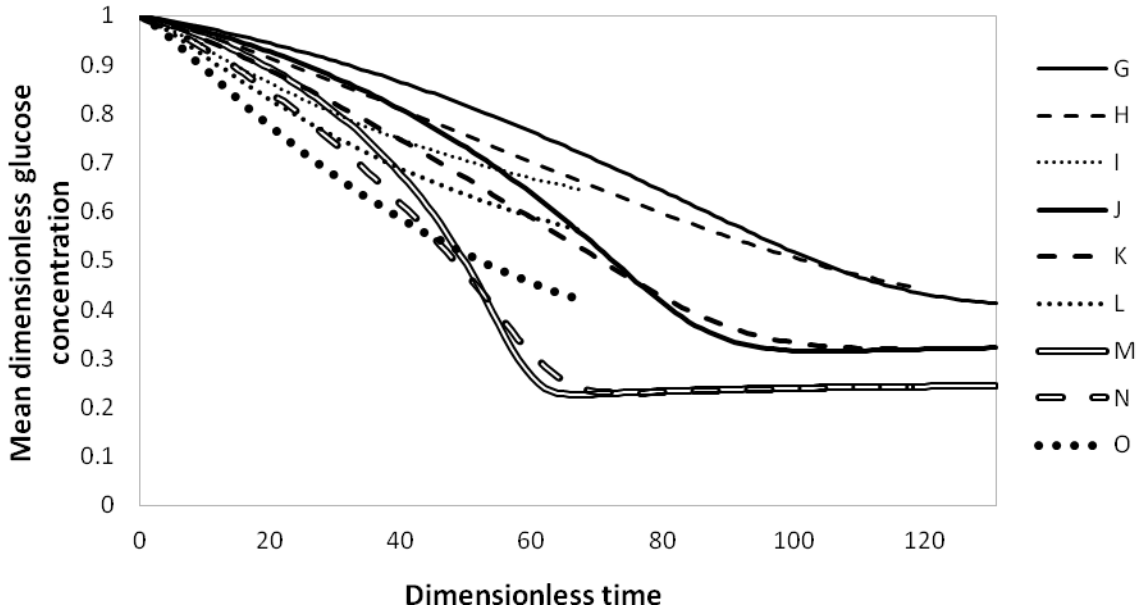

Figure 6.9: Time evolution of mean dimensionless glucose concentration for scaffold thickness of 0.088, 0.116 and 0.168 cm, with high initial glucose concentration. G: [$\varepsilon/\varepsilon_{max}$ H/H_{max}] = [100 28.95], H: [$\varepsilon/\varepsilon_{max}$ H/H_{max}] = [100 38.16], I: [$\varepsilon/\varepsilon_{max}$ H/H_{max}] = [100 55.26], J: [$\varepsilon/\varepsilon_{max}$ H/H_{max}] = [80 28.95], K: [$\varepsilon/\varepsilon_{max}$ H/H_{max}] = [80 38.16], L: [$\varepsilon/\varepsilon_{max}$ H/H_{max}] = [80 55.26], M: [$\varepsilon/\varepsilon_{max}$ H/H_{max}] = [60 28.95], N: [$\varepsilon/\varepsilon_{max}$ H/H_{max}] = [60 38.16], O: [$\varepsilon/\varepsilon_{max}$ H/H_{max}] = [60 55.26]

Figures 6.10 and 6.11 present the time evolution of mean cell volume fraction and dimensionless glucose concentration for the cases P to U (0.088, 0.116 and 0.168 cm of thickness, with low initial glucose concentration). For the low glucose concentration medium, the decrease of the dimensionless glucose concentration was higher for the cases with 60 % of porosity (cases S, T and U), indicating that a decrease in scaffold porosity increased transport limitations, since the mean cell volume fraction presented similar results when porosity was reduced from 80 to 60 % (cases P and S, Q and T, R and U, for scaffold thicknesses of 0.088 cm, 0.116 cm, and 0.168 cm, respectively). With low glucose medium, the presence of less substrate reduced the effect of the transport limitation on the proliferation. In addition, the cell growth was lower with low initial glucose concentration than for the cases with high glucose concentration medium (presented in Figure 6.8).

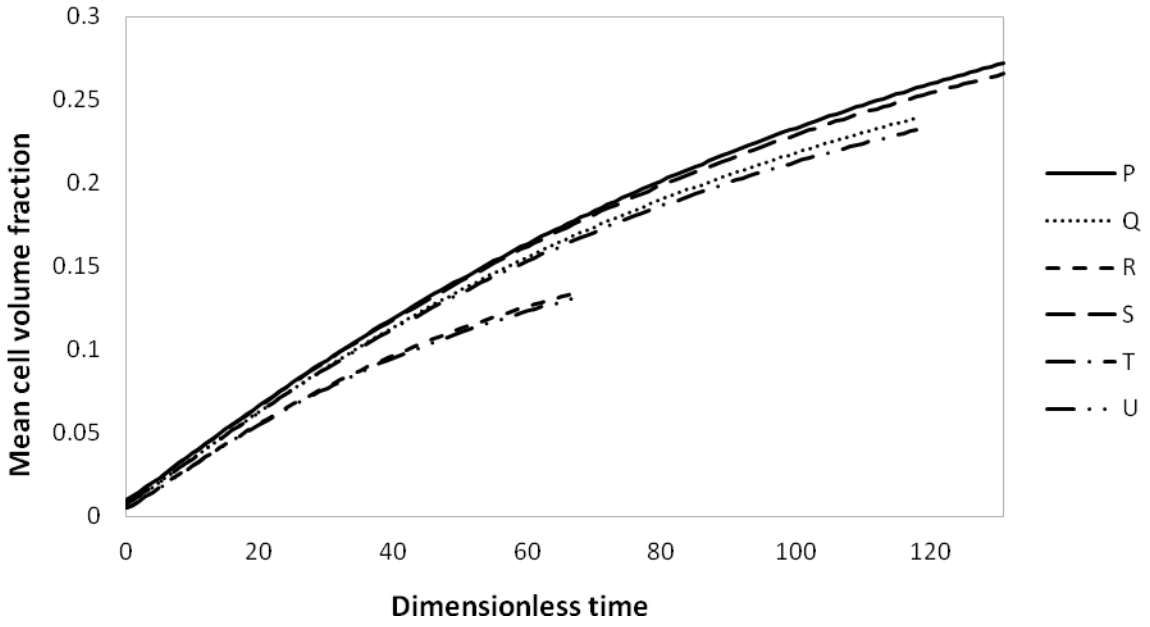

Figure 6.10: Time evolution of mean cell volume fraction for scaffold thickness of 0.088, 0.116 and 0.168 cm, with low initial glucose concentration. P: [$\varepsilon/\varepsilon_{max}$ H/H_{max}] = [80 28.95], Q: [$\varepsilon/\varepsilon_{max}$ H/H_{max}] = [80 38.16], R: [$\varepsilon/\varepsilon_{max}$ H/H_{max}] = [80 55.26], S: [$\varepsilon/\varepsilon_{max}$ H/H_{max}] = [60 28.95], T: [$\varepsilon/\varepsilon_{max}$ H/H_{max}] = [60 38.16], U: [$\varepsilon/\varepsilon_{max}$ H/H_{max}] = [60 55.26]

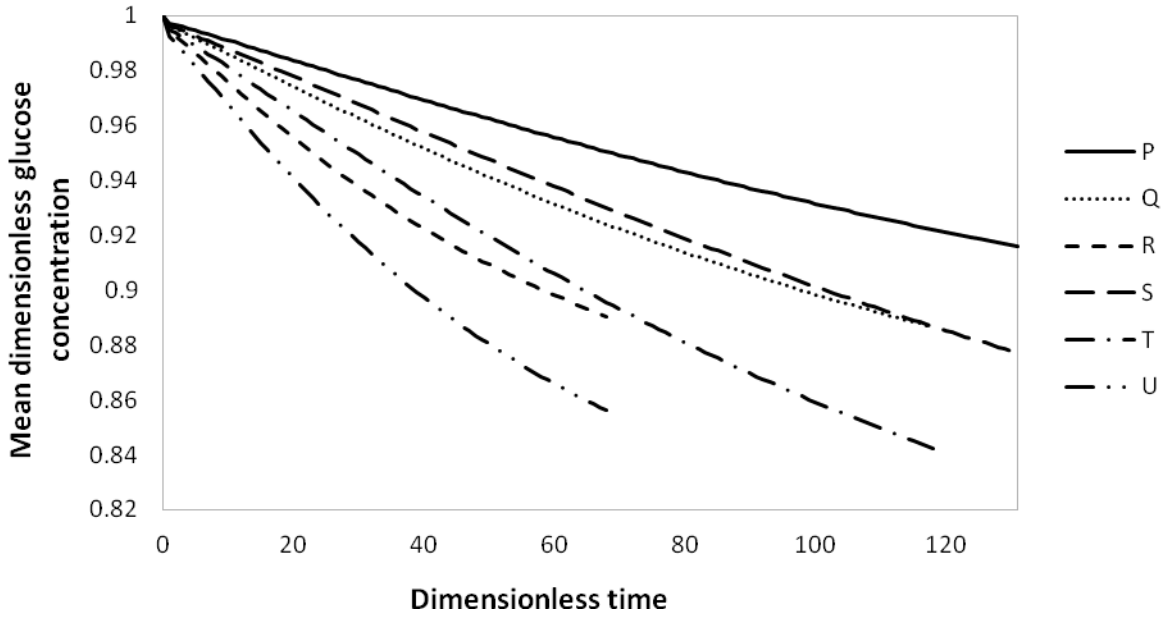

Figure 6.11: Time evolution of mean dimensionless glucose concentration for scaffold thickness of 0.088, 0.116 and 0.168 cm, with low initial glucose concentration. P: [$\varepsilon/\varepsilon_{max}$ H/H_{max}] = [80 28.95], Q: [$\varepsilon/\varepsilon_{max}$ H/H_{max}] = [80 38.16], R: [$\varepsilon/\varepsilon_{max}$ H/H_{max}] = [80 55.26], S: [$\varepsilon/\varepsilon_{max}$ H/H_{max}] = [60 28.95], T: [$\varepsilon/\varepsilon_{max}$ H/H_{max}] = [60 38.16], U: [$\varepsilon/\varepsilon_{max}$ H/H_{max}] = [60 55.26]

In addition to the above analysis, the results were compared to the experimental data plotted by Chung et al. [10]. Figure 6.12 presents the relative error of cell volume fraction with this data for the different input variations. Comparing the cases with equivalent initial conditions, regarding the experimental data (A, E, F; G, J, M; H, K, N; I, L, O), only case G presented less deviation when compared to the cases with porosity values lower than the 100%. This can indicate that a porosity of 100 % may not fully represent the experimental condition, as proposed by Chung et al. [10].

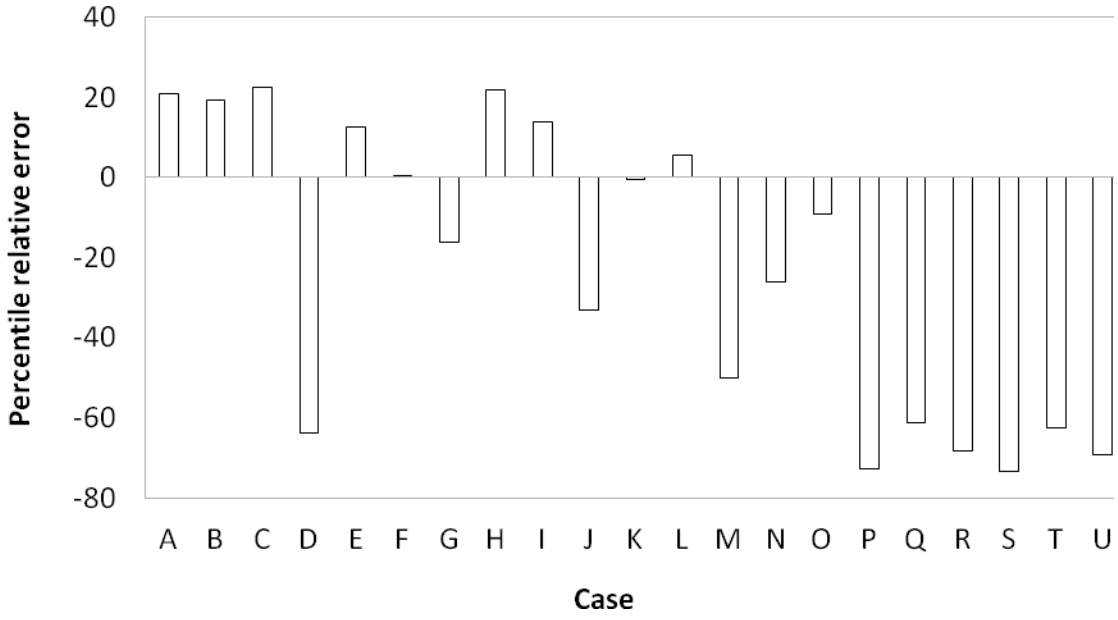

Figure 6.12: Percent relative error of calculated mean cell volume fraction at the final time, for input variation cases. The cases A to F have H/H_{max} = 100. A: [$\varepsilon_{cell,0}/\varepsilon_{cell,0,max}$ $\varepsilon/\varepsilon_{max}$ $C_{G,0}/C_{G,0,max}$] = [40 100 100], B: [$\varepsilon_{cell,0}/\varepsilon_{cell,0,max}$ $\varepsilon/\varepsilon_{max}$ $C_{G,0}/C_{G,0,max}$] = [10 100 100], C: [$\varepsilon_{cell,0}/\varepsilon_{cell,0,max}$ $\varepsilon/\varepsilon_{max}$ $C_{G,0}/C_{G,0,max}$] = [100 100 100], D: [$\varepsilon_{cell,0}/\varepsilon_{cell,0,max}$ $\varepsilon/\varepsilon_{max}$ $C_{G,0}/C_{G,0,max}$] = [40 100 22.22], E: [$\varepsilon_{cell,0}/\varepsilon_{cell,0,max}$ $\varepsilon/\varepsilon_{max}$ $C_{G,0}/C_{G,0,max}$] = [40 80 100], F: [$\varepsilon_{cell,0}/\varepsilon_{cell,0,max}$ $\varepsilon/\varepsilon_{max}$ $C_{G,0}/C_{G,0,max}$] = [40 60 100]. The cases G to U have $\varepsilon_{cell,0}/\varepsilon_{cell,0,max}$ = 20, the cases G to O have $C_{G,0}/C_{G,0,max}$ = 100. G: [$\varepsilon/\varepsilon_{max}$ H/H_{max}] = [100 28.95], H: [$\varepsilon/\varepsilon_{max}$ H/H_{max}] = [100 38.16], I: [$\varepsilon/\varepsilon_{max}$ H/H_{max}] = [100 55.26], J: [$\varepsilon/\varepsilon_{max}$ H/H_{max}] = [80 28.95], K: [$\varepsilon/\varepsilon_{max}$ H/H_{max}] = [80 38.16], L: [$\varepsilon/\varepsilon_{max}$ H/H_{max}] = [80 55.26], M: [$\varepsilon/\varepsilon_{max}$ H/H_{max}] = [60 28.95], N: [$\varepsilon/\varepsilon_{max}$ H/H_{max}] = [60 38.16], O: [$\varepsilon/\varepsilon_{max}$ H/H_{max}] = [60 55.26]. The cases P to U have $C_{G,0}/C_{G,0,max}$ = 22.22. P: [$\varepsilon/\varepsilon_{max}$ H/H_{max}] = [80 28.95], Q: [$\varepsilon/\varepsilon_{max}$ H/H_{max}] = [80 38.16], R: [$\varepsilon/\varepsilon_{max}$ H/H_{max}] = [80 55.26], S: [$\varepsilon/\varepsilon_{max}$ H/H_{max}] = [60 28.95], T: [$\varepsilon/\varepsilon_{max}$ H/H_{max}] = [60 38.16], U: [$\varepsilon/\varepsilon_{max}$ H/H_{max}] = [60 55.26]

In Figure 6.12, it can also be seen that cases F (60 % porosity), K and L (porosity of 80 %) presented the smallest percent relative errors of mean cell volume fraction at the final time from the experimental data. This could be due to the slight increase in transport limitation (smaller void fraction) and consequent reduction of cell volume fraction, what can balance an overestimation of cell growth rate (observed in cases A, B, C, E, H, and I).

The deviations for the cases with different initial conditions compared to the experimental ones provide information about the model prediction capacity. As can be seen in

Figure 6.10, different initial cell numbers (cases B and C) with relation to the experimental one (case A) led to different final cell volume fractions. Also, the reduction of initial glucose media concentration led to high and negative deviation, as it implies a radical reduction of glucose availability when compared to the experimental one (high glucose culture media), and consequent decrease of cell growth (cases D, P, Q, R S, T, and U).

With the exception of case G, the cases with 0.088 cm of thickness (J, M, P, and S) presented higher deviations with relation to the experimental data when compared to the cases with higher thickness. The fact of the errors all being negative could be due to the underestimation of maximum cell growth rate for this thickness, which was convenient only for the case with 100 % porosity (G).

Positive variations (increase) of R_m, η and/or λ, and the negative variations (decrease) of K_{eq}, D_β, D_α and/or α, considering the reference values for the dimensionless parameters presented in Table 6.1, reduced the percent relative error between the experimental and calculated mean cell volume fractions, when compared to the relative error obtained with the reference values. The dimensionless parameter variations presented in Table 6.6 led to the higher deviations from the reference case concerning the relative error between the experimental and calculated mean cell volume fractions at the final time.

Table 6.6: Percent reduction of the relative error between the experimental and calculated cell volume fractions at the final time, with dimensionless parameter variation

Dimensionless parameter	Dimensionless parameter variation (%)	Reduction in the relative error between the experimental and calculated cell volume fractions at the final time (%)
Rm	+ 50	54.6
Db	- 50	93.2
η	+ 25	91.6
λ	+ 50	98.8

According to the results in Table 6.6, with the increase in λ, higher the cell death or smaller the cell proliferation. Higher η requires smaller glucose concentration or higher Contois saturation coefficient, what would reduce the effect of glucose on cell growth. A positive variation of R_m could be associated to higher glucose uptake or higher transport limitations (smaller D_β), which would affect cell growth negatively. Thus, all the variations that reduced the relative error, with relation to the experimental data, led to the reduction of

the final cell volume fraction value. Since in the experiments performed by Freed, Vunjak-Novakovic and Marquis [36] there was media exchange over the culture that was not considered in the model, perhaps the cell growth rate was overestimated to account for the higher glucose availability and the consequent slight increase in cell growth that occurred every time the medium was replaced.

According to Chung et al. [10] and Vunjak-Novakovic and Marquis [36], volumetric cell growth rate decreases for higher scaffold thickness. Therefore, different maximum cell growth rates - proposed by Chung et al. [10] - were used in this study for each scaffold thickness. Moreover, different initial cell densities did not change significantly the growth rate in the present computational study, as occurred in the experiments of Vunjak-Novakovic and Marquis [36].

According to Vunjak-Novakovic and Marquis [36], cell growth rate decreases with the increase of cell density over time. The model captured this behavior, once the glucose uptake increased with time due to proliferation and higher cell number, and consequently, the glucose concentration decreased, leading to a reduction of cell growth rate over time.

According to Gomes, Holtorf, Reis and Mikos [51], higher porosities lead to higher cell proliferation, due to higher diffusion of nutrients and metabolic waste removal. The model also captured this behavior, since higher glucose concentrations and cell volume fractions were observed for higher porosities.

6.4 Conclusions

Through a sensitivity analysis, it was observed that the model is more sensitive to the dimensionless parameters related to cell proliferation (η), death (λ) and nutrient uptake (R_m), in this order of importance. The impact of different input variables on the model output variables was also studied. It was possible to analyze the effects of transport limitations and of the glucose availability on cell growth. The model presented higher sensitivity to initial glucose concentration and scaffold porosity. When compared to experimental studies, the results showed that the model is capable of representing the phenomena involved in tissue development *in vitro*.

6.5 Acknowledgments

This research was developed at the National Center of Supercomputing from the Federal University of Rio Grande do Sul. The authors would like to thank CAPES

(Coordination for the Improvement of Higher Education Personnel), FINEP (Financing Agency for Studies and Projects) and Stem Cell Research Institute for their financial support.

6.6 References

[1] M. Cioffi, J. Küffer, S. Ströbel, G. Dubini, I. Martin, D. Wendt, Computational evaluation of oxygen and shear stress distributions in 3D perfusion culture systems: Macro-scale and micro-structured models, J. Biomech. 41 (2008) 2918–2925. doi:10.1016/j.jbiomech.2008.07.023.

[2] W.L. Grayson, D. Marolt, S. Bhumiratana, M. Fröhlich, X.E. Guo, G. Vunjak-Novakovic, Optimizing the medium perfusion rate in bone tissue engineering bioreactors, Biotechnol. Bioeng. 108 (2011) 1159–1170. doi:10.1002/bit.23024.

[3] J. Malda, J. Rouwkema, D.E. Martens, E.P. Le Comte, F.K. Kooy, J. Tramper, C. a. Van Blitterswijk, J. Riesle, Oxygen Gradients in Tissue-Engineered PEGT/PBT Cartilaginous Constructs: Measurement and Modeling, Biotechnol. Bioeng. 86 (2004) 9–18. doi:10.1002/bit.20038.

[4] B. Obradovic, J.H. Meldon, L.E. Freed, G. Vunjak-Novakovic, Glycosaminoglycan deposition in engineered cartilage: Experiments and mathematical model, AIChE J. 46 (2000) 1860–1871. doi:10.1002/aic.690460914.

[5] M. Radisic, W. Deen, R. Langer, G. Vunjak-Novakovic, Mathematical model of oxygen distribution in engineered cardiac tissue with parallel channel array perfused with culture medium containing oxygen carriers., Am. J. Physiol. Heart Circ. Physiol. 288 (2005) H1278–H1289. doi:10.1152/ajpheart.00787.2004.

[6] G.D.S. Tan, G.W. Toh, E. Birgersson, J. Robens, D. van Noort, H.L. Leo, A thin-walled polydimethylsiloxane bioreactor for high-density hepatocyte sandwich culture, Biotechnol. Bioeng. 110 (2013) 1663–1673. doi:10.1002/bit.24822.

[7] S. Zhou, Z. Cui, J.P.G. Urban, Nutrient gradients in engineered cartilage: Metabolic kinetics measurement and mass transfer modelings, Biotechnol. Bioeng. 101 (2008) 408–421. doi:10.1002/bit.21887.

[8] M. Campolo, F. Curcio, A. Soldati, Minimal perfusion flow for osteogenic growth of mesenchymal stem cells on lattice scaffolds, AIChE J. 59 (2013) 3131–3144. doi:10.1002/aic.14084.

[9] P. Causin, R. Sacco, A computational model for biomass growth simulation in tissue engineering, Commun. Appl. Ind. Math. 2 (2011). doi:10.1685/journal.caim.370.

[10] C.A. Chung, S.-Y. Ho, Analysis of Collagen and Glucose Modulated Cell Growth within Tissue Engineered Scaffolds, Ann. Biomed. Eng. 38 (2010) 1655–1663. doi:10.1007/s10439-010-9909-5.

[11] C.A. Chung, C.W. Chen, C.P. Chen, C.S. Tseng, Enhancement of cell growth in tissue-engineering constructs under direct perfusion: Modeling and simulation, Biotechnol. Bioeng. 97 (2007) 1603–1616. doi:10.1002/bit.21378.

[12] C.A. Chung, C.P. Chen, T.H. Lin, C.S. Tseng, A compact computational model for cell construct development in perfusion culture, Biotechnol. Bioeng. 99 (2008) 1535–1541. doi:10.1002/bit.21701.

[13] M. Flaibani, E. Magrofuoco, N. Elvassore, Computational modeling of cell growth heterogeneity in a perfused 3D scaffold, Ind. Eng. Chem. Res. 49 (2010) 859–869. doi:10.1021/ie900418g.

[14] C.J. Galban, B.R. Locke, Effects of spatial variation of cells and nutrient and product concentrations coupled with product inhibition on cell growth in a polymer scaffold, Biotechnol. Bioeng. 64 (1999) 633–643. doi:10.1002/(SICI)1097-

0290(19990920)64:6<633::AID-BIT1>3.0.CO;2-6.
[15] C.J. Galban, B.R. Locke, Analysis of cell growth kinetics and substrate diffusion in a polymer scaffold, Biotechnol. Bioeng. 65 (1999) 121–132. doi:10.1002/(SICI)1097-0290(19991020)65:2<121::AID-BIT1>3.0.CO;2-6.
[16] T.Y. Kang, H.W. Kang, C.M. Hwang, S.J. Lee, J. Park, J.J. Yoo, D.W. Cho, The realistic prediction of oxygen transport in a tissue-engineered scaffold by introducing time-varying effective diffusion coefficients, Acta Biomater. 7 (2011) 3345–3353. doi:10.1016/j.actbio.2011.05.015.
[17] C.Y.J. Ma, R. Kumar, X.Y. Xu, A. Mantalaris, A combined fluid dynamics, mass transport and cell growth model for a three-dimensional perfused biorector for tissue engineering of haematopoietic cells, Biochem. Eng. J. 35 (2007) 1–11. doi:10.1016/j.bej.2006.11.024.
[18] M.M. Nava, M.T. Raimondi, R. Pietrabissa, A multiphysics 3D model of tissue growth under interstitial perfusion in a tissue-engineering bioreactor, Biomech. Model. Mechanobiol. 12 (2013) 1169–1179. doi:10.1007/s10237-013-0473-4.
[19] M. Radisic, J. Malda, E. Epping, W. Geng, R. Langer, G. Vunjak-Novakovic, Oxygen gradients correlate with cell density and cell viability in engineered cardiac tissue, Biotechnol. Bioeng. 93 (2006) 332–343. doi:10.1002/bit.20722.
[20] M. Shakeel, P.C. Matthews, R.S. Graham, S.L. Waters, A continuum model of cell proliferation and nutrient transport in a perfusion bioreactor., Math. Med. Biol. 30 (2013) 21–44. doi:10.1093/imammb/dqr022.
[21] B.G. Sengers, Modeling the development of tissue engineered cartilage, Technische Universiteit Eindhoven, 2005.
[22] M.T. Raimondi, F. Boschetti, L. Falcone, G.B. Fiore, a. Remuzzi, E. Marinoni, M. Marazzi, R. Pietrabissa, Mechanobiology of engineered cartilage cultured under a quantified fluid-dynamic environment, Biomech. Model. Mechanobiol. 1 (2002) 69–82. doi:10.1007/s10237-002-0007-y.
[23] H. Singh, S.H. Teoh, H.T. Low, D.W. Hutmacher, Flow modelling within a scaffold under the influence of uni-axial and bi-axial bioreactor rotation, J. Biotechnol. 119 (2005) 181–196. doi:10.1016/j.jbiotec.2005.03.021.
[24] B. Porter, R. Zauel, H. Stockman, R. Guldberg, D. Fyhrie, 3-D computational modeling of media flow through scaffolds in a perfusion bioreactor, J. Biomech. 38 (2005) 543–549. doi:10.1016/j.jbiomech.2004.04.011.
[25] R. Voronov, S. VanGordon, V.I. Sikavitsas, D. V. Papavassiliou, Computational modeling of flow-induced shear stresses within 3D salt-leached porous scaffolds imaged via micro-CT, J. Biomech. 43 (2010) 1279–1286. doi:10.1016/j.jbiomech.2010.01.007.
[26] M. Laganà, M.T. Raimondi, A miniaturized, optically accessible bioreactor for systematic 3D tissue engineering research, Biomed. Microdevices. 14 (2012) 225–234. doi:10.1007/s10544-011-9600-0.
[27] C. Jungreuthmayer, M.J. Jaasma, a. a. Al-Munajjed, J. Zanghellini, D.J. Kelly, F.J. O'Brien, Deformation simulation of cells seeded on a collagen-GAG scaffold in a flow perfusion bioreactor using a sequential 3D CFD-elastostatics model, Med. Eng. Phys. 31 (2009) 420–427. doi:10.1016/j.medengphy.2008.11.003.
[28] Y. Chen, S. Zhou, Q. Li, Mathematical modeling of degradation for bulk-erosive polymers: Applications in tissue engineering scaffolds and drug delivery systems, Acta Biomater. 7 (2011) 1140–1149. doi:10.1016/j.actbio.2010.09.038.
[29] M. Heljak, W. Swieszkowski, K.J. Kurzydlowski, A phenomenological model for the degradation of polymeric tissue engineering scaffolds, (2011).
[30] M. Heljak, W. Swieszkowski, K.J. Kurzydlowski, Modeling of the degradation kinetics

of biodegradable scaffolds: The effects of the environmental conditions, J. Appl. Polym. Sci. 131 (2014) 1–7. doi:10.1002/app.40280.
[31] T. Shazly, V.B. Kolachalama, J. Ferdous, J.P. Oberhauser, S. Hossainy, E.R. Edelman, Assessment of material by-product fate from bioresorbable vascular scaffolds, Ann. Biomed. Eng. 40 (2012) 955–965. doi:10.1007/s10439-011-0445-8.
[32] J. Ferdous, V.B. Kolachalama, T. Shazly, Impact of polymer structure and composition on fully resorbable endovascular scaffold performance, Acta Biomater. 9 (2013) 6052–6061. doi:10.1016/j.actbio.2012.12.011.
[33] G. Lemon, D. Howard, M.J. Tomlinson, L.D. Buttery, F.R. a J. Rose, S.L. Waters, J.R. King, Mathematical modelling of tissue-engineered angiogenesis, Math. Biosci. 221 (2009) 101–120. doi:10.1016/j.mbs.2009.07.003.
[34] P. Pathi, Mathematical Modeling of Transport and Reaction in Cellular and Tissue Engineering, Florida State University, 2005.
[35] M. Lovett, K. Lee, A. Edwards, D.L. Kaplan, Vascularization strategies for tissue engineering., Tissue Eng. Part B. Rev. 15 (2009) 353–70. doi:10.1089/ten.TEB.2009.0085.
[36] F. LE, V.-N. G, M. JC, L. R., Kinetics of chondrocyte growth in cell-polymer implants, Biotechnol Bioeng. 43 (1994) 597–604.
[37] C.A. Chung, S.Y. Ho, Analysis of collagen and glucose modulated cell growth within tissue engineered scaffolds, Ann. Biomed. Eng. 38 (2010) 1655–1663. doi:10.1007/s10439-010-9909-5.
[38] T.-H. Lin, C.-H. Lin, C.A. Chung, Comutational Study of Oxygen and Glucose Transport in Engineered Cartilage Constructs, J. Mech. 27 (2011) 337–346. doi:10.1017/jmech.2011.36.
[39] C. Bandeiras, A. Completo, A. Ramos, Influence of the scaffold geometry on the spatial and temporal evolution of the mechanical properties of tissue-engineered cartilage: insights from a mathematical model, Biomech. Model. Mechanobiol. 14 (2015) 1057–1070. doi:10.1007/s10237-015-0654-4.
[40] D. Liu, C.K. Chua, K.F. Leong, A mathematical model for fluid shear-sensitive 3D tissue construct development, Biomech. Model. Mechanobiol. 12 (2013) 19–31. doi:10.1007/s10237-012-0378-7.
[41] M. Izadifar, Biomanufacturing versus Superficial Cell Seeding: Simulation of Chondrocyte Proliferation in a Cylindrical Cartilage Scaffold, Int. J. Tissue Eng. 2013 (2013) 1–9. doi:10.1155/2013/407047.
[42] L. Tang, A.L. van de Ven, D. Guo, V. Andasari, V. Cristini, K.C. Li, X. Zhou, Computational Modeling of 3D Tumor Growth and Angiogenesis for Chemotherapy Evaluation, PLoS One. 9 (2014) e83962. doi:10.1371/journal.pone.0083962.
[43] H.B. Henninger, S.P. Reese, A.E. Anderson, J.A. Weiss, Validation of computational models in biomechanics, Proc Inst Mech Eng H. 224 (2010) 801–812.
[44] P. Causin, R. Sacco, M. Verri, A multiscale approach in the computational modeling of the biophysical environment in artificial cartilage tissue regeneration, Biomech. Model. Mechanobiol. 12 (2013) 763–780. doi:10.1007/s10237-012-0440-5.
[45] M. Pisu, A. Concas, S. Fadda, A. Cincotti, G. Cao, A simulation model for stem cells differentiation into specialized cells of non-connective tissues, Comput. Biol. Chem. 32 (2008) 338–344.
[46] T.I. Croll, S. Gentz, K. Mueller, M. Davidson, A.J. O'Connor, G.W. Stevens, J.J. Cooper-White, Modelling oxygen diffusion and cell growth in a porous, vascularising scaffold for soft tissue engineering applications, Chem. Eng. Sci. 60 (2005) 4924–4934. doi:10.1016/j.ces.2005.03.051.
[47] D. Cook, B.A. Ogunnaike, R. Vadigepalli, Systems analysis of non-parenchymal cell

modulation of liver repair across multiple regeneration modes, BMC Syst. Biol. 9 (2015) 1–24.
[48] B.D. Wood, M. Quintard, S. Whitaker, Calculation of effective diffusivities for biofilms and tissues, Biotechnol. Bioeng. 77 (2002) 495–516. doi:10.1002/bit.10075.
[49] D.E. Contois, Kinetics of bacterial growth: Relationship between population density and specific growth rate of continuous cultures, J Gen Microbil. 21 (1959) 40–50.
[50] T. Holzmann, The pimple algorithm in OpenFOAM., (2016). https://openfoamwiki.net/index.php/OpenFOAM_guide/The_PIMPLE_algorithm_in_OpenFOAM (accessed July 14, 2016).
[51] M.E. Gomes, H.L. Holtorf, R.L. Reis, A.G. Mikos, Influence of the porosity of starch-based fiber mesh scaffolds on the proliferation and osteogenic differentiation of bone marrow stromal cells cultured in a flow perfusion bioreactor., Tissue Eng. 12 (2006) 801–809. doi:10.1089/ten.2006.12.801.

Capítulo 7

Comparação entre modelos do desenvolvimento de tecidos

A partir de um modelo bastante utilizado na engenharia de tecidos, foram analisadas contribuições sugeridas por outros trabalhos da literatura. Desta forma, este capítulo buscou responder a seguinte questão de pesquisa:

→ Qual a contribuição do oxigênio e do aumento da porosidade com a degradação do polímero ao modelo em estudo sob diferentes cenários (variação nas variáveis de entrada)?

O trabalho apresentado neste capítulo teve o objetivo de avaliar a contribuição da adição de complexidade ao modelo, através da variação temporal da porosidade e da associação do consumo e transporte de oxigênio com a cinética dupla de Contois, para poder estabelecer os fenômenos que devem ser descritos pelo modelo. O capítulo está estruturado na forma de artigo científico, na língua inglesa, o qual foi submetido para a revista *Brazilian Journal of Chemical Engineering* e está sob revisão.

Artigo 6

SENSITIVITY ANALYSIS FOR MODEL COMPARISON AND SELECTION IN TISSUE ENGINEERING

Ágata Paim [*1,2], Nilo S. M. Cardozo [1], Patricia Pranke[2,3], Isabel C. Tessaro[1]

[1]Department of Chemical Engineering, Universidade Federal do Rio Grande do Sul (UFRGS), R. Eng. Luis Englert, s/n. Porto Alegre, Rio Grande do Sul 90040-040, Brazil.

[2]Faculty of Pharmacy, Universidade Federal do Rio Grande do Sul (UFRGS), Av. Ipiranga, 2752. Porto Alegre, Rio Grande do Sul 90610-000, Brazil.

[3]Stem Cell Research Institute, Universidade Federal do Rio Grande do Sul (UFRGS), Av. Ipiranga, 2752. Porto Alegre, Rio Grande do Sul 90610-000, Brazil.

Corresponding author (Ágata Paim)

Present address: Department of Chemical Engineering, Universidade Federal do Rio Grande do Sul (UFRGS), R. Eng. Luis Englert, s/n. Porto Alegre, Rio Grande do Sul 90040-040, Brazil

Phone/Fax: +55 51 33085257

E-mail address: agata@enq.ufrgs.br

Abstract

Computational modeling has been proven to be very useful in tissue engineering over the past years. Because the model is a simplification of the experimental system, the processes accounted in the model should be analyzed carefully. However, new and complex models are usually proposed without a clear comparison with the basic ones. In this study, the contribution of oxygen in Contois growth kinetics and porosity variation with time due to polymer degradation was evaluated through a sensitivity analysis. The effect of initial glucose concentration, porosity and thickness of the scaffold on the cell volume fraction and substrate concentration was analyzed for three models. Even with the inclusion of oxygen concentration in the model, the output variables are more affected by the initial cell number, while the model with variable porosity is considerably robust to variations on the input variables.

Keywords: computational modeling, tissue engineering, scaffold porosity, mass transport, cell growth

Symbols

$C_{g,\beta,}$	average glucose concentration in the fluid phase	$kg \cdot m^{-3}$
C_o	average oxygen concentration in the fluid phase	$mol \cdot m^{-3}$
$C_{g,0,\beta}$	initial average glucose concentration in the fluid phase	$kg \cdot m^{-3}$
$C_{g,0,\beta,max}$	maximum value used for the initial average glucose concentration in the fluid phase	$kg \cdot m^{-3}$
$C_{o,0}$	initial average oxygen concentration	$mol \cdot m^{-3}$
$D_{g,eff}$	glucose effective diffusivity in the tissue scaffold	$m^2\ s^{-1}$
$D_{o,eff}$	oxygen effective diffusivity in the tissue scaffold	$m^2\ s^{-1}$
$D_{g,\sigma}$	glucose diffusivity in the cell phase	$m^2\ s^{-1}$
$D_{g,\beta}$	glucose diffusivity in the fluid phase	$m^2\ s^{-1}$
D_o	oxygen molecular diffusivity in the fluid phase	$m^2\ s^{-1}$
$D_{g,eff,\sigma}$	glucose effective diffusivity in the cell phase	$m^2\ s^{-1}$
$D_{o,eff,\sigma}$	oxygen effective diffusivity in the cell phase	$m^2\ s^{-1}$
$D_{g,eff,\beta}$	glucose effective diffusivity in the fluid phase	$m^2\ s^{-1}$
$D_{o,eff,\beta}$	oxygen effective diffusivity in the fluid phase	$m^2\ s^{-1}$
$D_{eff,cell}$	coefficient for random migration of cells	$m^2\ s^{-1}$
H	scaffold thickness	m
H_{max}	maximum value used for the scaffold thickness	m
K_c	Contois saturation coefficient	
K_{eq}	equilibrium of the cellular and fluid phases coefficient	
R_d	cell death rate	s^{-1}
R_g	cell growth rate	s^{-1}
S_g	volumetric rate of cell consumption for glucose	$kg \cdot s^{-1} \cdot m^{-3}$

S_o	volumetric rate of cell consumption for oxygen	$mol \cdot s^{-1} \cdot cell^{-1}$
R_m	glucose uptake rate	s^{-1}
R_{gm}	maximum glucose metabolic rate	$kg \cdot s^{-1} \cdot m^{-3}$
R_{om}	maximum oxygen metabolic rate	$mol \cdot s^{-1} \cdot cell^{-1}$
K_{gm}	glucose saturation coefficient	$kg \cdot m^{-3}$
K_{om}	oxygen saturation coefficient	$mol \cdot m^{-3}$

Greek letters

α	parameter from Maxwell formula for glucose effective diffusivity	
ε	scaffold porosity	
ε_0	initial scaffold porosity	
ε_β	fluid phase volume fraction	
ε_σ	volumetric fraction of cells in the scaffold	
$\varepsilon_{\sigma,0}$	initial number of cells	cells
$\varepsilon_{\sigma,0,max}$	maximum value used for the initial number of cells	
ε_{max}	maximum value used for the scaffold porosity	
ρ_{cell}	single cell mass density	$cell \cdot m^{-3}$
μ_{max}	maximum cell growth rate	s^{-1}
τ	scaffold tortuosity	
Ω	degradation coefficient	s

7.1 Introduction

Modeling techniques have been used recently to determine scaffold properties and/or to analyze the impact of them on tissue development. The properties considered in these works include porosity [1,2], permeability [1,3,4], mean pore size [3,5], surface energy [6], roughness [6] and effective Young's modulus [7]. Besides this, modeling techniques have also been used in the comparison of different bioreactor designs [8–10] and seeding techniques [11–13]. The processes most studied in tissue development are nutrient diffusion and convection [1,2,14–20], cell growth [1–3,14–20], cell adhesion strength [6], morphology [5], and cell deformation and detachment [5].

Galban and Locke [21] used moving boundary equations to develop a mathematical model for cell growth in a porous polymeric matrix. The computational results were compared to the experimental data from Freed et al. [22], which studied chondrocyte growth kinetics on polyglycolic acid (PGA) scaffolds under static and well-mixed conditions. The authors then improved this model by the inclusion of a nutrient diffusion term to study the performance of different kinetic functions on the prediction of the rate of cell growth [15]. Using this model, the authors evaluated the impact of spatial variation of cell numbers and nutrient and product concentrations on cell growth [14].

Chung et al. [16] developed a mathematical model to describe chondrocyte growth in a porous scaffold. In addition to cell growth kinetics and nutrient consumption, their model included a term of cell diffusion. Chung et al. [12] considered both glucose and collagen modulation on chondrocyte culture and used the Michaelis–Menten model to describe the glucose uptake. Lin et al. [20] adapted this model to evaluate the simultaneous effects of glucose and oxygen on cartilaginous constructs under static culture. In these three works the computational results have also been compared with the experimental data from Freed et al. [22]. However, in the three cases, this comparison was only performed graphically by means of figures where model predictions and experimental points are plotted together, and without including any comparison with predictions of the other models.

Highly porous scaffolds are desirable for tissue engineering applications because they can support cellular migration and adhesion, promote vascularization, and also encourage angiogenesis. However, the porosity must be optimized because scaffolds with too high void fractions cannot maintain enough mechanical integrity and become unable to support cellular growth [23]. The models based on the volume average method, such as the model proposed by Chung et al. [16], usually consider the reduction of space for the culture media due to the

increase in the cell volume fraction. However, with scaffold degradation and extracellular matrix formation, it becomes interesting to also consider the porosity variation in mathematical models.

Yan et al. [2] incorporated the effect of scaffold degradation on the porosity of the construct. The data of chondrocytes growth in PGA scaffolds in rotating bioreactors from Freed et al. [24] were adopted to obtain a porosity function. Although they evaluated the effect of different porosities considering the perfusion of the medium through the scaffold, the model was validated only with the static culture data of Freed et al. [22]. In addition, the behavior obtained for static condition was less similar to the experimental data from Freed et al. [22], when compared to the results from Chung et al. [12] and Lin et al. [20].

As can be seen, the models for tissue development available in the literature differ greatly from one another with respect to the mechanisms considered and the specific model used for a given mechanism. However, in most cases, each of these models was presented without a detailed comparison with the others, in such a way that the contribution of each model improvement in terms of adequacy or predictive capacity is not completely understood. The overall objective of this work has been to evaluate the contribution of the oxygen transport in Contois proliferation kinetics and the porosity variation with time due to polymer degradation, using the model of Chung et al. [16] considering the Michaelis-Menten model for the nutrient consumption. A sensitivity analysis was used to compare the models and to verify the impact of each variable on the model outputs.

7.2 Methodology

7.2.1. Modeling

The governing equations for cell growth, considering only the effect of random walk on cell diffusion, can be described by the following equation [2,16,19]:

$$\frac{\partial \varepsilon_\sigma}{\partial t} = \nabla\left(D_{eff,cell}\nabla\varepsilon_\sigma\right) + \left[R_g - R_d\right]\varepsilon_\sigma \tag{7.1}$$

where $D_{eff,cell}$ is the coefficient for random migration of cells, ε_σ is the volumetric fraction of cells in the scaffold, R_g is the cell growth rate, and R_d is the cell death rate.

The classical Contois growth model is widely used for cell growth kinetics [16] and is given by Equation 7.2:

$$R_g = \frac{\mu_{max} C_{g,\beta}}{K_{eq}^{-1} K_c \rho_{cell} \varepsilon_\sigma + C_{g,\beta}} \tag{7.2}$$

where μ_{max} is the maximum cell growth rate, $C_{g,\beta}$ is the average glucose concentration in the fluid phase, K_{eq} is the equilibrium of the cellular and fluid phases coefficient, ρ_{cell} is the single cell mass density and K_c is the Contois saturation coefficient.

When more than one substrate can limit growth kinetics, a double-Contois can be used [2]. Therefore, considering combined oxygen and glucose modulation on cell growth rate, this model can be written as:

$$R_g = \mu_{max} \frac{C_o}{K_c \rho_{cell} \varepsilon_\sigma + C_o} \frac{C_{g,\beta}}{K_{eq}^{-1} K_c \rho_{cell} \varepsilon_\sigma + C_{g,\beta}} \tag{7.3}$$

where C_o is the average oxygen concentration in the fluid phase.

The governing equations for glucose and oxygen transport in static culture are given by Equations 7.4 and 7.5:

$$\frac{\partial[(\varepsilon_\sigma K_{eq} + \varepsilon_\beta) C_{g,\beta}]}{\partial t} = \nabla\left[D_{g,eff} \nabla C_{g,\beta}\right] - S_g \tag{7.4}$$

$$\frac{\partial C_o}{\partial t} = \nabla\left[D_{o,eff} \nabla C_o\right] - S_o \tag{7.5}$$

where $C_{g,\beta}$ and C_o, $D_{g,eff}$ and $D_{o,eff}$, and S_g and S_o are, respectively, the concentration in the culture media, the effective diffusivity in the tissue scaffold, and the volumetric rate of cell consumption for glucose (subindex *g*)and oxygen (subindex *o*).

The volume fraction of the fluid phase (ε_β) is given by:

$$\varepsilon_\beta = \varepsilon - \varepsilon_\sigma \tag{7.6}$$

where ε is the scaffold porosity.

For the glucose volumetric rate of cell consumption, Chung et al. [16] used the following expression:

$$S_g = R_m \varepsilon_\sigma K_{eq} C_{g,\beta} \tag{7.7}$$

while the corresponding expression by the Michaelis-Menten kinetic is given by [2,20]:

$$S_g = \left[\frac{R_{gm} C_{g,\beta}}{K_{gm} + C_{g,\beta}}\right] \varepsilon_\sigma \tag{7.8}$$

where R_{gm} is the maximum glucose metabolic rate and K_{gm} is the glucose saturation coefficient.

Similarly, the oxygen cell consumption is given by:

$$S_o = \left[\frac{R_{om} C_o}{K_{om} + C_o}\right] \varepsilon_\sigma \tag{7.9}$$

where R_{om} is the maximum oxygen metabolic rate and K_{om} is the oxygen saturation coefficient.

For effective diffusivity, Chung et al. [16] used the following expression:

$$D_{g,eff} = \varepsilon_\sigma K_{eq} D_{g,\sigma} + \varepsilon_\beta D_{g,\beta} \tag{7.10}$$

where $D_{g,\sigma}$ and $D_{g,\beta}$ are the diffusivities of the glucose in the cells and in the fluid phase, respectively.

Conversely, Yan et al. [2] evaluated the effective diffusivity as:

$$D_{i,eff} = \frac{D_{i,eff,m}\varepsilon}{\tau} \tag{7.11}$$

where τ is the scaffold tortuosity, and $D_{i,eff,m}$ is the component i effective diffusivity in the phase m (cell or fluid), which is evaluated by the Maxwell formula for glucose and oxygen:

$$D_{g,eff,m} = D_{g,\beta}\left(\frac{\left(3\alpha - 2\left(\frac{\varepsilon_\beta}{\varepsilon}\right)(\alpha-1)\right)}{\left(3+\left(\frac{\varepsilon_\beta}{\varepsilon}\right)(\alpha-1)\right)}\right), \quad D_{o,eff,m} = \frac{D_o 2\left(1-\frac{\varepsilon_\sigma}{\varepsilon}\right)}{\left(2+\frac{\varepsilon_\sigma}{\varepsilon}\right)} \tag{7.12}$$

where $\alpha = K_{eq} \cdot D_{g,\sigma} \cdot D_{g,\beta}^{-1}$ and D_o, is the oxygen molecular diffusivity in the fluid phase.

The time evolution of the scaffold porosity was evaluated using the function adopted by Yan et al. [2], which is given by Equation 7.13:

$$\varepsilon = 1 - (1 - \varepsilon_0)e^{-t/\Omega} \tag{7.13}$$

where ε_0 is the initial porosity of the scaffold, and Ω is the degradation coefficient.

Based on the previously described set of equations, three models of different levels of complexity were obtained. The mechanisms and equations included in each of these models are summarized in Table 7.1.

Table 7.1: Models

Model	Mechanisms	Equations
I	Glucose limitation of cell growth (Contois)	7.2
	Glucose transport (Michaelis-Menten)	7.8
II	Glucose and oxygen limitation of cell growth (double Contois)	7.3
	Glucose and oxygen transport (Michaelis-Menten)	7.8, 7.9
III	Glucose and oxygen limitation of cell growth (double Contois)	7.3
	Glucose and oxygen transport (Michaelis-Menten)	7.8, 7.9
	Time dependence of the scaffold porosity	7.13

Model I is basically the same as that proposed by Chung et al. [16], but including the Michaelis-Menten kinetic for glucose transport. Model II is similar to the model suggested by Lin et al. [20], including limitation of growth and the Michaelis-Menten kinetic for both glucose and oxygen. Finally, Model III also includes the time dependence of the scaffold porosity as a variable, such as in the model of Yan et al. [2].

As proposed by Chung et al. [16], the following boundary conditions were specified: (i) zero cell mass flux on the boundaries, and (ii) nutrient concentration at the extremities of the scaffold surface equal to the bulk concentration of the medium surrounding the scaffold. Thus, the nutrient transport occurs from the extremities to the center of the scaffold.

7.2.2. Implementation and Sensitivity Analysis

Models I-III were implemented in a finite volume code using the open source OpenFOAM *package*. The numerical scheme used in the simulations was the algorithm for transient processes PIMPLE [25]. Four rectangular geometries were studied, with proportions between length and height of 3.26 × 1, 5.95 × 1, 8.62 × 1 and 11.36 × 1, corresponding to the cases with thicknesses of 3.07×10^{-3} m, 1.69×10^{-3} m, 1.16×10^{-3} m and 0.88×10^{-3} m, respectively. The meshes were created with the tool blockMesh with 100 elements per dimensionless unit of length in each direction, what satisfies the convergence condition, as established preliminarily.

The processes of cell proliferation and nutrient transfer through a PGA scaffold seeded with chondrocytes reported by Freed et al. [22] was used as the basis of analysis, considering a culture time of 21 days. The set of model parameters used in the simulations is given in Table 7.2. A static seeding efficiency of 60% was assumed.

Table 7.2: Values of parameters used in the simulations

Parameter	Value	Unit	Reference
$D_{g,\beta}$	1×10^{-8}	$m^2\cdot s^{-1}$	[16]
$D_{g,\sigma}$	1×10^{-7}	$m^2\cdot s^{-1}$	[16]
D_o	3.093×10^{-7}	$m^2\cdot s^{-1}$	[20]
τ	1.93	---	[2]
μ_{max}	$1.6\text{-}4.5\times10^{-6}$	s^{-1}	[16]
ρ_{cell}	0.182×10^{6}	$cell\cdot m^{-3}$	[16]
R_{om}	1.86×10^{-18}	$mol\cdot s^{-1}\cdot cell^{-1}$	[1]
R_{gm}	8×10^{-3}	$kg\cdot s^{-1}\cdot m^{-3}$	[20]
K_{om}	6×10^{-3}	$mol\cdot m^{-3}$	[20]
K_{gm}	6.3×10^{-2}	$kg\cdot m^{-3}$	[20]
K_c	0.154	---	[16]
Ω	2.1×10^{6}	s	[2]
R_d	3.3×10^{-7}	s^{-1}	[16]
R_m	3×10^{-2}	s^{-1}	[16]
V_{cell}	5.49×10^{-16}	$m^3\cdot cell^{-1}$	[16]
K_{eq}	0.1	---	[16]
$D_{eff,cell}$	1.7×10^{-12}	$m^2\cdot s^{-1}$	[16]

In the input sensitivity analysis of Models I-III, the influence of four inputs - initial number of cells ($\varepsilon_{\sigma,0}$), scaffold porosity (ε), scaffold thickness (H), and initial average glucose concentration in the fluid phase ($C_{g,0,\beta}$) - on the output variables (glucose and oxygen concentrations, and volumetric fraction of cells in the scaffold) was evaluated. The set of different combinations of input values used for the sensitivity analysis are presented in Table 7.3, expressed in terms of percentage of the maximum value used for each input. The maximum values used for the initial number of cells, scaffold porosity, scaffold thickness, and average glucose concentration in the fluid phase were, respectively, $\varepsilon_{\sigma,max} = 1\times10^{7}$ cells,

ε_{max} = 100 %, H_{max} = 3.07×10^{-3} m, and $C_{g,0,\beta,max}$ = 4.5 kg·m^{-3}. In all cases an initial oxygen concentration of 0.119 mol·m^{-3} was used.

Table 7.3: Cases for the sensitivity analysis

Case	$\varepsilon_\sigma/\varepsilon_{\sigma,max}$ (%)	$\varepsilon/\varepsilon_{max}$ (%)	H/H_{max} (%)	$C_{g,0,\beta}/C_{g,0,\beta,max}$ (%)
A	40	100	100	100
B	10	100	100	100
C	100	100	100	100
D	40	100	100	22.22
E	40	80	100	100
F	40	60	100	100
G	20	100	28.95	100
H	20	100	38.16	100
I	20	100	55.26	100
J	20	80	28.95	100
K	20	80	38.16	100
L	20	80	55.26	100
M	20	60	28.95	100
N	20	60	38.16	100
O	20	60	55.26	100

7.3 Results and Discussion

Figure 7.1 presents the time evolution of ε_σ predicted with Model I for the cases with scaffold thickness of 3.07×10^{-3} m (Cases A to F). It can be observed that porosity did not have a significant impact on the cell volume fraction for the Cases A, E and F. According to Gomes et al. [26], the enhanced cell growth related with highly porous scaffolds is associated to a higher diffusion of nutrients and metabolic waste removal. Thus, in the range of porosity values considered in this work (100- 60 %) the decrease of porosity could not decrease the nutrient transport sufficiently to affect cell growth. In addition, the production and/or accumulation of toxic metabolites were not considered in this work. Furthermore, with less glucose in the medium at the beginning of the culture (Case D), cell growth is not much higher than the cell death, resulting in an almost constant cell volume fraction.

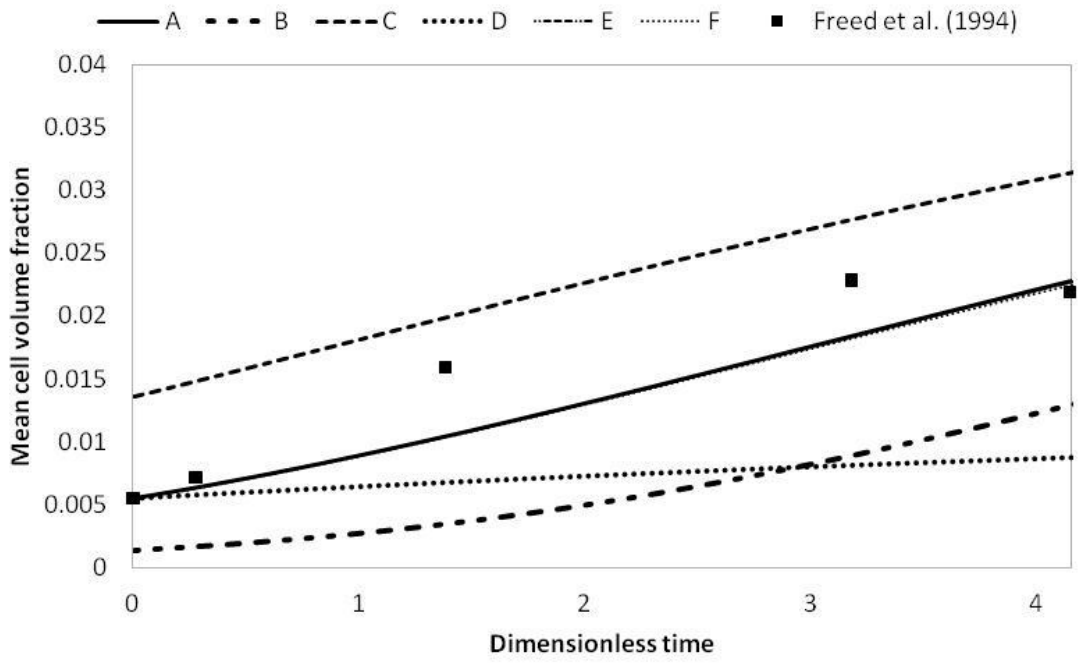

Figure 7.1: Model I time evolution of mean cell volume fraction for scaffold thickness of 3.07×10^{-3} m. A: $[\varepsilon_{cell,0}/\varepsilon_{cell,0,max}\ \ \varepsilon/\varepsilon_{max}\ \ C_{G,0}/C_{G,0,max}] = [40\ 100\ 100]$, B: $[\varepsilon_{cell,0}/\varepsilon_{cell,0,max}\ \ \varepsilon/\varepsilon_{max}\ \ C_{G,0}/C_{G,0,max}] = [10\ 100\ 100]$, C: $[\varepsilon_{cell,0}/\varepsilon_{cell,0,max}\ \ \varepsilon/\varepsilon_{max}\ \ C_{G,0}/C_{G,0,max}] = [100\ 100\ 100]$, D: $[\varepsilon_{cell,0}/\varepsilon_{cell,0,max}\ \ \varepsilon/\varepsilon_{max}\ \ C_{G,0}/C_{G,0,max}] = [40\ 100\ 22.22]$, E: $[\varepsilon_{cell,0}/\varepsilon_{cell,0,max}\ \ \varepsilon/\varepsilon_{max}\ \ C_{G,0}/C_{G,0,max}] = [40\ 80\ 100]$, F: $[\varepsilon_{cell,0}/\varepsilon_{cell,0,max}\ \ \varepsilon/\varepsilon_{max}\ \ C_{G,0}/C_{G,0,max}] = [40\ 60\ 100]$

In Figure 7.2, the dimensionless glucose concentration distribution over the scaffold width at the final time is presented for cases with 3.07×10^{-3} m of thickness to Model I. The increase of mass transport limitation with smaller porosities can be observed through the higher difference between the glucose concentrations at the extremities and at the center of the scaffold observed for Cases E and F when compared to Case A.

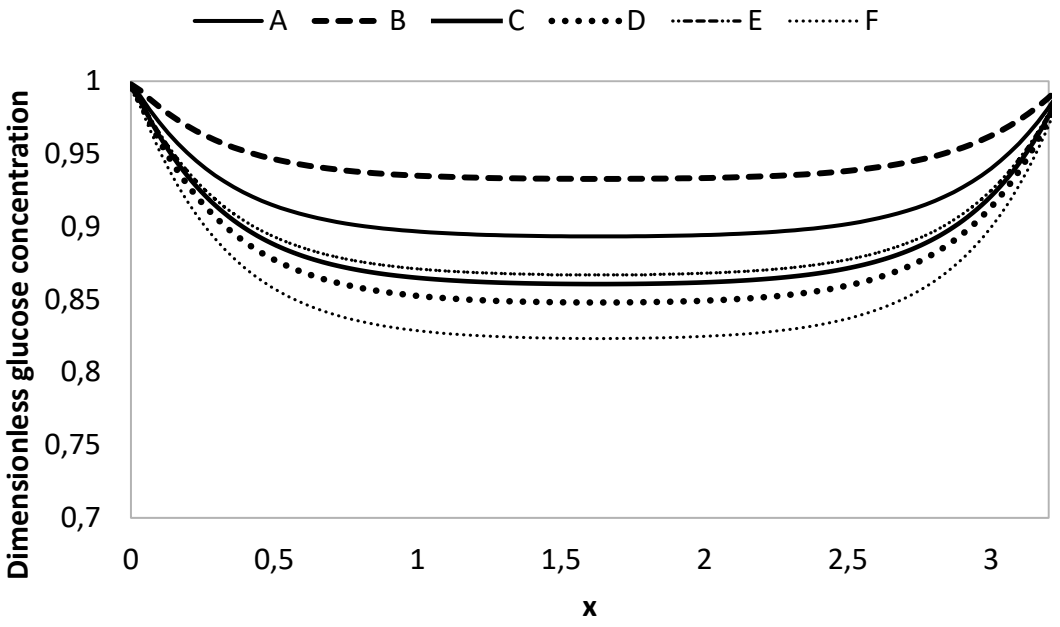

Figure 7.2: Distribution of dimensionless glucose concentration for scaffolds with 3.07×10^{-3} m thickness at the final time using Model I. A: [$\varepsilon_{cell,0}/\varepsilon_{cell,0,max}$ $\varepsilon/\varepsilon_{max}$ $C_{G,0}/C_{G,0,max}$] = [40 100 100], B: [$\varepsilon_{cell,0}/\varepsilon_{cell,0,max}$ $\varepsilon/\varepsilon_{max}$ $C_{G,0}/C_{G,0,max}$] = [10 100 100], C: [$\varepsilon_{cell,0}/\varepsilon_{cell,0,max}$ $\varepsilon/\varepsilon_{max}$ $C_{G,0}/C_{G,0,max}$] = [100 100 100], D: [$\varepsilon_{cell,0}/\varepsilon_{cell,0,max}$ $\varepsilon/\varepsilon_{max}$ $C_{G,0}/C_{G,0,max}$] = [40 100 22.22], E: [$\varepsilon_{cell,0}/\varepsilon_{cell,0,max}$ $\varepsilon/\varepsilon_{max}$ $C_{G,0}/C_{G,0,max}$] = [40 80 100], F: [$\varepsilon_{cell,0}/\varepsilon_{cell,0,max}$ $\varepsilon/\varepsilon_{max}$ $C_{G,0}/C_{G,0,max}$] = [40 60 100]

Mean cell volume fraction presented an increase of 2.3, 4.2, and 9.5 fold in 30 days (corresponding to a 4.15 dimensionless time) for initial cell numbers of 1×10^7, 4×10^6 and 1×10^6 cells (Cases C, A and B, respectively). This is in agreement with the behavior observed experimentally by Freed et al. [22], for which initial cell numbers of 4×10^7, 2×10^7 and 0.5×10^7 presented increases of 2.7, 4.2 and 15.8 fold. The increase of cell growth for smaller initial cell density could be due to the higher availability of glucose caused by the smaller consumption. Higher glucose concentrations for Case B (when compared to Cases A and C), with the smallest initial cell number, can be observed in Figure 7.3, which presents the mean dimensionless glucose concentration evolution in time.

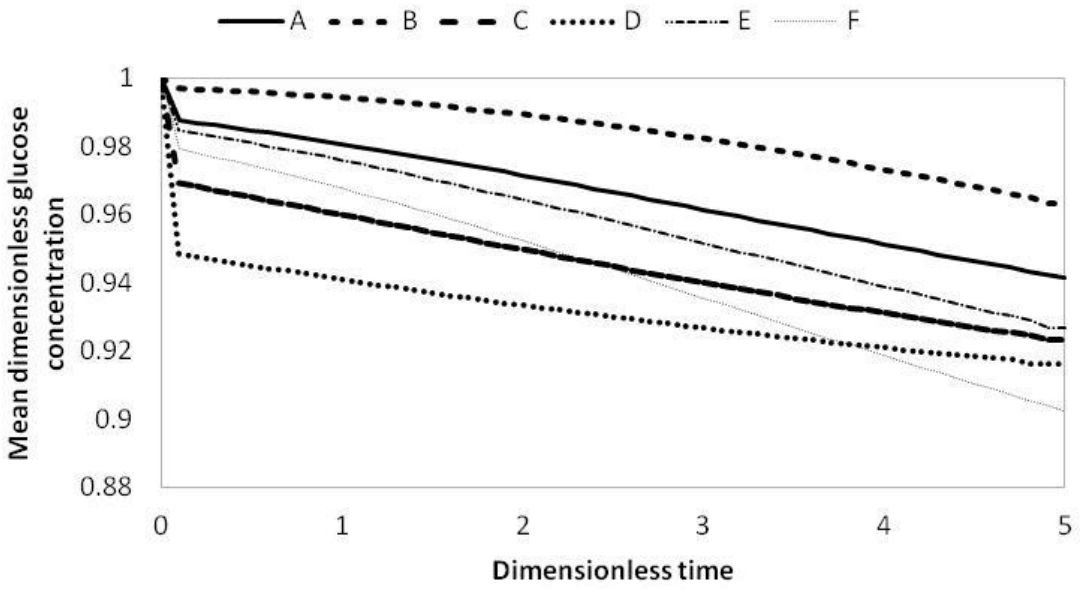

Figure 7.3: Model I time evolution of mean dimensionless glucose concentration for scaffold thickness of 3.07×10^{-3} m. A: [$\varepsilon_{cell,0}/\varepsilon_{cell,0,max}$ $\varepsilon/\varepsilon_{max}$ $C_{G,0}/C_{G,0,max}$] = [40 100 100], B: [$\varepsilon_{cell,0}/\varepsilon_{cell,0,max}$ $\varepsilon/\varepsilon_{max}$ $C_{G,0}/C_{G,0,max}$] = [10 100 100], C: [$\varepsilon_{cell,0}/\varepsilon_{cell,0,max}$ $\varepsilon/\varepsilon_{max}$ $C_{G,0}/C_{G,0,max}$] = [100 100 100], D: [$\varepsilon_{cell,0}/\varepsilon_{cell,0,max}$ $\varepsilon/\varepsilon_{max}$ $C_{G,0}/C_{G,0,max}$] = [40 100 22.22], E: [$\varepsilon_{cell,0}/\varepsilon_{cell,0,max}$ $\varepsilon/\varepsilon_{max}$ $C_{G,0}/C_{G,0,max}$] = [40 80 100], F: [$\varepsilon_{cell,0}/\varepsilon_{cell,0,max}$ $\varepsilon/\varepsilon_{max}$ $C_{G,0}/C_{G,0,max}$] = [40 60 100]

Figure 7.4 presents the time evolution of ε_σ of these cases for Model I. It can be seen that the effect of the porosity on the mean cell volume fraction was much lower than that of the scaffold thickness, as scaffolds of the same thickness presented similar mean cell volume fraction evolution for the three levels of porosity considered: 0.88×10^{-3} m (G, J and M), 1.16×10^{-3} m (H, K and N), and 1.69×10^{-3} m (I, L and O).

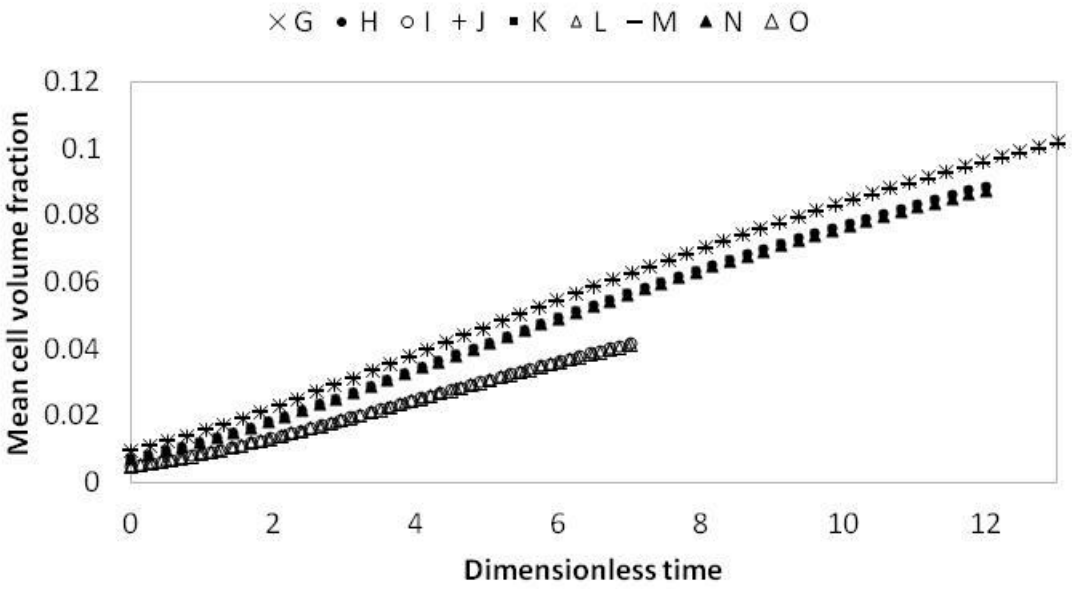

Figure 7.4: Model I time evolution of mean cell volume fraction for scaffold thickness of 0.88, 1.16 and 1.68 $\times 10^{-3}$ m. G: [$\varepsilon/\varepsilon_{max}$ H/H_{max}] = [100 28.95], H: [$\varepsilon/\varepsilon_{max}$ H/H_{max}] = [100 38.16], I: [$\varepsilon/\varepsilon_{max}$ H/H_{max}] = [100 55.26], J: [$\varepsilon/\varepsilon_{max}$ H/H_{max}] = [80 28.95], K: [$\varepsilon/\varepsilon_{max}$ H/H_{max}] = [80 38.16], L: [$\varepsilon/\varepsilon_{max}$ H/H_{max}] = [80 55.26], M: [$\varepsilon/\varepsilon_{max}$ H/H_{max}] = [60 28.95], N: [$\varepsilon/\varepsilon_{max}$ H/H_{max}] = [60 38.16], O: [$\varepsilon/\varepsilon_{max}$ H/H_{max}] = [60 55.26]

As can be observed in Figure 7.4, the increase in scaffold thickness reduces the initial cell volume fraction as the initial cell number is maintained. Thus, the mean cell volume fraction at the final time is smaller for thicker scaffolds, which is observed for Cases G to I, J to L and M to O. The mean cell volume fraction after 30 days in a scaffold with thickness of 0.88×10^{-3} m (Case G) is 2.26 fold that obtained with a scaffold of 1.68×10^{-3} m (Case I), which is nearly the fold increase of 2.25 observed by Freed et al. [22]. Because Model I does not include oxygen concentration, Model II was used to evaluate the mean dimensionless oxygen concentration evolution in time of scaffolds with 3.07×10^{-3} m, which is shown in Figure 7.5. The observed changes of oxygen concentration over time were below 1 %. The same occurred for other cases with different thicknesses and also when using Model III. This could be due to a small maximum oxygen consumption rate, which should be estimated for the experimental system in study to check if this parameter is in an acceptable range.

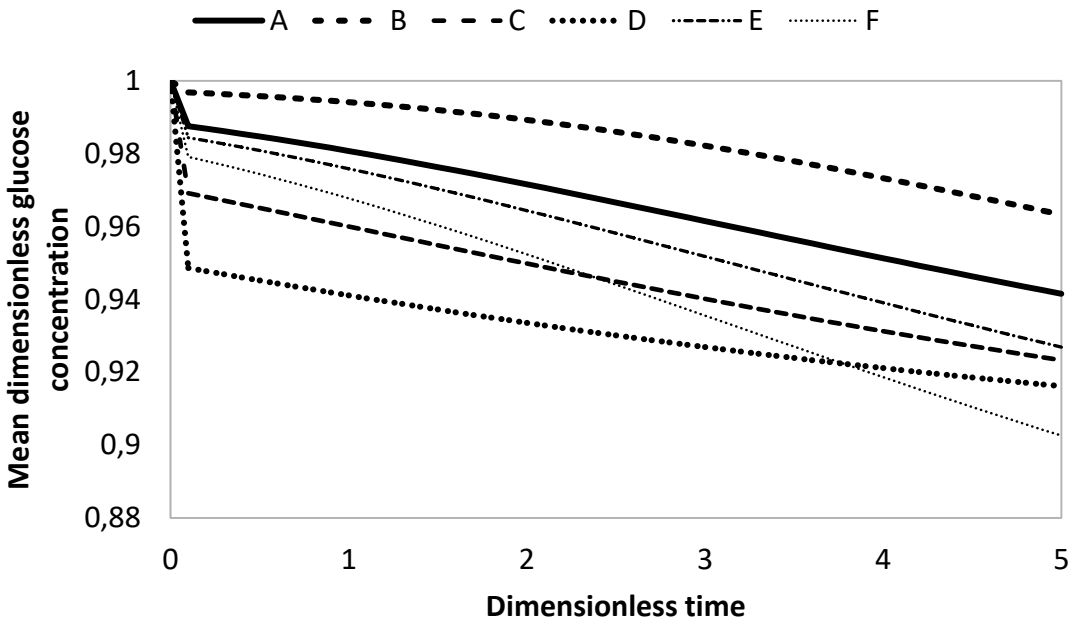

Figure 7.5: Model II time evolution of mean dimensionless oxygen concentration for scaffold thickness of 3.07×10^{-3} m. A: [$\varepsilon_{cell,0}/\varepsilon_{cell,0,max}$ $\varepsilon/\varepsilon_{max}$ $C_{G,0}/C_{G,0,max}$] = [40 100 100], B: [$\varepsilon_{cell,0}/\varepsilon_{cell,0,max}$ $\varepsilon/\varepsilon_{max}$ $C_{G,0}/C_{G,0,max}$] = [10 100 100], C: [$\varepsilon_{cell,0}/\varepsilon_{cell,0,max}$ $\varepsilon/\varepsilon_{max}$ $C_{G,0}/C_{G,0,max}$] = [100 100 100], D: [$\varepsilon_{cell,0}/\varepsilon_{cell,0,max}$ $\varepsilon/\varepsilon_{max}$ $C_{G,0}/C_{G,0,max}$] = [40 100 22.22], E: [$\varepsilon_{cell,0}/\varepsilon_{cell,0,max}$ $\varepsilon/\varepsilon_{max}$ $C_{G,0}/C_{G,0,max}$] = [40 80 100], F: [$\varepsilon_{cell,0}/\varepsilon_{cell,0,max}$ $\varepsilon/\varepsilon_{max}$ $C_{G,0}/C_{G,0,max}$] = [40 60 100]

Figure 7.6 presents the maximum values of mean cell volume fraction deviation obtained with Models II and III when compared to the results obtained with Model I (Figures 7.1 to 7.4). The values of cell volume fraction predicted by Model II were slightly smaller than those predicted by Model I, being the maximum deviation of approximately 24 % for the thinnest scaffolds (Case G, J and M). Thus, scaffold thickness was the factor that most affected the difference between the predictions of Models I and II, followed by initial glucose concentration and initial cell density. This may be related to the inclusion of oxygen contribution to the cell growth in the Contois equation, which reduced the effect of glucose concentration on cell growth, and also to the fact that the smaller the scaffold thickness the higher the cell growth and glucose consumption, increasing the difference between the two models.

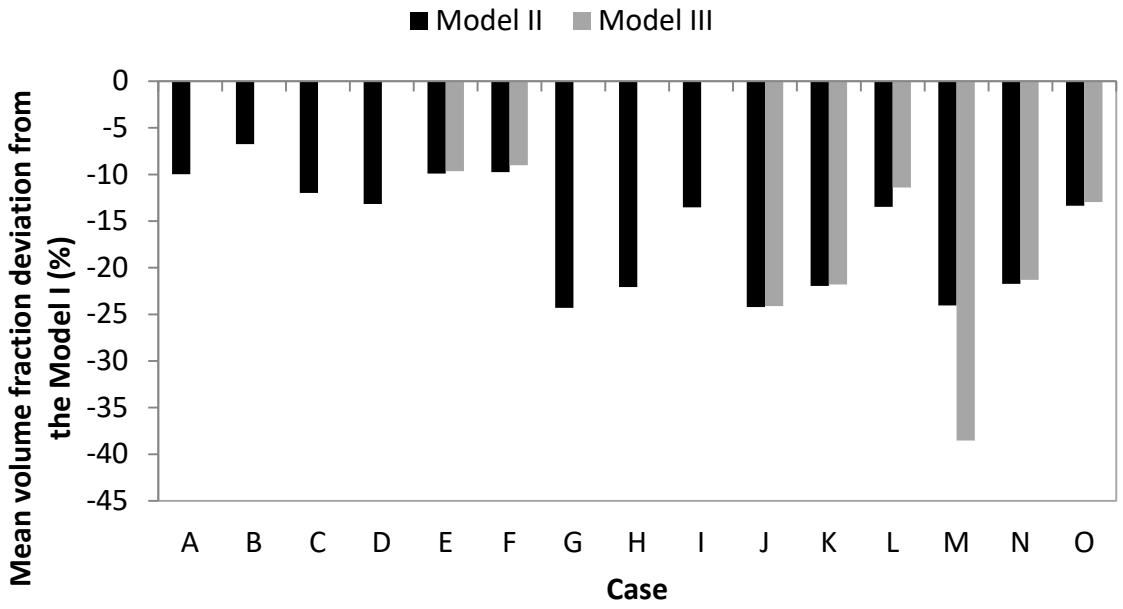

Figure 7.6: Maximum values of Model II and III mean cell volume fraction deviation from Model I for all cases. The cases A to F have H/H_{max} = 100. A: [$\varepsilon_{cell,0}/\varepsilon_{cell,0,max}$ $\varepsilon/\varepsilon_{max}$ $C_{G,0}/C_{G,0,max}$] = [40 100 100], B: [$\varepsilon_{cell,0}/\varepsilon_{cell,0,max}$ $\varepsilon/\varepsilon_{max}$ $C_{G,0}/C_{G,0,max}$] = [10 100 100], C: [$\varepsilon_{cell,0}/\varepsilon_{cell,0,max}$ $\varepsilon/\varepsilon_{max}$ $C_{G,0}/C_{G,0,max}$] = [100 100 100], D: [$\varepsilon_{cell,0}/\varepsilon_{cell,0,max}$ $\varepsilon/\varepsilon_{max}$ $C_{G,0}/C_{G,0,max}$] = [40 100 22.22], E: [$\varepsilon_{cell,0}/\varepsilon_{cell,0,max}$ $\varepsilon/\varepsilon_{max}$ $C_{G,0}/C_{G,0,max}$] = [40 80 100], F: [$\varepsilon_{cell,0}/\varepsilon_{cell,0,max}$ $\varepsilon/\varepsilon_{max}$ $C_{G,0}/C_{G,0,max}$] = [40 60 100]. The cases G to O have $\varepsilon_{cell,0}/\varepsilon_{cell,0,max}$ = 20 and $C_{G,0}/C_{G,0,max}$ = 100. G: [$\varepsilon/\varepsilon_{max}$ H/H_{max}] = [100 28.95], H: [$\varepsilon/\varepsilon_{max}$ H/H_{max}] = [100 38.16], I: [$\varepsilon/\varepsilon_{max}$ H/H_{max}] = [100 55.26], J: [$\varepsilon/\varepsilon_{max}$ H/H_{max}] = [80 28.95], K: [$\varepsilon/\varepsilon_{max}$ H/H_{max}] = [80 38.16], L: [$\varepsilon/\varepsilon_{max}$ H/H_{max}] = [80 55.26], M: [$\varepsilon/\varepsilon_{max}$ H/H_{max}] = [60 28.95], N: [$\varepsilon/\varepsilon_{max}$ H/H_{max}] = [60 38.16], O: [$\varepsilon/\varepsilon_{max}$ H/H_{max}] = [60 55.26]

Cell volume fractions predicted by Model III were also smaller when compared to those obtained with Model I, with maximum deviation of approximately 38 % for Case M (thinnest and less porous scaffold), as it can be seen in Figure 7.6. Besides this, the differences between the models increased with time and reached the maximum value at the final time for all cases, except for Case M with Model III. In Case M, with smaller porosity at the beginning of the culture, the cell growth was lower, resulting in higher deviation at the middle of the culture time. As the porosity increase with time, the cell growth increased, reaching the final time with a smaller divergence from Model I.

When the mean cell volume fraction at the final time was compared for different porosities, the effect of the porosity in Model I was slightly more accentuated than that in

Models II and III. This could be due to the low oxygen consumption and consequent attenuation of glucose diffusion limitation impact on cell growth with the inclusion of a term related to the oxygen concentration in the model (Models II and III). It is important to observe that this effect could be significant with a higher cell growth rate. With polymer degradation and increasing void fraction (Model III), the initial porosity effect was reduced with time.

Figure 7.7 presents the percent relative errors for the simulation results obtained for the three models when compared to the experimental data of Freed et al. [22]. Model I presented higher relative errors for intermediate times for Cases A, B, D, E, F, I, L, and O and smaller errors at the final time, except for Cases C, M, H, K and N. Case C presented the highest relative error at the smallest time, which could be related to the consideration of a higher initial cell volume fraction. For Model III, relative error decreased with time except for Cases K and N, for which the minimum error occurred for the cell volume fraction at the sixteenth day of cultivation.

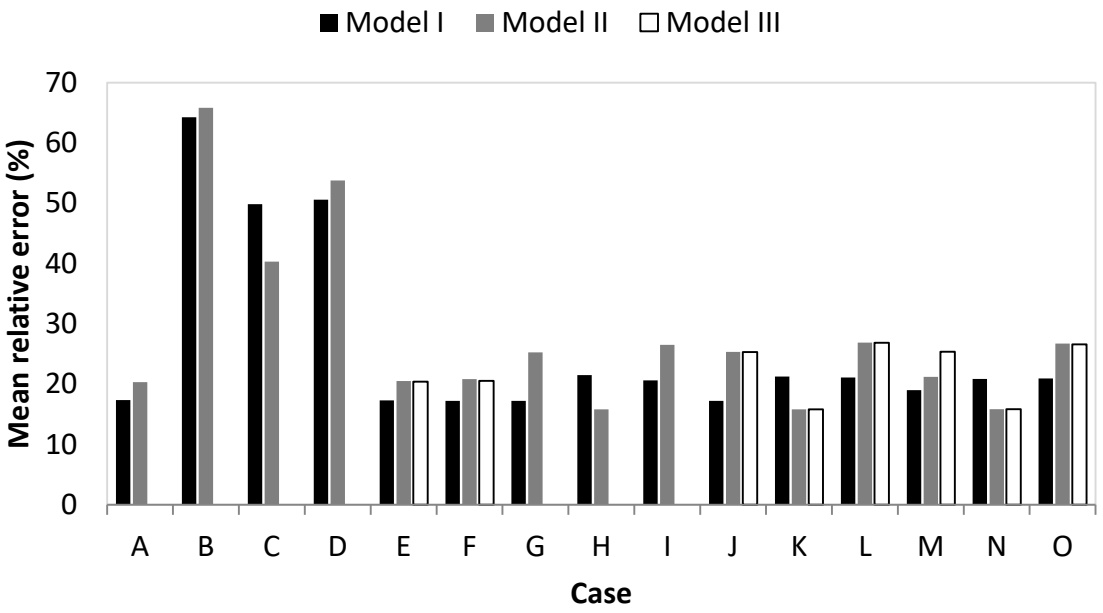

Figure 7.7: Percent relative errors for Model I, II and III. The cases A to F have H/H_{max} = 100. A: [$\varepsilon_{cell,0}/\varepsilon_{cell,0,max}$ $\varepsilon/\varepsilon_{max}$ $C_{G,0}/C_{G,0,max}$] = [40 100 100], B: [$\varepsilon_{cell,0}/\varepsilon_{cell,0,max}$ $\varepsilon/\varepsilon_{max}$ $C_{G,0}/C_{G,0,max}$] = [10 100 100], C: [$\varepsilon_{cell,0}/\varepsilon_{cell,0,max}$ $\varepsilon/\varepsilon_{max}$ $C_{G,0}/C_{G,0,max}$] = [100 100 100], D: [$\varepsilon_{cell,0}/\varepsilon_{cell,0,max}$ $\varepsilon/\varepsilon_{max}$ $C_{G,0}/C_{G,0,max}$] = [40 100 22.22], E: [$\varepsilon_{cell,0}/\varepsilon_{cell,0,max}$ $\varepsilon/\varepsilon_{max}$ $C_{G,0}/C_{G,0,max}$] = [40 80 100], F: [$\varepsilon_{cell,0}/\varepsilon_{cell,0,max}$ $\varepsilon/\varepsilon_{max}$ $C_{G,0}/C_{G,0,max}$] = [40 60 100]. The cases G to O have $\varepsilon_{cell,0}/\varepsilon_{cell,0,max}$ = 20 and $C_{G,0}/C_{G,0,max}$ = 100. G: [$\varepsilon/\varepsilon_{max}$ H/H_{max}] = [100 28.95], H: [$\varepsilon/\varepsilon_{max}$ H/H_{max}] = [100 38.16], I: [$\varepsilon/\varepsilon_{max}$ H/H_{max}] = [100 55.26], J: [$\varepsilon/\varepsilon_{max}$ H/H_{max}] = [80 28.95], K:

$[\varepsilon/\varepsilon_{max}\ H/H_{max}]$ = [80 38.16], L: $[\varepsilon/\varepsilon_{max}\ H/H_{max}]$ = [80 55.26], M: $[\varepsilon/\varepsilon_{max}\ H/H_{max}]$ = [60 28.95], N: $[\varepsilon/\varepsilon_{max}\ H/H_{max}]$ = [60 38.16], O: $[\varepsilon/\varepsilon_{max}\ H/H_{max}]$ = [60 55.26]

The smallest mean relative errors obtained with Models II and III were of approximately 16 %, for the cases with scaffold thickness of 1.16×10^{-3} m. Regarding Model I, the smallest errors (around 17 %) were found for Cases A, E, F, G and J. This is probably due to the fact that the parameter estimation performed by Chung et al. [16] with the model without the oxygen term in the Contois equation and was based on experimental conditions more similar to those of Case A. The higher mean relative errors obtained for scaffold thicknesses of 1.68 and 1.16×10^{-3} m may be associated to the inclusion of the Michaelis-Menten equation and the consequent changes on the cell volume fraction profile due to the variable glucose consumption rate. Models II and III seemed to capture the experimental behavior of the cells in scaffolds with 1.16×10^{-3} m of thickness, which may be related to their smaller cell growth in the initial times.

The highest mean relative errors were of approximately 65 % for the case with the smallest initial cell number (B) for Models I and II, and of 26 % for the cases with scaffold thickness of 1.68×10^{-3} m (L and O) for Model III. Thus, models I and II can be said to be more affected by the initial cell number, while Model III is quite robust to variations on the input variables.

7.4 Conclusions

The contribution of oxygen in the Contois growth kinetics and the porosity variation with time due to polymer degradation was evaluated through a sensitivity analysis. The inclusion of oxygen concentration in the model affected both the cell volume fraction and the glucose concentration. In addition, the oxygen concentration behavior was not modified by considering a variable porosity on the model. On the other hand, the initial cell number had a more significant impact on mass transport than on cell growth. The inclusion of different processes in the model led to significant differences on the predictions. This indicates that, in order to achieve definitive conclusions in terms of model adequacy and selection, more extensive experimental data generation and specific measuring techniques development is required.

7.5 Acknowledgments

This research was developed at the National Center of Supercomputing from the Federal University of Rio Grande do Sul. The authors would like to thank CAPES (Coordination for the Improvement of Higher Education Personnel), FINEP (Financing Agency for Studies and Projects) and Stem Cell Research Institute for their financial support.

7.6 References

[1] F. Coletti, S. Macchietto, N. Elvassore, Mathematical Modeling of Three-Dimensional Cell Cultures in Perfusion Bioreactors, Ind. Eng. Chem. Res. 45 (2006) 8158–8169. doi:10.1021/ie051144v.

[2] X. Yan, D.J. Bergstrom, X.B. Chen, Modeling of cell cultures in perfusion bioreactors, IEEE Trans. Biomed. Eng. 59 (2012) 2568–2575. doi:10.1109/TBME.2012.2206077.

[3] S. Truscello, G. Kerckhofs, S. Van Bael, G. Pyka, J. Schrooten, H. Van Oosterwyck, Prediction of permeability of regular scaffolds for skeletal tissue engineering: A combined computational and experimental study, Acta Biomater. 8 (2012) 1648–1658. doi:10.1016/j.actbio.2011.12.021.

[4] V.A.A. Santamaría, M. Malvè, a. Duizabo, a. Mena Tobar, G. Gallego Ferrer, J.M. García Aznar, M. Doblaré, I. Ochoa, Computational methodology to determine fluid related parameters of non regular three-dimensional scaffolds, Ann. Biomed. Eng. 41 (2013) 2367–2380. doi:10.1007/s10439-013-0849-8.

[5] R.J. McCoy, C. Jungreuthmayer, F.J. O'Brien, Influence of flow rate and scaffold pore size on cell behavior during mechanical stimulation in a flow perfusion bioreactor, Biotechnol. Bioeng. 109 (2012) 1583–1594. doi:10.1002/bit.24424.

[6] P. Decuzzi, M. Ferrari, Modulating cellular adhesion through nanotopography, Biomaterials. 31 (2010) 173–179. doi:10.1016/j.biomaterials.2009.09.018.

[7] E.Y. Gómez-Pachón, F.M. Sánchez-Arévalo, F.J. Sabina, A. Maciel-Cerda, R.M. Campos, N. Batina, I. Morales-Reyes, R. Vera-Graziano, Characterisation and modelling of the elastic properties of poly(lactic acid) nanofibre scaffolds, J. Mater. Sci. 48 (2013) 8308–8319. doi:10.1007/s10853-013-7644-7.

[8] P. Pathi, T. Ma, B.R. Locke, Role of nutrient supply on cell growth in bioreactor design for tissue engineering of hematopoietic cells, Biotechnol. Bioeng. 89 (2005) 743–758. doi:10.1002/bit.20367.

[9] M. Devarapalli, B.J. Lawrence, S. V. Madihally, Modeling nutrient consumptions in large flow-through bioreactors for tissue engineering, Biotechnol. Bioeng. 103 (2009) 1003–1015. doi:10.1002/bit.22333.

[10] L.A. Hidalgo-Bastida, S. Thirunavukkarasu, S. Griffiths, S.H. Cartmell, S. Naire, Modeling and design of optimal flow perfusion bioreactors for tissue engineering applications, Biotechnol. Bioeng. 109 (2012) 1095–1099. doi:10.1002/bit.24368.

[11] I.O. Doagă, T. Savopol, M. Neagu, a. Neagu, E. Kovács, The kinetics of cell adhesion to solid scaffolds: An experimental and theoretical approach, J. Biol. Phys. 34 (2008) 495–509. doi:10.1007/s10867-008-9108-x.

[12] C.A. Chung, T.-H. Lin, S.-D. Chen, H.-I. Huang, Hybrid cellular automaton modeling of nutrient modulated cell growth in tissue engineering constructs, J. Theor. Biol. 262 (2010) 267–278. doi:10.1016/j.jtbi.2009.09.031.

[13] D. Jeong, A. Yun, J. Kim, Mathematical model and numerical simulation of the cell growth in scaffolds, Biomech. Model. Mechanobiol. 11 (2012) 677–688.

doi:10.1007/s10237-011-0342-y.
[14] C.J. Galban, B.R. Locke, Analysis of cell growth kinetics and substrate diffusion in a polymer scaffold, Biotechnol. Bioeng. 65 (1999) 121–132. doi:10.1002/(SICI)1097-0290(19991020)65:2<121::AID-BIT1>3.0.CO;2-6.
[15] C.J. Galban, B.R. Locke, Effects of spatial variation of cells and nutrient and product concentrations coupled with product inhibition on cell growth in a polymer scaffold, Biotechnol. Bioeng. 64 (1999) 633–643. doi:10.1002/(SICI)1097-0290(19990920)64:6<633::AID-BIT1>3.0.CO;2-6.
[16] C.A. Chung, C.W. Yang, C.W. Chen, Analysis of Cell Growth and Diffusion in a Scaffold for Cartilage Tissue Engineering, Wiley Period. 94 (2006) 1138–1146.
[17] C.A. Chung, C.W. Chen, C.P. Chen, C.S. Tseng, Enhancement of cell growth in tissue-engineering constructs under direct perfusion: Modeling and simulation, Biotechnol. Bioeng. 97 (2007) 1603–1616. doi:10.1002/bit.21378.
[18] C.A. Chung, C.P. Chen, T.H. Lin, C.S. Tseng, A compact computational model for cell construct development in perfusion culture, Biotechnol. Bioeng. 99 (2008) 1535–1541. doi:10.1002/bit.21701.
[19] M. Shakeel, Continuum modelling of cell growth and nutrient transport in a perfusion bioreactor, The University of Nottingham, 2011. http://etheses.nottingham.ac.uk/1772/.
[20] T.-H. Lin, C.-H. Lin, C.A. Chung, Comutational Study of Oxygen and Glucose Transport in Engineered Cartilage Constructs, J. Mech. 27 (2011) 337–346. doi:10.1017/jmech.2011.36.
[21] C.J. Galban, B.R. Locke, Analysis of cell growth in a polymer scaffold using a moving boundary approach, Biotechnol. Bioeng. 56 (1997) 422–432. doi:10.1002/(SICI)1097-0290(19971120)56:4<422::AID-BIT7>3.0.CO;2-Q.
[22] F. LE, V.-N. G, M. JC, L. R., Kinetics of chondrocyte growth in cell-polymer implants, Biotechnol Bioeng. 43 (1994) 597–604.
[23] J.M. Gluck, Electrospun Nanofibrous Poly(ε-caprolactone) (PCL) Scaffolds for Liver Tissue Engineering, Graduate Faculty of North Carolina State University, 2007.
[24] L.E. Freed, A.P. Hollander, I. Martin, J.R. Barry, R. Langer, G. Vunjak-Novakovic, Chondrogenesis in a cell-polymer-bioreactor system., Exp. Cell Res. 240 (1998) 58–65. doi:10.1006/excr.1998.4010.
[25] T. Holzmann, The pimple algorithm in OpenFOAM., (2016). https://openfoamwiki.net/index.php/OpenFOAM_guide/The_PIMPLE_algorithm_in_OpenFOAM (accessed July 14, 2016).
[26] M.E. Gomes, H.L. Holtorf, R.L. Reis, A.G. Mikos, Influence of the porosity of starch-based fiber mesh scaffolds on the proliferation and osteogenic differentiation of bone marrow stromal cells cultured in a flow perfusion bioreactor., Tissue Eng. 12 (2006) 801–809. doi:10.1089/ten.2006.12.801.

Capítulo 8

Considerações finais

Nas últimas décadas, o cultivo de células-tronco mesenquimais em *scaffolds* tridimensionais tem sido utilizado para o desenvolvimento de diversos tipos de tecidos. No entanto, um dos desafios do cultivo tridimensional é a formação de gradiente de nutrientes. Visando a otimização do processo, as limitações de transporte de massa podem ser estudadas e minimizadas através do uso de biorreatores e de técnicas de modelagem.

Neste trabalho, foi estudado o cultivo de células-tronco mesenquimais da polpa de dente decíduo em *scaffolds* eletrofiados de PCL. Para isto, foram desenvolvidos protocolos de cultivo estático e dinâmico, para posterior comparação dos fenômenos de transporte de massa e de crescimento e metabolismo celular nos dois tipos de cultivo. Além disso, um modelo bastante referenciado na literatura foi analisado para verificar a capacidade do mesmo em representar o sistema experimental deste estudo.

Inicialmente, buscou-se estabelecer os parâmetros de eletrofiação e a composição da solução polimérica (concentração, solvente) de modo a produzir *scaffolds* com fibras micrométricas. As questões de pesquisa, hipóteses e objetivo referentes a esta etapa estão listadas a seguir.

→ Questões de pesquisa: É possível eletrofiar *scaffolds* de PCL com poros de diâmetro adequado para a infiltração de DPSCs? O cultivo tridimensional afeta o crescimento, o consumo de nutrientes e produção de metabólitos das células?

→ Hipótese: A técnica de *electrospinning* é capaz de produzir *scaffolds* de PCL com fibras micrométricas e poros grandes o suficiente para permitir a infiltração das células para dentro da matriz.

→ Objetivos específicos:

a. estabelecer o protocolo de eletrofiação de *scaffolds* com poros de diâmetro adequados para o cultivo tridimensional de DPSCs;

b. comparar o tempo de dobramento e as taxas de consumo de glicose e de produção de lactato das células em cultivos bidimensionais e tridimensionais.

Foi observado que a adição de metanol melhorou a eletrofiabilidade da solução de clorofórmio e PCL, e diminuiu o diâmetro médio de fibra e de poro do *scaffold* (conforme apresentado nas Figuras 4.5 e 4.6). De acordo com a Figura 4.8, apenas a solução de PCL com uma proporção de clorofórmio/metanol de 9:1 foi capaz de produzir uma estrutura com poros adequados para a infiltração celular. Assim, com diâmetro de fibra de 3,95±0,73 μm (conforme Tabela 4.3) e de poro de 21,35±8,89 μm (conforme Tabela 4.4), os *scaffolds* produzidos com esta solução foram utilizados nos experimentos posteriores de cultivo de DPSC (diâmetro da célula entre 12,2 e 16,6 μm).

Apesar de apresentarem diferentes distribuições celulares, os diferentes *scaffolds* testados tiveram tempos de dobramento e taxas específicas de consumo de glicose e de produção de lactato similares, diferenciando-se apenas do controle (poço). É provável que o baixo número de células aderidas nos *scaffolds* não tenha propiciado uma situação de competitividade por espaço e nutrientes, não sendo possível evidenciar a influência da arquitetura do *scaffold* na atividade celular. Quando uma densidade de semeadura mais alta foi utilizada nos *scaffolds* que permitiam a infiltração celular, a disposição das células após a adesão se deu de forma a cobrir a superfície do *scaffold*, obstruindo os poros. Isto ficou evidente após análises de microscopia confocal (Figura 5.4) e de MEV (Figura 5.5a).

Então foram estabelecidas as condições de cultivo dinâmico no biorreator de perfusão. Neste processo, buscou-se responder as seguintes questões de pesquisa:

→ É possível minimizar o arraste de DPSCs de um *scaffold* eletrofiado de PCL sob perfusão diminuindo a vazão?

→ Qual a vazão máxima ou ótima de operação?

→ O tempo de semeadura e a densidade das células afetam o processo de adesão e o posterior arraste das células?

De acordo com a literatura, contanto que a tensão de cisalhamento não atinja um limite máximo dentro dos poros, não irá ocorrer desprendimento e arraste das células com a perfusão de meio. Desta forma, é necessário determinar a vazão máxima de operação para minimizar o arraste sob perfusão, o que está relacionado com a seguinte hipótese:

→ a célula é capaz de se proliferar com a perfusão direta do meio de cultivo, contanto que a tensão de cisalhamento não ultrapasse um limite crítico.

No entanto, com a passagem de fluxo, as células que ocupavam os poros da superfície do *scaffold* eram arrastadas independentemente da vazão de perfusão (Figura 5.5b e Figura 5.8b), indicando que a tensão de cisalhamento não era a única variável a influenciar o arraste das células. Assim sendo, a metodologia utilizada para a adesão das células foi revista, e novas hipóteses foram formuladas:

→ com o aumento do tempo de adesão é possível favorecer a formação de adesão focal entre as células e as fibras do *scaffold*, diminuindo o arraste de células;

→ com a diminuição da densidade de semeadura é possível reduzir o preenchimento dos poros da superfície.

O aumento do tempo de adesão possibilitou maior espalhamento em condições estáticas (Figura 5.4) e reduziu o arraste das células sob perfusão (Figura 5.7). Já a diminuição da densidade de semeadura diminuiu o arraste das células (Figura 5.8a). Sendo assim, as hipóteses acima foram validadas e o protocolo de cultivo dinâmico foi estabelecido a uma densidade de semeadura de $0{,}5\times10^5$ células por *scaffold* e uma vazão de 0,05 mL/min, atingindo o seguinte objetivo específico:

c. estabelecer protocolo de cultivo dinâmico de células-tronco mesenquimais da polpa de dente em *scaffolds* de PCL;

Paralelamente a estes experimentos *in vitro*, foram realizados testes *in silico*. Para poder comparar os cultivos estático e dinâmico, inicialmente foi estudado um modelo de proliferação celular e transporte e consumo de nutrientes sob condições estáticas. Nesta etapa, visou-se responder as seguintes questões de pesquisa:

→ Qual o efeito dos parâmetros e das variáveis de entrada nas variáveis de saída do modelo?

→ O modelo estudado é adequado para representar o sistema experimental deste estudo?

O estudo do efeito dos parâmetros e entradas no modelo é de extrema importância para verificar se o comportamento das seguintes hipóteses pode ser representado pelo modelo:

→ o crescimento celular é modulado pela disponibilidade de nutrientes;

→ a célula é capaz de migrar através de uma estrutura 3D com poros de diâmetro maior que o diâmetro da célula em suspensão.

Conforme pode ser observado no Capítulo 6, este comportamento é representado pelo modelo. Através de uma análise de sensibilidade, foi possível determinar os parâmetros e as variáveis de entrada com maior impacto no modelo em estudo. Verificou-se que os parâmetros relacionados aos processos de proliferação e morte celular e ao consumo de nutrientes (Figuras 6.3 e 6.4), assim como as variáveis de entrada relacionadas à disponibilidade de nutrientes (concentração adimensional de glicose inicial e porosidade do *scaffold*) (Figuras 6.6 a 6.11), tiveram maior impacto nas variáveis de saída do modelo (fração volumétrica de células e concentração adimensional de glicose). Nesta etapa foi possível atingir os seguintes objetivos específicos:

d. modelar a proliferação celular e o transporte de massa em *scaffolds* porosos;
e. realizar análise de sensibilidade (simulação com diferentes valores de parâmetros e entradas) para determinar os parâmetros significativos do modelo.

O segundo estudo *in silico* realizado buscou responder a seguinte questão de pesquisa:

→ Qual a contribuição do oxigênio e do aumento da porosidade com a degradação do polímero ao modelo em estudo em diferentes cenários (variação nas variáveis de entrada)?

Este trabalho foi realizado para verificar se a determinação da concentração de oxigênio e da variação da porosidade com a degradação do polímero poderia trazer uma contribuição significativa para a posterior validação do modelo. Foi verificado que a inclusão da concentração de oxigênio no modelo afetou as variáveis de saída, enquanto o modelo com porosidade variável se mostrou consideravelmente robusto a variações nas variáveis de entrada (Figura 7.6). Nesta etapa atingiu-se o objetivo específico a seguir:

f. avaliar a contribuição da adição de complexidade ao modelo e estabelecer os fenômenos que devem ser descritos.

Desta forma, a primeira principal conclusão deste estudo é que a técnica de *electrospinning* permite a produção de *scaffolds* com poros adequados para a infiltração de DPSCs. A segunda, que a tensão de cisalhamento não é a única variável que influencia no desprendimento das células no sistema dinâmico em estudo, visto que foi possível minimizar o arraste aumentando o tempo de adesão e diminuindo a densidade de semeadura. Com as simulações, pôde-se concluir que o modelo em estudo é sensível às variáveis de entrada

concentração inicial de nutrientes e porosidade do *scaffold*, e aos parâmetros adimensionais relacionados à atividade celular (proliferação e morte, e consumo de nutrientes).

A validade de se incorporar ao modelo termos que considerem a concentração de oxigênio e o aumento da porosidade com a degradação do *scaffold* depende do comportamento observado experimentalmente para o sistema em estudo. Como o PCL possui um tempo de degradação relativamente prolongado, espera-se que a variação temporal da porosidade apresente uma contribuição ainda menor do que a observada nas simulações. Além disso, tendo em vista a capacidade de adaptação das células-tronco mesenquimais, a concentração de oxigênio pode não influenciar significativamente a modulação da atividade celular como previsto nas simulações com condrócitos. Por fim, a perfusão direta, combinada com a semeadura estática e *scaffolds* eletrofiados, foi capaz de propiciar um ambiente favorável para o crescimento celular. No entanto, mais testes com um maior número de culturas e de amostras são necessários para reduzir o erro experimental e gerar dados para a validação de um modelo fenomenológico.

Capítulo 9

Perspectivas

Cabe ressaltar que o este estudo buscou combinar as técnicas de *electrospinning* e de modelagem com o cultivo de células-tronco em biorreatores, o que acarretou em limitações específicas para este sistema. Esta pesquisa pode ser ampliada para sistemas com outros tipos de *scaffolds*, células e biorreatores, o que possibilita a realização de inúmeros trabalhos futuros, como:

- verificar se é possível minimizar o arraste em *scaffolds* através da funcionalização do *scaffold* para aumentar a adesão celular;
- realizar o cultivo de células-tronco mesenquimais em outros tipos de biorreatores;
- realizar o co-cultivo de células-tronco mesenquimais e células diferenciadas nos biorreatores;
- realizar o cultivo dinâmico nos *scaffolds* eletrofiados de PCL com outros tipos de células;
- realizar o cultivo dinâmico das células-tronco mesenquimais em *scaffolds* produzidos a partir de outros polímeros;
- realizar o cultivo dinâmico das células-tronco mesenquimais em *scaffolds* produzidos a partir de outras técnicas.